ERDC/CHL TR-15-5

US Army Corps
of Engineers®
Engineer Research and
Development Center

ERDC
INNOVATIVE SOLUTIONS
for a safer, better world

North Atlantic Coast Comprehensive Study (NACCS)

Coastal Storm Hazards from Virginia to Maine

Norberto C. Nadal-Caraballo, Jeffrey A. Melby,
Victor M. Gonzalez, and Andrew T. Cox

November 2015

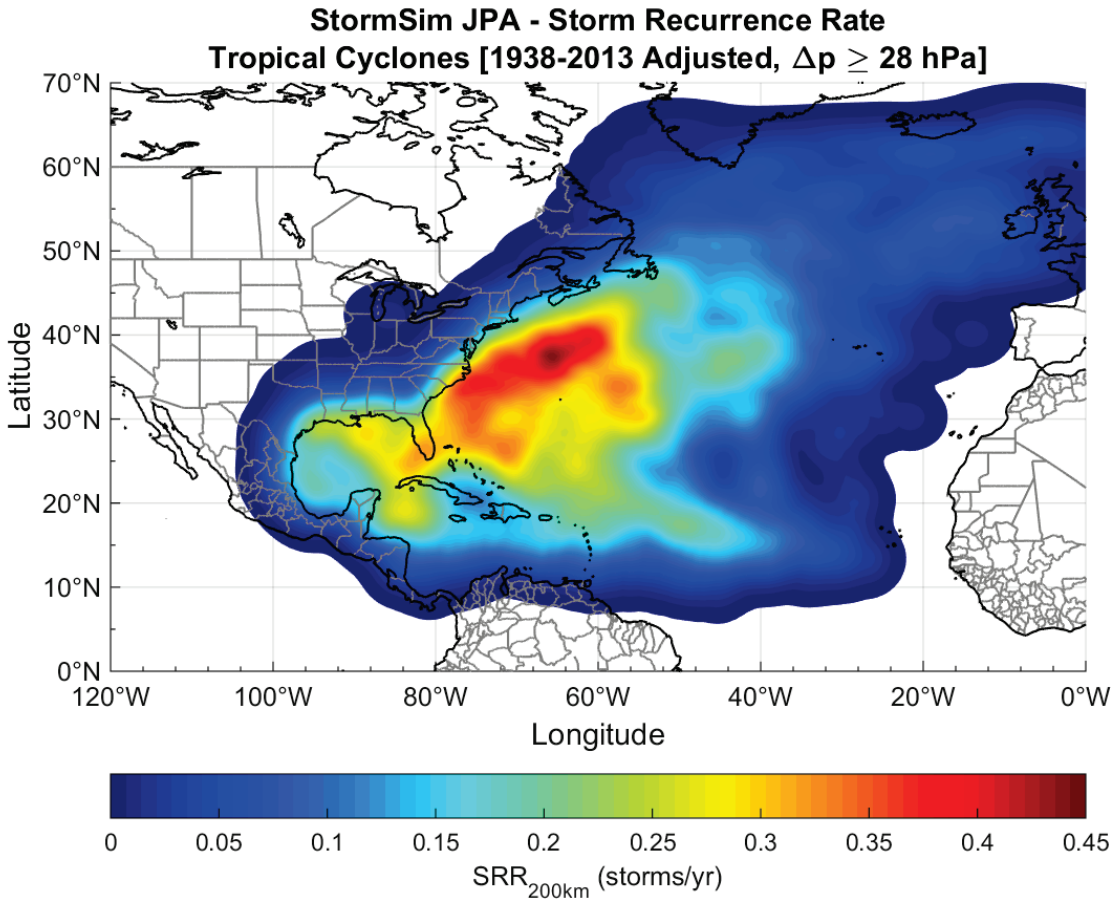

Coastal and Hydraulics Laboratory

The U.S. Army Engineer Research and Development Center (ERDC) solves the nation's toughest engineering and environmental challenges. ERDC develops innovative solutions in civil and military engineering, geospatial sciences, water resources, and environmental sciences for the Army, the Department of Defense, civilian agencies, and our nation's public good. Find out more at www.erdc.usace.army.mil.

To search for other technical reports published by ERDC, visit the ERDC online library at http://acwc.sdp.sirsi.net/client/default.

ERDC/CHL TR-15-5
November 2015

Coastal Storm Hazards from Virginia to Maine

Norberto C. Nadal-Caraballo, Jeffrey A. Melby, and Victor M. Gonzalez

Coastal and Hydraulics Laboratory
U.S. Army Engineer Research and Development Center
3909 Halls Ferry Road
Vicksburg, MS 39180—6199

Andrew T. Cox

Oceanweather Inc.
5 River Road, Suite 1
Cos Cob, CT 06807

Prepared for U.S. Army Engineer District, Baltimore
City Crescent Building, 10 South Howard Street
Baltimore, MD 21201

Under Project 401426, North Atlantic Coast Comprehensive Study

Abstract

The U.S. North Atlantic coast is subject to coastal flooding as a result of tropical cyclones (e.g., hurricanes) and severe extratropical cyclones (e.g., Nor'easters). The North Atlantic Coast Comprehensive Study (NACCS) seeks to quantify existing and future forcing for use in assessing potential engineering projects that would reduce flooding risk and increase resiliency. The study encompasses the coastal region from Virginia to Maine. This report describes the characterization of storm climate and statistical analysis of coastal storm hazards for the NACCS. The overall NACCS wave and water level modeling goals included simulating an efficient number of storms that blanketed a sufficient range of storm characteristics in order to accurately describe the statistical nature of coastal storm response over the entire region. This information is required for modern probabilistic project design and for risk assessments. For this study, storm surge, tide, waves, wind, atmospheric pressure, and currents were the dominant storm responses computed. The effect of sea level change on these storm responses was assessed. The significant advancements in this study included a dense spatial coverage of nearshore storm response for the region, high-fidelity computations, a comprehensive description of the aleatory variability of response from frequent storm events to extremely rare events, a description of epistemic uncertainty, characterization of the statistical nature of the data in easily ingestible, relatively simple data formats, and public distribution of data and statistics within the Coastal Hazards System, a web-based coastal storm data resource.

Contents

Figures and Tables

Figures

Tables

Preface

The study summarized in this report was conducted as a task within the North Atlantic Coast Comprehensive Study. The study was funded by the U.S. Army Corps of Engineers (USACE) Headquarters through the USACE Baltimore District (NAB) and conducted at the U.S. Army Engineer Research and Development Center (ERDC), Coastal and Hydraulics Laboratory (CHL), Vicksburg, MS, during the period of April 2013–February 2015. Lynn M. Bocamazo, Chief, Hurricane Sandy Relief Branch, New York District (NAN), Engineering Division, was the primary engineering point of contact.

This report was prepared by Dr. Norberto C. Nadal-Caraballo, Dr. Jeffrey A. Melby, and Victor M. Gonzalez, Harbors, Entrances, and Structures (HES) Branch, CHL.

Dr. Nadal-Caraballo, Dr. Melby, and Gonzalez were under the general supervision of James D. Gutshall, Chief, HES Branch, and Dr. Jackie Pettway, Chief, Navigation Division. José Sánchez was Director, CHL, and Dr. Kevin Barry was Deputy Director, CHL.

At the time of publication of this report, COL Bryan S. Green was Commander of ERDC. Dr. Jeffery P. Holland was Director.

Unit Conversion Factors

Most measurements and calculations for this study were done in SI units. The following table can be used to convert SI units to English customary units.

Multiply	By	To Obtain
m	3.28084	ft
km	0.621371	mi
km	0.539957	nmi
km/h	0.621371	mph
km/h	0.539957	kn

Notation

Δp	central pressure deficit of tropical cyclone, computed as the difference between a far-field atmospheric pressure of 1,013 hPa and central pressure (hPa)
θ	heading direction of tropical cyclone (deg)
R_{max}	radius of maximum winds of tropical cyclone (km)
V_t	translational speed of tropical cyclone (km/h)
x_0	tropical cyclone track location
AEP	annual exceedance probability (yr^{-1})
ARI	average recurrence interval (yr)
BFE	base flood elevation, a flood having a one percent chance of being equaled or exceeded in a given year (m)
CCDF	complementary cumulative distribution function
CDF	cumulative distribution function
CHS	Coastal Hazards System
CL	confidence limit
CSS	composite storm set
CRL	coastal reference location
DSRR	directional storm recurrence rate
DTWD	doubly truncated Weibull distribution
EVA	extreme value analysis
GKF	Gaussian kernel function

GPD	generalized Pareto distribution
GSLC	global sea level change (m)
JPA	joint probability analysis
JPM	joint probability method
JPM-OS	joint probability method with optimal sampling
JPM-OS-RS	joint probability method with optimal sampling by response surface
JPM-OS-BQ	joint probability method with optimal sampling by Bayesian quadrature
LRP	landfall reference point
LTWD	left truncated Weibull distribution
NLR	nonlinear residual, defined as the difference in storm water level response between the linearly superimposed components and the full numerical simulation of total storm water level (m)
NTR	nontidal residual (m)
ODGP	ocean data gathering program
ORP	offshore reference point
PBL	planetary boundary layer numerical model
PDF	probability density function
SLC	sea level change (m)
SRR	storm recurrence rate (storms/yr/km)

SRR_{200km}	recurrence rate associated with storms passing within 200 km of a given location (storms/yr)
SSHWS	Saffir-Simpson hurricane wind scale
TC	tropical cyclone
XC	extratropical cyclone

1 Introduction

1.1 Problem

The North Atlantic Coast Comprehensive Study (NACCS) sought the quantification of coastal storm hazards for the Virginia to Maine coastal region. The main goal was to determine the magnitude and uncertainty of existing and future forcing for use in assessing coastal planning and engineering projects for flood-risk reduction and increased resiliency, for example. The project was motivated by the catastrophic consequences from Hurricane Sandy and also by a pre-existing need to accurately quantify the coastal storm hazards and vulnerability nationally (USACE 2015). NACCS goals also included evaluating the effect of future sea level change (SLC) on coastal storm hazards such as water level and wave climate. In the NACCS, rigorous regional statistical analyses, storm climatology, and detailed high-fidelity numerical hydrodynamic modeling were conducted for the northeast Atlantic coastal region in order to quantify coastal storm wave, wind, and water level extremal statistics. These results will be used in coastal studies to assess risk from storm events and evaluate resiliency following storm events.

Flood and wind damage from coastal storms result in dramatic negative impacts to the national economy with an estimated direct cost of over $400 billion for the top seven hurricanes (Blake et al. 2011). Six of the top seven most damaging storms have occurred since 2004. Over 52% of the U.S. population lives in coastal watershed counties, and the coastal population is expected to increase 10% by 2020 (Burkett et al. 2012). SLC and increasing storminess are exacerbating the vulnerability of coastal communities. In 2012, Hurricane Sandy accounted for more than 60 deaths, 600,000 damaged homes, and 8.5 million customers without electricity, totaling over $65 billion in damages in New York, New Jersey, and Connecticut alone (Pirani and Tolkoff 2014).

1.2 North Atlantic Coast Comprehensive Study (NACCS) area

Coastal flooding is primarily caused by rainfall, storm-induced water levels, and waves. For the northeastern U.S. Atlantic coastline, tides can have a significant influence on the degree of flooding given their large amplitudes. For the region from Virginia to Maine, tropical and

extratropical cyclones (TCs and XCs, respectively) have historically caused significant coastal flooding.

Portions of the region are low lying and sinking as a result of land subsidence (NOAA 2012; USACE 2015). Combined with global sea level change (GSLC) from ocean warming and melting ice (Church and White 2011; Burkett et al. 2012), relative SLC is an important issue for much of the study region due to increased flood risk. A regional map showing the area under consideration is presented in Figure 1-1 (USACE 2015). This image also provides a color-coded overview of the impact of Hurricane Sandy in the NACCS area:

- Very High (Purple): County population greater than 10,000 experienced storm surge flooding impacts.
- High (Red): County population of 500 to 10,000 experienced storm surge impacts or modeled wind damages greater than $100 million or precipitation greater than 0.2 m.
- Moderate (Yellow): County population of 100 to 500 experienced storm surge impacts or modeled wind damages of $10 to $100 million or precipitation of 0.1 to 0.2 m.
- Low (Green): No storm surge impacts or modeled wind damages less than $10 million or precipitation less than 0.1 m.

Figure 1-1. Regional map of area considered in this report.

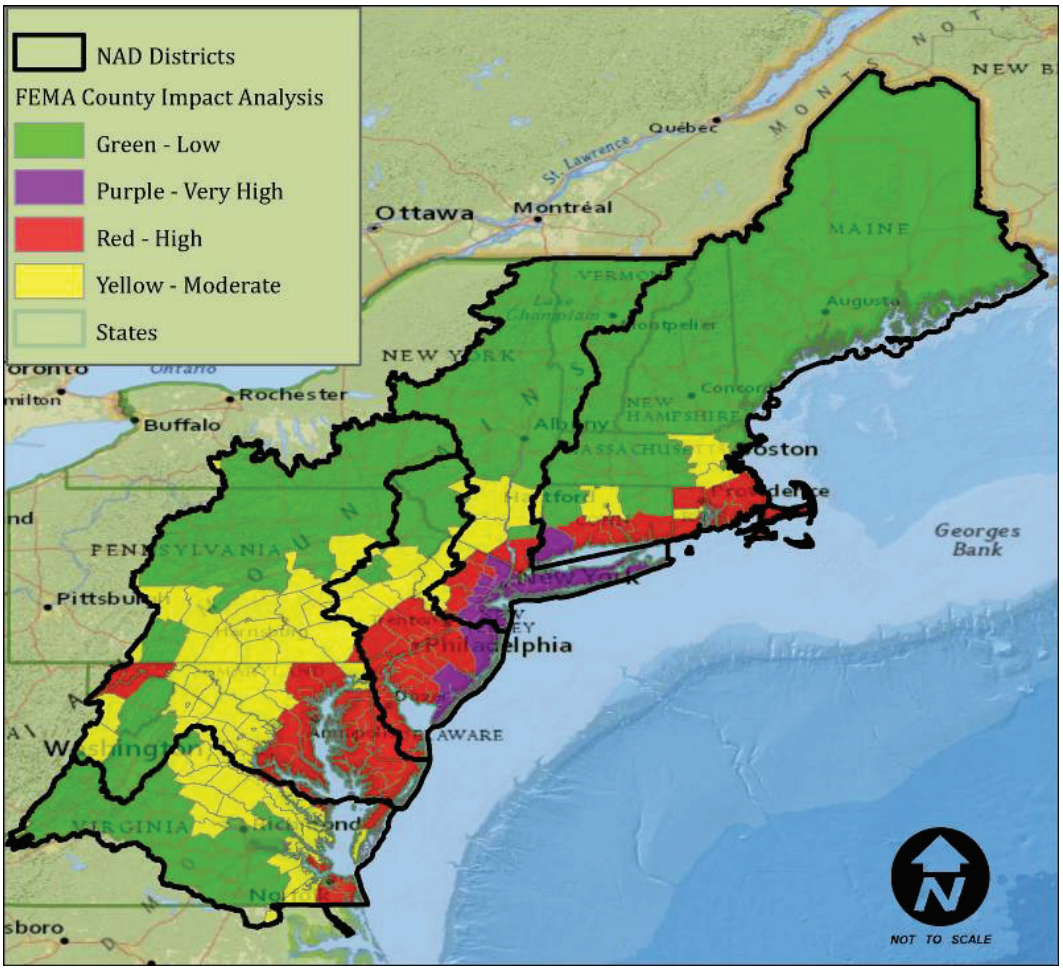

1.3 NACCS statistical methodology

The NACCS methodology was focused on detailed high-fidelity modeling of storm processes and the statistical quantification of the regional storm climatology and responses. The statistical assessment of coastal storm hazards performed for the NACCS required the development of a joint probability analysis (JPA) model of TC forcing parameters and extreme value analysis (EVA) of historical XC responses. For both XC and TC populations, extreme storms were efficiently sampled to accurately compute extreme statistical from high-fidelity modeling results. For TC, synthetic storms were efficiently sampled from the JPA model in order to span the parameter and probability spaces. The term *storm response* is used to describe physical reactions to storm forcing. The primary storm responses evaluated as part of this JPA include storm surge, water level (combined astronomical tide and surge response), and wave climate (height, peak period, and direction). The probability of storm responses is

expressed in terms of annual exceedance probability (AEP). *Storm forcing* refers to the meteorological characterization of a storm, including wind and atmospheric pressure fields. Typical storm forcing parameters used to describe storms are track (position and heading direction), intensity (central pressure deficit), size (radius of maximum winds), structure (Holland *B*), and translational speed. As discussed in Toro et al. (2010), the range of potential storm surge is primarily a function of storm intensity and size as well as the along-shore location in proximity to the storm center.

The overall NACCS wave and water level modeling study goals included simulating an efficient number of storms that blanketed the range of storm and astronomical tide characteristics necessary to accurately describe the statistical nature of coastal storm response over the entire study region. This information is required for modern probabilistic project design and for risk assessment. The processes of these storms were modeled from basin scale down to local scale, where the probabilities of storm responses were computed. For this study, the computed high-fidelity responses included storm surge, astronomical tide, waves, wave effects on water levels, storm duration, wind, currents, and the effect of SLC.

In this study, predominant basin scale and local hydrodynamic processes that impact nearshore waves and water levels were quantified. In addition to those mentioned above, interannual or steric water levels were accounted for by using the peak summer steric water level adjustment in the modeling. This is noted in Cialone et al. (2015). Wave setup was included in the coupled surge-wave modeling. However, neither wave runup, infragravity waves, or harbor seiching were modeled.

In this report, the focus is primarily on coastal storm hazards. *Coastal storm hazards* can be described in different ways. Herein, reference is made to the extreme storm responses of water level, depth, and wave climate as hazards as they are the primary contributions to flooding and damaging wave forces. Flooding from coastal storms is primarily a function of depth, tide and storm surge with some influence from wave setup. While this study did not quantify flooding and wave forcing explicitly, the wave, depth, and water level parameters quantified in this study are quite often sufficient to compute those hazards or can be used as boundary conditions for near-field computations of those hazards. In the nearshore, wave runup extent is important, but that has not been

considered herein. A coastal storm response does not necessarily constitute a hazard unless its magnitude reaches a specific threshold to impact vulnerable assets; therefore, this study focused on relatively extreme responses that could constitute a hazard. Over the entire NACCS region, the vulnerability covers a wide range from highly vulnerable assets (at or near the mean higher high water elevation) to assets located well outside of any coastal storm hydraulic vulnerability. Although use of the term *hazards* to describe the extreme nature of the responses that are quantified in this study, for any specific location along the coast, the values of the extreme responses may or may not constitute hazards to the local communities. The combination of hazard and vulnerability is done through risk studies, which are beyond the scope of this report.

The significant advancements in this study included

1. dense spatial coverage of nearshore storm response for the region
2. high-fidelity simulation of storm forcing and responses
3. description of the aleatory variability of response from frequent storm events to extremely rare events, corresponding to AEP ranging from 1 to 10^{-4}
4. comprehensive quantification of epistemic uncertainty associated with meteorological and hydrodynamic modeling, astronomical tide variability and SLC scenarios
5. public distribution of data and statistics within the Coastal Hazards System (CHS).

The density of spatial coverage is reported in Cialone et al. (2015) and includes highly defined nearshore numerical modeling grids with minimum nodal distances on the order of 10 m. These surge and wave models produced global validation errors with relatively small bias and scatter, compared to other regional modeling studies. The model errors from validation studies are described in detail in Chapter 6 and are incorporated into the epistemic uncertainty values reported in the CHS.

The CHS (https://chs.erdc.dren.mil) is a coastal storm hazards data storage and mining system. It stores comprehensive, high-fidelity, storm-response numerical modeling results including storm climatology, storm surge, water level, waves, and currents with corresponding epistemic uncertainties. CHS also stores extreme value statistics of observed waves and water level responses. Observations in CHS include water levels,

waves, and meteorological parameters such as wind and atmospheric pressure. The data can be easily accessed, mined, plotted, and downloaded through a user-friendly web tool.

1.3.1 Storm selection

The NACCS region coastal storm hazard is primarily dependent on large ocean-based storms consisting of TCs, XCs, and transitional cyclones. It is common to group the storms into statistical families of TCs and XCs with transitional cyclones that originated as tropical being categorized as tropical. A TC is a rotating, organized, warm-core system originating over tropical or subtropical waters and has a closed surface wind circulation about a well-defined center (e.g., tropical depression, tropical storm, hurricane). An XC is a low-pressure system that primarily relies on baroclinic processes, getting its energy from the temperature contrast between warm and cold air masses in the atmosphere (e.g., Nor'easter).

In this study, both TCs and XCs were strategically selected to characterize the regional storm hazard. The storm suite was specifically designed to simulate coastal hydrodynamic response that efficiently spans the required parameter and probability spaces for each studied area. XCs were selected using the methods of Nadal-Caraballo and Melby (2014) and Nadal-Caraballo et al. (2012) using an observation screening and sample-space optimization process. Storm surge and meteorological measurements corresponding to the 1938–2013 period were sampled to define significant extratropical events. The result was an efficient sample that yielded 100 historical XCs that were then modeled using high-fidelity climate and hydrodynamic numerical models.

The methods used for sampling historical XCs from historical measurements of response, such as storm surge, are not very useful for TCs because their response records on any specific section of coast are usually too sparse to derive accurate statistical models.

The TCs suite was developed using a modified version of the joint probability method (JPM) with Bayesian optimal sampling techniques where synthetic TCs are defined from a probabilistic model of TC parameters. The primary parameters considered were track location, heading direction, central pressure deficit, radius of maximum winds, and translational speed. Optimal sampling of the joint distributions of these parameters yielded 1,050 unique TCs that spanned the region spatially and

encompassed the full range of practical hazard, from frequent to very rare events. Storm parameters, such as size and intensity, of historical TCs that impacted the region were collected from the National Oceanographic and Atmospheric Administration (NOAA) National Hurricane Center HURDAT2 (HURricane DATa 2nd generation) for the 1938–2013 period, corresponding to a few years before the dawn of Hurricane Hunter aircraft reconnaissance missions. These TCs were also simulated using high-fidelity climate and hydrodynamic models.

1.3.2 Storm response statistical analysis

For the present study, a new JPA model was developed for the North Atlantic coast taking advantage of more rigorous methods recently developed at the U.S. Army Engineer Research and Development Center (ERDC). The NACCS JPA model was built based on the historical storm climatology of both TCs and XCs. High-fidelity numerical simulation results (Cialone et al. 2015) were extracted at locations where probabilities of coastal storm hazards were sought. These model save point locations were chosen to ensure optimal coverage of the study region. Storm surge, astronomical tide, waves, wind, atmospheric pressure, currents, and the effect of SLC were the dominant responses computed. These climatological and hydrodynamic responses are stochastic because storms are random in both recurrence and intensity. The joint probabilities of these responses were computed for separate and combined TC and XC statistical families. The statistical analysis of the response of the 1150 simulated storms was conducted at nearly 19,000 save point locations to produce response statistics including AEP and average recurrence interval (ARI). In addition, epistemic uncertainty was quantified and represented as confidence limits (CLs). Both storm response and the statistical results are distributed through the CHS and are directly useable in USACE project studies.

The NACCS JPA model employs the joint probability method with optimal sampling (JPM-OS) scheme for the statistical analysis of TCs. The JPM considers all possible combinations of TC meteorological parameters (i.e., track location, heading direction, translational speed, central pressure deficit, and radius of maximum winds) along with their associated probabilities and the storm responses generated by each combination of parameters. Each of these combinations constitutes a synthetic TC. The probabilities of the TCs are combined by means of the JPM multidimensional integral in order to compute the AEP of each storm

response. The JPM was adopted by federal agencies in the aftermath of Hurricane Katrina (Toro et al. 2009). In the past, a criticism of the JPM is that it requires the simulation of tens of thousands of synthetic storms to accurately represent the parameter space. The JPM-OS approach overcomes this limitation accurately covering the storm parameter space through optimal sampling of a reduced number of storms. The recommended number of storms when using a process of optimization is 100 to 300 per study area with coarse coastline on the order of 100 km. Here, the word *coarse* is intended to describe a coastline distance that ignores inlets and embayments and other irregularities.

The JPM is considered a robust approach because rather than relying on extrapolation beyond the historical record, the marginal probability distributions of TC parameters are discretized and weights, or probability masses, are computed for each combination of parameters. As will be shown in Chapter 5, the extrapolation done on the marginal probability distributions is constrained and typically not far beyond the extent of the historical record. In other words, parameter sampling is either inside the historical record or slightly outside. Therefore, this approach minimizes the effect of the uncertainty typically associated with extrapolation of marginal parametric distributions. As an example, marginal water level distributions were developed by Nadal-Caraballo and Melby (2014) from EVA of historical gage measurements using record lengths of 30 years to 100 years. An AEP of, for example, 10^{-3} computed from those results would require significant extrapolation. However, using the JPM approach discussed herein, there is very little extrapolation required to calculate water levels with an AEP of 10^{-3}. The synthetic TCs represent the full range of storm characteristics contained in the historical record. Using the JPM approach, the statistical characterization of storms results in combinations of TC parameters that match those of the historical storms but also encompass a much wider range of plausible storms without introducing significant uncertainty.

1.3.3 Storm set simulations

The study sought to characterize waves and water levels associated with a wide range storm hazards. In the NACCS region, a large tidal range is possible. As shown by Nadal-Caraballo and Melby (2014), Hurricane Sandy produced an extreme surge, but what made it particularly devastating was that it made landfall at high tide in the New York bight area. In this study, it was critical to define plausible extreme water levels

as a combination of surge and tide with the combination represented both hydrodynamically and a statistically correct.

As described in Cialone et al. (2015), three variations of the 1,050 TCs and 100 XCs were modeled using the full climatological, WAM (offshore waves), and coupled ADCIRC and STWAVE hydrodynamic system for nearshore waves and water levels:

- The first set (TCS1, XCS1) represents the base condition, modeled on mean sea level with wave effects but without astronomical tides or long-term SLC.
- The second set (TCS2, XCS2) consisted of the same base condition as in the first set but with each storm modeled on a unique, randomly selected tide phase.
- The third set (TCS3, XCS3) was the same as the second set except that it was modeled with a static water level adjustment of 1.0 m to simulate a future GSLC scenario of the same magnitude.
- A tide-only suite of 96 simulations was also run where each simulation had a random phase selected from historical tides occurring in September 2010.

A fourth TC set (TCS4) of results was developed by linear superposition of 96 tide-only simulations with the base condition set (TSC1), and these are provided in the CHS.

The three storm modeling suites were required for several reasons. Storms can produce peak surge on any tide phase from low tide to high tide. Tide and surge represent two long waves that interact nonlinearly in shallow water as discussed in Chapter 7 and, in more detail, Appendix D. Accurate simulation of combined tide and surge requires high-fidelity modeling of both processes simultaneously. Unfortunately, full hydrodynamic modeling of all 1150 storms on a wide range of tide phases was not feasible given the time and funding constraints of this study. The modeling suites were devised to provide sufficient modeling to accurately define the combined tide and surge response on varied sea level rise scenarios. As discussed in Chapter 7, over most of the coastline, linear superposition of tide, surge, and SLC can be done with little error. The first suite of modeling on mean sea level (MSL; relative to the 1983–2001 epoch) was intended to be applied using linear superposition with the 96 tide realizations and SLC. The second and third suites with simulation of

all processes together for one tide realization were intended to be used to quantify linear superposition errors and to be used for the estimation of response in the case where nonlinear errors were considered to be unacceptably high. Because the total number of regional storms modeled was relatively high and the sampling of parameter space very efficient, the single, random, tide-per-storm realization produced only a small error in statistics in most cases.

1.4 StormSim statistical analysis software system

StormSim is a software system developed for the statistical analysis of extreme coastal hazards due to TCs and XCs. The research to develop the StormSim system resulted in standardized, robust, state-of-the-art extremal statistical methods and software tools that span a wide range of federal needs including coastal applications within research, emergency management, coastal planning, and coastal engineering. These applications include extremal marginal and joint statistical analysis of storm climatological parameters for TCs and XCs. Also, the methods provide statistical tools for characterizing, analyzing, and simulating response parameters such as surge elevation, wave height, wave direction, wave period, wave power index, total water level, and storm duration in a statistical context. The development of the StormSim software system is an ongoing effort that has been funded through USACE Navigation Systems and Flood & Coastal Storm Reduction Civil Works Research programs.

2 Probabilistic Coastal Hazard Assessment (PCHA)

Probabilistic coastal hazard assessment (PCHA) is characterized by the relationship between storm hazards, such as water level, storm surge, waves or wind, and corresponding AEP. Storm surge typically represents the most significant source of flooding in the coastal environment. Storm surge can be described as a storm-induced increase in the surface water elevation above the expected astronomical tide. It is primarily a result of winds, atmospheric pressure, and waves associated with TCs and XCs. The quantification of storm surge hazard is an integral component of the flood hazard assessment near the coastline. Approaches to evaluating the contribution of storm surge to the overall flood frequency at a coastal location can be direct or indirect. Direct methods rely on the EVA of historical storm response observations. Indirect methods are based on the JPA of storm forcing parameters. In the latter, synthetic storms based on the statistical characterization of historical TCs are developed and their associated wind and pressure fields used as inputs to hydrodynamic models for the simulation of storm surge response.

Direct methods are still widely used for the statistical analysis of storm responses in areas affected primarily by extratropical atmospheric events, such as the U.S. Pacific coast and the Great Lakes region. In the past, however, the quantification of surge hazard in hurricane-prone areas also relied on direct methods based on the EVA of water level measurements. EVA of measured water levels for probabilistic assessment in hurricane-exposed areas is shown herein to be inadequate mainly due to spatially sparse storm occurrences. Along the U.S. Atlantic coast, more so than other hurricane-prone areas, the TC population is statistically underrepresented in the historical record. At any given location along the Atlantic coast, the number of TC responses in water level observations is very limited.

In addition, this approach has limitations arising from the heterogeneous storm responses that result from mixed populations of XCs and TCs. Doing so violates the *independent* and *identically distributed* (IID) principle that is central to extreme value theory (Coles 2001).

In past studies, the IID principle was often overlooked, perhaps due to lack of alternatives, and the EVA was performed on heterogeneous populations instead of separating extratropical and tropical events.

The end result of an EVA done for regions with mixed populations is usually characterized by excessive uncertainty. Nadal-Caraballo and Melby (2014) performed an EVA of historical water level measurements for the study area to serve as a benchmark for the validation of the JPA. The EVA exhibited the previously discussed limitations related to the inclusion of multiple populations and the underrepresentation of TCs. The results of the EVA study, referred to as Phase I of the NACCS, were considered interim and are superseded by results from the JPA summarized in this report.

For hurricane-prone areas, the standard of practice is to develop probabilistic models based on the JPA of storm forcing and associated high-fidelity numerical modeling results. One indirect method is the JPM (Resio et al. 2007; Toro 2008). The main intent of these indirect methods is to overcome the limited number of samples of TC responses in the historical record. Coastal regions of the contiguous United States where the assessment of surge hazard due to TCs is based on the JPA of storm forcing parameters include the Atlantic and Gulf of Mexico coasts. Surge hazard in coastal areas that are affected by XCs in addition to TCs, such as the Atlantic coast, can also be assessed using a combined JPA where the water level probabilities due to tropical and extratropical events are estimated independently and then integrated into a single probability distribution.

The PCHA done as part of the NACCS required the development of synthetic TCs in order to adequately cover the parameter and probability spaces. Once the parameter and probability spaces were efficiently and sufficiently sampled, a suite of parameterized storms was created. A planetary boundary layer (PBL) numerical model was then used to generate wind and pressure fields for the storms to drive high-fidelity storm surge and wave hydrodynamic models such as the Advanced Circulation (ADCIRC) model (Westerink et al. 1992) and the Steady-State Spectral Wave (STWAVE) model (Smith et al. 2001). Since the NACCS coastal areas are also affected by XCs, coastal responses from this type of storm were also assessed using EVA. The uncertainties associated with the storm forcing parameters and the numerical modeling were quantified and

integrated into the JPA. The information pertaining to the uncertainty is conveyed as CLs ranging from 84% to 98%.

2.1 Statistical analysis of tropical cyclones (TCs)

Statistical analysis of water level response resulting from TCs in most cases suffers from a lack of historical observations, which results in a small sample size. Moreover, some of the characteristics of the TCs that impact a particular area may make it necessary to consider them as belonging to different populations, further reducing the sample sizes. Storm intensity has been identified as such a characteristic (Resio et al. 2007) since intense TCs tend to behave differently from weak ones. The JPM overcomes this problem by focusing on the forcing instead of the response. In broad terms, TCs are defined by a number of forcing parameters that are used to generate the corresponding wind and pressure fields required for the simulation of storm water level and waves. Therefore, the JPM has become the dominant probabilistic model used to assess coastal storm hazard in hurricane-prone areas. Although the JPM approach has been implemented since the 1970s, recent advancements in sampling techniques and the development of the JPM-OS have made it possible to reduce the necessary number of synthetic storms, more efficiently characterizing the parameter and probability spaces. Different implementations of the JPM-OS methodology emerged as a result of several studies done in the aftermath of Hurricane Katrina after 2005.

2.1.1 Joint probability method (JPM)

Early characterization and probabilistic analyses of individual hurricane parameters were performed by Myers (1954). The precursor of the JPM was pioneered in the late 1960s (Russell 1968a, 1968b) as a full Monte Carlo simulation to estimate probabilities of wind, storm surge, and wave loads on offshore structures. Beginning in the 1970s, NOAA further developed and adapted the JPM for hurricane climatology and probabilistic storm surge studies in the U.S. Atlantic and Gulf coastal areas. The total annual frequency of water level was determined adding the separately calculated frequencies from landfalling hurricanes, bypassing hurricanes, and XCs. Several publications refined the methodology and expanded it to sections of the U.S. Atlantic and Gulf of Mexico coasts (e.g., Myers 1970, 1975; Ho 1974; Ho and Myers 1975). By the late 1980s, Federal Emergency Management Agency (FEMA) had

adopted the JPM (FEMA 1988) as presented in the National Weather Service report NWS-38 (Ho et al. 1987).

2.1.2 JPM with optimal sampling

The destruction caused by Hurricane Katrina in 2005 led to the proliferation of surge hazard studies that brought further improvements to the JPM. Of particular importance was the work done by the Interagency Performance Evaluation Taskforce (IPET 2009) in the aftermath of Hurricane Katrina in which JPM-OS methods were developed for the statistical analysis of water level extremes to evaluate the performance of the Southeast Louisiana hurricane surge reduction system. This study provided the basic framework for the storm surge and modeling approaches used in later works. This effort, led by a team of USACE, FEMA, NOAA, and private sector and academic researchers, was documented in the IPET (2009) report.

The main accomplishment of these new developments was the reduction in number of storms required for populating the parameter space. This reduction was accomplished by optimizing the sampling of the storm parameters (Resio et al. 2007; Toro 2008; Vickery and Blanton 2008). The number of sampled storms decreased from thousands, or even tens of thousands, to hundreds of storms. Present approaches include the JPM-OS by Bayesian Quadrature (JPM-OS-BQ), the JPM with augmented sampling by means of Response Surface (JPM-OS-RS), and other JPM applications that use hybrid optimal sampling techniques. Regional studies conducted after Hurricane Katrina that stood out included the Louisiana Coastal Protection and Restoration (LACPR) (USACE 2009a), the Mississippi Coastal Improvements Program (MSCIP) (USACE 2009b), the Mississippi Coastal Analysis Project (FEMA 2008) and the Flood Insurance Study for the Coastal Counties in Texas (USACE 2011). The JPM-OS-BQ, in particular, was adopted as part of FEMA's National Flood Insurance Program Risk MAP program best practices, as documented in the Operating Guidance No. 8-12 (FEMA 2012).

Although the details in the application of the JPM can vary significantly by study, the different approaches typically follow a common general methodology, depending on the dominant processes and respective solution strategies.

The JPM methodology generally includes the following steps:

- characterization of historical storm climatology
- computation of historical spatially varying storm recurrence rate (SRR)
- storm parameterization and development of probability distributions of historical storm parameters
- discretization of probability distributions of storm parameters
- development of synthetic storm set
- meteorological and hydrodynamic simulation of synthetic storms
- estimation of errors and other secondary terms
- integration of joint probability of storm responses, including extratropical events.

A diagram summarizing the JPM methodology is presented in Figure 2-1.

Figure 2-1. JPA of coastal storm hazards.

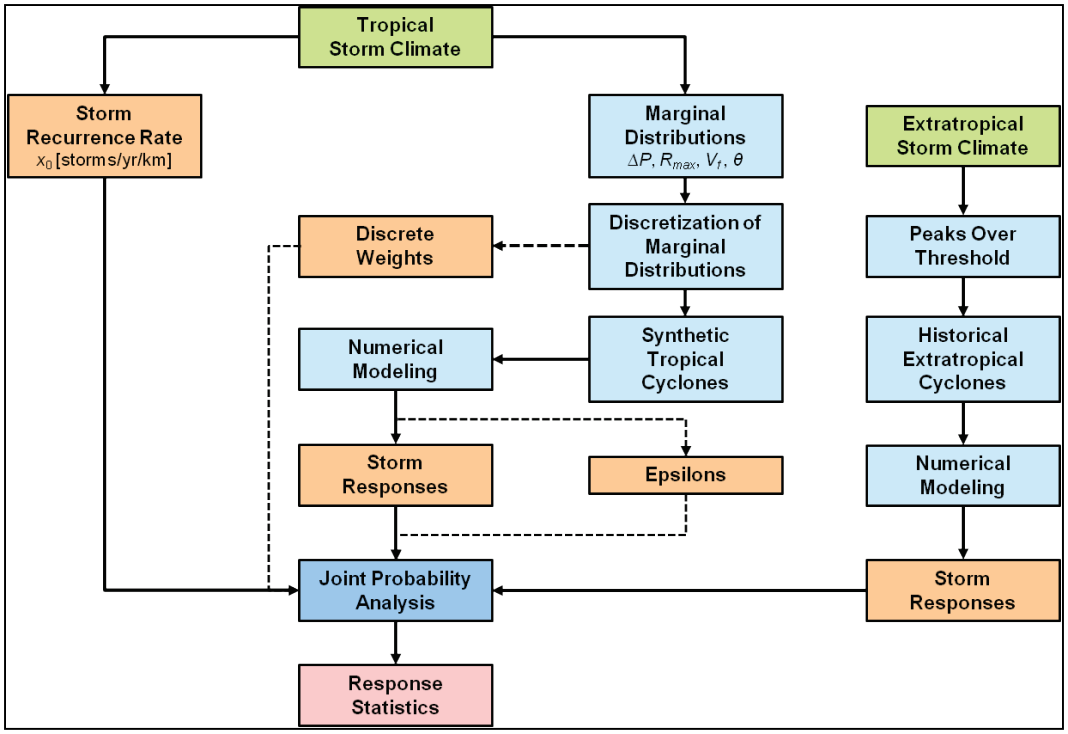

The AEP of coastal storm hazards at a given site is a function of three main components: the SRR, the joint probability of characteristic storm parameters, and the storm responses.

The JPA of coastal storm hazards can be summarized by means of the JPM integral:

$$\lambda_{r(\hat{x})>r} = \lambda \int P[r(\hat{x}) > r|\hat{x}]\, f_{\hat{x}}(\hat{x}) d\hat{x}$$
$$\approx \sum_i^n \lambda_i\, P[r(\hat{x}) > r|\hat{x}] \quad (2\text{-}1)$$

where $\lambda_{r(\hat{x})>r}$ = AEP of storm response r due to forcing vector $\hat{x}$ and $P[r(\hat{x}) > r|\hat{x}]$ = conditional probability that storm i with parameters $\hat{x}_i$ generates a response larger than r.

The storm parameters commonly used in JPM for the characterization of TCs and included in the forcing vector $\hat{x}$ are

1. track location (x_0)
2. heading direction (θ)
3. central pressure deficit (Δp)
4. radius of maximum winds (R_{max})
5. translational speed (V_t).

In order to develop the set of synthetic storms, each parameter is treated as a correlated random variable and either a marginal or a conditional probability distribution is sought for each parameter based on the TCs observed in the historical record. The probability distributions are then discretized, and the corresponding weights are assigned to the range of discrete values. Synthetic storms are developed as possible combinations of samples from the marginal or conditional distributions. Each synthetic storm must consist of a physically and meteorologically realistic combination of the aforementioned parameters. The parameterized TCs are used as inputs to the PBL model. This model is used as part of the JPM methodology to estimate the time histories of the wind and pressure fields that drive high-fidelity storm surge and wave numerical hydrodynamic models such as ADCIRC and STWAVE.

A central issue surrounding the application of the JPM is number of storm parameters required to adequately represent TCs and their forcing. In current practice, it has been shown that the five parameters listed above are sufficient to characterize TCs and their wind and pressure fields for the purpose of quantifying coastal storm hazards. Sources of epistemic uncertainty often accounted for in the JPM include

1. hydrodynamic modeling errors potentially arising from unresolved physical processes, inadequate resolution, and bathymetry inaccuracy

2. meteorological modeling errors due to idealized wind and pressure fields and wind variations not captured by the PBL model
3. track variations not captured in synthetic storm set
4. random variations in the peakedness of the wind fields represented by the Holland *B* parameter.

The AEP of a particular storm hazard is computed by integration of Equation 2-1. Epistemic uncertainty is quantified and incorporated in the JPM as CLs (e.g., 84%, 90%, 95%, and 98%).

2.1.3 Application of planetary boundary layer (PBL) model in JPM

The PBL model solves the storm wind and pressure fields by means of numerical integration of the equations of motion of the boundary layer and the physics of a moving vortex (Cardone and Cox 2009). The model is dynamic as it is solved along the storm track, taking into account the variations of the storm parameters. This model, first developed into a practical tool in the ocean data gathering program (ODGP) (Cardone et al. 1976), can provide a fairly complete description of time-space evolution of the surface winds in the boundary layer of a TC from the simple model parameters available in historical storms. The model is an application of a theoretical model of the horizontal airflow in the boundary layer of a moving vortex. That model solves, by numerical integration, the vertically averaged equations of motion that govern a boundary layer subject to horizontal and vertical shear stresses. The equations are resolved in a Cartesian coordinate system whose origin translates at constant velocity (V_t) with the storm center of the pressure field associated with the cyclone. Variations in storm intensity and motion are represented by a series of quasi-steady state solutions. The original theoretical formulation of the model is given by Chow (1971). A similar model was described more recently in the open literature by Shapiro (1983).

The version of the model applied in this study is the result of two major upgrades, one described by Cardone et al. (1992) and the second by Cardone et al. (1994) and Thompson and Cardone (1996). The first upgrade involved mainly replacement of the empirical scaling law by a similarity boundary layer formulation to link the surface drag, surface wind, and the model vertically averaged velocity components. The second upgrade added spatial resolution and generalized the pressure field specification. A more complete description of the theoretical development of the model as upgraded is given by Thompson and Cardone (1996).

The model pressure field is described as the sum of an axially symmetric part and a large-scale pressure field of constant gradient. The symmetric part is described in terms of an exponential pressure profile, which has the following parameters shown in Equation 2-2:

$$P(r) = P_o + \sum_i^n dp_i e^{-\left(\frac{R_{p_i}}{r}\right)^{B_i}} \quad (2\text{-}2)$$

where P_o = minimum central pressure; dp_i = total pressure deficit; R_{p_i} = scale radius of exponential pressure profile; B_i = profile peakedness parameter (Holland *B*); and r = radius.

Holland *B* is an additional scaling parameter whose significance was discussed by Holland (1980). This analytical form is also used to explicitly model the storm pressure field for use in the hydrodynamic model.

The PBL model is driven from parameters that are derived from data in historical meteorological records and the ambient pressure field. The entire wind field history is computed from knowledge of the variation of those parameters along the storm track by computing solutions, or so-called *snapshots* on the nested grid as often as is necessary to describe different stages of intensity, and then interpolating the entire time history from the snapshots. The model was validated originally against winds measured in several ODGP storms. It has since been applied to nearly every recent hurricane to affect the U.S. offshore area, to all major storms to affect the South China Sea since 1945, and to storms affecting many other foreign basins including the Northwest Shelf of Australia, Tasman Sea of New Zealand, Bay of Bengal, Arabian Sea, and Caribbean Sea. Many comparisons have been published (e.g., Ross and Cardone 1978; Cardone and Ross 1979; Forristall et al. 1977, 1978; Forristall 1980; Forristall and Greenwood 1998; Cardone et al. 1992; Cardone and Grant 1994).

As presently formulated, the wind model is free of arbitrary calibration constants, which might link the model to a particular storm type or region. For example, differences in latitude are handled properly in the primitive equation formulation through the Coriolis parameter. The variations in structure between TC types manifest themselves basically in the characteristics of the pressure field of the vortex itself and of the surrounding region. The interaction of a TC and its environment, therefore, can be accounted for by a proper specification of the input

parameters. The assignable parameters of the PBL formulation, namely PBL depth and stability, and of the sea surface roughness formulation, can safely be taken from studies performed in the Gulf of Mexico, since TCs world-wide share a common set of thermodynamic and kinematic constraints.

2.2 Statistical analysis of extratropical cyclones (XCs)

The probabilistic analysis of coastal storm hazards due to XCs relies on EVA of historical storm responses. The JPM method, based on storm parameters, is not suitable for XCs due to the difficulties of XC parameterization. When a water level station exists near a study site and sufficient historical water level observations are available, an EVA of water level measurements can be performed. However, where there are no or limited measurements close to a study site, the probabilistic assessment should be based on simulated responses developed from high-fidelity numerical modeling. The first step in this methodology is to collect time-series data from water level stations and analyze the time series to estimate the nontidal residuals (NTRs). The way in which NTRs are estimated varies depending on the geographical region. In the North Atlantic and Pacific coasts, for example, the approach used to compute the NTR consists of subtracting a predicted astronomical tide time series from a time series of verified water level measurements (Nadal-Caraballo and Melby 2014). For the Great Lakes, the NTRs are identified by detrending the water level time series, since tides are negligible in this region. The second step consists of identifying storm events within the NTR time series. A method known as peaks-over-threshold (POT) is used for censoring the time series. When performing POT, all NTRs above a certain threshold are identified and sampled from the historical record. An additional screening process of wind and pressure measurements is required to verify that sampled NTRs are actually wind-driven surges.

Nadal-Caraballo et al. (2012) developed the composite storm set (CSS) methodology for estimating extreme water level statistics for the FEMA flood hazard mapping efforts in the Great Lakes region that exemplifies the assessment of surge hazard due to XCs. The CSS methodology was adopted for the NACCS. In this approach, the most significant XCs are sampled from water level stations throughout the study area using the POT method. If measurements are too sparse, then available hindcasts or surrogate models can be used to generate additional data as described in Nadal-Caraballo et al. (2012). The CSS constitutes an optimized regional

set of storms that is representative of the entire study area. Enough storms should be sampled for the water level distributions derived from the CSS to adequately match the distributions at the locations of the water level stations from which the CSS was sampled. Once sampled, the CSS storms are simulated using climatological and hydrodynamic numerical simulation. Hindcast wind and pressure fields are used to drive high-fidelity storm surge and wave hydrodynamic models such as ADCIRC and STWAVE. As part of the EVA, the simulated water level responses are fitted with a parametric distribution model. The most widely used parametric approach to model POT extremes is the generalized Pareto distribution (GPD) (Coles 2001). The best estimates of the distribution parameters can be obtained using fitting approaches such as using the maximum likelihood method (MLM).

3 Characterization of Storm Climatology

The U.S. North Atlantic coast is subject to coastal flooding as a result of TCs and XCs. The climatology of each of these two storm populations is assessed separately.

3.1 Tropical cyclones

As previously discussed, the characterization of historical TCs for purposes of the statistical analysis of coastal storm hazards is based on the primary storm parameters accounted for in the JPM: track location (x_o), heading direction (θ), central pressure deficit (Δp), radius of maximum winds (R_{max}), and translational speed (V_t).

The storms were divided according to whether they were landfalling or bypassing. This was done because, although TCs tend to decay as they move to higher latitudes, cyclones that make landfall normally decay at a much faster rate than bypassing cyclones. In this report, the definition of track and landfall conforms to that used within HURDAT2. The TC track is defined as the center of the eye which is computed as the location of minimum central pressure within HURDAT2. Landfall occurs when the track crosses the coastline, which is defined as the interface between the MSL and land. In this study, an idealized coastline was constructed from data obtained from NOAA National Geophysical Data Center (NGDC). The idealized coastline is depicted in Figure 3-1.

The Virginia-to-Maine coastline was divided into three subregions for the computation of TC landfalling and bypassing statistics. A midpoint coastal reference location (MPCRL) was established at the center of each subregion's coastline to facilitate spatial discretization of the storm climatology and the development of synthetic TCs. In general, a coastal reference location (CRL) is a point along the idealized coastline where the SRR and joint probability distribution of TC parameters are defined in order to characterize the storm climate at that given location. The three NACCS subregions are similar to FEMA Regions I, II, and III, respectively, with some modifications to make the three regions more spatially uniform (Figure 3-2). For example, the northern boundary of Region II was extended to include Rhode Island and the southern coastline of Massachusetts (Cape Cod area).

Figure 3-1. Idealized coastline for sampling of landfalling TCs.

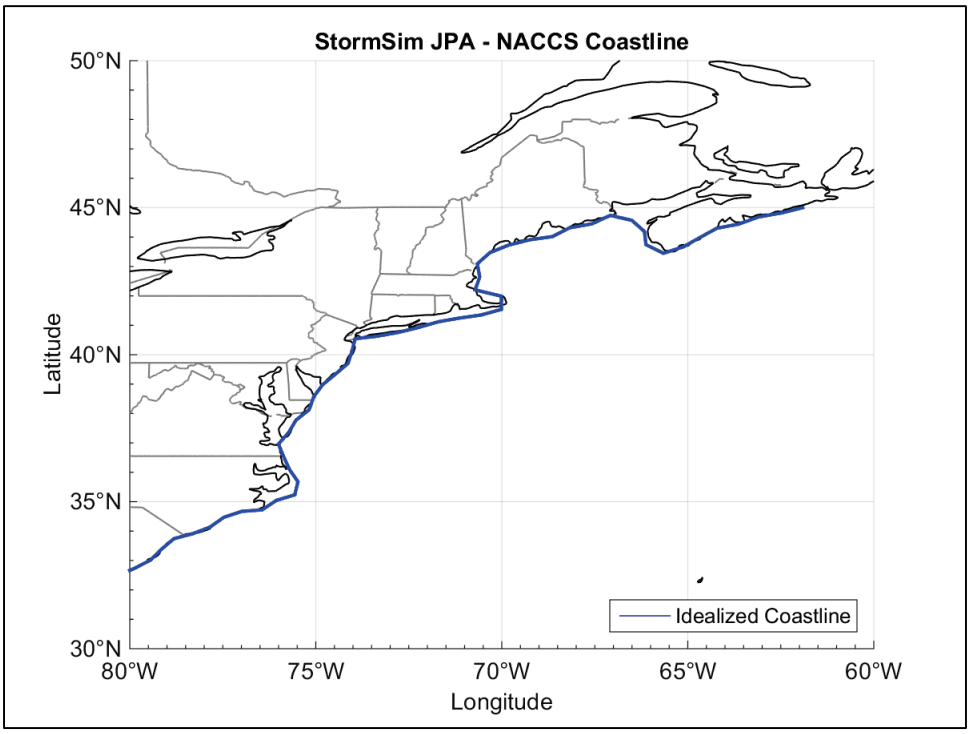

The southern and northern boundaries, as well as the CRL of each subregion, are listed in Table 3-1.

Table 3-1. Regional boundaries within the NACCS study area.

Subregion	Southern Boundary	Northern Boundary	MPCRL
3	36.5°N	39.0°N	37.75°N
2	39.0°N	41.5°N	40.25°N
1	41.5°N	45.0°N	43.25°N

The following sections of this chapter discuss the data sources used for the characterization of the storm climatology in the NACCS region, as well as the identification and selection process for historical tropical and XCs.

Figure 3-2. Three NACCS subregions identified for historical storm selection.

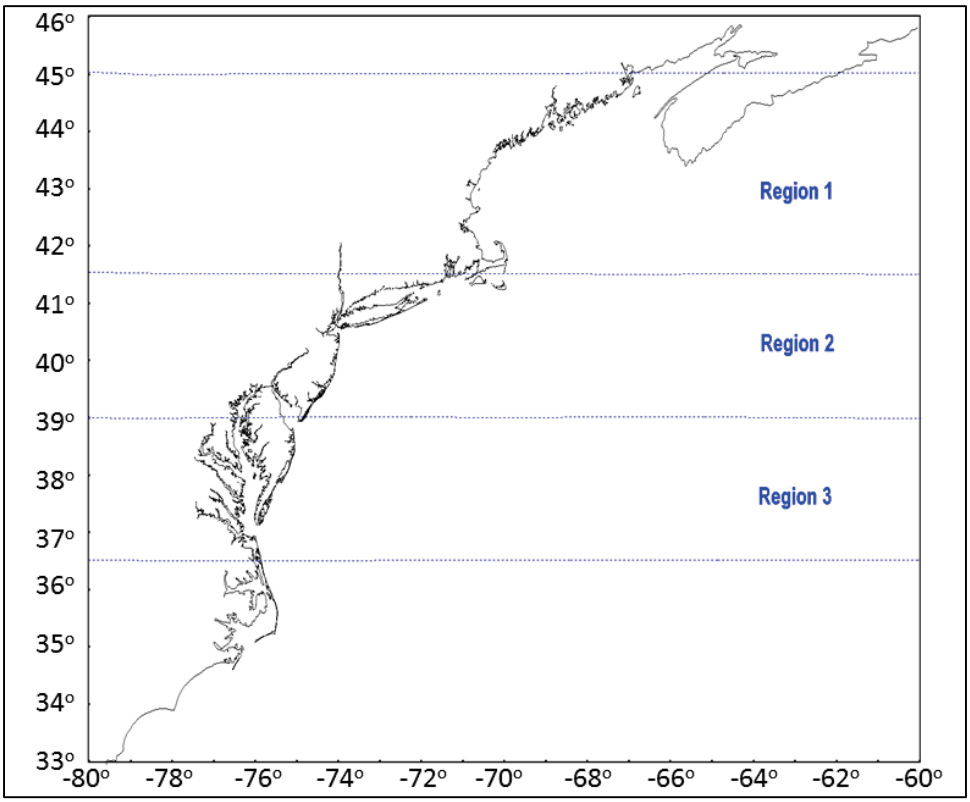

3.1.1 Data sources

For TC screening, the main data source was HURDAT2 (Landsea and Franklin 2013). HURDAT2 is a product of the NOAA National Hurricane Center (NOAA-NHC) and consists of the reanalysis of all historical TCs recorded in the North Atlantic basin (i.e., North Atlantic Ocean, Gulf of Mexico, and the Caribbean Sea) from 1851 to the present. Table 3-2 lists the sources used in this study for the primary TC parameters.

Table 3-2. Sources for TC parameters.

Tropical Cyclone Parameters	Sources
Central pressure deficit	HURDAT2 historical data
Radius of maximum winds	Vickery and Wadhera (2008) stochastic model
Translational speed	HURDAT2 historical data
Heading direction	HURDAT2 historical data
Holland *B*	Vickery and Wadhera (2008) stochastic model

The JPA performed in this study focused on TCs with $\Delta p \geq 28$ hPa. The Δp were computed as the difference between a far-field atmospheric pressure of 1,013 hPa and central pressure (c_p). TCs of this intensity are expected to be classified, on average, as category 1 hurricanes based on the Saffir-Simpson hurricane wind scale (SSHWS) but generally fall within the tropical storm to category 2 range. The correlation between Δp and maximum wind speed (W_{max}) is examined in Section 4.3. The W_{max} for TCs within the context of the standard JPM methodology is a storm response parameter estimated by the PBL model.

3.1.2 Period of record for the statistical analysis

Prior to the selection of historical TCs, the specific period of record to be used for the JPA was assessed. The SRR and the marginal distributions of storm parameters are sensitive to the historical record length. The 1940s decade marked the dawn of modern aircraft reconnaissance missions to measure hurricane parameters, resulting in much more reliable estimates of storm characteristics, including frequency and intensity.

Prior to 1944, the main data sources were land stations and ship reports (Jarvinen et al. 1984). During this period it was typical for relatively weak storms to go undetected and for the intensity of strong storms to be underestimated. After 1944 and as a consequence of World War II, aerial reconnaissance led to increased data collection incidence and measurement accuracy, including storm position, track, wind speed, and pressure. The use of satellite imagery was introduced during the 1964 hurricane season (Neumann et al. 1985) and was considered one of the major advances in TC tracking (Jarvinen et al. 1984).

The high frequency of unsampled TCs prior to the 1940s has been well documented. Mann et al. (2007) estimated an undercount in the preaircraft reconnaissance era (1870–1943) ranging from 0.5 to 2.0 TC/yr, with a mean of 1.2 TC/yr. Landsea et al. (2010) discussed that the increase in reported TCs during the 1940s and until approximately 1960 had been interpreted as a result of climate change. This increase, however, is likely to be the consequence of improved observing and recording of short-lived TCs coinciding with the advent of aircraft reconnaissance and satellite imagery.

Worley et al. (2005) identified spikes in the number of unrecorded moderate to long-lived TCs during the 1910s and 1940s as due to reduced

ship observations during World War I and World War II, respectively. Vecchi and Knutson (2011), after adjusting HURDAT data for unrecorded TCs, concluded that the midtwentieth century was a high-activity period that extended from the 1940s to the 1960s.

The review of technical literature indicates that although the 1940s decade saw improvements in the observation and recording of TCs, there was still a significant undercount during this period. In recent flood hazard studies where the JPM-OS methodology has been used, the period of record that was considered started in the early 1940s (FEMA 2008, 2012; Resio et al. 2007).

For the NACCS, the need to extend the period of record back to 1938 was identified in order to include the The Great New England Hurricane of 1938, a high intensity TC that significantly affected the study area. This TC, which is also known as The Long Island Express, is still the highest recorded water level at some locations within the NACCS region, including Kings Point, NY. The adequacy of the 1938–2013 period was assessed by computing the SSR corresponding to this period and then comparing it to alternative periods, from 1851–2013 to 1965–2013. This analysis was performed by screening HURDAT2 data using the StormSim software system.

For convenience, the SRR is depicted in the following assessment as SRR_{200km}, which corresponds to the recurrence rate associated with storms passing within a radius of 200 km of a given location. SRR_{200km} (storms/yr) is computed as SRR (storms/yr/km) × $2r_i$, where r_i is a user-determined radius of influence.

SRR_{200km} were computed for the five different periods and listed in Table 3-3 for 23 locations within the NACCS region corresponding to NOAA water level stations. SRR_{200km} averaged over these 23 CRLs, representing region-wide trends, are also provided in this table. Figures 3-3 through 3-7 show estimates of SRR_{200km} for the entire Atlantic basin, corresponding to the five periods listed in Table 3-3. Methods for estimating SRR are discussed in greater detail in Chapter 5.

Table 3-3. SRR_{200km} for different record periods at different CRLs.

Coastal Reference Location (CRL)	SRR_{200km} (storms/yr) for $\Delta p \geq 28$ hPa				
	NACCS	Other Record Periods			
	1938–2013	1851–2013	1851–1937	1945–2013	1965–2013
Eastport, ME	0.11	0.06	0.01	0.11	0.15
Bar Harbor, ME	0.11	0.06	0.01	0.11	0.14
Portland, ME	0.10	0.06	0.02	0.10	0.11
Boston, MA	0.13	0.09	0.03	0.13	0.14
Woods Hole, MA	0.18	0.12	0.03	0.18	0.20
Nantucket Island, MA	0.18	0.12	0.03	0.18	0.20
Newport, RI	0.18	0.11	0.03	0.17	0.19
Providence, RI	0.18	0.11	0.03	0.17	0.19
New London, CT	0.17	0.11	0.03	0.17	0.18
Montauk Point Light, NY	0.17	0.11	0.03	0.17	0.18
Kings Point, NY	0.14	0.09	0.02	0.13	0.15
The Battery, NY	0.14	0.09	0.02	0.13	0.15
Sandy Hook, NJ	0.14	0.09	0.02	0.13	0.15
Atlantic City, NJ	0.17	0.11	0.03	0.17	0.18
Cape May, NJ	0.18	0.11	0.03	0.17	0.18
Lewes, DE	0.18	0.11	0.03	0.18	0.19
Cambridge, MD	0.19	0.12	0.03	0.19	0.20
Baltimore, MD	0.18	0.11	0.03	0.18	0.19
Annapolis, MD	0.18	0.11	0.03	0.18	0.19
Solomons Island, MD	0.20	0.13	0.03	0.21	0.22
Washington, DC	0.19	0.12	0.03	0.19	0.20
Sewells Point, VA	0.22	0.14	0.04	0.24	0.25
Chesapeake Bay Bridge Tunnel, VA	0.22	0.14	0.04	0.24	0.25
Mean	0.17	0.11	0.03	0.17	0.18
Difference compared to 1938–2013	–	-37%	-84%	0%	9%

Figure 3-3. SRR_{200km} of TCs in the North Atlantic basin for the 1938–2013 period.

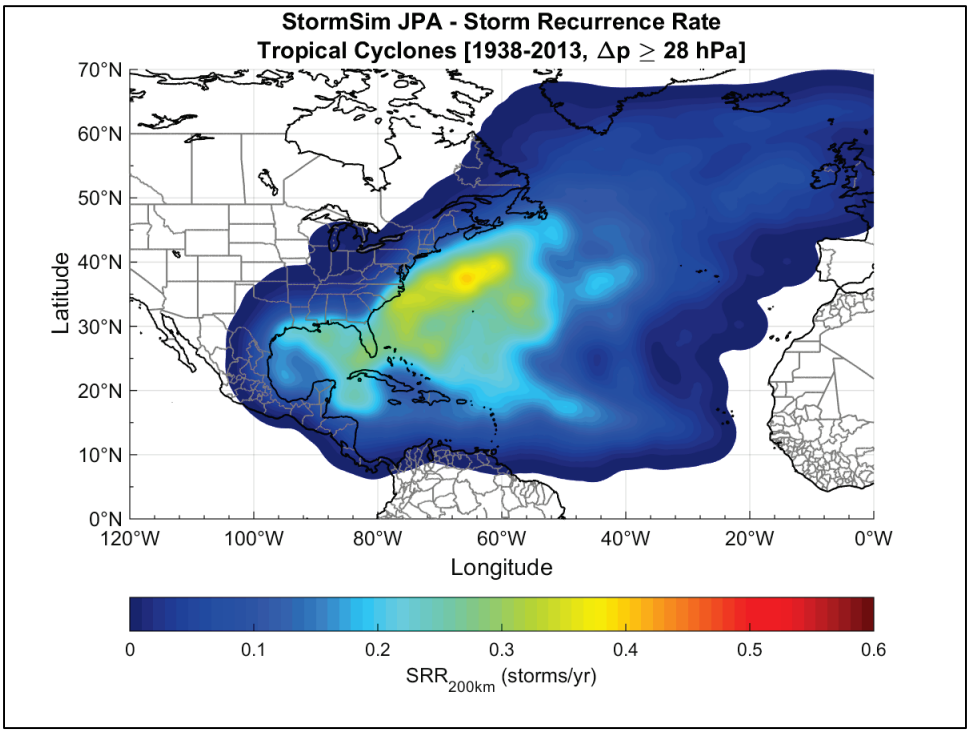

Figure 3-4. SRR_{200km} of TCs in the North Atlantic basin for the 1851–2013 period.

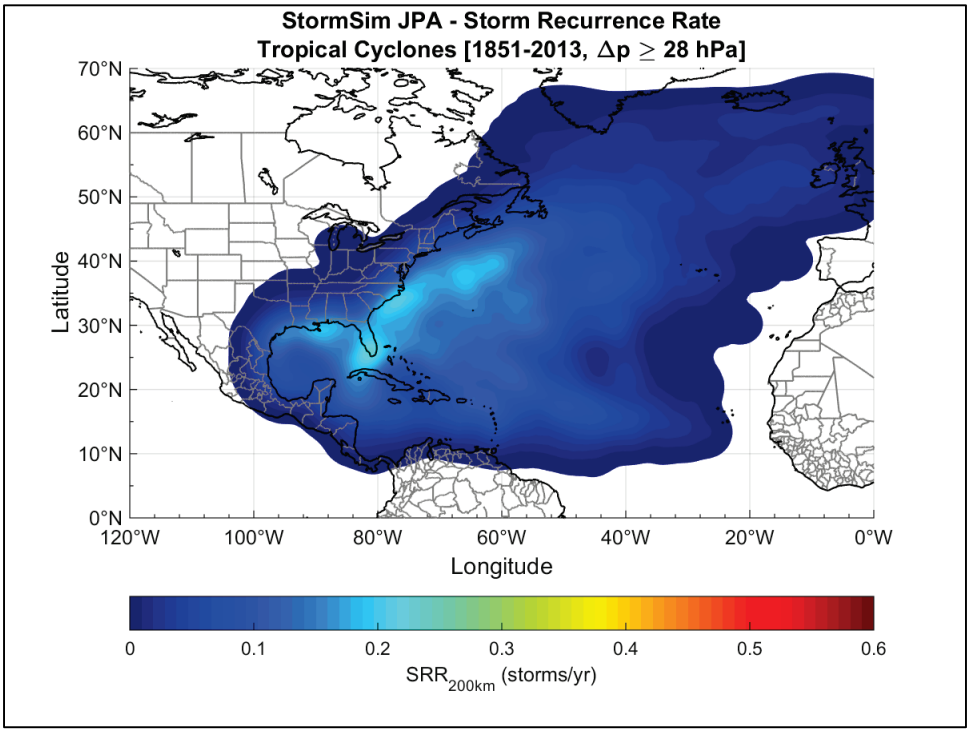

Figure 3-5. SRR_{200km} of TCs in the North Atlantic basin for the 1851–1937 period.

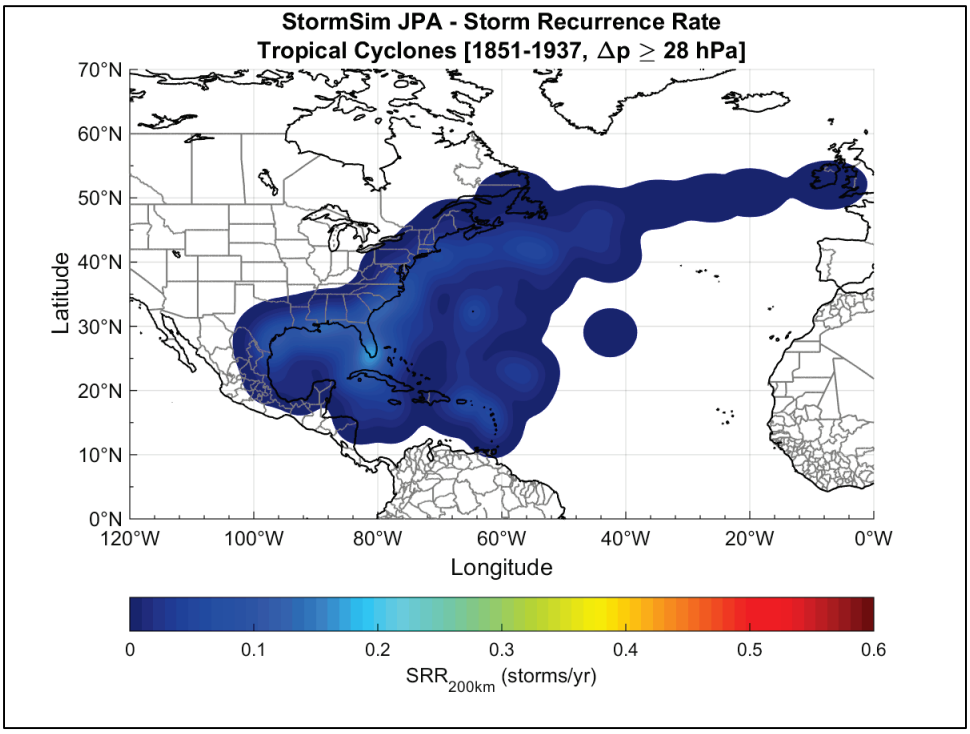

Figure 3-6. SRR_{200km} of TCs in the North Atlantic basin for the 1945–2013 period.

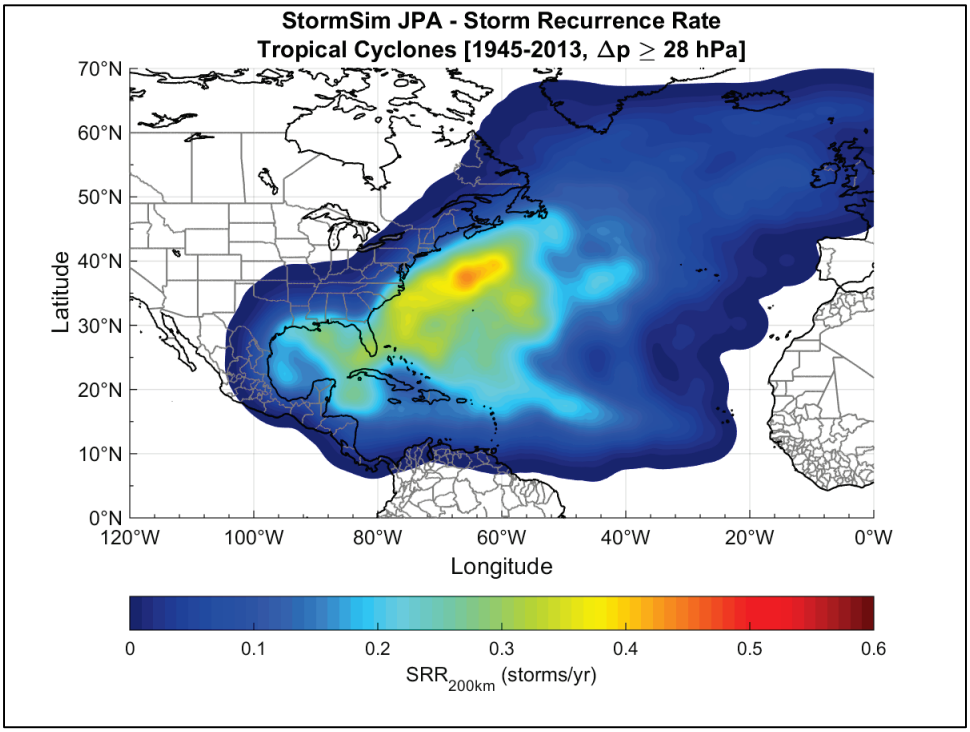

Figure 3-7. SRR_{200km} of TCs in the North Atlantic basin for the 1965–2013 period.

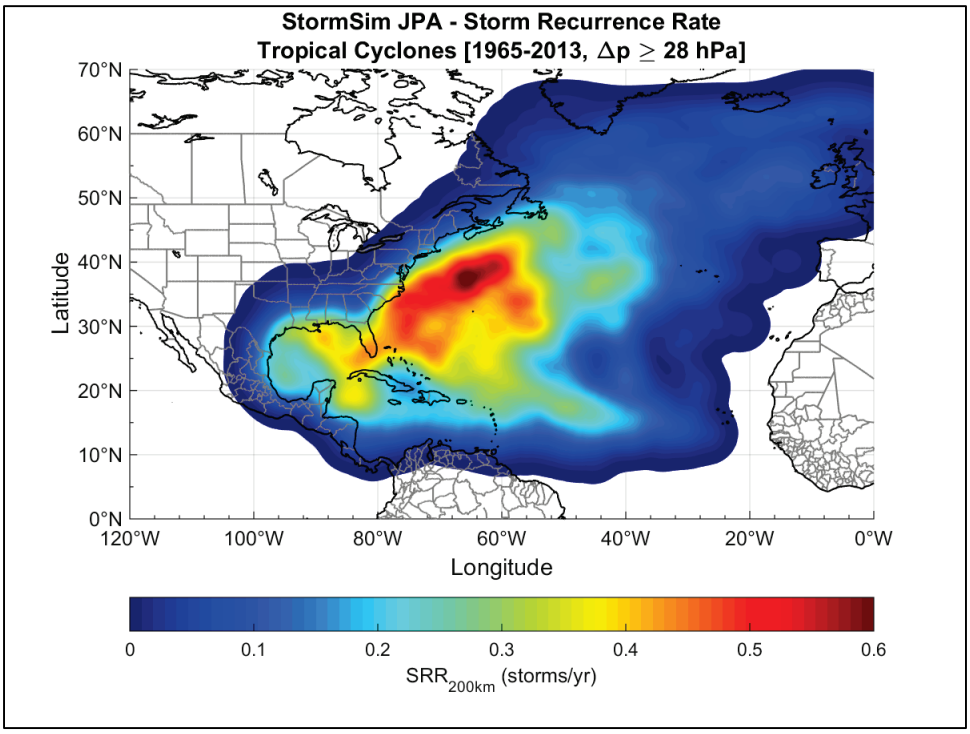

The mean SRR_{200km} for the 1938–2013 period was estimated to be 0.17 storms/yr. Using the entire 1851–2013 record, instead of the 1938–2013 period, would have resulted in an mean SRR_{200km} of 0.11 storms/yr. This represents an underestimation of the mean SRR_{200km} by -37%. This is mainly due to the scarce recorded data during the 1851–1937 period. The mean SRR_{200km} corresponding to the 1851–1937 period alone was 0.03 storms/yr; this resulted in underestimation of -84% when compared to the 1938–2013 period. The mean SRR_{200km} for the 1938–2013 period was also compared to two additional periods: post aircraft reconnaissance (1945–2013) and post satellite imagery (1965–2013). The difference in mean SRR_{200km} between the 1938–2013 and 1945–2013 was negligible. However, results showed that the using the 1938–2013 period underestimated the SRR_{200km} by -9% when compared to the 1965–2013 period.

In order to assess the stability of the SRR and to determine a *true* value, SRR_{200km} were estimated for all time periods from 1851–2013 to 1970–2013, at a 1 yr interval. The average of all locations shown in Table 3-3 is plotted in Figure 3-8.

Figure 3-8. SRR_{200km} for different record periods starting in 1851.

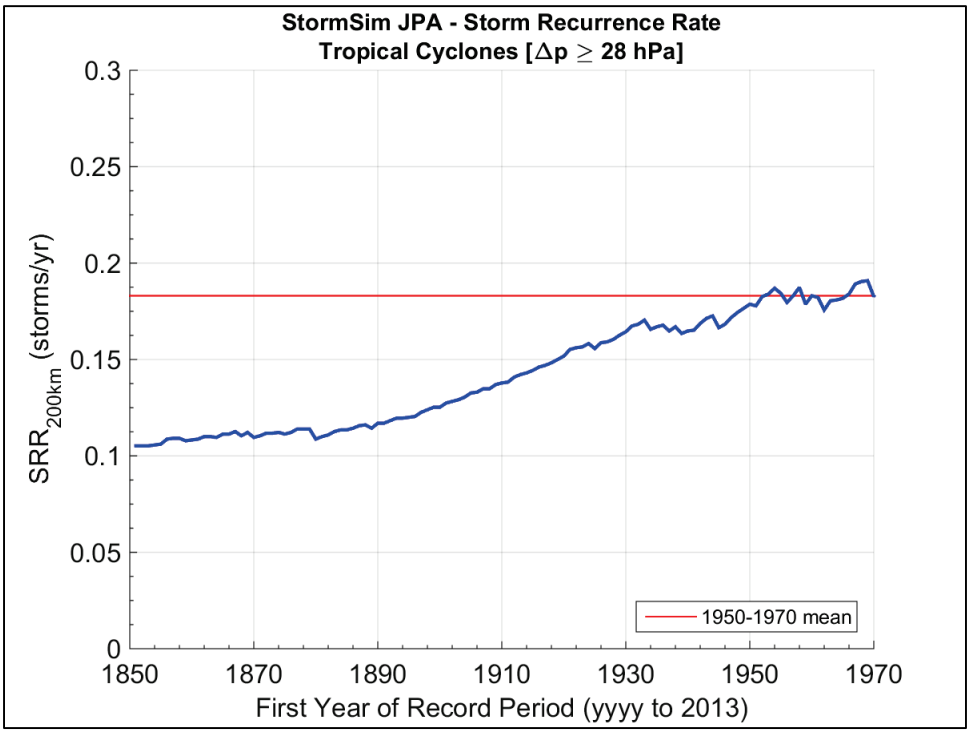

The true value of the mean SRR_{200km} was assumed to be approximated by the mean SRR_{200km} from 1950–2013 to 1970–2013, which resulted in 0.18 storms/yr. This is equivalent to the mean SRR_{200km} of 0.18 storms/yr corresponding to the 1964–2013 period. Using the 1938–2013 period to compute SRR resulted in an underestimation of -10% compared to the true value. The use of the 1938–2013 period is necessary for the NACCS in order to properly characterize the storm climatology of this region, but the SRR were adjusted by +10% to avoid the bias brought by the undercounting of TCs prevalent during the early part of this period.

3.1.3 Selection of historical TCs

Statistical characterization of TC climatology for each of the NACCS subregions requires sampling a set of storms from the historical record (i.e., HURDAT2). The JPA is then performed with this set of storms as basis, including the development of statistical distributions of individual storm parameters. The sampling of historical storms was limited to the 1938–2013 period, as previously discussed.

A sample (or capture) zone was established for each of the NACCS subregions based on the following criteria:

- Each subregion's southern and northern boundaries were extended by 300 km (latitude-wise) to sample landfalling TCs.
- The coastline was extended also by 300 km (longitude-wise) to sample bypassing TCs.
- Sampling was expanded to include cyclones with $\Delta p \geq 25$ hPa (in order to properly characterize TCs near the 28 hPa threshold).

The TCs that affected subregions 3, 2, and 1 are shown in Figures 3-9, 3-10 and 3-11, respectively. These include both landfalling and bypassing tracks, screened from a total of 1,771 cyclones available in the HURDAT2 database (from 1851 to 2013). In each plot, the subregion is the coastal area between the dashed lines.

Figure 3-9. Landfalling and bypassing TC tracks for NACCS subregion 3,

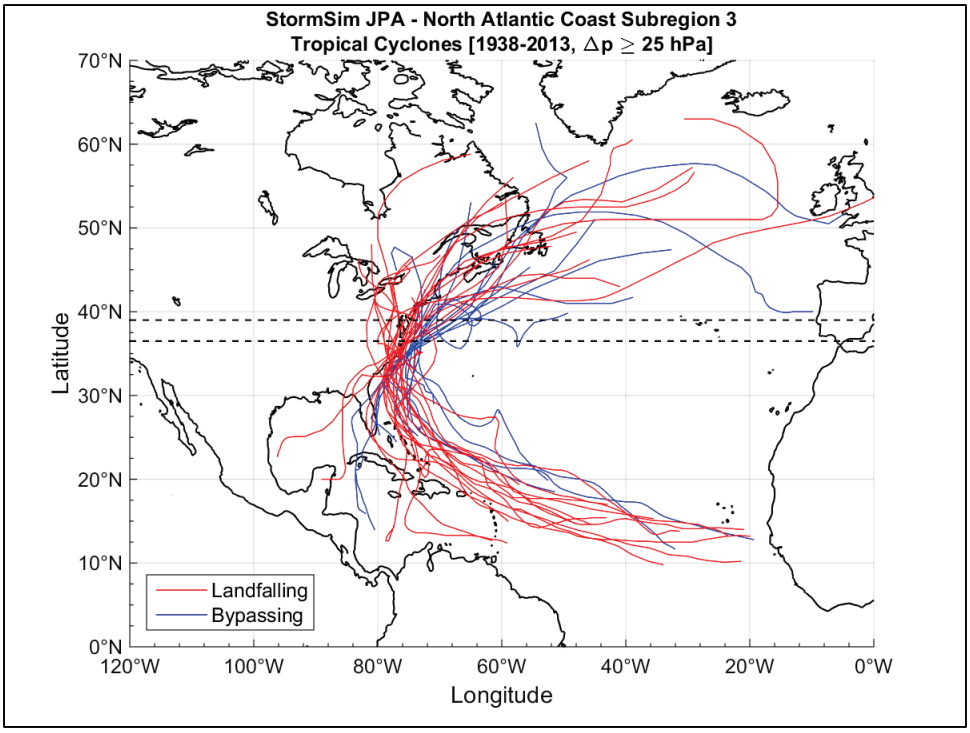

Figure 3-10. Landfalling and bypassing TC tracks for NACCS subregion 2.

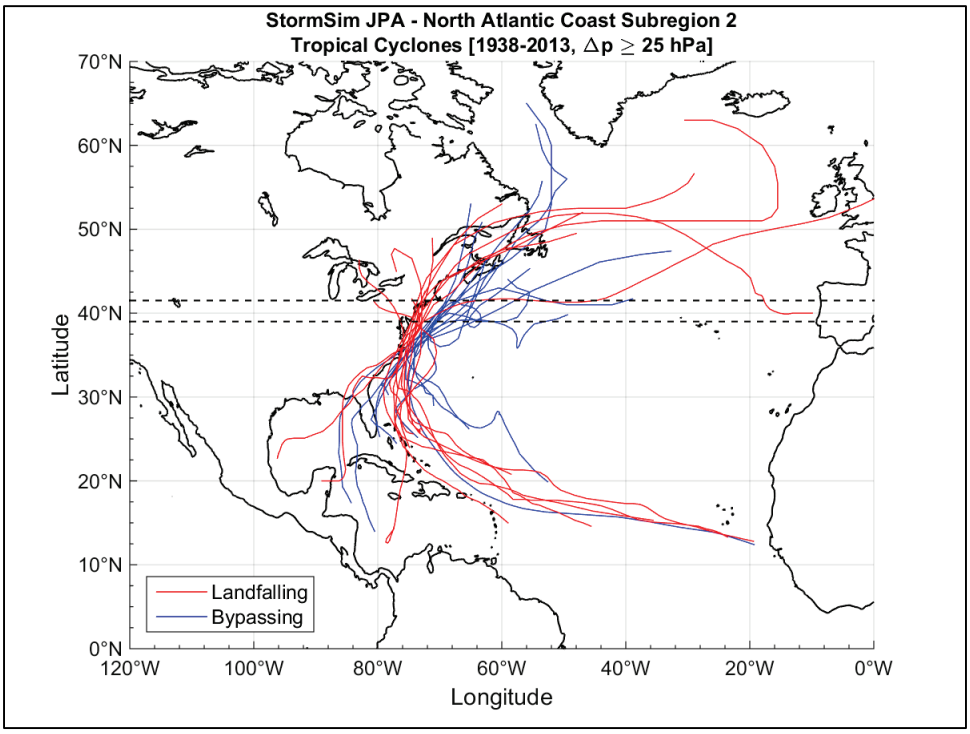

Figure 3-11. Landfalling and bypassing TC tracks for NACCS subregion 1.

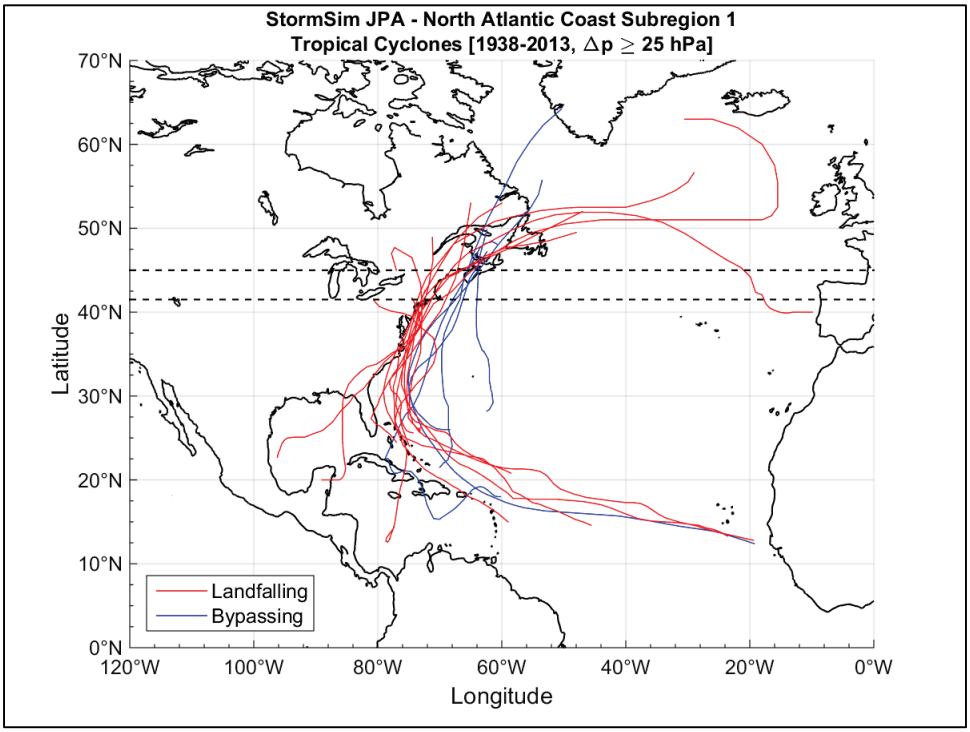

The major TCs identified from the HURDAT2 database as either making landfall or passing within 300 km of the study area during the 1938–2013 period are listed in Table 3-4.

Table 3-4. Historical TCs affecting the NACCS region during the 1938–2013 period.

NACCS Historical Tropical Cyclone ID	Name	Year	National Hurricane Center ID	Maximum Wind Speed (km/h)	Minimum Central Pressure (hPa)
1	UNNAMED	1938	6	204	940
2	UNNAMED	1940	4	167	961
3	UNNAMED	1944	7	194	940
4	BARBARA	1953	2	167	987
5	CAROL	1954	3	139	976
6	HAZEL	1954	9	204	937
7	CONNIE	1955	2	232	936
8	DIANE	1955	3	194	969
9	IONE	1955	9	185	938
10	DAISY	1958	4	194	935
11	HELENE	1958	8	204	934
12	DONNA	1960	5	222	932
13	ESTHER	1961	5	213	927
14	ALMA	1962	1	120	986
15	GLADYS	1964	9	232	945
16	GERDA	1969	16	204	979
17	AGNES	1972	2	111	977
18	BLANCHE	1975	4	139	980
19	BELLE	1976	7	194	957
20	UNNAMED	1981	22	111	978
21	GLORIA	1985	9	232	920
22	CHARLEY	1986	5	83	980
23	HUGO	1989	11	259	918
24	BOB	1991	3	185	950
25	UNNAMED	1991	12	111	972
26	EMILY	1993	5	185	960
27	ALLISON	1995	1	93	982
28	BERTHA	1996	2	185	960
29	FRAN	1996	6	194	946
30	JOSEPHINE	1996	10	83	970
31	BONNIE	1998	2	185	954
32	DENNIS	1999	5	167	962
33	FLOYD	1999	8	250	921

NACCS Historical Tropical Cyclone ID	Name	Year	National Hurricane Center ID	Maximum Wind Speed (km/h)	Minimum Central Pressure (hPa)
34	IRENE	1999	13	176	958
35	GUSTAV	2002	8	148	960
36	ISABEL	2003	13	269	915
37	JUAN	2003	15	167	969
38	ALEX	2004	1	194	957
39	ERNESTO	2006	6	111	985
40	NOEL	2007	16	120	965
41	HANNA	2008	8	139	977
42	KYLE	2008	11	130	984
43	EARL	2010	7	232	927
44	IRENE	2011	9	167	942
45	SANDY	2012	18	148	940

3.2 Historical XCs

In contrast to TCs, XCs cannot be described by a set of parameters because the cyclone is rarely a well-defined relatively uniform symmetric cyclone. XCs are formed as a result of the interaction of two air masses of cold and warm air. The greater the difference in temperature between the air masses, the greater the instability and stronger the storm. This contributes to the occurrence of more intense storms during the winter. One of the most recognized names for these storms is Nor'easters. They are characterized by storm winds with counterclockwise circulation, and they move towards the north east (Myers 1975). XCs tend to produce smaller surge than TCs since they typically exhibit lower intensity. TCs can convert to extratropical as they move from the tropics to the poles. When this occurs, it is referred to as an extratropical transition.

3.2.1 Data sources

For XCs, approximately 40 NOAA water level stations within the NACCS study area were initially evaluated. Twenty-three stations were selected based on the criterion of hourly measurement record lengths of at least 30 years. The 23 NOAA stations are listed in Table 3-5. The station identification number (ID) is listed in the first column. NOAA-verified hourly water level data were acquired for each station.

Table 3-5. NOAA-NOS CO-OPS water level stations.

Station ID	Station Name	Start Date	End Date	Record Length (years)
8410140	Eastport, ME	10/1/1958	3/31/2013	55
8413320	Bar Harbor, ME	3/2/1950	3/31/2013	63
8418150	Portland, ME	3/4/1910	3/31/2013	103
8443970	Boston, MA	5/3/1921	4/30/2013	92
8447930	Woods Hole, MA	2/25/1958	4/30/2013	55
8449130	Nantucket Island, MA	2/1/1965	4/30/2013	48
8452660	Newport, RI	9/10/1930	3/31/2013	83
8454000	Providence, RI	5/24/1979	3/31/2013	34
8461490	New London, CT	6/12/1938	4/30/2013	75
8510560	Montauk Point Light, NY	1/7/1959	4/30/2013	54
8516945	Kings Point, NY	1/1/1957	4/30/2013	56
8518750	The Battery, NY	6/1/1920	4/30/2013	93
8531680	Sandy Hook, NJ	1/7/1910	4/30/2013	103
8534720	Atlantic City, NJ	8/19/1911	4/30/2013	102
8536110	Cape May, NJ	11/21/1965	4/30/2013	48
8557380	Lewes, DE	1/1/1957	4/30/2013	56
8571892	Cambridge, MD	5/31/1979	3/31/2013	34
8574680	Baltimore, MD	7/1/1902	3/31/2013	111
8575512	Annapolis, MD	8/6/1928	4/30/2013	85
8577330	Solomons Island, MD	4/1/1979	3/31/2013	34
8594900	Washington, DC	4/15/1931	3/31/2013	82
8638610	Sewells Point, VA	7/22/1927	3/31/2013	86
8638863	Chesapeake Bay Bridge Tunnel, VA	1/29/1975	4/30/2013	38

Also, as part of the XC selection process, meteorological data (e.g., wind speed, atmospheric pressure) were obtained from meteorological stations within the NACCS region. The meteorological data used in this study were acquired from the NOAA National Climatic Data Center (NCDC) land-based stations. The Station IDs, names, and locations of the 18 meteorological stations used in this study are listed in Table 3-6. Two distinct station IDs are listed per station: U.S. Air Force (USAF) and Weather Bureau, Air Force, and Navy (WBAN).

Table 3-6. NCDC meteorological stations.

Station ID		Station Name	State
USAF	WBAN		
723080	13737	NORFOLK INTL ARPT	VIRGINIA
724070	93730	ATLANTIC CITY INTL	NEW JERSEY
724080	13739	PHILADELPHIA INTL	PENNSYLVANIA
724088	13707	DOVER AFB	DELAWARE
724096	14706	MC GUIRE AFB	NEW JERSEY
725020	14734	NEWARK INTL AIRPORT	NEW JERSEY
725030	14732	NEW YORK/LA GUARDIA	NEW YORK
725038	14714	STEWART INTL	NEW YORK
725040	94702	BRIDGEPORT/IGOR I.	CONNECTICUT
725046	14707	GROTON NEW LONDON	CONNECTICUT
725070	14765	PROVIDENCE/GREEN ST	RHODE ISLAND
725080	14740	HARTFORD/BRADLEY IN	CONNECTICUT
725087	14752	HARTFORD BRAINARD	CONNECTICUT
725090	14739	BOSTON/LOGAN INTL	MASSACHUSETTS
726050	14745	CONCORD MUNICIPAL	NEW HAMPSHIRE
744865	14719	WESTHAMPTON BEACH	NEW YORK
744910	14703	CHICOPEE FALLS/WEST	MASSACHUSETTS
745980	13702	LANGLEY AFB/HAMPTON	VIRGINIA

3.2.2 Period of record for statistical analysis

The 1938–2013 period used for the TCs was also used for the XCs. Reasons for the selection of this period were discussed in Section 3.1.2.

3.2.3 Selection of historical XCs

Unlike the JPM methodology where an attempt is made to quantify significant uncertainties, generally, this has not been taken into account in surge hazard studies for areas influenced only by XCs, such as those summarized in Nadal-Caraballo et al. (2012) and FEMA (2005). Nadal-Caraballo and Melby (2014), as part of the Phase I of the North Atlantic Coast Comprehensive Study, quantified uncertainty using a bootstrap resampling method. The mean curve and CL curves were calculated at 23 water level gages. The uncertainty from bootstrap resampling includes an aleatory component related to the selected sample and an epistemic component related to the best estimate parameters of the distribution. Uncertainty related to measurement errors or undersampling of TCs was not quantified in this gage analysis.

The sampling of XCs was done by identifying storms from time series of storm surge. The screening process was performed to screen out nonwind events based on meteorological observations. As part of this process, the storm surge response, quantified as the NTR, is estimated as the difference between the verified observed water level and the astronomical tide. A final storm screening was done by Oceanweather Inc. (OWI) to remove any remaining nonwind event. The methodology to estimate storm surge from water level measurements is explained in detail in Nadal-Caraballo and Melby (2014). As discussed in Section 3.2.1, 23 stations were selected based on the criterion of having at least 30 years of verified hourly measurements (these stations were listed in Table 3-5).

The preliminary screening of the 23 NOAA stations resulted in the sampling of approximately 250 XCs for the entire NACCS region. This number was reduced to an optimal amount using the CSS method (Nadal-Caraballo et al. 2012). Employing this approach, storms were screened and sampled using the POT technique from the 23 NOAA gages, and the highest ranked storms (largest water level values) among all stations were retained to constitute the CSS.

The general steps in this extratropical CSS methodology (Nadal-Caraballo et al. 2012) are as follows:

1. Use the POT technique to sample storms with approximately equal representation among the three regions.
2. Isolate the XC population by eliminating TCs, convective storms, and any other nonwind driven events from the CSS.
3. Develop full storm set (FSS) probability distributions by fitting GPD to storm surge values estimated from each of the 23 gages.
4. Fit GPD to the CSS storm surge values using different numbers of storms (e.g., 250, 225–100).
5. Minimize the number of storms in the CSS by selecting the fewest number of storms that match the FSS distributions.
6. Validate the CSS by comparing to the FSS water levels for different return periods at both tails of the probability distributions.

The CSS validation was done by comparing the root mean square deviation (RMSD) error between the CSS and FSS distributions over the record length. Although the sampling of the XCs is primarily based on the screening of storm surge responses estimated from the historical record of

observed water levels, the selection process was further validated by cross-checking the water level and surge time series of each event against wind speed and atmospheric pressure data obtained from adjacent meteorological stations, as shown in Figure 3-12. The locations of the 18 meteorological gages were listed in Table 3-6.

Statistical analyses showed that a CSS of 100 storms was adequate to capture the XC response statistics in the NACCS region. As a result of the CSS method, the number of sampled storms was reduced to an optimal set of 100 historical XCs. This sample set of XCs captures the historical range of storm intensity and variability of storm duration. These storms are listed in Appendix A: NACCS Historical Extratropical Cyclones. The GPD-based approach defined above was used to compute the final storm response statistics for XCs.

Figure 3-12. Example of synoptic time series of astronomical tide, water level, surge (NTR), wind speed, and atmospheric pressure for storm screening.

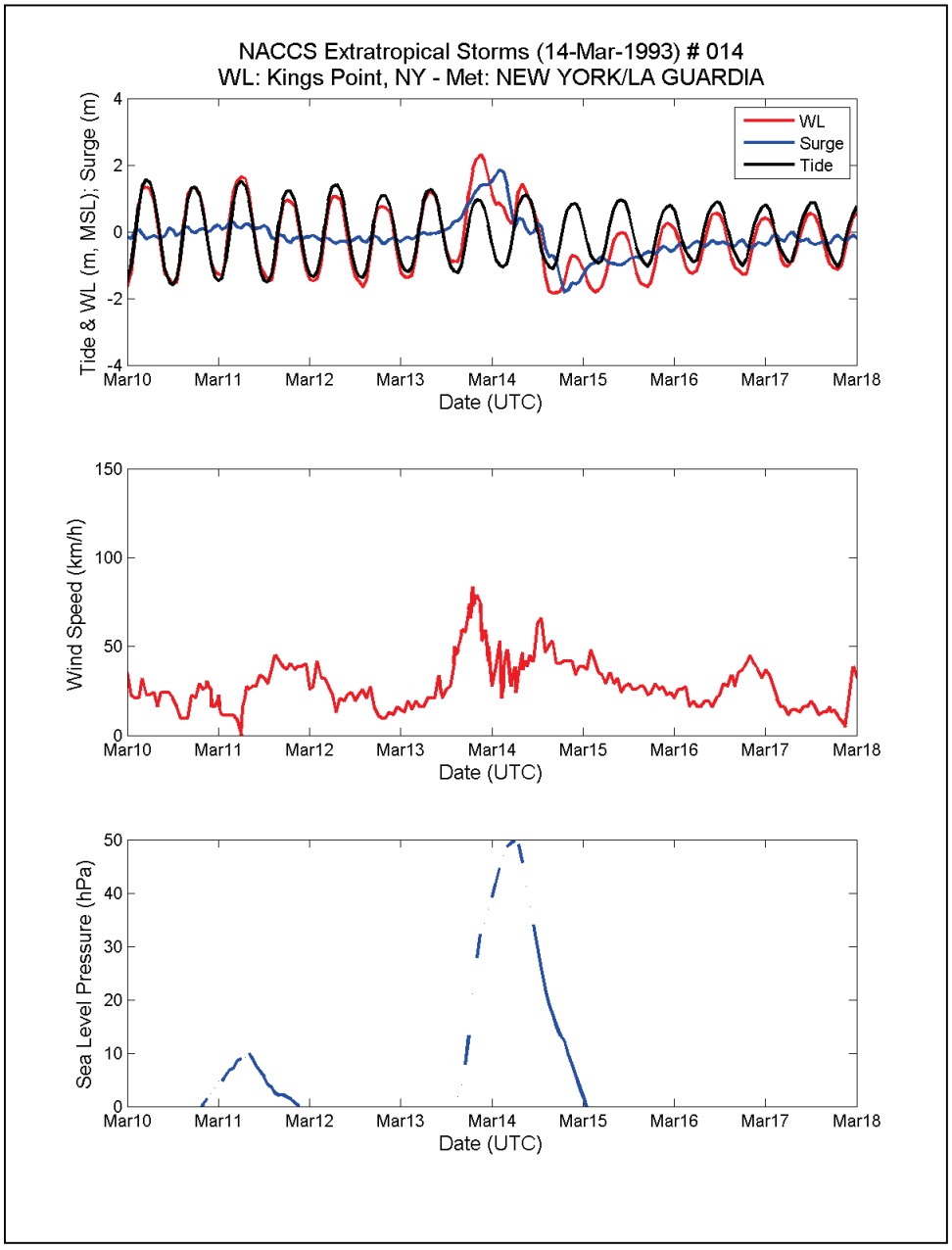

4 Spatially Varying Storm Recurrence Rate (SRR)

Efficient storm sampling from the historical record and statistical computation of SRR can be achieved using several different approaches. In recent studies, some of the approaches used to compute the spatial variation of SRR have included area-crossing, line-crossing, Gaussian kernel function (GKF), and other combined methods. Area-crossing and line-crossing are examples of capture zone methods. In the area-crossing approach, only storms passing through a particular area are counted in the computation of the SRR. The line-crossing approach usually consists of an idealized coastline or a reference line representing a segment of coastline. Only storms making landfall along the chosen segment of coastline are captured and counted towards the computation of the SRR.

Capture zones can also be defined in other ways, such as a rectangular or circular window, or any other finite spatial region. In past studies, the standard had been to apply any of the capture zone methods in order to count the storms and to assign uniform weights to all captured storms. The main limitation of the capture zone approach is that, while all storms within the chosen capture zone are given uniform weights, storms outside this zone are given a weight of zero. The conundrum lies in establishing a capture zone large enough to reduce the uncertainty associated with sample size by capturing an adequate number of storms from which significant statistics can be derived but small enough to balance the uncertainty associated with spatial variability and population heterogeneity.

The use of the GKF method, developed by Chouinard and Liu (1997), can overcome the main limitations of capture zone approaches. The standard application of the GKF consists of establishing a grid of nodes where estimates of the SRR are sought. All storms within this gridded space can be counted at any given node, but the weight assigned to each storm decreases with increasing distance from storm to node. The distance-adjusted weights are computed using a Gaussian probability distribution function (PDF) with an optimal kernel size.

The GKF equations are as follows:

$$\lambda = \frac{1}{T}\sum_i^n w(d_i) \tag{4-1}$$

$$w(d_i) = \frac{1}{\sqrt{2\pi}h_d} exp\left[-\frac{1}{2}\left(\frac{d_i}{h_d}\right)^2\right] \tag{4-2}$$

where λ = SRR in storms/yr/km; T = record length (yr); $w(d_i)$ = distance-adjusted weights from the Gaussian PDF (km^{-1}); d_i = distance from location of interest to a storm data point (km); h_d = optimal kernel size (km). Use of the GKF weights minimizes sample size uncertainty by taking full advantage of all available storm data while significantly reducing the uncertainty associated with spatial variability and potentially heterogeneous populations.

4.1 Optimal Gaussian kernel size

For purposes of this study, the optimal kernel size was determined from a series of sensitivity analyses performed using all TCs in the HURDAT2 database with $\Delta p \geq 28$ hPa within the 1938–2013 period. For validation purposes, the SRR computed from the GKF were compared to the observed SRR estimated using the capture zone approach. The analysis consisted of first estimating the observed SRR using circular capture zones with radii ranging from 100 km to 500 km and then computing the mean observed SRR corresponding to this range of radii; second, the squared error of the GKF results was computed from the difference between the mean observed SRR and GKF estimates using kernel sizes from 100 km to 500 km. For each cyclone, only track data points with $\Delta p \geq 28$ hPa were accounted for in this analysis.

Figure 4-1 shows the variation of SRR as a function of capture zone radius (red curve), as well as the mean observed SRR (blue horizontal line), for a CRL in Atlantic City, NJ. The observed SRR for this CRL varied from 1.79E-4 to 5.26E-4 storms/yr/km, depending on the capture zone radius, with a mean of 4.20E-4 storms/yr/km. Figure 4-2 shows the variation of SRR for a CRL in The Battery, NY. The observed SRR varied from 2.57E-4 to 4.76E-4 storms/yr/km, and had a mean of 3.56E-4 storms/yr/km. Figure 4-3 shows the variation of SRR for a CRL in Providence, RI. The observed SRR varied from roughly 2.19E-4 to 5.48E-4 storms/yr/km, depending on the capture zone radius, with a mean of 4.31E-4 storms/yr/km.

Figure 4-1. Mean observed SRR for Atlantic City, NJ.

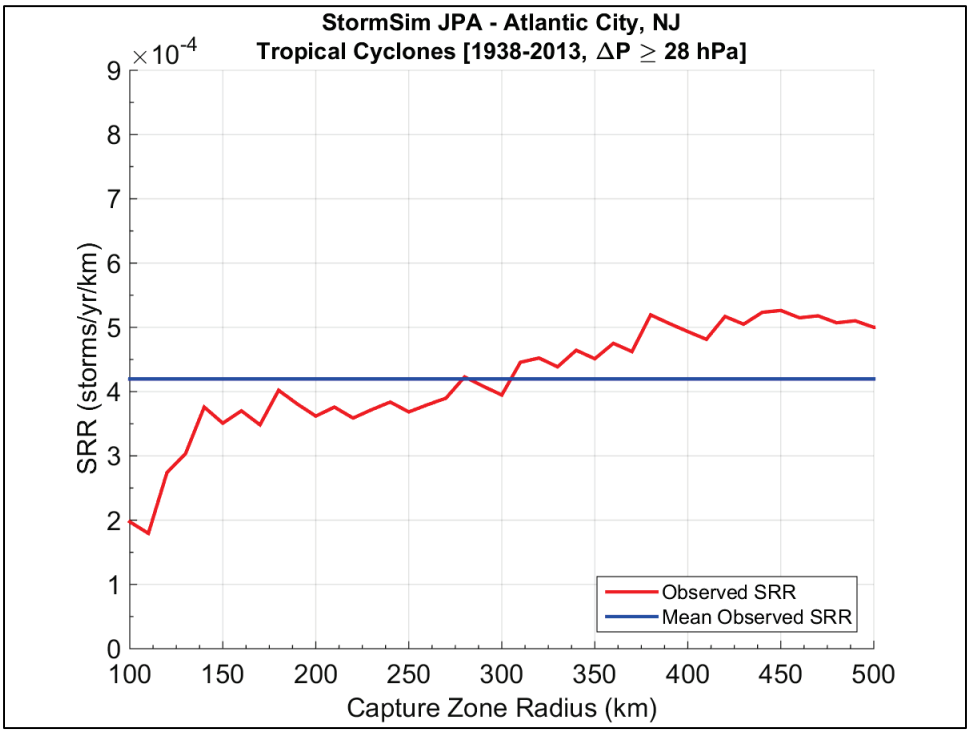

The squared error of the difference between the observed SRR and GKF SRR for Atlantic City, NJ; The Battery, NJ; and Providence, RI, are presented in Figures 4-4 through 4-6, respectively. In general, the differences between observed and GKF SRR exhibit asymmetric-parabolic shapes with minima corresponding to kernel sizes consistently in the range of 190 km to 210 km.

Figure 4-2. Mean observed SRR for The Battery, NY.

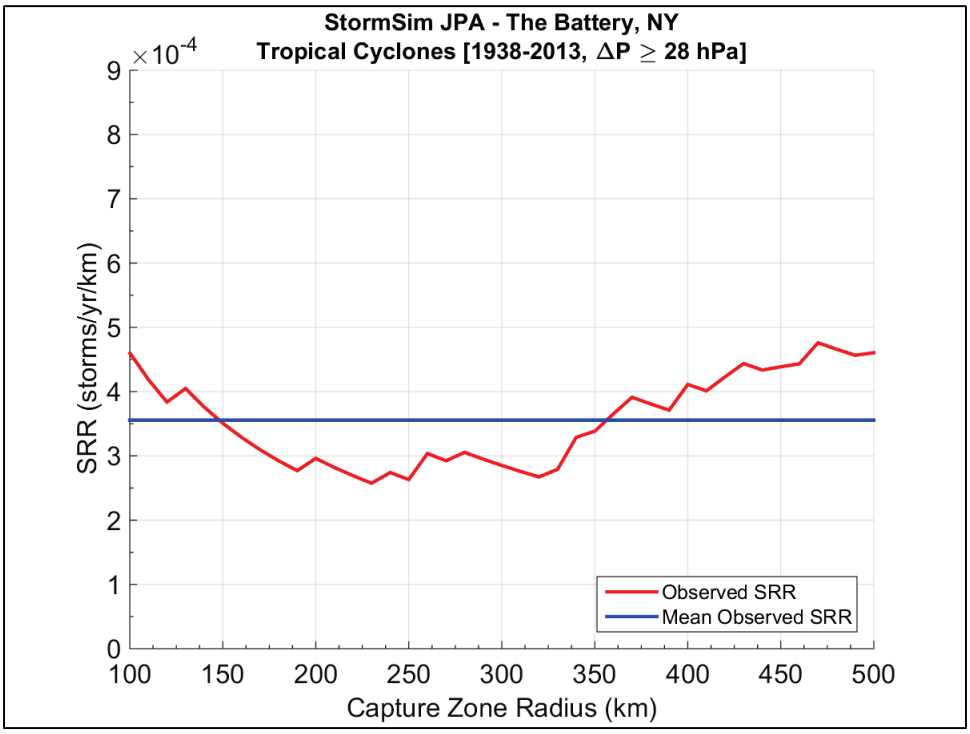

Figure 4-3. Mean observed SRR for Providence, RI.

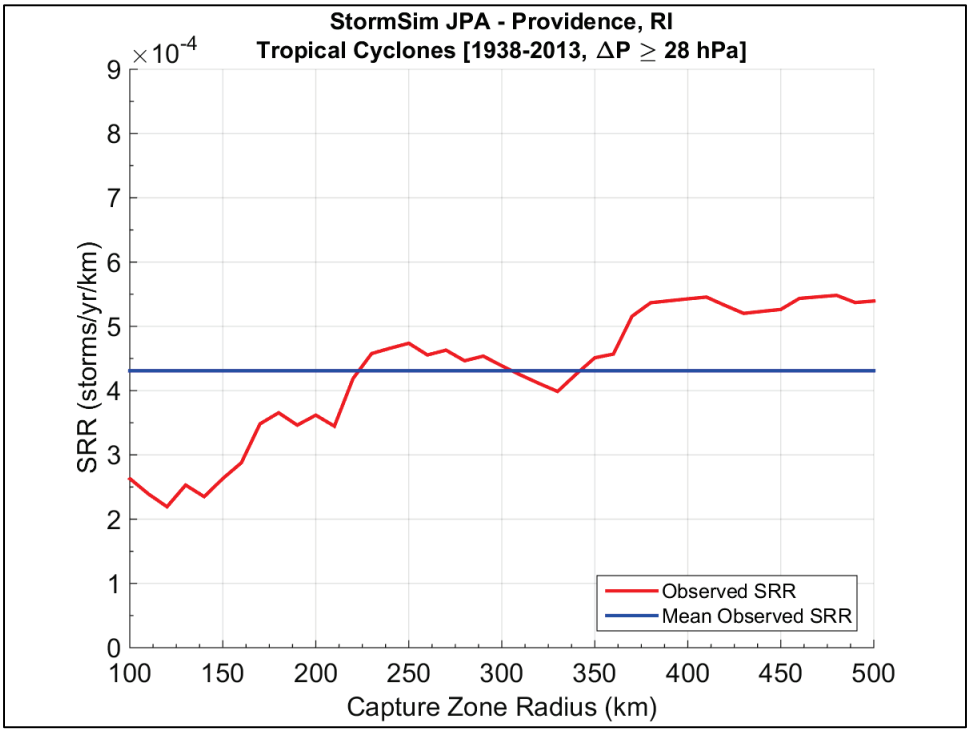

Figure 4-4. SRR squared error for Atlantic City, NJ.

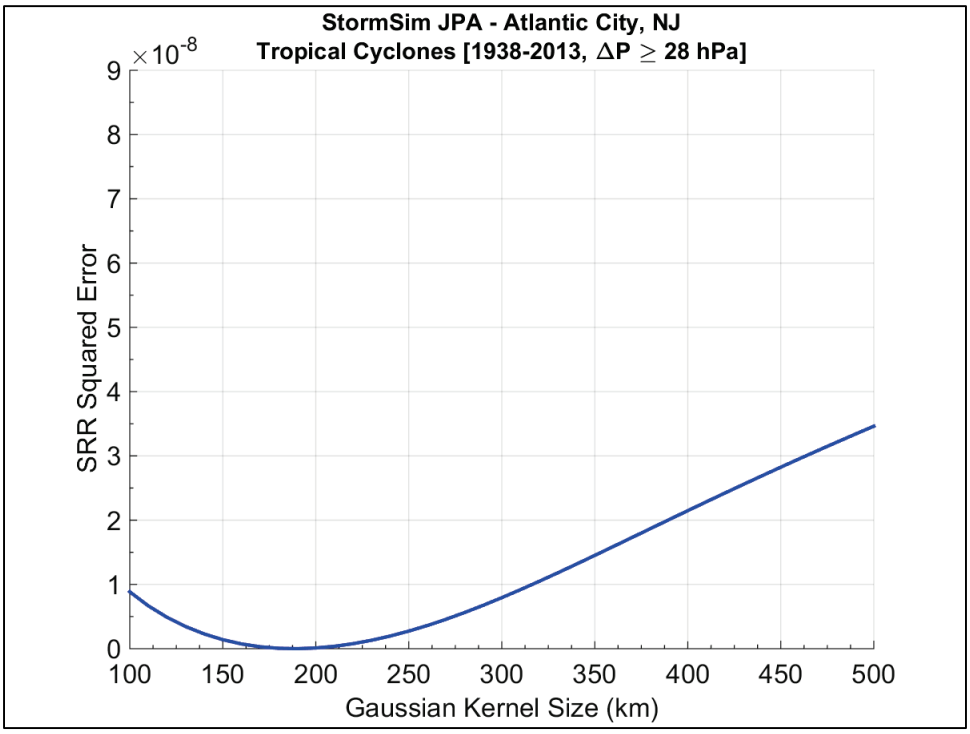

Figure 4-5. SRR squared error for The Battery, NY.

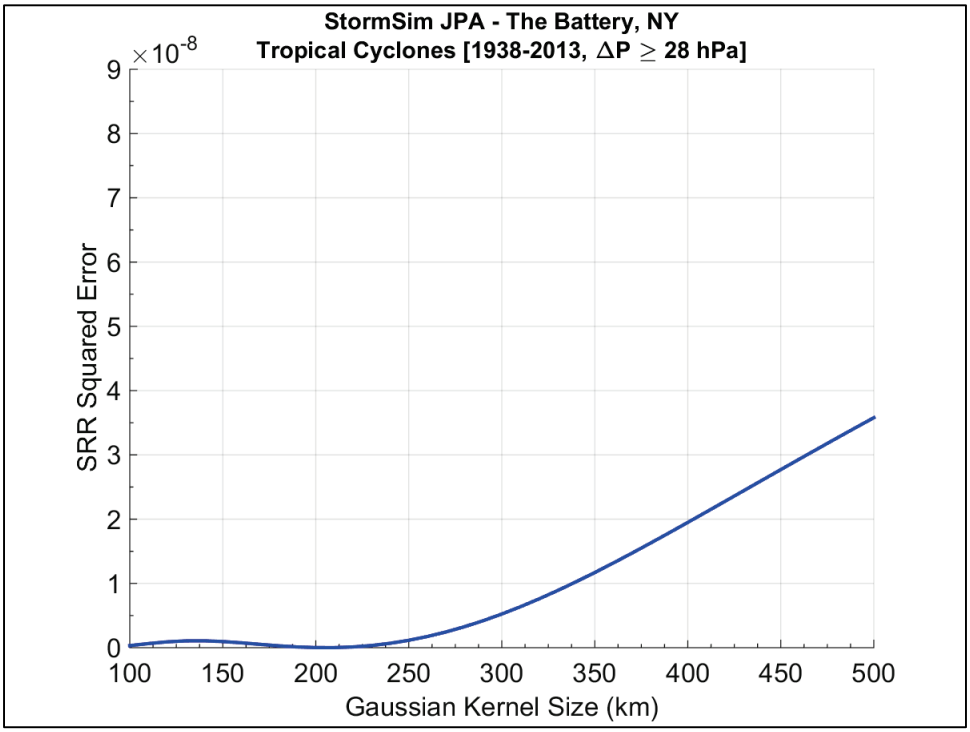

Figure 4-6. SRR squared error for Providence, RI.

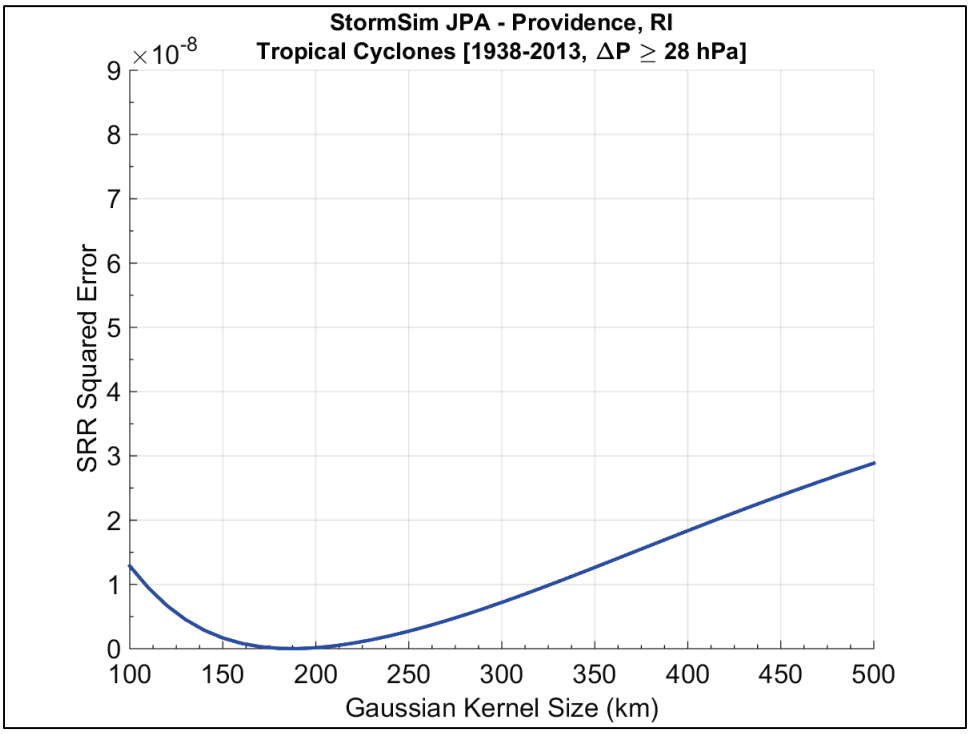

4.2 Capture zone and Gaussian kernel function (GKF) SRR results

This study adopted a global optimal kernel size of 200 km. An optimal kernel size of 200 km was also chosen in a recent FEMA study of coastal Mississippi (FEMA 2008; Toro 2008) and in the latest FEMA Region II study (FEMA 2014). Table 4-1 lists the observed and GKF SRR for the 23 select locations within the NACCS region. These SRR have been adjusted by +10%, as discussed in Section 3.1.2.

Table 4-1. Observed and GKF SRR for 23 locations within the NACCS region.

Coastal Reference Location (CRL)	Mean Observed SRR (storms/yr/km)	Mean Observed SRR_{200km} (storms/yr)	GKF SRR (storms/yr/km)	GKF SRR_{200km} (storms/yr)
Eastport, ME	2.68E-04	0.11	2.78E-04	0.11
Bar Harbor, ME	2.72E-04	0.11	2.77E-04	0.11
Portland, ME	2.46E-04	0.10	2.53E-04	0.10
Boston, MA	3.23E-04	0.13	3.36E-04	0.13
Woods Hole, MA	4.39E-04	0.18	4.53E-04	0.18
Nantucket Island, MA	4.42E-04	0.18	4.61E-04	0.18
Newport, RI	4.29E-04	0.17	4.40E-04	0.18
Providence, RI	4.31E-04	0.17	4.43E-04	0.18
New London, CT	4.30E-04	0.17	4.31E-04	0.17
Montauk Point Light, NY	4.30E-04	0.17	4.31E-04	0.17
Kings Point, NY	3.58E-04	0.14	3.57E-04	0.14
The Battery, NY	3.56E-04	0.14	3.52E-04	0.14

Coastal Reference Location (CRL)	Mean Observed SRR (storms/yr/km)	Mean Observed SRR_{200km} (storms/yr)	GKF SRR (storms/yr/km)	GKF SRR_{200km} (storms/yr)
Sandy Hook, NJ	3.56E-04	0.14	3.52E-04	0.14
Atlantic City, NJ	4.20E-04	0.17	4.30E-04	0.17
Cape May, NJ	4.27E-04	0.17	4.38E-04	0.18
Lewes, DE	4.42E-04	0.18	4.51E-04	0.18
Cambridge, MD	4.57E-04	0.18	4.65E-04	0.19
Baltimore, MD	4.42E-04	0.18	4.51E-04	0.18
Annapolis, MD	4.42E-04	0.18	4.51E-04	0.18
Solomons Island, MD	4.84E-04	0.19	4.97E-04	0.20
Washington, DC	4.57E-04	0.18	4.65E-04	0.19
Sewells Point, VA	5.43E-04	0.22	5.60E-04	0.22
Chesapeake Bay Bridge Tunnel, VA	5.43E-04	0.22	5.60E-04	0.22

The weights computed using the GKF with a kernel size of 200 km are illustrated in Figure 4-7. These weights are shown relative to the weight of a storm track point located on the CRL (d = 0 km), or

$$Relative\ weight = \frac{w(d_i)}{w(d=0)} \qquad \text{for } d_i \geq 0 \qquad (4\text{-}3)$$

Data from a storm track point located on the CRL would have a relative weight of 1.0 whereas a track point located at a distance 200 km away from the CRL would have a relative weight of 0.60. The weights decrease as distance from the CRL increases, based on the Gaussian PDF, until becoming negligible. The relative weight of track points located at 600 km and 800 km from the CRL, for example, have relative weights 1.11E-2 and 3.35E-4, respectively.

Figure 4-7. Relative weight of storm parameters as a function of distance from CRL.

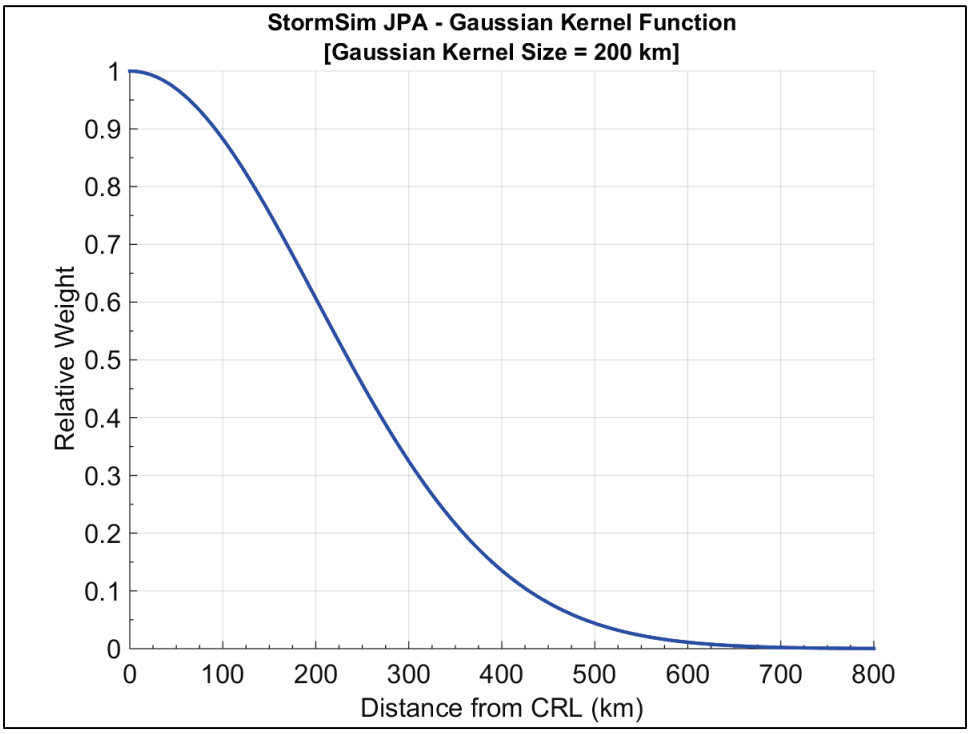

The SRR_{200km} results of low-intensity TCs (28 hPa ≤ Δp < 48 hPa) in the entire Atlantic for the 1938–2013 period (unadjusted) are presented in Figure 4-8. The SRR_{200km} corresponding to high-intensity TCs (Δp ≥ 48 hPa) for the same period are shown in Figure 4-9. The GKF SRR for low- and high-intensity TCs at 23 locations within the NACCS region are presented in Table 4-2. As discussed in Section 3.2.1, SRR_{200km}, which is used here for convenience of illustration, corresponds to the SRR associated with storms passing within a radius of 200 km of a given location.

Figure 4-8. SRR_{200km} for low-intensity TCs recorded in the Atlantic basin from 1938–2013.

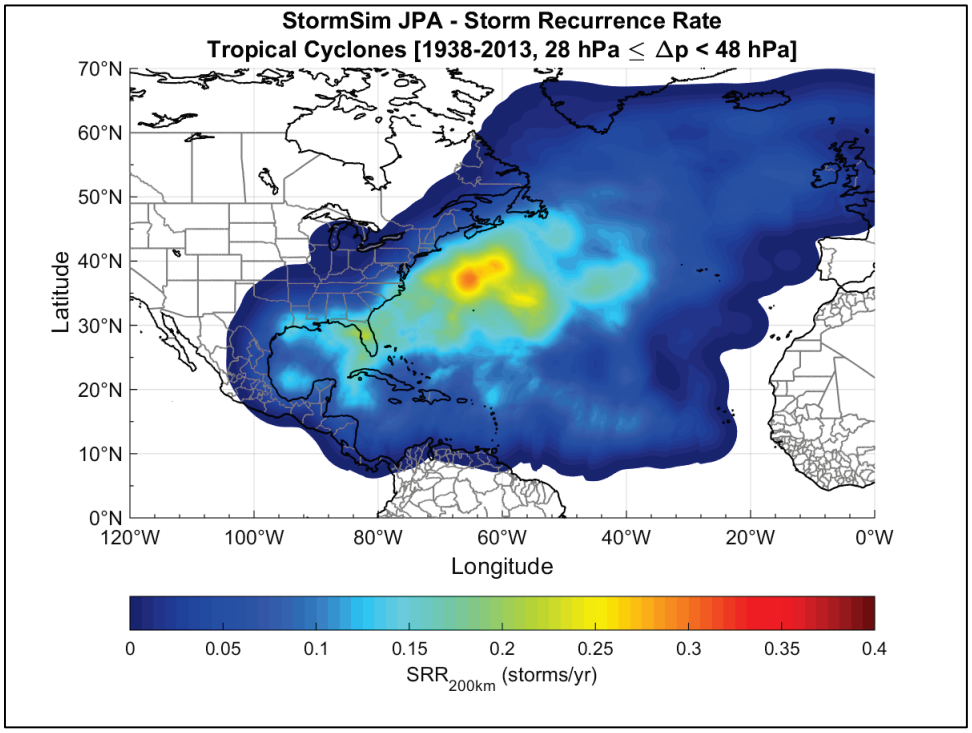

Figure 4-9. SRR_{200km} for high-intensity TCs recorded in the Atlantic basin from 1938–2013.

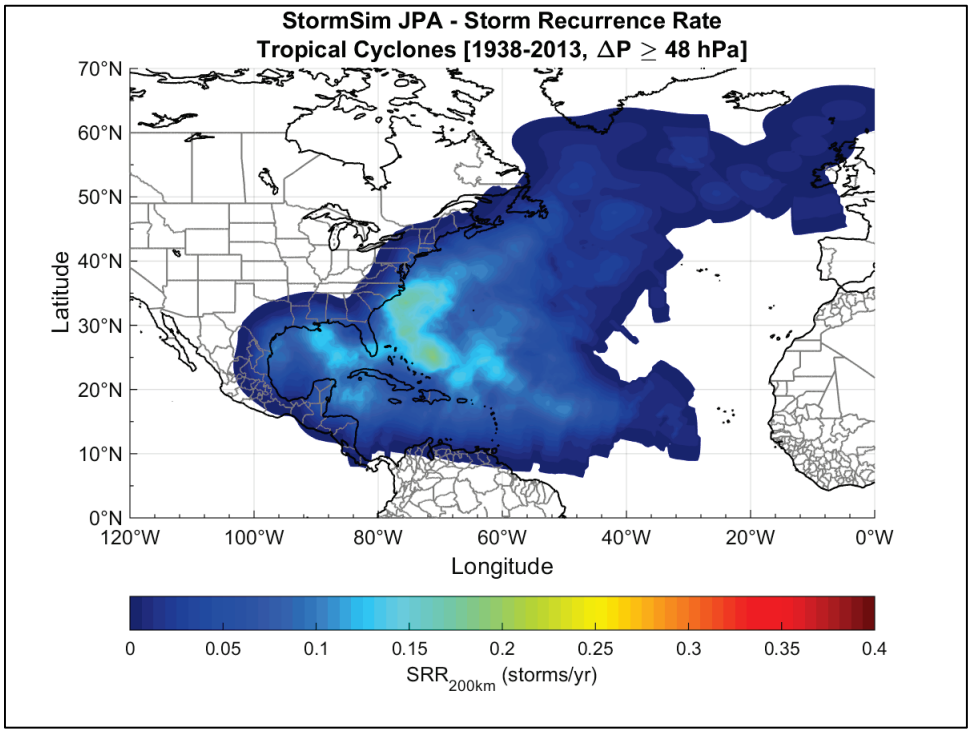

Table 4-2. GKF SRR for low- and high-intensity TCs.

Coastal Reference Location	Low-Intensity TCs (28 hPa ≤ Δp < 48 hPa)		High-Intensity TCs (Δp ≥ 48 hPa)	
	GKF SRR (storms/yr/km)	GKF SRR_{200km} (storms/yr)	GKF SRR (storms/yr/km)	GKF SRR_{200km} (storms/yr)
Eastport, ME	2.24E-04	0.09	5.32E-05	0.02
Bar Harbor, ME	2.23E-04	0.09	5.32E-05	0.02
Portland, ME	2.18E-04	0.09	3.53E-05	0.01
Boston, MA	2.40E-04	0.10	9.59E-05	0.04
Woods Hole, MA	3.18E-04	0.13	1.35E-04	0.05
Nantucket Island, MA	3.24E-04	0.13	1.37E-04	0.05
Newport, RI	2.89E-04	0.12	1.51E-04	0.06
Providence, RI	2.92E-04	0.12	1.51E-04	0.06
New London, CT	2.79E-04	0.11	1.52E-04	0.06
Montauk Point Light, NY	2.79E-04	0.11	1.52E-04	0.06
Kings Point, NY	1.89E-04	0.08	1.68E-04	0.07
The Battery, NY	1.84E-04	0.07	1.67E-04	0.07
Sandy Hook, NJ	1.84E-04	0.07	1.67E-04	0.07
Atlantic City, NJ	2.36E-04	0.09	1.94E-04	0.08
Cape May, NJ	2.47E-04	0.10	1.91E-04	0.08
Lewes, DE	2.63E-04	0.11	1.88E-04	0.08
Cambridge, MD	2.76E-04	0.11	1.89E-04	0.08
Baltimore, MD	2.63E-04	0.11	1.88E-04	0.08
Annapolis, MD	2.63E-04	0.11	1.88E-04	0.08
Solomons Island, MD	2.94E-04	0.12	2.03E-04	0.08
Washington, DC	2.76E-04	0.11	1.89E-04	0.08
Sewells Point, VA	3.43E-04	0.14	2.17E-04	0.09
Chesapeake Bay Bridge Tunnel, VA	3.43E-04	0.14	2.17E-04	0.09

5 Development of Synthetic TCs

The development of synthetic TCs and respective storm parameters included landfalling and bypassing storms covering the entire Virginia-to-Maine coastal region. In the JPM, the primary parameters considered, as discussed in Section 2.1.2, are

1. track location (x_0)
2. heading direction (θ)
3. central pressure deficit (Δp)
4. radius of maximum winds (R_{max})
5. translational speed (V_t).

These storm parameters are required as inputs to the PBL model used for generation of wind and pressure fields. The work described here consists of the development and discretization of storm parameter marginal or conditional distributions, generation of synthetic TC track paths and along-track variation of storm parameters, and finalization of the set of synthetic TCs.

Section 5.1 describes the development of the marginal distributions of storm parameters. Section 5.2 presents a discussion of the discretization of the marginal distributions, and Section 5.3 discusses the correlation between central pressure deficit and maximum wind speed. Section 5.4 presents the generation of the synthetic TC tracks. Section 5.5 describes how TC parameters were used and how the storm parameters were modified for prelandfall and postlandfall changes.

5.1 Probability distributions of TC parameters

The characterization of storm climatology at each of the NACCS subregions required developing probability distributions of individual storm parameters. These distributions were developed from HURDAT2 data limited to the 1938–2013 period and $\Delta p \geq 28$ hPa. However, the entire 1851–2013 record was used for assessing the historical maxima and variances of the TC parameters. The marginal distributions discussed in this section were developed as part of the process that sought the generation of synthetic TCs. A set of marginal distributions was developed for each of the MPCRLs in order to characterize the storm climatology corresponding to each of the three NACCS subregions and to properly

reflect the latitude-dependency of the TC parameters. As will be discussed in Chapter 8, the final JPA required separate statistical analyses to be performed at a much higher spatial resolution, resulting in the establishment of 200 CRLs equally spaced throughout the NACCS region idealized coastline.

The distance-weighting GKF methodology, which was developed by Chouinard and Liu (1997) and afterwards applied in several flood hazards studies (Resio et al. 2007; FEMA 2008, 2012, 2014; IPET 2009; Niedoroda et al. 2010; Toro et al. 2010; USACE 2011), was used to compute the TC parameter mean values and marginal probabilistic distributions for each of the three NACCS subregions. As discussed in Section 3.1, a MPCRL was established at the center of each subregion coastline in order to facilitate spatial discretization of the storm climatology and development of synthetic TCs. The latitudes of these MPCRLs were listed in Table 3-1.

A unique set of marginal probability distributions was developed for each subregion. In the case of landfalling TCs, the heading direction (θ) was computed at landfall, as defined in Section 3.1. The central pressure deficit or deviation (Δp) was determined at the peak intensity of each TC, identified as the highest Δp within 300 km of the landfall location. The translational speed (V_t) was computed at the same location as the highest Δp. In the case of bypassing TCs, the θ was computed at the closest track point within 300 km of the MPCRL of the corresponding subregion. The Δp was identified as the highest Δp within 300 km of the MPCRL. The V_t was computed at the location of the highest Δp.

For each of the TC parameter distributions, a distance-weighted mean was computed based on the distances between the track point of higher intensity and the MPCRL of the subregion. The marginal distributions are then fitted to the distance-adjusted TC parameters. The purpose of this Gaussian process is to maximize the use of available historical data while properly characterizing the storm climatology of each subregion given the latitude-dependency of the TC parameters.

The distance-weighted mean (μ_{dist}) was computed as follows:

$$\mu_{dist} = \frac{\sum_{i=1}^{n} w(d_i) x_i}{\sum_{i=1}^{n} w(d_i)} \tag{5-1}$$

where $w(d_i)$ = distance weights computed using the GKF (Equation 4-2); x_i = individual parameter values of sampled TCs (e.g., one set of values per TC taken at the location of highest intensity); and n = number of sampled TCs corresponding to each subregion.

The parameters x_i are adjusted by μ', which is the ratio of the μ_{dist} to the arithmetic mean (μ)

$$x'_i = x_i \, \mu' \tag{5-2}$$

where:

$$\mu' = \frac{\mu_{dist}}{\mu} \tag{5-3}$$

and

$$\mu = \frac{\sum_{i=1}^{n} x_i}{n} \tag{5-4}$$

This Gaussian process was followed for all TC parameters discussed at the beginning of this chapter.

5.1.1 Central pressure deficit (Δp)

The c_p is a measurement of TC intensity and is inversely proportional to intensity. However, for convenience and to facilitate statistical analyses, hurricane intensity is usually expressed in terms of Δp. It is common practice to use these parameters interchangeably. The c_p is measured at the center or eye of a storm while Δp is the difference between the c_p and the far-field atmospheric pressure outside of the storm influence (FEMA 2008). In most JPM studies, the Δp has been computed from an assumed far-field atmospheric pressure of 1,013 hPa.

A JPA was performed using StormSim to further assess the correlation between storm central pressure deficit and latitude. Figure 5-1 shows the marginal distribution of Δp for the U.S. North Atlantic coast for latitudes 25° N to 50° N and longitudes 60° W to 80° W. The red values represent the empirical distribution while the blue curve is the GPD best fit that was determined using the maximum likelihood MLM.

Several parametric distributions were tested to fit the empirical distribution of storm location (degrees of latitude), including the GPD, the Gaussian (normal) distribution, and the lognormal distribution. The best overall fit was obtained with the lognormal distribution (Figure 5-2).

The Δp and latitude marginal distributions were used to determine the conditional probability of Δp as a function of latitude for the North Atlantic coast. A multivariate Gaussian model was employed to compute the joint probability between both parameters and subsequently the conditional probability, $P(\Delta p|x_o)$.

The $P(\Delta p|x_o)$ as well as 85%, 50%, and 16% CLs are plotted in Figure 5-3. These results confirm that, within the study area, Δp decreases as a function of latitude.

Figure 5-1. Marginal distribution of central pressure deficit (GPD) for latitudes 25°N to 50°N and longitudes 60°W to 80°W.

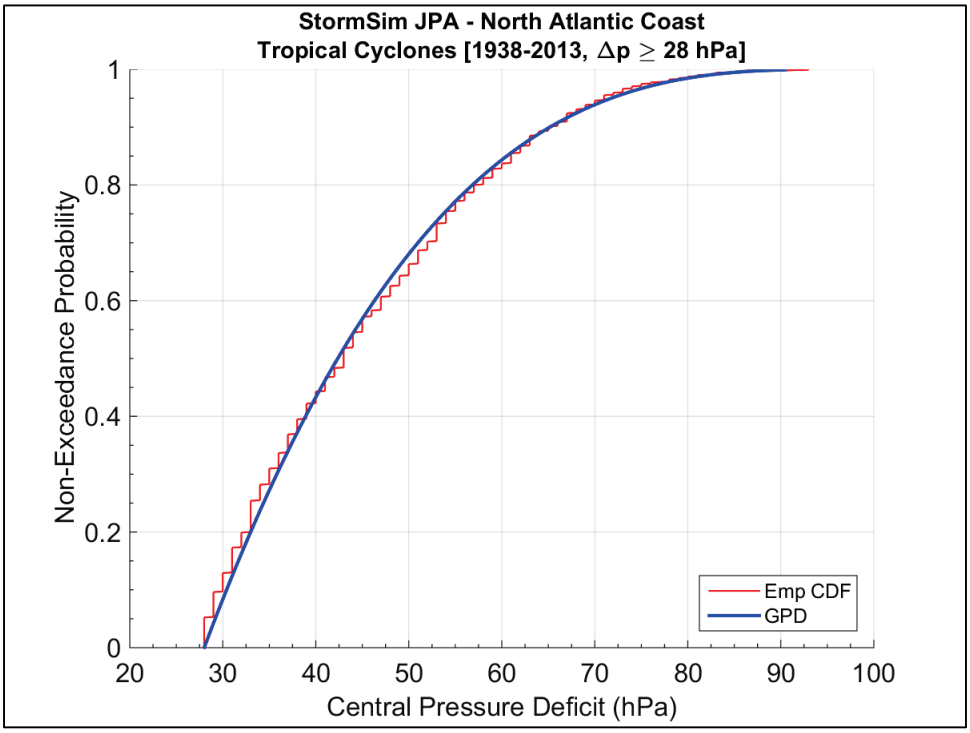

Figure 5-2. Lognormal marginal distribution of storm location (latitude).

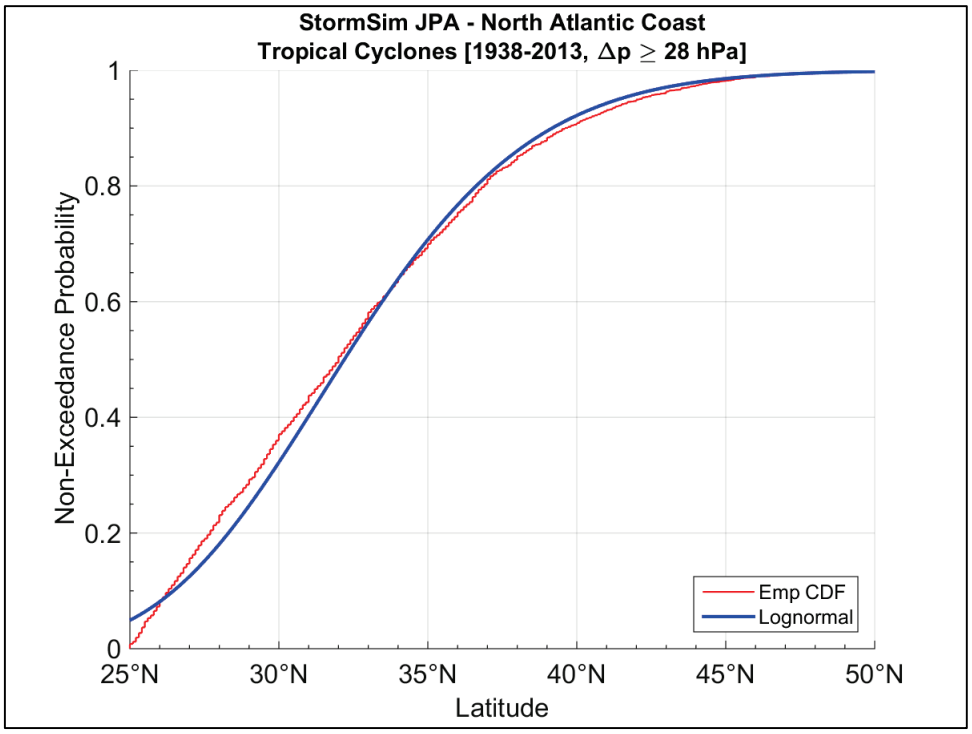

Figure 5-3. Conditional probability between storm location (latitude) and central pressure deficit.

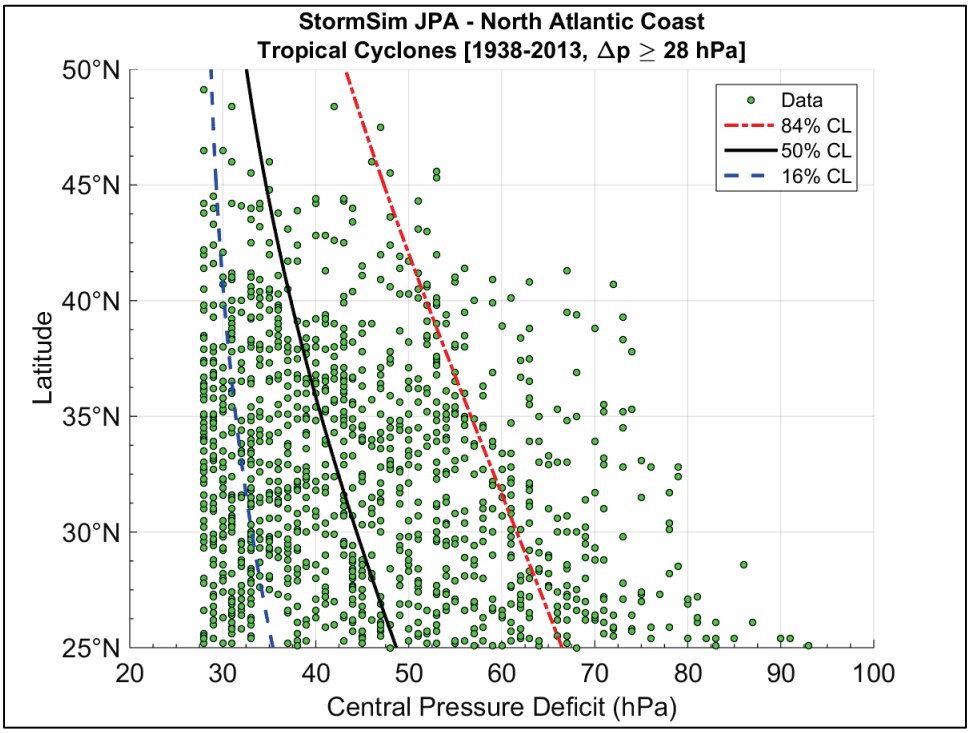

For the development of synthetic TCs , the doubly truncated Weibull distribution (DTWD) (Equation 5-5) was fit to the historical Δp data for the NACCS subregions. The probability distributions for subregions 3, 2, and 1 were truncated at 103, 93, and 83 hPa, respectively. The values of the DTWD parameters are listed in Table 5-1.

$$F[\Delta p > x] = \frac{exp\left[-\left(\frac{x}{U}\right)^k\right] - exp\left[-\left(\frac{\Delta p_2}{U}\right)^k\right]}{exp\left[-\left(\frac{\Delta p_1}{U}\right)^k\right] - exp\left[-\left(\frac{\Delta p_2}{U}\right)^k\right]} \tag{5-5}$$

where: U = scale parameter; k = shape parameter; Δp_1 = lower limit of Δp; and Δp_2 = upper limit of Δp.

Table 5-1. Central pressure deficit marginal distribution parameters.

NACCS Subregion	U (hPa)	k	Δp_1 (hPa)	Δp_2 (hPa)
3	33.27	1.00	25	103
2	35.77	1.41	25	93
1	24.76	1.00	25	83

The Δp marginal distributions for subregions 3, 2, and 1 are plotted in Figures 5-4, 5-5, and 5-6, respectively. The CLs corresponding to the marginal distributions discussed in this chapter were developed through bootstrap resampling.

Figure 5-4. Marginal distribution of central pressure deficit for NACCS subregion 3.

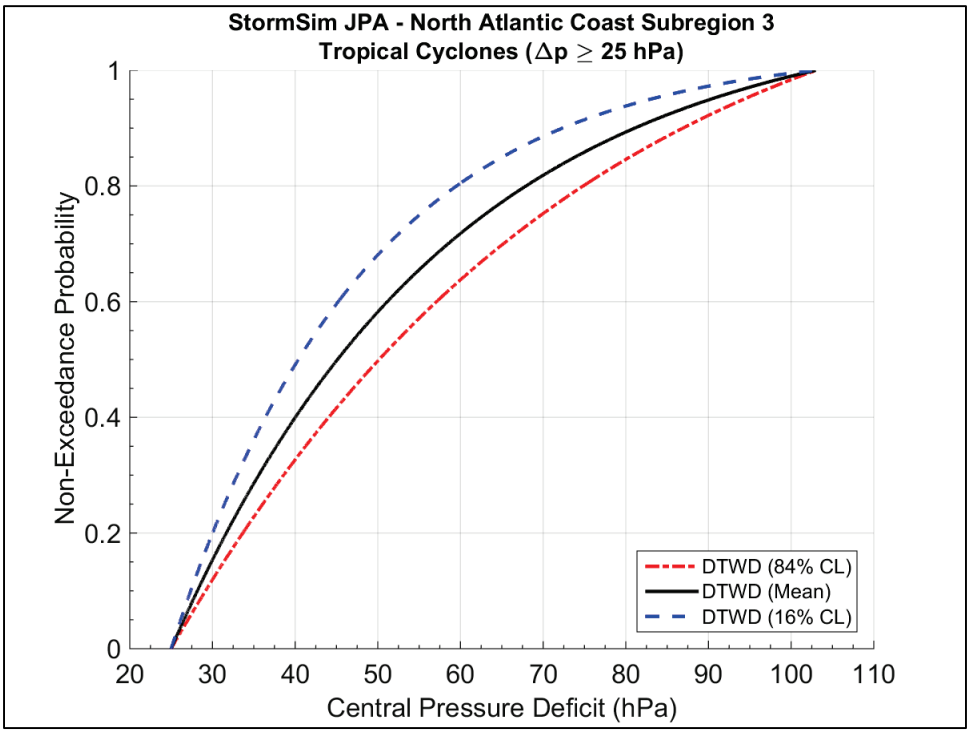

Figure 5-5. Marginal distribution of central pressure deficit for NACCS subregion 2.

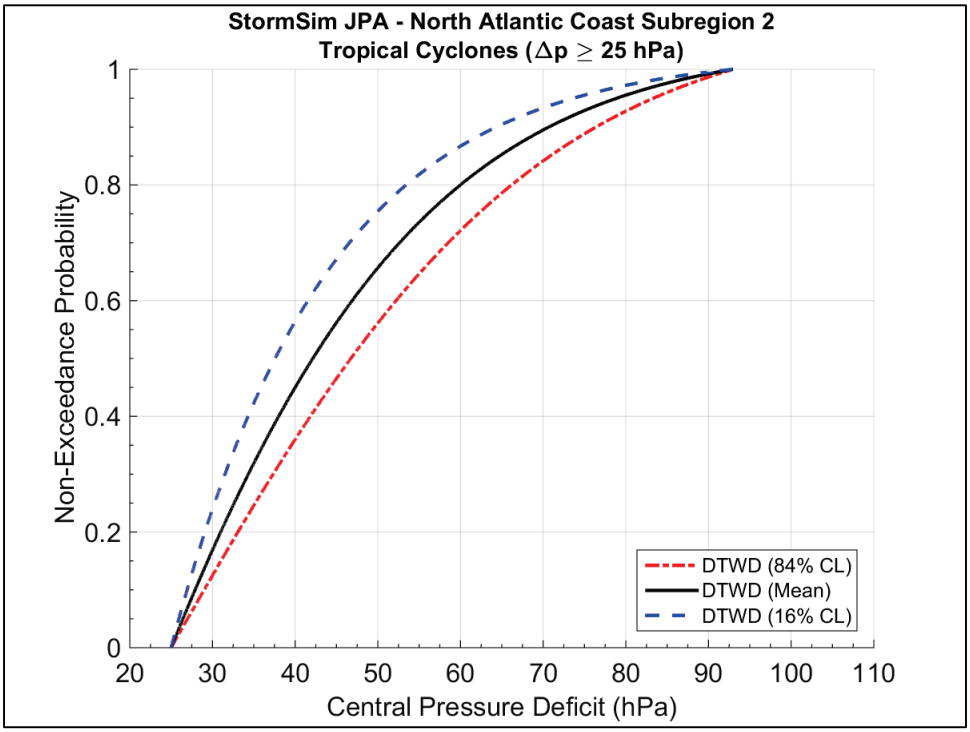

Figure 5-6. Marginal distribution of central pressure deficit for NACCS subregion 1.

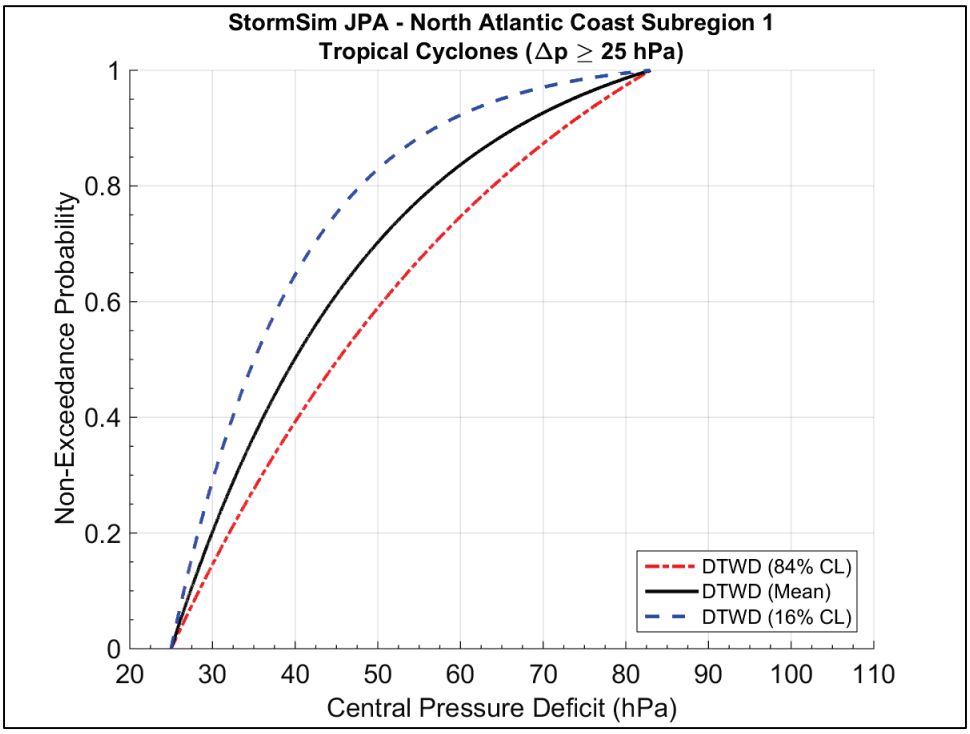

5.1.2 Radius of maximum winds (R_{max})

In this study, the parameter R_{max} is represented by the lognormal distribution which has the form

$$f(x) = \frac{1}{x\sigma\sqrt{2\pi}} exp\left[-\frac{1}{2}\left(\frac{ln(x)-\mu}{\sigma}\right)^2\right] \quad (5\text{-}6)$$

The lognormal distribution parameters are estimated from a statistical model of R_{max} developed by Vickery and Wadhera (2008). In this model, the expected value of R_{max} is estimated as a function of both Δp and latitude (ψ). The statistical model of R_{max} is as follows:

$$ln(R_{max}) = 3.015 - 6.291 \times 10^{-5}\Delta p^2 + 0.0337\psi \quad (5\text{-}7)$$

$$\sigma_{ln(R_{max})} = 0.441$$

The values of the lognormal distribution parameters for each subregion are listed in Table 5-2. These are the mean values of the natural logarithms of R_{max}, or $\mu_{ln(Rmax)}$, and the standard deviation of the natural logarithms of R_{max}, or $\sigma_{ln(Rmax)}$. The latter, which in this case is a measure of the

dispersion of the historical data, was increased from 0.441 to 0.45 after sensitivity analyses of the entire HURDAT2 1851–2013 record.

Table 5-2. Radius of maximum winds marginal distribution parameters.

NACCS Subregion	$\mu_{ln(x)}$	$\sigma_{ln(x)}$
3	4.090	0.45
2	4.215	0.45
1	4.316	0.45

The R_{max} marginal distributions for subregions 3, 2, and 1 are plotted in Figures 5-7, 5-8, and 5-9, respectively.

Figure 5-7. Marginal distribution of radius of maximum winds for NACCS subregion 3.

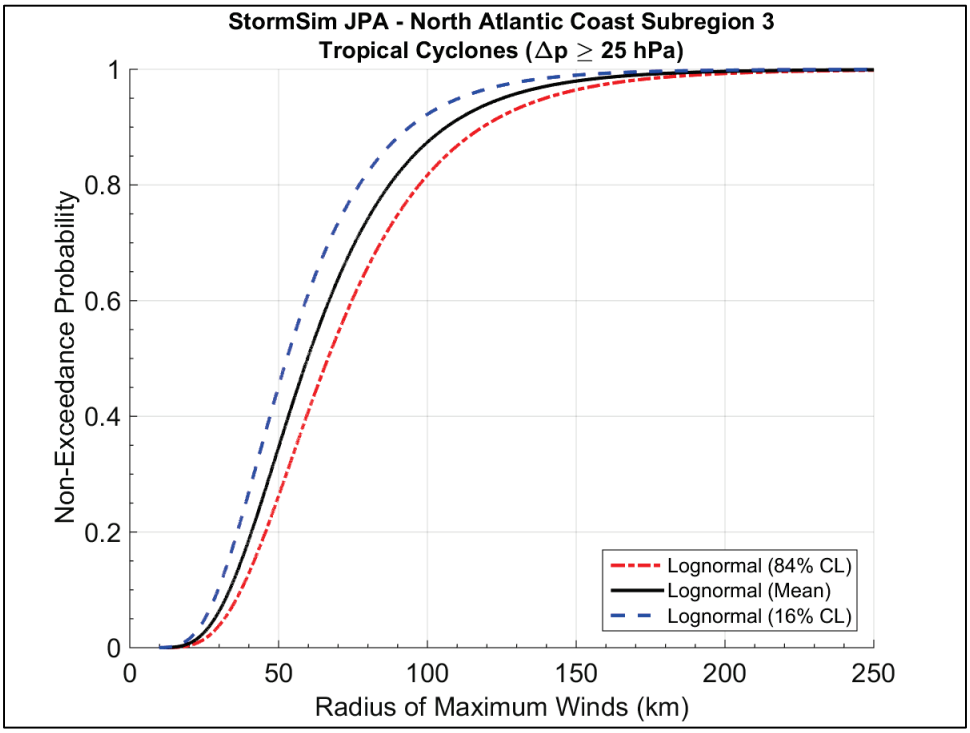

Figure 5-8. Marginal distribution of radius of maximum winds for NACCS subregion 2.

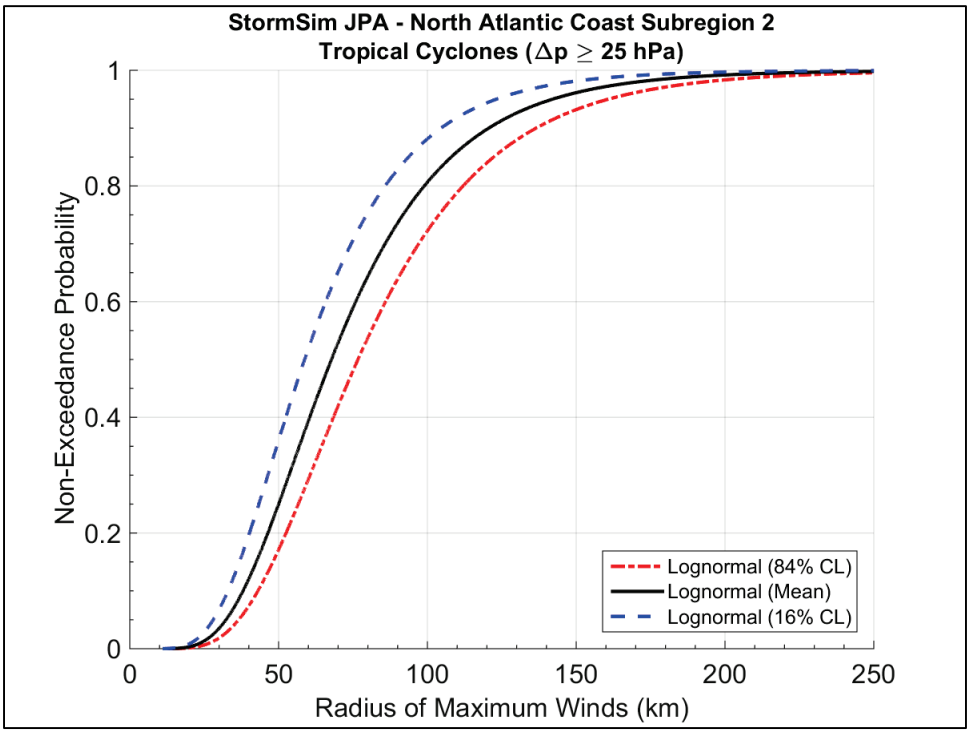

Figure 5-9. Marginal distribution of radius of maximum winds for NACCS subregion 1.

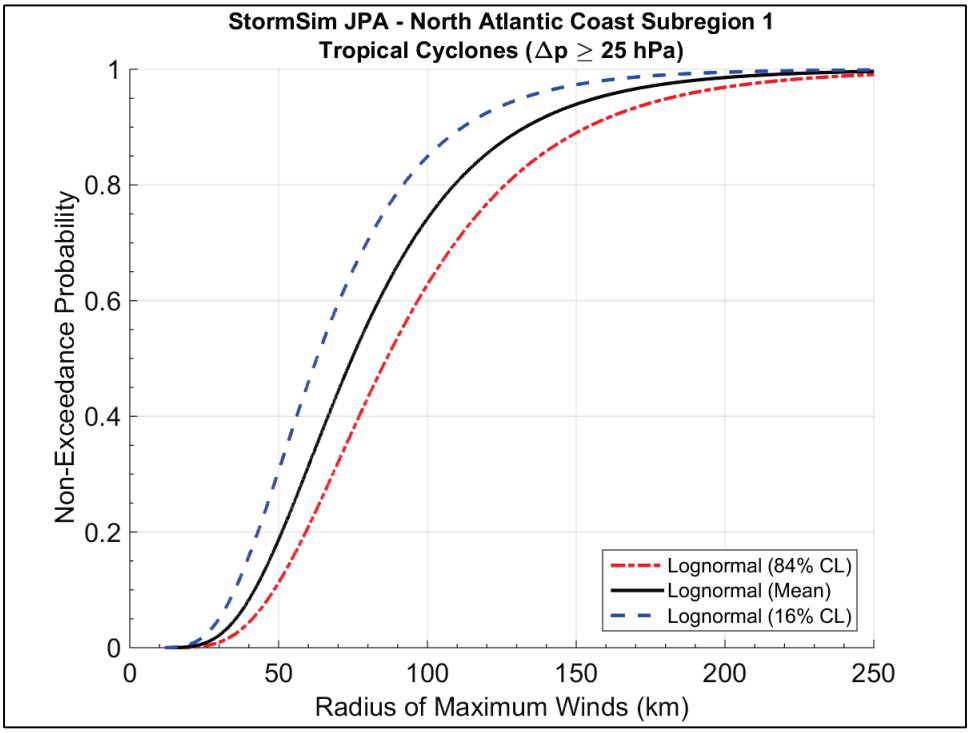

5.1.3 Translational speed (V_t)

The V_t marginal distribution is represented by the Gaussian or normal distribution model that has the form shown in Equation 5-8. The normal distribution has two parameters: mean (μ) and standard deviation (σ).

$$f(x) = \frac{1}{\sigma\sqrt{2\pi}} exp\left[-\frac{1}{2}\left(\frac{x-\mu}{\sigma}\right)^2\right] \quad (5\text{-}8)$$

The values of the normal distribution parameters for each subregion are listed in Table 5-3.

Table 5-3. Translational speed marginal distribution parameters.

NACCS Subregion	μ (km/h)	σ (km/h)
3	27.12	12.18
2	44.05	16.06
1	49.20	15.19

The translational speed marginal distributions for subregions 3, 2, and 1 are plotted in Figures 5-10, 5-11, and 5-12, respectively.

Figure 5-10. Marginal distribution of translational speed for NACCS subregion 3.

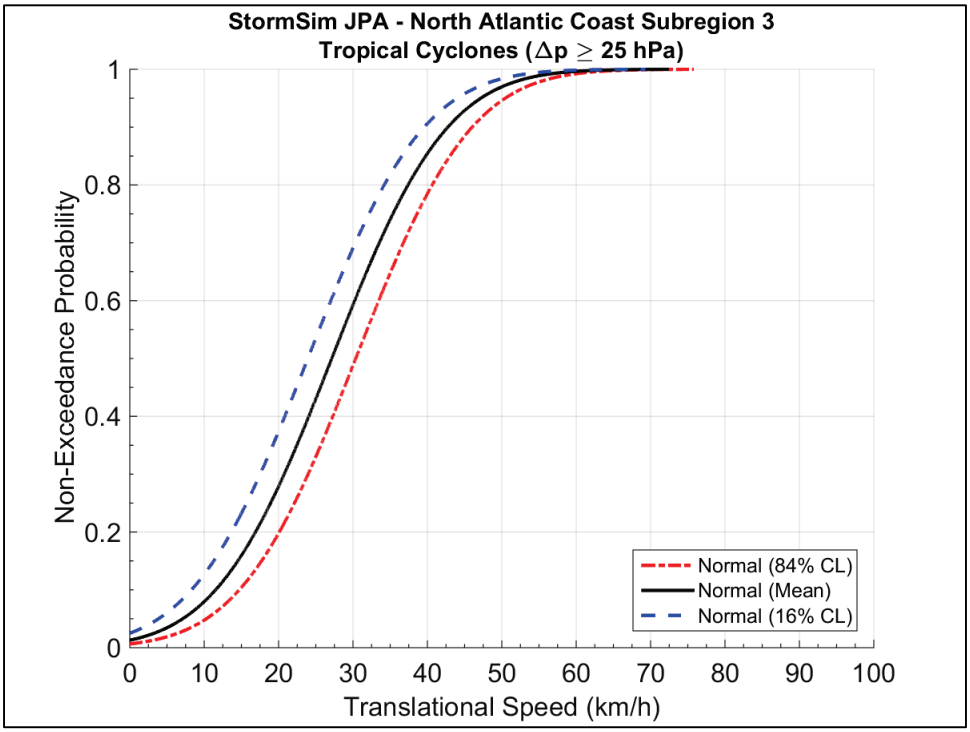

Figure 5-11. Marginal distribution of translational speed for NACCS subregion 2.

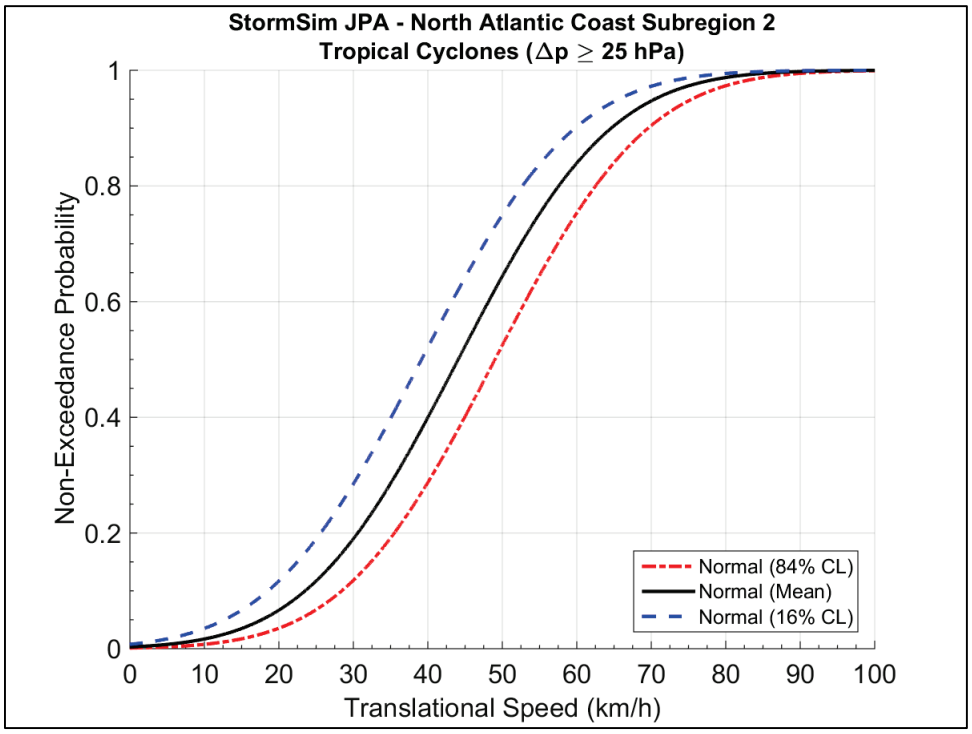

Figure 5-12. Marginal distribution of translational speed for NACCS subregion 1.

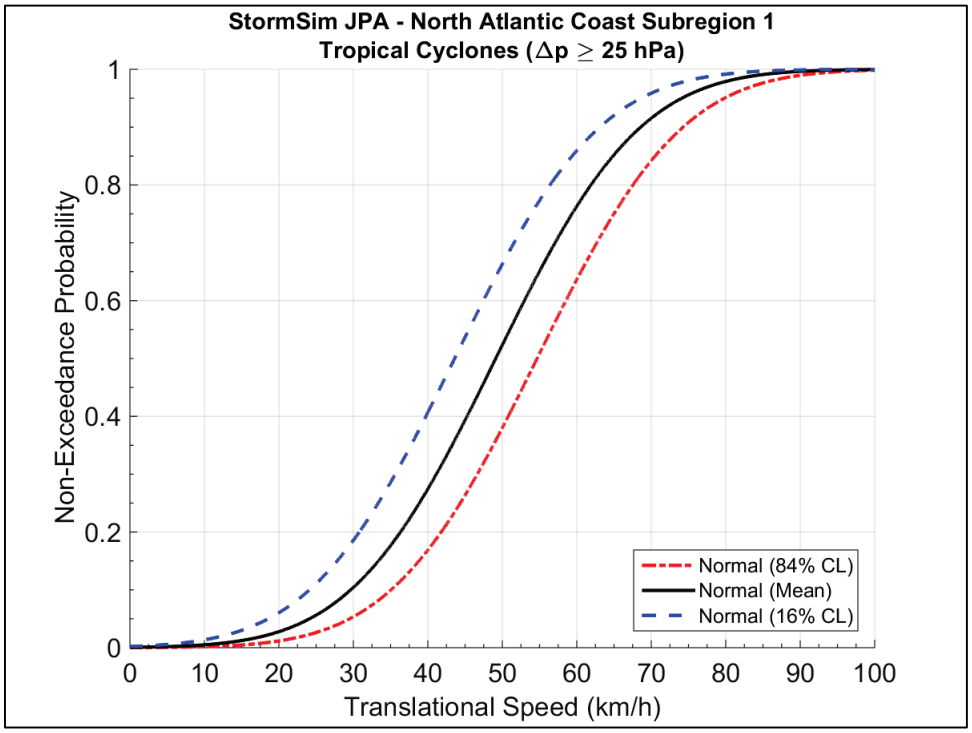

5.1.4 Heading direction

The normal distribution (Equation 5-4) is also employed to represent the TCs' θ, measured clockwise from North, where 0° indicates a TC track heading North. The values of the normal distribution parameters, μ and σ, for each subregion are listed in Table 5-4.

Table 5-4. Heading direction marginal distribution parameters.

NACCS Subregion	μ (deg)	σ (deg)
3	20.28	30.41
2	16.48	36.17
1	22.08	21.67

The θ marginal distributions for subregions 3, 2, and 1 are plotted in Figures 5-13, 5-14, and 5-15, respectively.

Figure 5-13. Marginal distribution of heading direction for NACCS subregion 3.

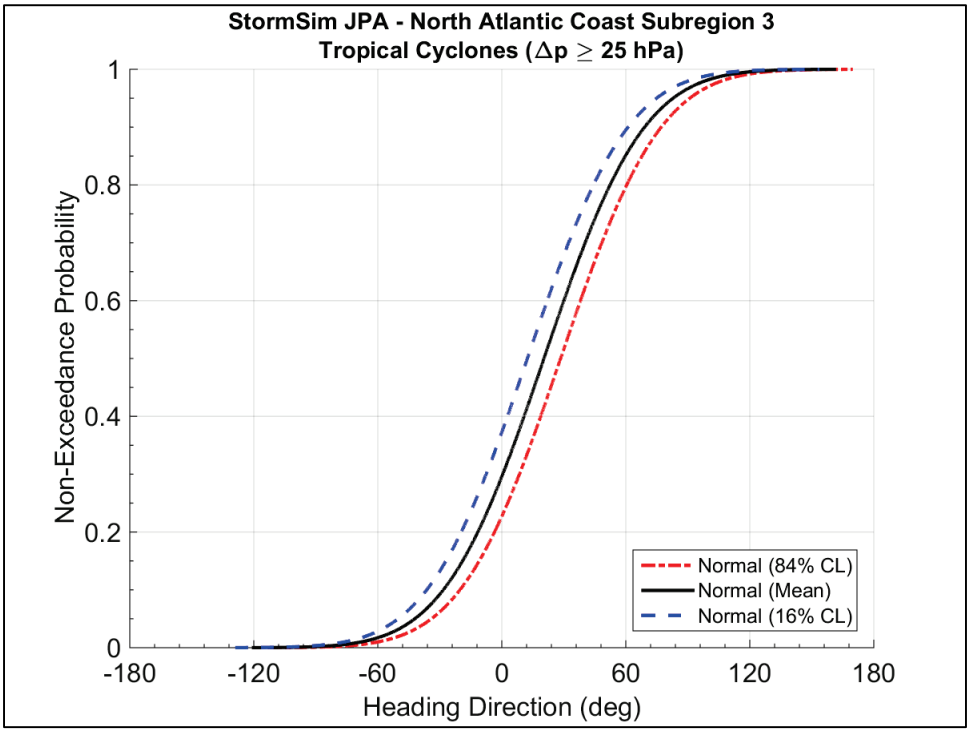

Figure 5-14. Marginal distribution of heading direction for NACCS subregion 2.

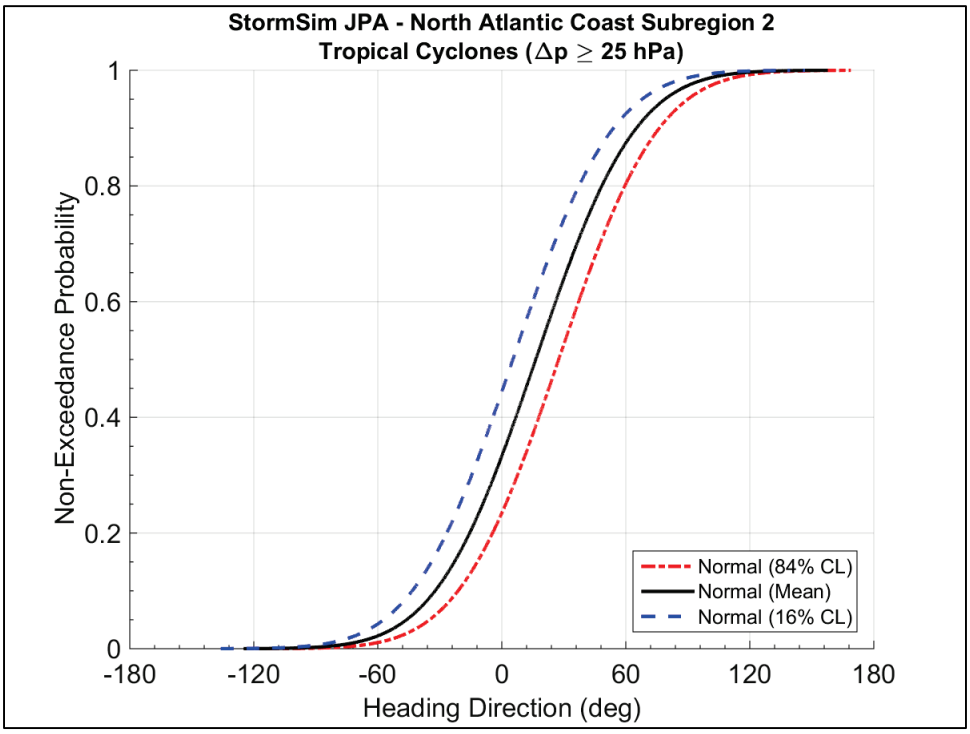

Figure 5-15. Marginal distribution of heading direction for NACCS subregion 1.

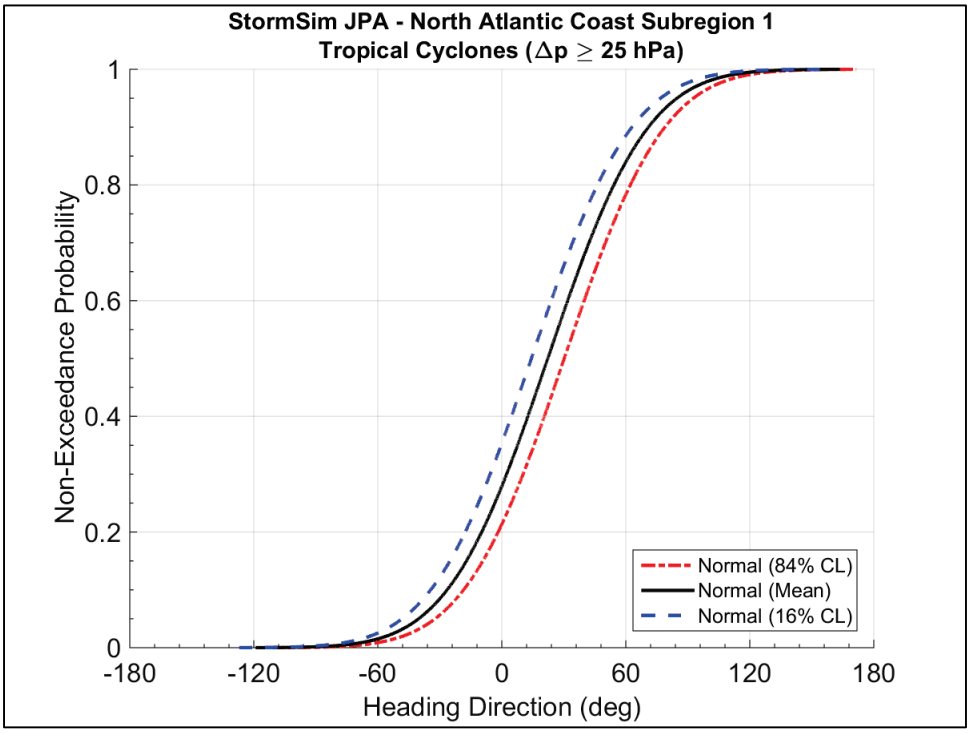

5.1.5 Holland *B*

The Holland *B* is considered a secondary JPM parameter. For this study, it was estimated based on the statistical model from Vickery and Wadhera (2008) that requires R_{max} and the latitude (ψ) associated with each track's reference location as inputs. The Holland *B* statistical model has the following form:

$$B = 1.881 - 0.00557R_{max} - 0.01295\psi \quad (5\text{-}9)$$

$$\sigma_B = 0.221$$

The Holland *B* is a dimensionless scaling parameter that controls the peakedness of the wind profile (Holland 1980). It has been found to decrease with increasing latitude and increase with decreasing radius of maximum winds. The Holland *B* parameter is directly related to the shape of the wind field and can also vary with changes in central pressure and translational speed.

5.2 Discretization of probability distributions

Most recent FEMA studies of hurricane-prone coastal areas have been based on some implementation of the JPM-OS methodology. The two most well-established JPM-OS approaches are the JPM-OS Response Surface (Resio et al. 2007) and the JPM-OS Bayesian Quadrature (Toro 2008). The Response Surface approach (JPM-OS-RS) has been used in studies throughout the Gulf coast, including Louisiana (IPET 2009) and Texas (USACE 2011). The Bayesian Quadrature Approach (JPM-OS-BQ) has been used in areas of the Gulf coast region such as Mississippi (FEMA 2008).

The focus of the JPM-OS-RS is to augment the storm sampling by interpolating intermediate values from response surfaces. The interpolated values have been shown to introduce additional uncertainty with RMSD on the order of 0.70 m (CPRA 2013). The added uncertainty is seldom quantified in these studies. The JPM-OS-RS also requires expert judgment for the selection of the storm parameters and associated discrete weights. The JPM-OS-BQ approach employs a quadrature scheme that selects the optimal storm parameters and assigns the appropriate discrete weights.

In this study, a hybrid optimal sampling method was employed for the discretization of the marginal distributions of TC parameters. To ensure optimum coverage of both probability and parameter spaces, as well as spatial coverage of the study area, a structured discretization approach was used for the Δp and θ marginal distributions. The discretization of the R_{max} and V_t marginal distributions were performed using the Bayesian Quadrature method. The values resulting from the discretization of the marginal distributions are listed in Table 5-5. These values are applicable from the genesis of each TC up to the corresponding offshore reference point (ORP) 250 km from landfall along the track path and then allowed prelandfalling filling as described in Section 5.5.

Table 5-5. Discrete values of synthetic TC parameter marginal distributions.

Tropical Cyclone Parameters	NACCS Subregion 3	NACCS Subregion 2	NACCS Subregion 1
Heading direction	-60°, -40°, -20°, 0°, +20°, +40°	-60°, -40°, -20°, 0°, +20°, +40°	-60°, -40°, -20°, 0°, +20°, +40°
Central pressure deficit	From 28 to 98 hPa at 5 hPa intervals	From 28 to 88 hPa at 5 hPa intervals	From 28 to 78 hPa at 5 hPa intervals
Radius of maximum winds	From 25 to 145 km, median of 54 km	From 25 to 158 km, median of 62 km	From 26 to 174 km, median of 74 km
Translational speed	From 12 to 59 km/h, median of 27 km/h	From 14 to 88 km/h, median of 45 km/h	From 16 to 83 km/h, median of 49 km/h
Holland *B*	From 0.45 to 1.32	From 0.56 to 1.35	From 0.66 to 1.37

Based on careful *H*Wind* (Powell et al. 2010) analyses by OWI, the R_{max} of Hurricane Sandy corresponding to the NACCS area ranged between 130 and 140 km. For comparison purposes, synthetic TCs resulting from the optimal sampling process have R_{max} as large as 170 km. This indicates that the storm-parameter optimization performed as part of the NACCS resulted in a suite of synthetic TCs with a wider range of parameter values than the historical occurrences, including cyclones more intense and of larger size than Hurricane Sandy. This allows accounting for storm responses generated by a wide range of storms from frequent (e.g., 1 yr AEP) to extremely rare (10^{-4} AEP).

5.3 Correlation between central pressure deficit and maximum wind speed

The correlation between Δp and W_{max}, considering all Atlantic basin TCs in HURDAT2, was 0.9211. The joint probability distribution of Δp and W_{max} is plotted in Figure 5-16 along with their respective marginal histograms.

Figure 5-16. Joint probability distribution of central pressure deficit and maximum wind speed with marginal histograms.

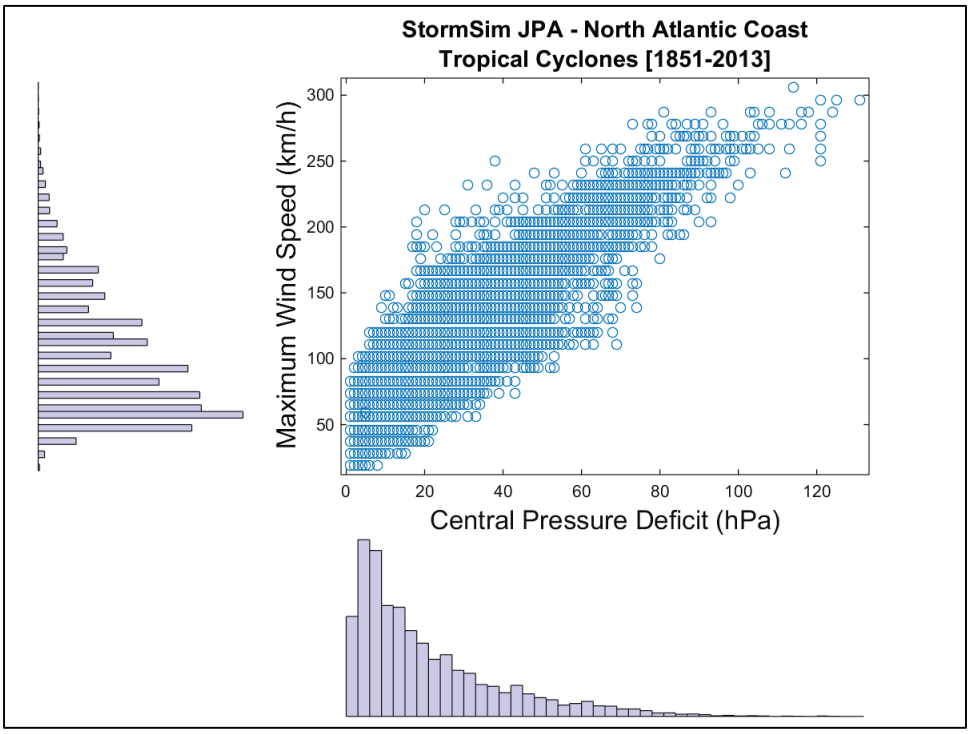

The relationship between Δp and W_{max} can be adequately described by a simple statistical model:

$$W_{max} = 42.4807 - 0.0084\Delta p^2 + 2.9752\Delta p \quad (5\text{-}10)$$

$$\sigma_{W_{max}} = 18.66$$

This model is plotted in Figure 5-17 with the mean, 98%, and 2% CL curves. Table 5-6 shows the range of intensities, based on the SSHWS, represented by the synthetic TCs as a function of Δp.

Figure 5-17. Joint probability distribution of central pressure deficit and maximum wind speed with polynomial regression.

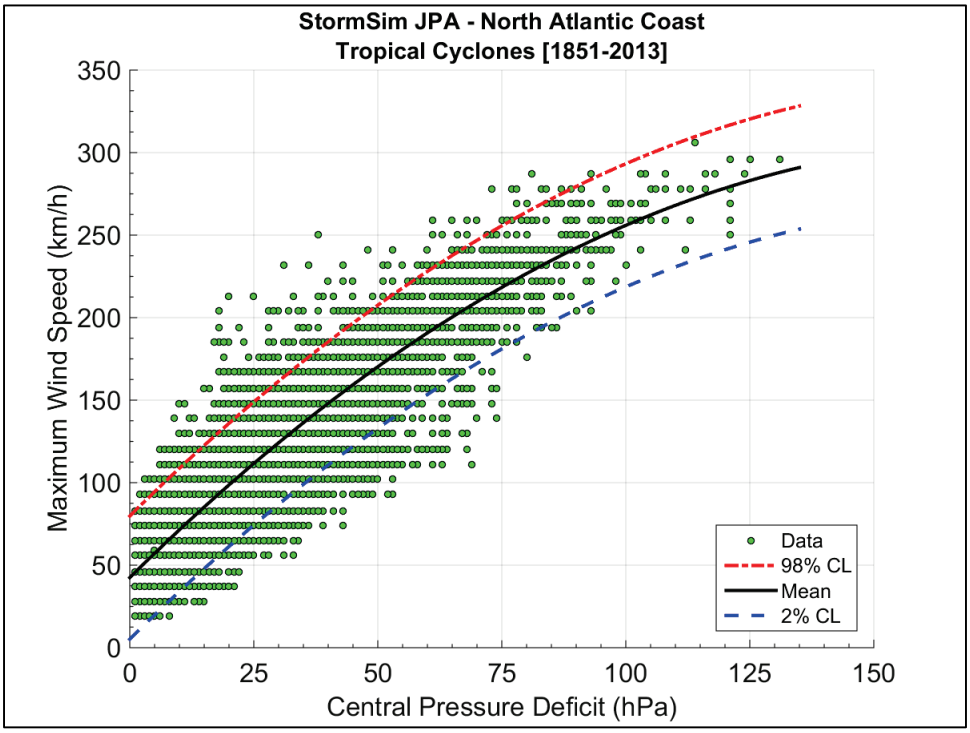

Table 5-6. Classification of synthetic TCs based on the SSHWS.

Central Pressure Deficit (hPa)	2% CL		Mean		98% CL	
	Maximum Wind Speed (km/h)	SSHWS Category	Maximum Wind Speed (km/h)	SSHWS Category	Maximum Wind Speed (km/h)	SSHWS Category
98	216	4	253	5	291	5
93	209	4	246	4	284	5
88	202	3	239	4	277	5
83	194	3	232	4	269	5
78	186	3	223	4	261	5
73	178	3	215	4	252	5
68	169	2	206	3	243	4
63	159	2	197	3	234	4
58	149	1	187	3	224	4
53	139	1	177	2	214	4
48	129	1	166	2	203	3
43	118	TS	155	2	192	3
38	106	TS	143	1	181	3
33	94	TS	132	1	169	2
28	82	TS	119	1	157	2

Note: TS = tropical storm ($W_{max} \leq 118$ km/h)

5.4 TC master tracks

For the NACCS, four landfalling track headings of -60°, -40°, -20°, and 0° (clockwise from North) and two bypassing track headings at +20° and +40° were applied in the JPM. In all, 130 master tracks were developed. Of these, 89 were landfall track paths, and the remaining 41 were bypassing tracks.

The set of track paths corresponding to landfalling storms apply track headings at the landfall reference point (LRP), which is defined as the intersection between a TC track and the generalized coastline. Generation of the landfall locations applied linear tracks with a starting location of 35.0° N 76.1° W with parallel track spacing determined by the landfall region location. All landfalling tracks apply a constant heading from the ORP 250 km prior to landfall, through landfall, and post landfall. A natural spline fit is applied prior to (farther offshore of) the ORP to result in track paths consistent with climatology. The significance of the ORP is that at this location, the synthetic TCs will be their peak intensity.

The bypassing sets of track paths apply track headings of 20° and 40° (clockwise from North). The bypassing storm set applies storm parameters specified over the entire latitudinal range of each region (i.e., NACCS subregions 3, 2, and 1). Generation of the landfall locations for the bypassing set applied linear tracks from the region's southern latitude with parallel track spacing. All bypassing tracks apply a constant heading within each region, and transitions using a spline fit to climatologically consistent track paths while outside the region's latitudinal limits.

The prelandfall track paths for the synthetic TCs are defined by the combinations of landfall location and angle of approach. Past JPM efforts have established a master track spacing equal to the mean storm R_{max}, which is typically in the neighborhood of 60–65 km (or approximately 0.54° to 0.58°) or a maximum track spacing of 0.60°. Resio et al. (2007) employed a master track spacing of approximately 0.60° that was determined based on studies of surge response. These studies showed that the distribution of surges along a coastline scale well with a track spacing of 0.60° for a wide range of storm sizes and offshore slopes. Another study (FEMA 2008) evaluated the maximum track spacing that could be used without compromising the validity of estimated surge heights. The results of that analysis showed that a master track spacing of one R_{max} provides adequate representation of storm tracks. FEMA (2012) recommends using

a master track spacing of R_{max} with a uniformly distributed offset from the master track.

For NACCS, a nominal master track spacing of 67 km (approximately 0.60°) was initially used to generate the synthetic storm track paths. The track paths were adjusted by varying spacing across the three NACCS subregions. The final master track spacings used for subregions 3, 2, and 1 were 60, 67, and 74 km, respectively, as shown in Table 5-7.

Table 5-7. Track spacing by NACCS subregion.

Subregion	Southern Boundary	Northern Boundary	Track Spacing (km)
3	36.5°N	39.0°N	60
2	39.0°N	41.5°N	67
1	41.5°N	45.0°N	74

The resulting 130 master tracks are listed in Appendix B: Synthetic Tropical Cyclone Master Tracks. Figures 5-18 through 5-21 show the track paths corresponding to landfalling TCs. The bypassing track paths are depicted in Figures 5-22 and 5-23. All 130 master track paths are displayed in Figure 5-24.

Figure 5-18. Landfalling -60° master tracks for the NACCS region.

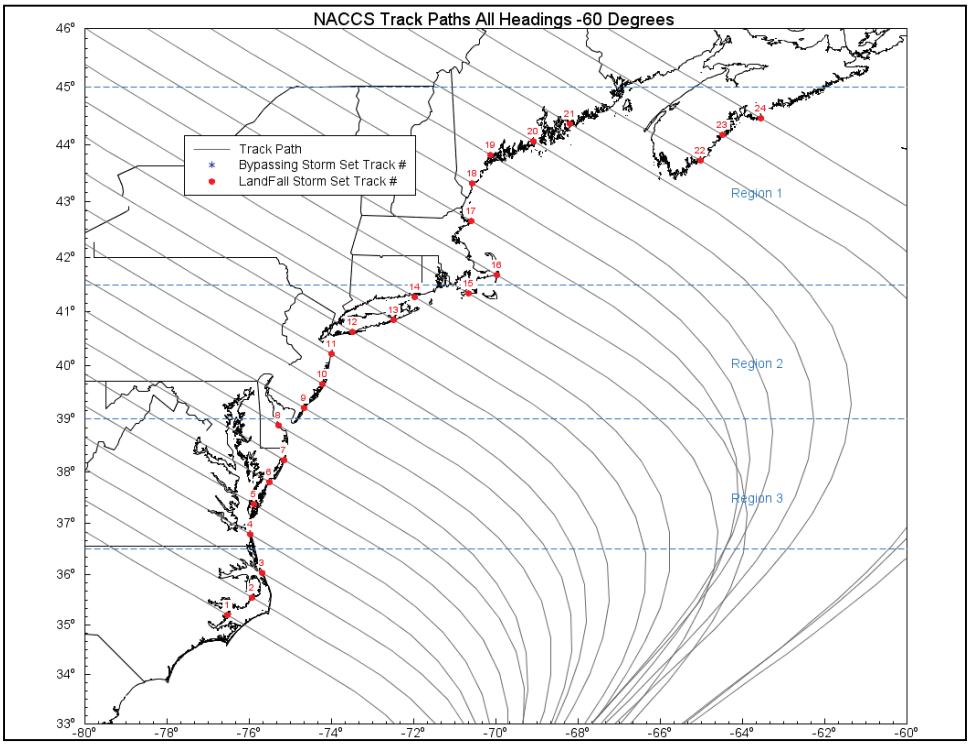

Figure 5-19. Landfalling -40° master tracks for the NACCS region.

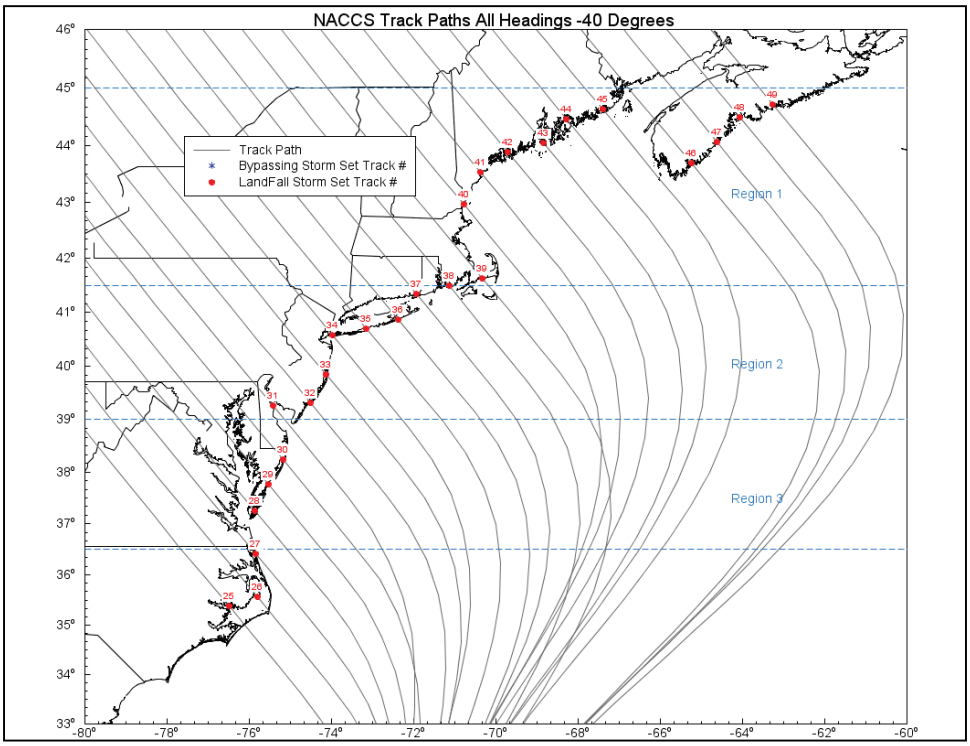

Figure 5-20. Landfalling -20° master tracks for the NACCS region.

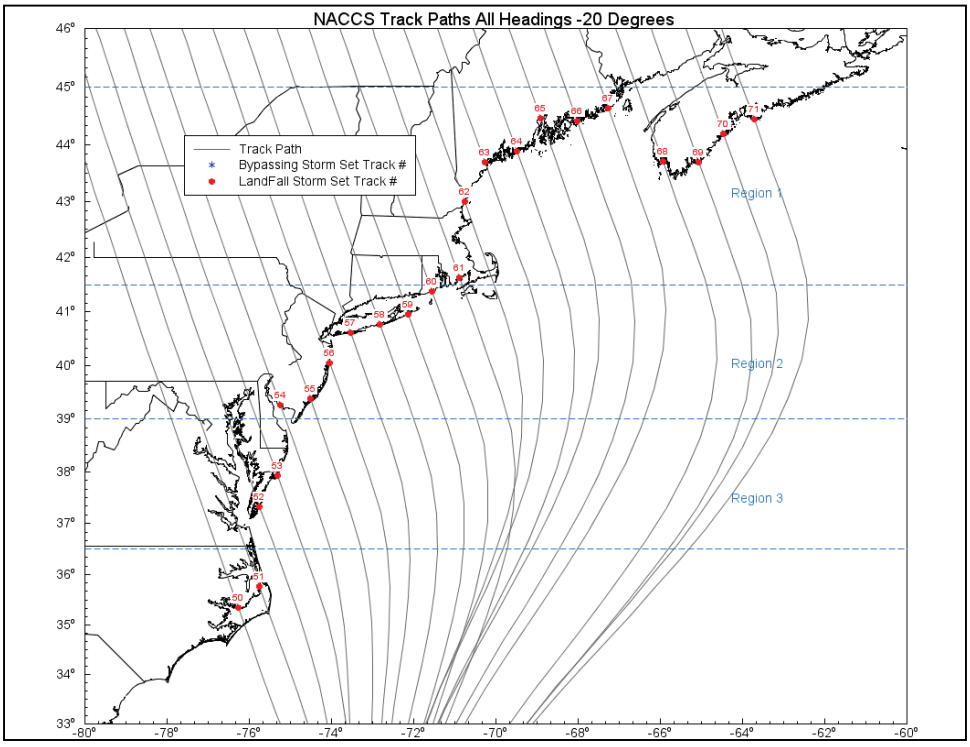

Figure 5-21. Landfalling 0° master tracks for the NACCS region.

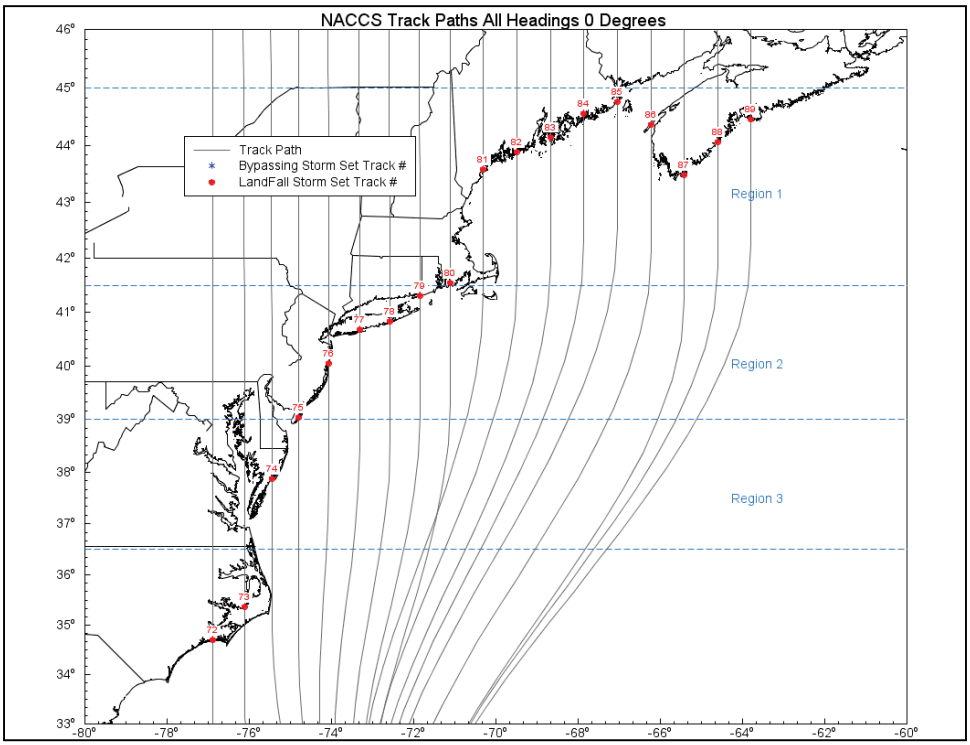

Figure 5-22. Bypassing +20° master tracks for the NACCS region.

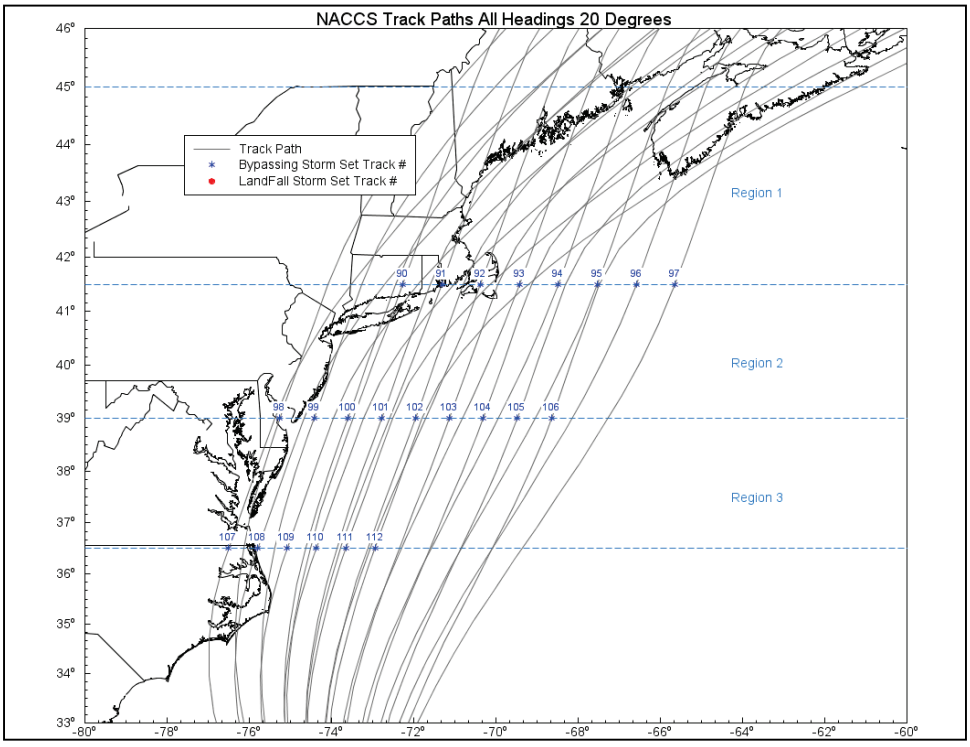

Figure 5-23. Bypassing +40° master tracks for the NACCS region.

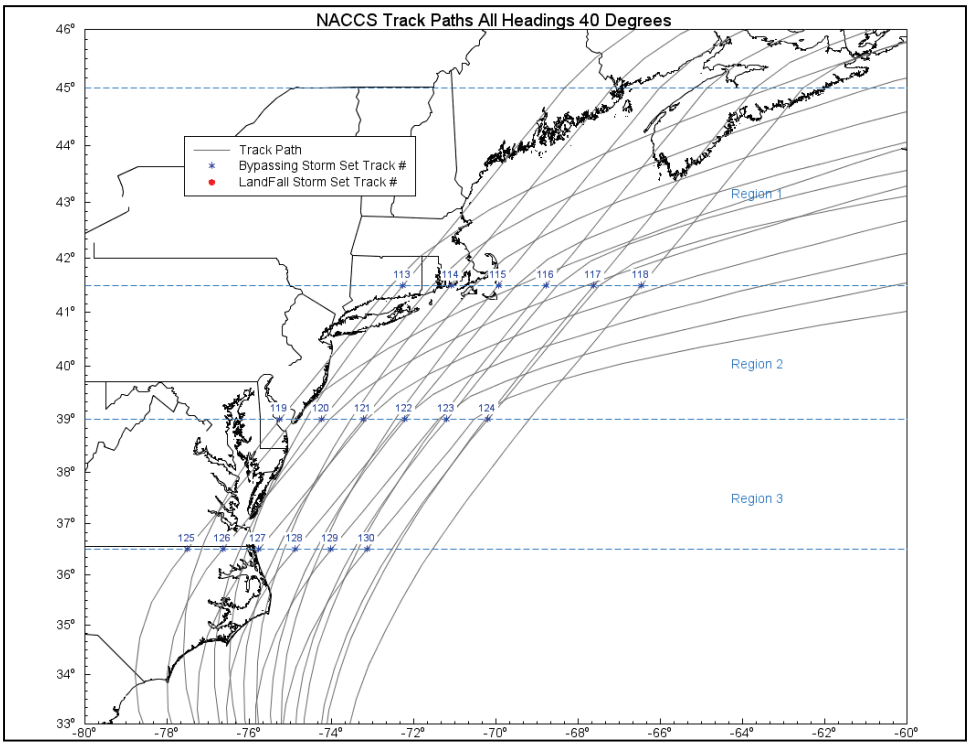

Figure 5-24. Master tracks (landfalling and bypassing) for the NACCS region.

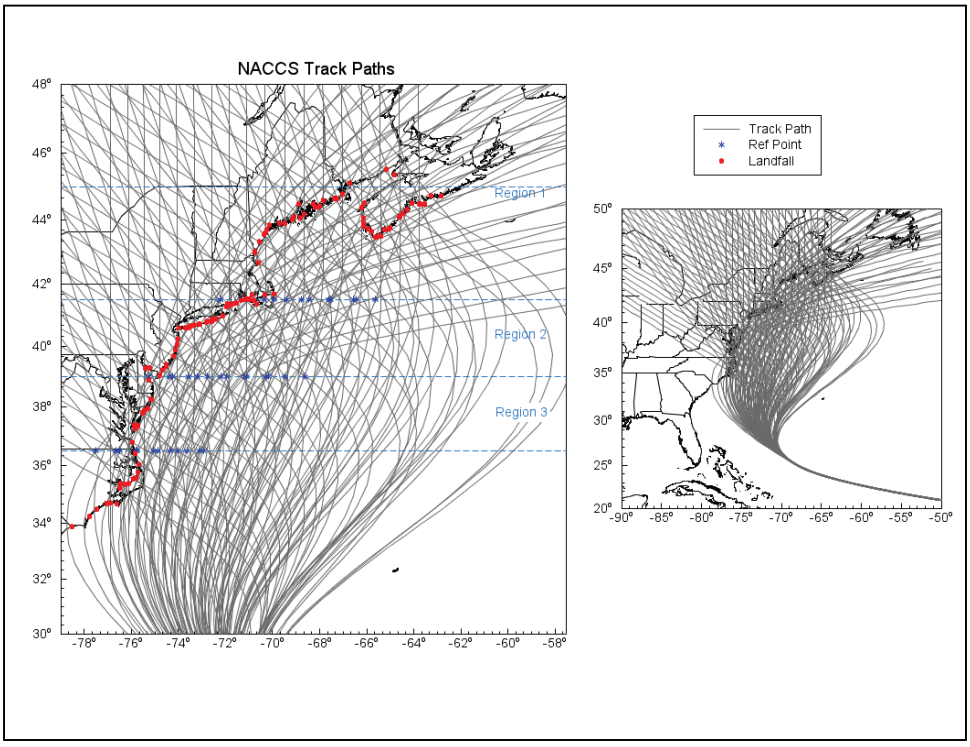

5.5 Along-track variations of TC parameters

As mentioned in Section 5.4, varying x_o and θ resulted in a total of 130 master tracks (see Appendix B). In order to complete the synthetic storm set, different combinations of the remaining parameters, Δp, R_{max}, V_t, have to be assigned to each of the master tracks. In Section 5.2 it was discussed that structured discretization was used for Δp and θ. Discretization of the marginal distributions through Bayesian Quadrature optimization was used for the remaining parameters: R_{max} and V_t. This process resulted in a total of 1,050 synthetic TCs for the NACCS region giving an average of 8 cyclones per master track. The final suite of synthetic TCs is listed in Appendix C: NACCS Synthetic Tropical Cyclones.

In the case of landfalling TCs, the storm parameters Δp, V_t, R_{max} are valid at the ORP and are allowed prelandfalling filling of the storm as described in Section 5.5.1. All track sets which include a landfall location apply the postlandfall filling model described in Section 5.5.2. The bypassing TCs use constant Δp, V_t, R_{max} across the respective region latitudinal limits (Table 3-1) and then apply a postregion filling model while over the ocean, which is described in Section 5.5.3. In the case of bypassing storms which make landfall prior to entering the region, the JPM parameters are specified at and prior to landfall and then apply the Vickery postlandfall filling model afterwards. All storms are allowed a maximum of one landfall location. Overall storm duration was determined by V_t as shown in Table 5-8. Subregion 2 and 3 bypassing storms are allowed a longer time period after exiting their respective regional latitudinal limits.

Table 5-8. Translational speeds and segment durations of JPM TCs.

Translational speed (km/h)	Hours Prior to ORP or Southern Boundary (Spin Up)	Hours Post ORP or Northern Boundary (Spin Down) Landfalling/Bypassing Subregion 1	Hours Post Northern Boundary (Spin Down) Bypassing Subregions 2 and 3
$V_t < 18.5$	240	48	96
$18.5 \le V_t < 37.0$	120	24	48
$37.0 \le V_t < 55.6$	90	18	36
$V_t \ge 55.6$	60	12	24

All storms applied a far-field pressure of 1,013 hPa to be consistent with the value applied in determination of pressure deficit in the JPM

development. The Holland *B* parameter, which controls the peakedness of the wind profile, was based on Equation 5-5 that applied the R_{max} and reference latitude (either at the ORP or at the crossing of the northern latitude subregional limit for bypassing storms).

5.5.1 Prelandfall filling of landfalling TCs

In the landfall set, the storm parameters are kept constant from the genesis of the TC until the ORP is reached. Then, prelandfall filling of the storm parameters is applied. The prelandfall filling rates were determined based on HURDAT2 data for the 45 historical TCs used for the development of the JPM synthetic TC set as listed in Table 5-9. Landfall locations and c_p were obtained from NWS38 (Ho et al. 1987), NOAA-NHC poststorm reports, and OWI analysis. In Table 5-9, yyyymm represents four digits for year and two for month; ddhhmm represents two digits for day, two digits for hour, and two digits for minute; LF = landfall; Lat = latitude; Lon = longitude; LF SLP = sea level pressure at landfall.

Figure 5-25 shows all the landfalling TCs within the 1938–2013 period along with the locations of c_p available in the HURDAT2 archive. Focusing on the prelandfall portion of the TCs, these pressures are expressed as the ratio of Δp offshore to the Δp at landfall as a function of distance to landfall in Figure 5-26. Since no statistically significant trend was found, based on the sampled central pressure data, a 5% decay rate was applied from the ORP to the LRP. This decaying profile was applied to the Δp prior to landfall for the JPM synthetic storm set. Since both Holland *B* and R_{max} functions from Vickery and Wadhera (2008) depend on Δp, these parameters were also recomputed during the prelandfall filling.

Table 5-9. Historical TC set considered for the computation of prelandfall filling rates.

NACCS Historical Tropical Cyclone ID	Name	Year	National Hurricane Center ID	LF yyyymm	LF ddmmhh	LF Lat (deg)	LF Lon (deg)	LF SLP (mb)	LF Reference
1	UNNAMED	1938	6	193809	211945	40.70	-72.90	946	NWS38
2	UNNAMED	1940	4	194009	030000	45.20	-66.40	990	OWI
3	UNNAMED	1944	7	194409	150300	40.91	-72.42	947	Landsea
4	BARBARA	1953	2	195308	140300	35.28	-75.91	987	Landsea
5	CAROL	1954	3	195408	311300	40.93	-72.63	960	Landsea
6	HAZEL	1954	9	195410	151445	33.97	-78.55	937	NWS38
7	CONNIE	1955	2	195508	121500	34.90	-76.20	962	Landsea
8	DIANE	1955	3	195508	171030	34.13	-77.90	987	Landsea

NACCS Historical Tropical Cyclone ID	Name	Year	National Hurricane Center ID	LF yyyymm	LF ddmmhh	LF Lat (deg)	LF Lon (deg)	LF SLP (mb)	LF Reference
9	IONE	1955	9	195509	191200	34.76	-76.70	960	NWS38 & Landsea
10	DAISY	1958	4	–	–	–	–	–	–
11	HELENE	1958	8	–	–	–	–	–	–
12	DONNA	1960	5	196009	122000	40.90	-72.55	959	NWS38
13	ESTHER	1961	5	196109	260600	41.51	-70.09	999	OWI LF in Cape Cod, NHC offshore
14	ALMA	1962	1	–	–	–	–	–	–
15	GLADYS	1968	14	–	–	–	–	–	–
16	GERDA	1969	16	196909	100100	44.75	-67.25	980	Landsea
17	AGNES	1972	2	197206	221930	40.60	-73.70	981	OWI
18	BLANCHE	1975	4	–	–	–	–	–	–
19	BELLE	1976	7	197608	100500	40.73	-73.25	980	Landsea
20	UNNAMED	1981	22	–	–	–	–	–	–
21	GLORIA	1985	9	198509	271600	40.73	-73.37	961	NHC
22	CHARLEY	1986	5	198608	171330	34.86	-76.42	992	NHC
23	HUGO	1989	11	198909	220400	32.90	-79.80	934	NHC
24	BOB	1991	3	199108	191800	41.40	-71.40	962	NHC
25	UNNAMED	1991	12	–	–	–	–	–	–
26	EMILY	1993	5	–	–	–	–	–	–
27	ALLISON	1995	1	–	–	–	–	–	–
28	BERTHA	1996	2	199607	122000	34.30	-77.80	974	NHC
29	FRAN	1996	6	199609	060030	33.95	-78.12	954	NHC
30	JOSEPHINE	1996	10	–	–	–	–	–	–
31	BONNIE	1998	2	199808	270400	34.40	-77.70	964	NHC
32	DENNIS	1999	5	199909	042100	34.80	-76.50	984	NHC
33	FLOYD	1999	8	199909	160630	33.80	-78.00	956	NHC
34	IRENE	1999	13	–	–	–	–	–	–
35	GUSTAV	2002	8	–	–	–	–	–	–
36	ISABEL	2003	13	200309	181700	34.90	-76.20	957	NHC
37	JUAN	2003	15	–	–	–	–	–	–
38	ALEX	2004	1	–	–	–	–	–	–
39	ERNESTO	2006	6	200609	010340	33.90	-78.10	985	NHC
40	NOEL	2007	16	–	–	–	–	–	–
41	HANNA	2008	8	200809	060720	33.80	-78.70	981	NHC
42	KYLE	2008	11	–	–	–	–	–	–
43	EARL	2010	7	–	–	–	–	–	–
44	IRENE	2011	9	201108	281300	40.60	-74.00	965	NHC
45	SANDY	2012	18	201210	292330	39.40	-74.40	945	NHC

Figure 5-25. HURDAT tracks and central pressures applied in JPM with landfall locations.

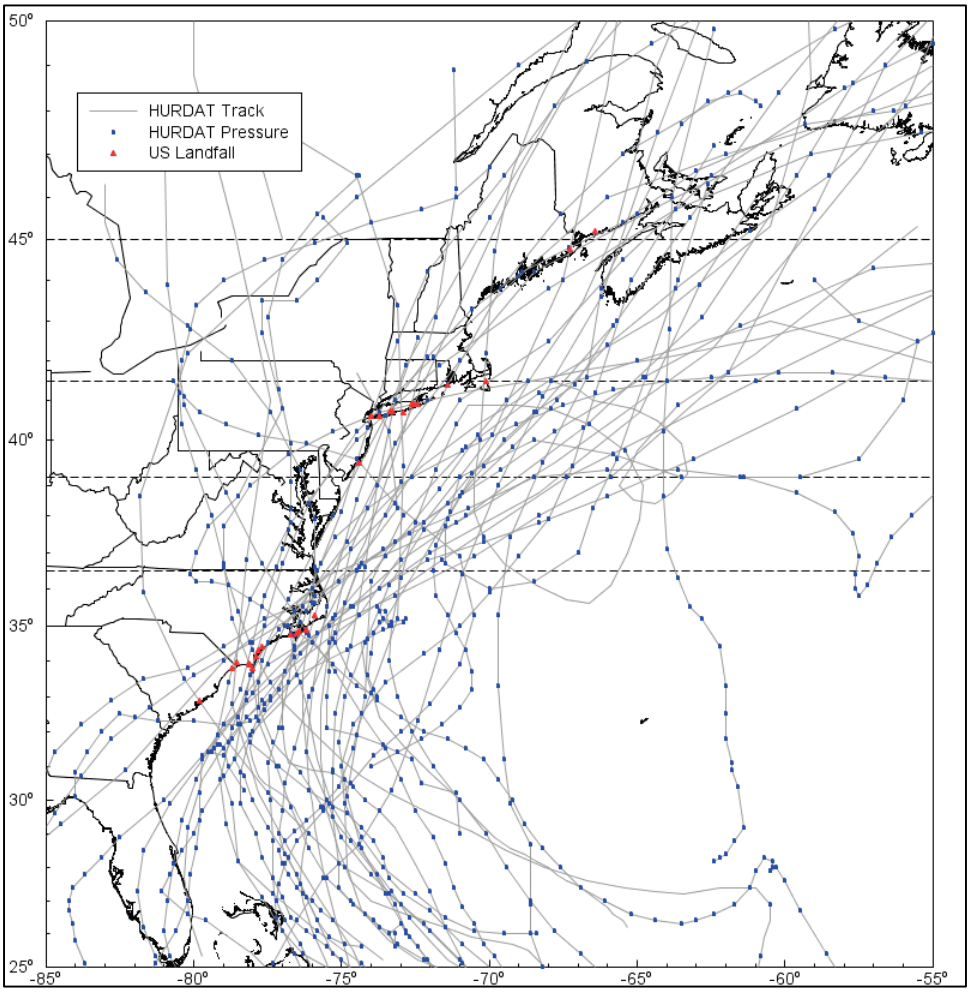

Figure 5-26. Historical data expressed as the ratio of offshore central pressure deficit to central pressure at landfall as a function of distance from landfall.

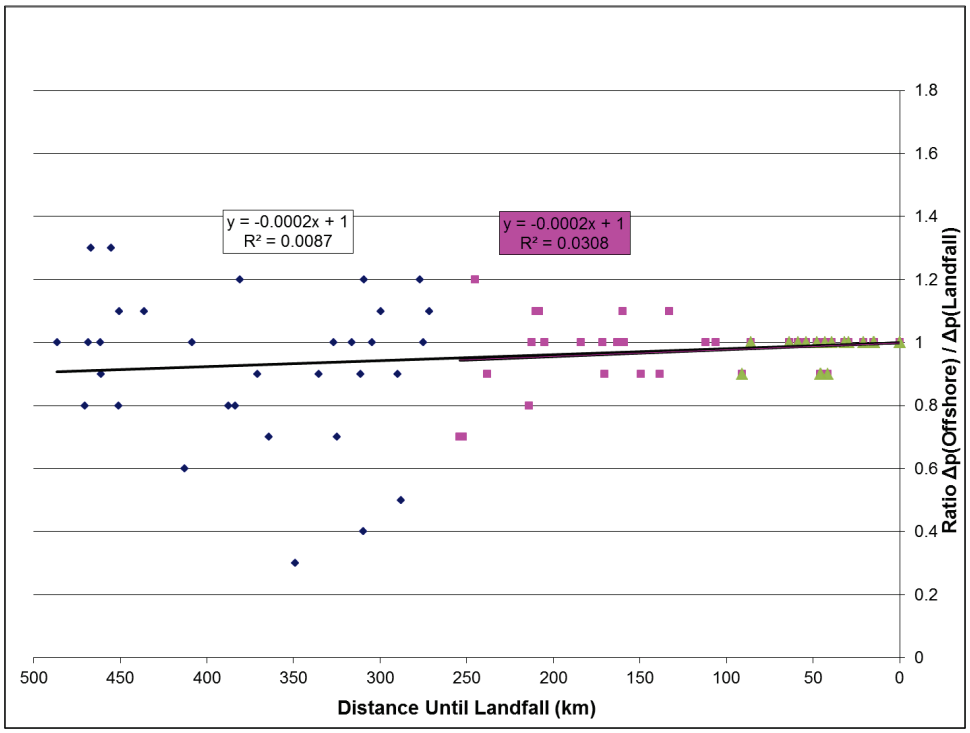

5.5.2 Postlandfall filling of landfalling TCs

All track sets which include a landfall location apply the postlandfall filling model described in Vickery (2005). The Holland B and R_{max} parameters were also recomputed during the postlandfall filling based on the functions from Vickery and Wadhera (2008).

5.5.3 Over-ocean filling of bypassing TCs

The bypassing storm set has constant TC parameters across the respective region latitudinal limits and then has postregion filling while over the ocean. The filling rates for bypassing TCs applied the same HURDAT2 data described in Section 5.5.1, but ratios were developed using the northern boundary of each region rather than landfall. Figure 5-27 through 5-29 depict all the HURDAT pressures northward of the region limits of 39°, 41.5°, and 45° for each of the historical tracks while each TC was still over the ocean.

Figure 5-27. HURDAT central pressures over the ocean northward of subregion 3.

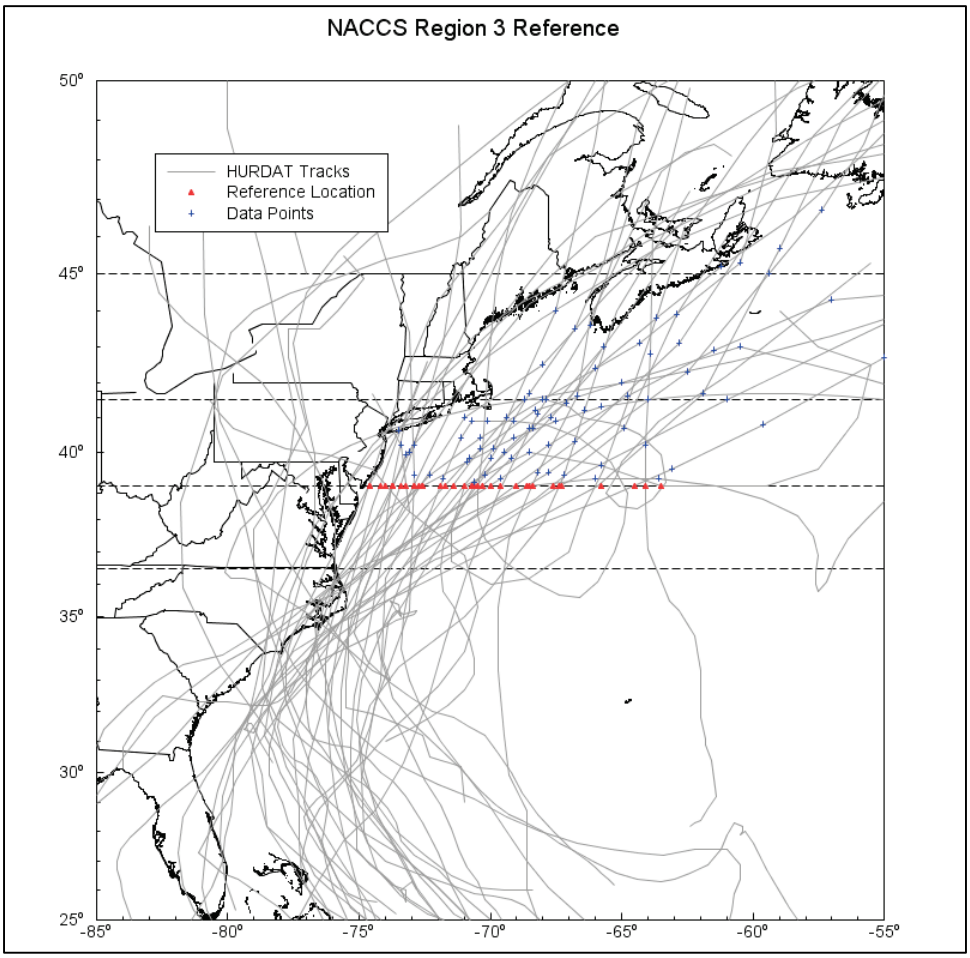

Figure 5-28. HURDAT central pressures over the ocean northward of subregion 2.

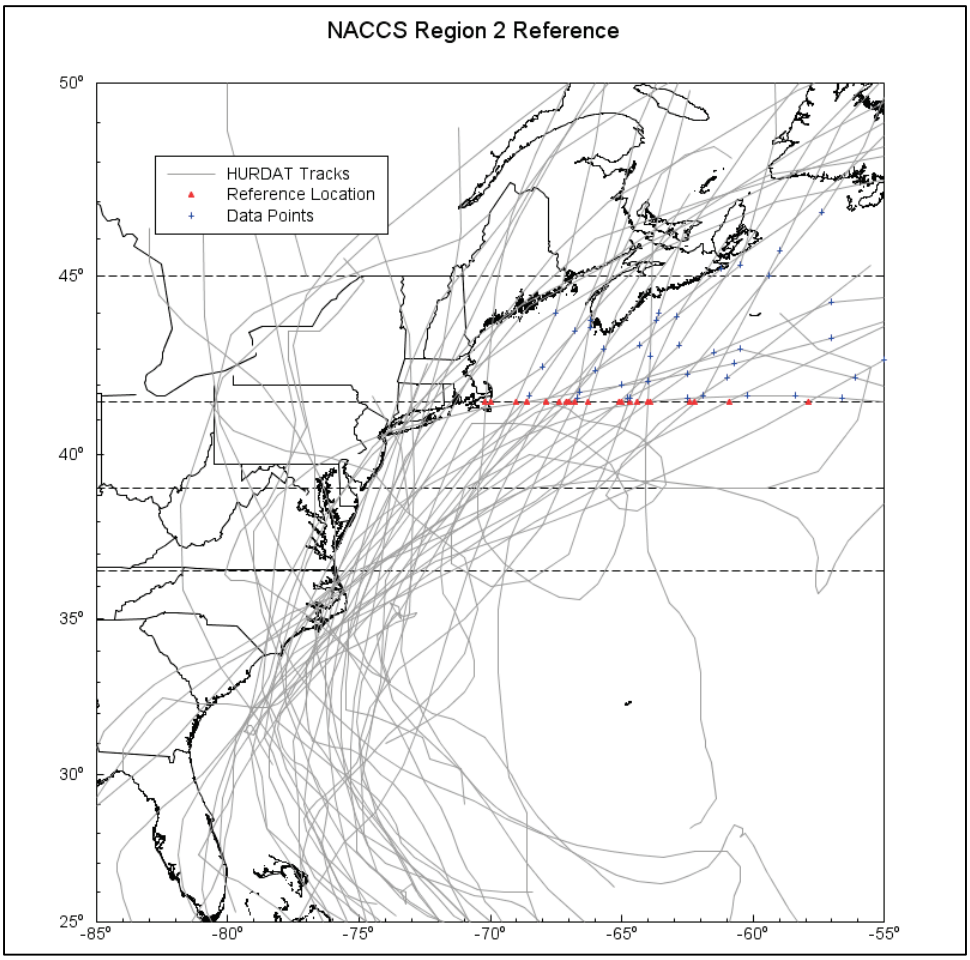

Figure 5-29. HURDAT central pressures over the ocean northward of subregion 1.

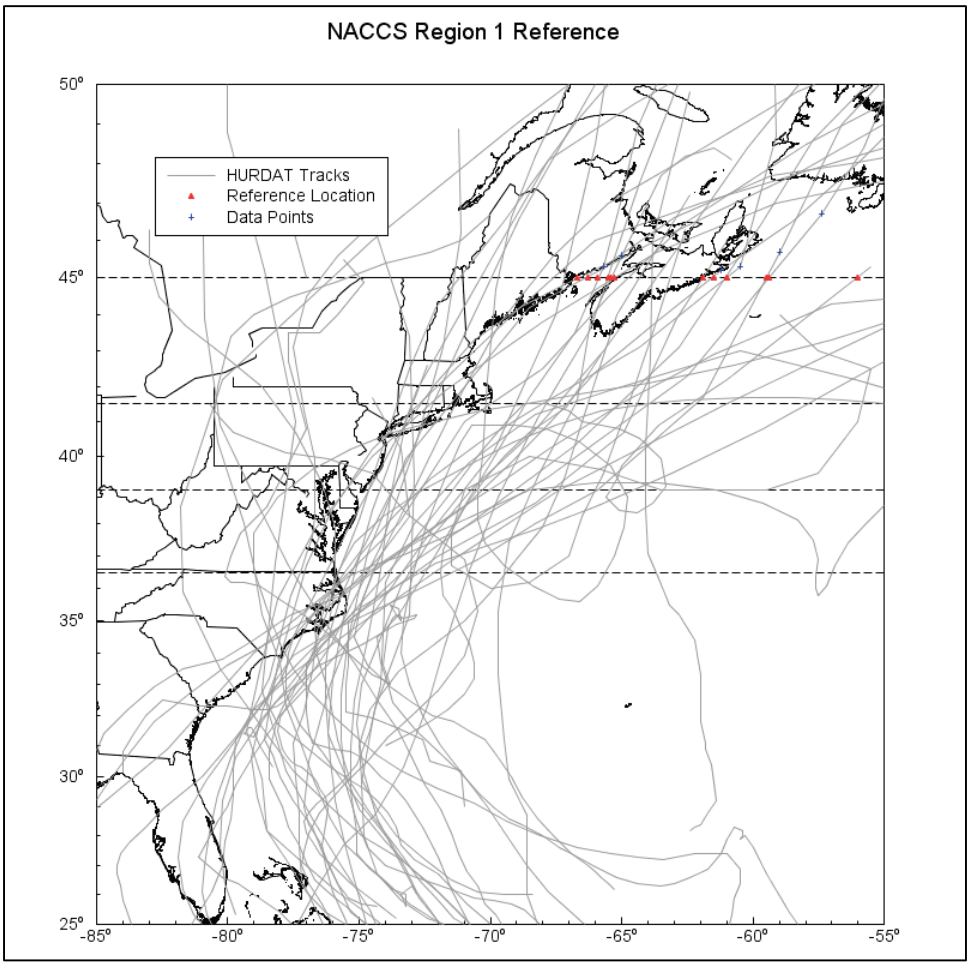

The filling rates for bypassing TCs were expressed as the ratio of Δp to the Δp at storm subregion crossing as a function of distance, as depicted in Figures 5-30 and 5-31. In this figure, reference latitude is defined as the northern boundary corresponding to each subregion. A regression fit was applied to each subregion separately and then combined to determine the applied rate. The trend shown in these figures seems to indicate that for this small sample of TCs, the Δp increases with higher latitudes, which is contrary to what was demonstrated in Section 5.1.1. Therefore, it was decided to instead apply a 5% filling rate, similar to the case of the landfalling TCs. As was also the case for landfalling TCs, both Holland B and R_{max} were adjusted using the functions from Vickery and Wadhera (2008) as TCs moved northward after closing each subregion's northern boundary.

Figure 5-30. Ratio of central pressure deficit as a function of distance from each subregion's northern boundary, separately.

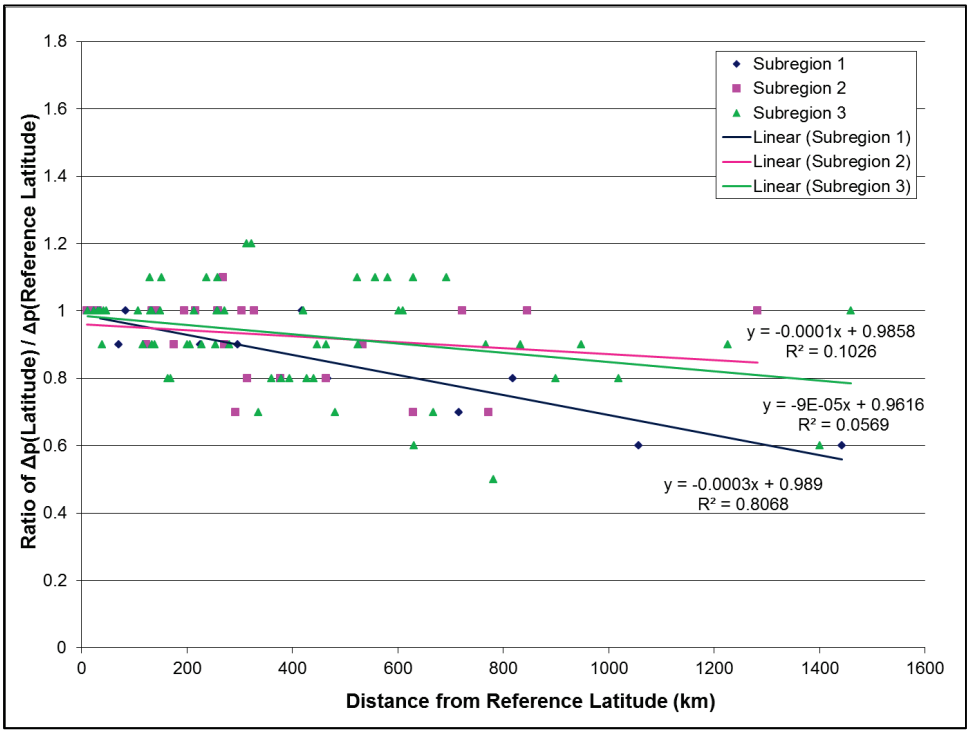

Figure 5-31. Ratio of central pressure deficit as a function of distance from each subregion's northern boundary, separately.

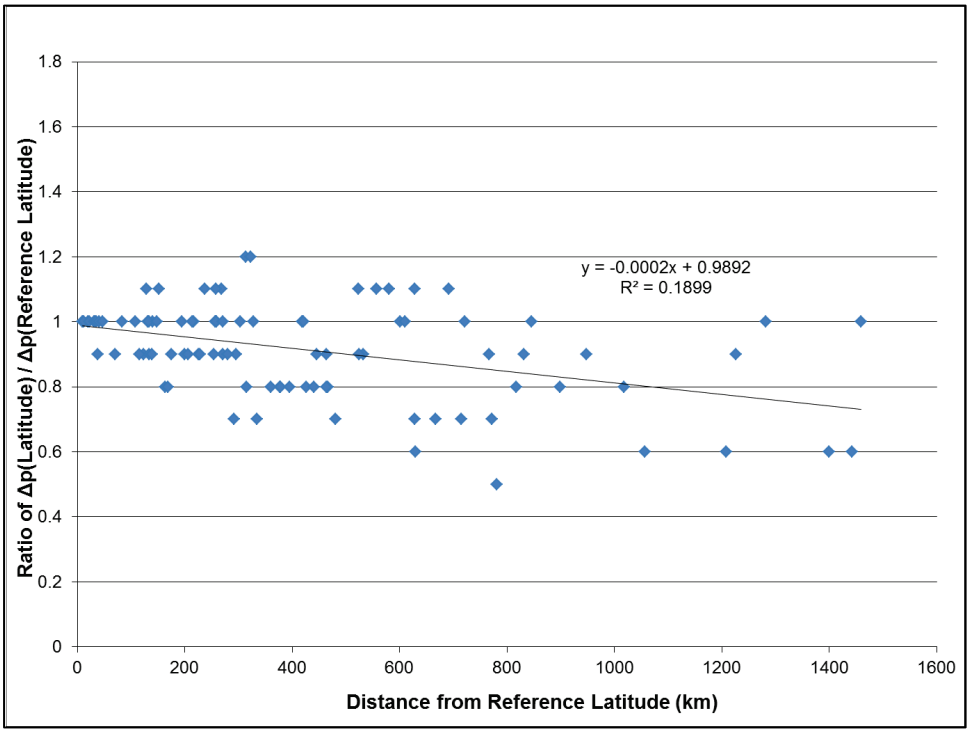

5.5.4 Scale pressure radius

In both the JPM development and in the prelandfall/postregion filling application the radius of maximum winds was used as a primary parameter to describe each storm. In the tropical model, the R_{max} is not an input value but rather the end result of running the model with the prescribed inputs. The size of a TC is primarily controlled by the scale pressure radius (R_p). A function was required to convert R_{max} to R_p. Equation 5-11 was developed by OWI and was based on a series of real historical storms of various radii, translational velocities, and latitudes.

$$R_p(nmi) = 1.1964089822 + 1.0833507089R_{max}(nmi) + 0.00697299296R_{max}^2(nmi) \quad (5\text{-}11)$$

To test if this conversion would be appropriate for use in NACCS, the PBL model was run at the reference points for the entire 1,050 storm set and R_{max} extracted. Figure 5-32 depicts the JPM R_{max} input and the PBL model R_{max} output which shows good agreement across the entire range of R_{max} required.

Figure 5-32. Input radius of maximum winds vs. OWI model output based on 1,050 synthetic TC set at reference location.

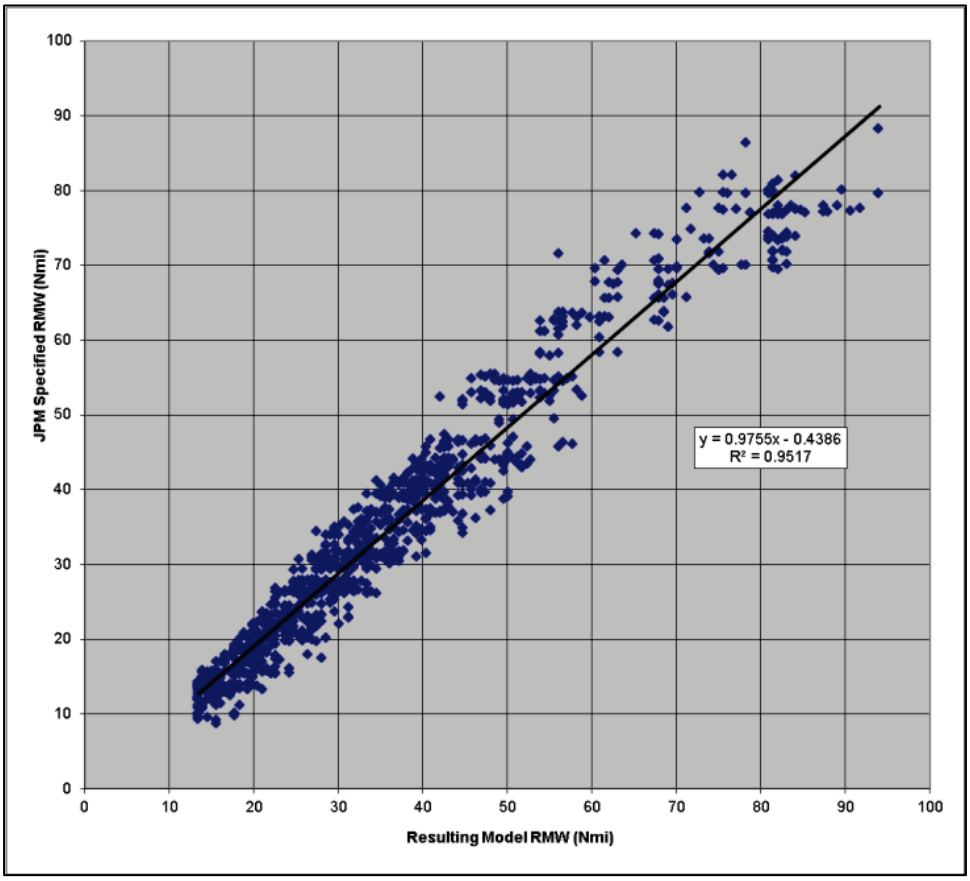

5.6 Summary of tropical wind and pressure forcing inputs

Detailed in Figure 5-33 is the summary of the track paths with model inputs R_p, Holland B, and V_t depicted as a function of c_p applied in the JPM. This figure includes the entire 1,050 JPM set and all prefilling/postfilling previously described.

Figure 5-34 is the summary graphic for NACCS_TC_0001, which is a subregion 3 landfalling storm with applied track number 1. This TC was specified with the following JPM input: Δp of 88 hPa, R_{max} of 39 km and V_t of 18 km/hr at the ORP (indicated in the upper left hand panel of Figure 5-34 by the blue-filled circle). Storm duration determined by Table 5-8 was 240 hours prior to the reference location and 48 hours afterwards. A date-time of 2000-Jul-15 00:00 UTC is arbitrarily applied for landfall. JPM parameters of Δp, V_t, R_p (Equation 5-11), and Holland B, calculated from Vickery and Wadhera (2008), were held constant from the beginning of the TC to the ORP. The parameter Δp was filled from the ORP to the LRP

using the prelandfall filling methodology, resulting in Δp of 83.6 hPa at landfall, with corresponding modifications in R_p and Holland B. Finally, Δp was modified using the postlandfall filling after landfall was made.

Figure 5-35 is the summary graphic for NACCS_TC_0268, which is a subregion 2 bypassing storm which applied track number 112. This TC was specified with the following JPM input: Δp of 38 hPa, R_{max} of 60 km and V_t of 12 km/h at the subregion 2 bypassing reference location of 39.0° N (indicated in the upper left-hand panel by the blue-filled circle). Storm duration determined by Table 4-8 was 240 hours prior to the reference location and 96 hours afterwards. A date-time of 2000- Jul-15 00:00 UTC was arbitrarily applied as the time at the northern boundary of subregion 3 (39.0° N). JPM parameters of Δp, V_t, R_p (Equation 5-11), and Holland B, calculated from Vickery and Wadhera (2008), were held constant from the beginning of the TC to the northern boundary. Although this TC is a bypassing storm, it makes landfall after it exits the subregion 2 upper latitudinal limits. The Δp of 38 hPa is applied up to region 1 (41.5° N), and then the postregion filling is applied until landfall, resulting in Δp of 32 hPa at landfall. After landfall, the landfall filling model is applied.

Figure 5-33. Summary of JPM track path and derived parameters for entire 1,050 synthetic TCs set.

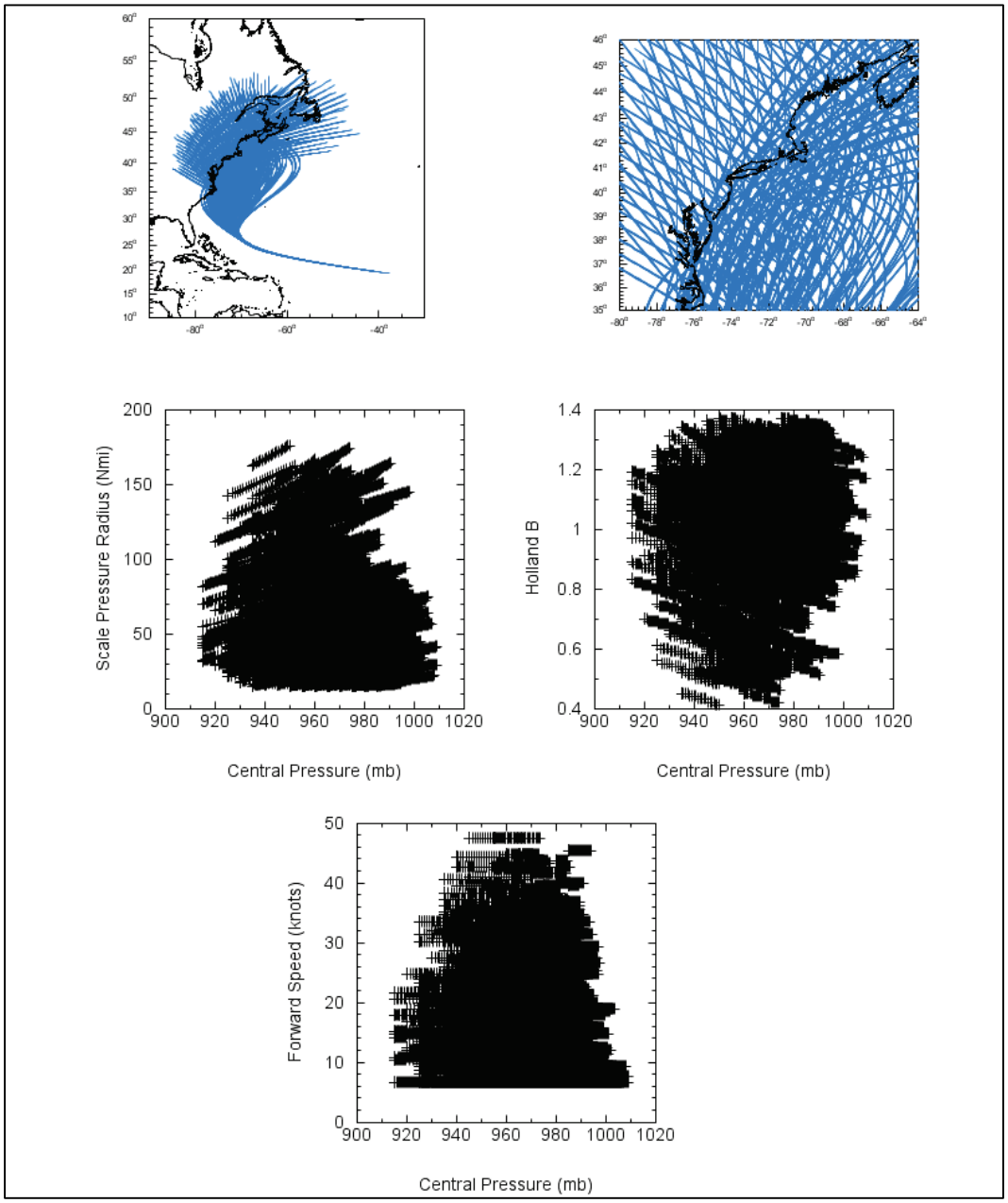

Figure 5-34. Example of along-track variation of storm parameters for a landfalling TC.

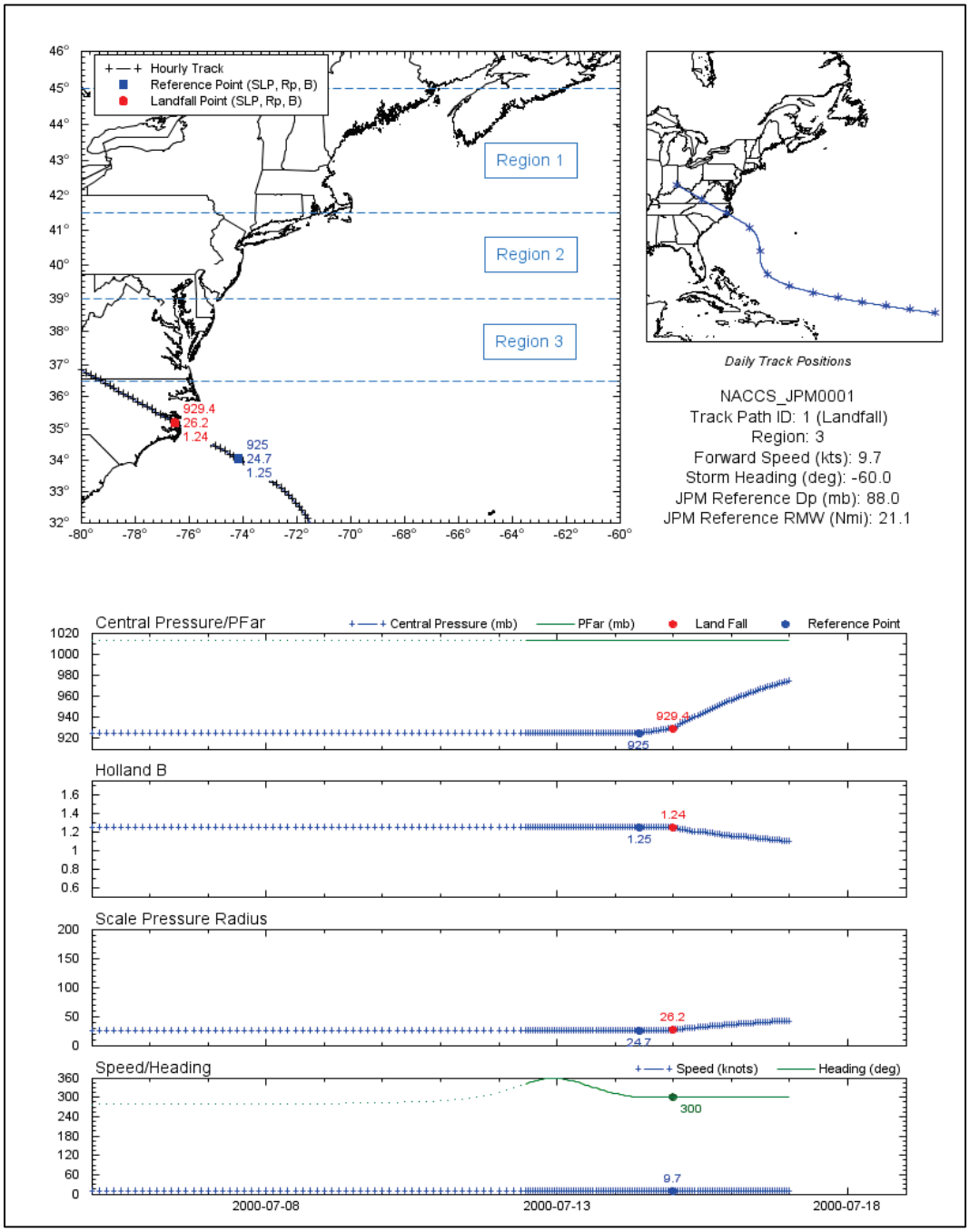

Figure 5-35. Example of along-track variation of storm parameters for a bypassing TC.

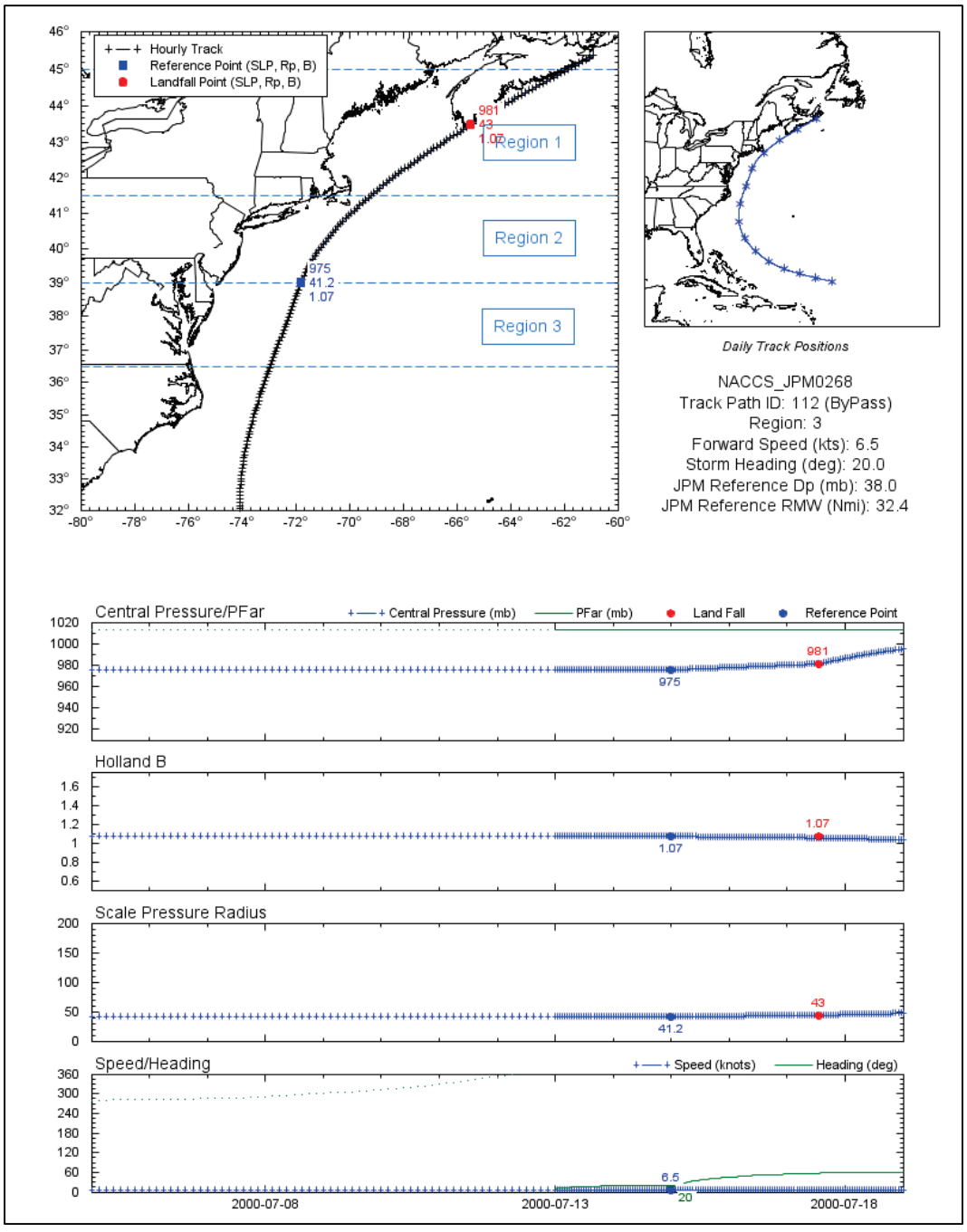

6 Quantification of Bias and Uncertainty

A natural consequence of the inherent simplification associated with the modeling of complex natural systems is that model outputs will differ in some degree from the true or actual values of the evaluated phenomena. Quantification of this difference or error is necessary in the calibration to set model parameters, in validation to ascertain the quality of the model results, and postvalidation to quantify uncertainty in a way that facilitates proper context for the data in a risk context. This chapter is primarily concerned with the third step: postvalidation quantification of model uncertainty. Two aspects of the error are typically quantified, which relate to the accuracy and precision of the results: bias and uncertainty. Bias occurs when there is a systematic difference between a model result and the corresponding true value. It is calculated as the mean of the error. A zero mean implies that there is no bias given that the model results are equally likely to fall on either side of the true value of the evaluated parameter. Once bias is identified, it can be corrected. The uncertainty of the error is given by the quantification of the variation of the result around the true value. It is calculated as the standard deviation of the error, and it is a measure of the precision of the model.

Two fundamentally distinct types of uncertainty are generally recognized: (1) aleatory uncertainty and (2) epistemic uncertainty. Aleatory uncertainty is the natural randomness of a process and is inherent in nondeterministic processes. It is often called stochastic or irreducible uncertainty, or aleatory variability. Epistemic uncertainty is associated with a lack of knowledge and is also called subjective or reducible uncertainty. Unlike aleatory variability, epistemic uncertainty can potentially be reduced through further analysis, by collecting more data, and/or performing additional research.

Epistemic uncertainty within the JPM methodology originates from several sources. These include historical observations, probabilistic models, and numerical simulation models. Application of the JPM requires correction of the bias and consideration of the epistemic uncertainty for each of its components. In the JPM methodology, it has been typically assumed that the error is unbiased and the epistemic uncertainty has been addressed through the use of an error term ε within the JPM integral, combining aleatory and epistemic uncertainties.

6.1 NACCS approach to bias and uncertainty quantification

The computation of the error term presupposes that the models used are unbiased. Biases arising from these components were estimated and corrected if they were significant. The total bias is computed as the summation of individual biases:

$$\mu_\varepsilon = \mu_{\varepsilon 1} + \mu_{\varepsilon 2} + \mu_{\varepsilon 3} + \cdots + \mu_{\varepsilon n} \quad (6\text{-}1)$$

where μ_ε = bias (mean of the error). In cases where the mean of the error is close to zero, the estimates are considered to be unbiased.

After the total bias is corrected, the unbiased uncertainty is estimated. Three assumptions regarding uncertainties that are routinely applied are that the error terms are independent, their effects can be combined by addition, and the combined error can be represented as a Gaussian distribution with mean zero. Total uncertainty can then be computed as

$$\sigma_\varepsilon = \sqrt{{\sigma_{\varepsilon 1}}^2 + {\sigma_{\varepsilon 2}}^2 + {\sigma_{\varepsilon 3}}^2 + \cdots + {\sigma_{\varepsilon n}}^2} \quad (6\text{-}2)$$

where σ_ε = uncertainty (standard deviation of the error). If there is correlation between error terms, it must be accounted for in Equation 6-2.

6.2 Errors associated with TCs

JPM components for which errors were quantified in this study include the hydrodynamic model, the meteorological model, the storm track variation, Holland *B*, and astronomical tide.

6.2.1 Hydrodynamic model results

The hydrodynamic modeling errors have been estimated as part of several recent FEMA studies. In a coastal storm surge study for Mississippi (FEMA 2008), for example, the hydrodynamic modeling or calibration error was computed from the differences between simulated and measured storm surge elevations, or high water marks. The uncertainty associated with this error, however, was estimated based on the difference between the standard deviations of the calibration and measurement errors. The measurement error was estimated as a standard deviation representing the variability in high water marks from the actual maximum water level. The calibration and measurement uncertainties were

estimated as 0.46 m and 0.40 m, respectively, resulting in a hydrodynamic modeling uncertainty of 0.23 m. In a flood insurance study for coastal Texas (USACE 2011), the hydrodynamic modeling uncertainty for the Gulf of Mexico region was estimated to be in the range of 0.53–0.76 m. In a more recent FEMA Region II study (FEMA 2014), the hydrodynamic modeling uncertainty for the New York-New Jersey region was estimated to be 0.39 m.

For the NACCS, the TC hydrodynamic modeling error was computed based on the differences between ADCIRC results and high water marks corresponding to the following North Atlantic TCs: Hurricane Isabel (2003), Hurricane Irene (2011), and Hurricane Sandy (2012). The TC hydrodynamic modeling error was found to have a bias of -0.10 m. The uncertainty associated with the hydrodynamic modeling error was estimated to be 0.48 m.

6.2.2 Meteorological model results

The errors in meteorological modeling are estimated from the variability in water levels when comparing levels simulated using PBL winds to those simulated using *handcrafted* best-winds. The wind and pressure fields derived from best-winds employ techniques that combine inputs from a variety of meteorological sources. For example, for the Mississippi coastal storm surge study (FEMA 2008), the meteorological modeling uncertainty was estimated to be 0.36 m. In USACE (2011), bias transformation functions were created to correct spatially varying biases in the meteorological modeling across the Texas coast. Bias correction factors were determined from Q-Q plots for five regions in the coast of Texas. The uncertainty for the Gulf of Mexico region was estimated to be in the 0.07–0.30 m range. In the recent FEMA (2014) study for the New York-New Jersey region, the meteorological modeling uncertainty was estimated as 0.36 m and later increased by 50% for added conservatism, resulting in 0.54 m.

For the NACCS, the TC meteorological modeling error was computed based on the differences in water level responses that were simulated using PBL winds and best-winds. For this assessment, the following five North Atlantic TCs were used: Hurricane Gloria (1985), Tropical Storm Josephine (1996), Hurricane Isabel (2003), Hurricane Irene (2011), and Hurricane Sandy (2012). The TC meteorological modeling error was found

to have a slight bias of -0.05 m. The uncertainty related to the meteorological modeling error was estimated to be 0.38 m.

6.2.3 Storm track variation

The natural random variation of storm tracks approaching the coast can have an effect on the storm surge response. In the JPM methodology, the TCs typically follow an idealized path with a straight-track approach to the coast or reference area, primarily affecting the development of wave fields. In past FEMA efforts, the uncertainty related to storm track variations not accounted for in the synthetic TC suite was estimated to be 20% of the wave setup contribution to the storm surge elevation (Resio et al. 2007; USACE 2011). Other FEMA (2008, 2014) studies have not explicitly accounted for this error.

For the NACCS, the TC track variation error was computed based on the differences in water level responses between those that were simulated using historical TC tracks to those responses from simplified, smooth, idealized JPM tracks. For this, the following five North Atlantic TCs were used: Hurricane Gloria (1985), Tropical Storm Josephine (1996), Hurricane Isabel (2003), Hurricane Irene (2011), and Hurricane Sandy (2012). The TC modeling error was found to have a small bias of -0.04 m. The uncertainty related to track idealization error was estimated to be 0.25 m.

6.2.4 Holland *B*

The effect of the Holland *B* parameter results in changes to the shape of the wind and pressure fields. It also captures the variability in W_{max} for a given Δp. The storm surge elevation has been found to vary almost linearly with changes in the Holland *B* parameter (Resio et al. 2007). The uncertainty associated with Holland *B* is typically assumed to be in the range of 10%–20% of the storm surge elevation. Some recent FEMA studies have adopted an uncertainty equal to 0.15 times the storm surge elevation (FEMA 2008; USACE 2011). In the more recent FEMA Region II study (FEMA 2014), the variation in Holland *B* was explicitly included in the storm suite, independent from of Δp and R_{max}.

Vickery et al. (2013), as part of the FEMA Region III Storm Surge Study production runs, initially used three discretizations of Holland *B* that increased the number of synthetic TCs from 156 to 468. These three

discretizations consisted of the mean Holland *B* and two values corresponding to the bounds given by $\pm 1.22\sigma_B$, where σ_B represents the uncertainty term from Equation 5-9. Based on sensitivity analyses of water level responses, the TCs corresponding to $\pm 1.22\sigma_B$ were deemed redundant and discarded since the water level statistics produced by using only the 156 TCs corresponding to the mean Holland *B* value matched the water level statistics from the full 468 TC set.

For the NACCS, the variation of Holland *B* was implicitly considered. The Holland *B* parameter was estimated from the Vickery and Wadhera (2008) model (Equation 5-9), as a function of R_{max} and latitude. This resulted in adequate variability in Holland *B* with values ranging from 0.45 to 1.37, as listed in Table 5-5 and depicted in Figure 5-33.

6.2.5 Astronomical tide and sea level change (SLC)

There are locations where the magnitude of the astronomical tide is small enough that it can be treated as an uncertainty associated with the total water level response. This has been the approach followed for the Gulf of Mexico (e.g., FEMA 2008; USACE 2011). In cases where the tide amplitude is relatively small compared to the storm surge, the purpose of this uncertainty is to capture the aleatory variability arising from the fact that the arrival of a TC can occur at any tide phase. This uncertainty is computed as the standard deviation of the predicted tide at any given location. FEMA (2008) estimated the uncertainty associated with the astronomical tide to be 0.20 m for coastal Mississippi. The large tidal amplitude along the North Atlantic coast, however, precludes its consideration as an uncertainty term. In FEMA (2014), the adopted approach consisted of simulating each storm with a random tide phase.

For the NACCS two different approaches were followed depending on the storm set type. As discussed in Section 1.3.3, a set of TCs was modeled on a unique, randomly selected tide phase. For this set, no uncertainty term was computed. Another set of TCs (TCS4) was modeled on MSL with wave effects but without astronomical tides, and after simulation, 96 randomly selected tide phases were linearly superimposed. Nonlinear residuals (NLRs) and uncertainty associated with the linear superposition of (1) storm surge and astronomical tide, and (2) storm surge and SLC were computed in this study as summarized in Chapter 7 and discussed in detail in Appendix D.

6.2.6 Summary of TC errors

The magnitudes of all biases discussed above are listed in Table 6-1. The total bias, excluding the NTR, was -0.19 m.

Table 6-1. Bias for various error components computed for the NACCS.

Type	Bias (m)
Hydrodynamic modeling	-0.10
Meteorological modeling	-0.05
Storm track variation	-0.04
Astronomical tide	variable

The values of the error terms used in the present study along with the previous JPM-OS studies for Mississippi (FEMA 2008) and Texas (USACE 2011) are listed in Table 6-2.

Table 6-2. Comparison of uncertainty estimates in JPM studies.

Uncertainty	FEMA 2008 (m)	USACE 2011 (m)	FEMA 2014 (m)	NACCS (m)
Hydrodynamic modeling	0.23	0.53 to 0.76	0.39	0.48
Meteorological modeling	0.36	0.07 to 0.30	0.54	0.38
Storm track variation	n/a	0.20* × wave setup	n/a	0.25
Holland *B*	0.15* × surge elevation	0.15* × surge elevation	n/a	elevation/a
NLR due to astronomical tide	0.20	n/a	n/a	variable
NLR due to SLC	n/a	n/a	n/a	variable

*Factor on storm surge elevation is dimensionless.

6.3 Errors associated with XCs

For the NACCS, the XC hydrodynamic modeling error was computed based on the differences between ADCIRC results and high water marks corresponding to several North Atlantic XCs. The XC hydrodynamic modeling error was found to have a bias of 0.06 m. The uncertainty associated with the hydrodynamic modeling error was estimated to be 0.25 m.

7 Analysis of Nonlinear Residuals (NLRs)

It is common practice when assessing water levels in coastal studies to separately consider components, such as storm surge, tide, and SLC, before combining them through linear superposition to determine the total water level. The use of linear superposition introduces an error due to the complex nonlinear interaction of the water level components. This error is referred to as the NLR. Although an ideal way to deal with the NLR is simply to model all water level components in a simulation to avoid using linear superposition; this would require modeling multiple scenarios to ensure that all possible variations of the components are captured. Given the complexity and extent of the NACCS hydrodynamic model, this would be impractical. For example, the peak storm surge for a modeled storm may occur on any phase of the tide. The simulation of only one random tide within the hydrodynamic model would not capture the variability represented by the possibility of the peak storm surge coinciding with a different tidal phase. To account for this variability, numerous simulations for different tide realizations would have to be run. For the NACCS study, linear superposition was used to incorporate tides and SLC in the water level results.

Methods for the quantification of NLRs and associated uncertainty were studied through a proof-of-concept study, as part of the NACCS effort, to inform the implementation of the use of linear superposition for the final modeling effort. As part of the NACCS hydrodynamic modeling effort, simulations were produced for the purpose of quantifying the bias and uncertainty associated with the NLRs. As discussed in section 1.3.3, three sets of simulations were produced from the NACCS hydrodynamic modeling. The first set or the base case corresponds to the modeling of the storms on MSL, without tide or SLC. The second set consisted of the base case plus a single random tide per storm. This set was used to assess the linear superposition of tide and surge for the NACCS results. The third set was used to assess the linear superposition of SLC in the NACCS results and consisted of the second case with a static water level adjustment of 1.0 m to simulate GSLC of the same magnitude. The storm set used for developing the hazard curves was created by linearly superimposing 96 random tides to the base condition and correcting for the nonlinearity. Refer to Section 8 of the report for a description of the development process of the hazard curves.

7.1 Proof-of-concept nonlinearity study

A proof-of-concept study was performed prior to the completion of the NACCS high-fidelity modeling to address the added uncertainty in applying linear superposition to the water level components. The results were documented in a white paper which is included in this report as Appendix D. The nonlinearity study was conducted using the computation mesh and storm climatology suite used for the FEMA Region II Risk MAP study for a smaller region of the East Coast. The study quantified the NLR and its variation for the purpose of applying this technique (linearly adding versus fully nonlinear modeling) to the more detailed domain of the NACCS modeling effort. As the intent of this effort was a proof-of-concept analysis, only one SLC realization (1.0 m) was evaluated for the smaller FEMA storm suite.

The goal of the proof-of-concept study was to answer these questions: (1) what is the magnitude and spatial variability of the NLR in assuming a linear sum of storm surge, tide and SLC, where each component is computed separately; (2) what is the statistical characterization of the NLR (bias and variability); (3) if the bias is significant, can one account for the linear assumption error with a correction term in the JPA; and furthermore, (4) can the NACCS modeling results still be used if the bias is large, and how can this be integrated with the data and statistics?

As discussed in Appendix D, the analysis showed that the linear superposition of water level components adequately represents extreme water levels with a correction factor for the small bias. Over the majority of the coastal region, the linear superposition bias was negligible (on the order of 0.1 m), and this bias can be incorporated into the results prior to the JPA. Any variability in the response (uncertainty) can be then accounted for in the JPA.

In some areas characterized by constrained geometric features like small interior bays and canals, the NLR can be non-negligible and can produce large errors in total water level elevations. In these areas, however, the NACCS results can still be applicable. For most of these areas, the NLR can still be accounted for within the statistical analysis. For the cases that the NLR is too large to account for within the JPA, the user can (1) use linear superposition of components from a nearby location that has an acceptable (lower) NLR , (2) in cases that the above method is not acceptable, the user can run additional site-specific modeling simulations,

using nearby save point locations as boundary conditions on a more detailed, localized model, or (3) use the full simulations with tide and SLC, as for example was done by FEMA (2014). The white paper (Appendix D) suggests that in the vast majority of cases, based on the full modeling suite of over 1100 storms, the NACCS results will require no additional modeling or complex statistical analysis.

7.2 NLRs due to linear superposition of astronomical tide

Results from the second storm-set simulation, which included one random realization of tide, were compared with the same random tide linearly added to the base-case scenario. A similar nonlinearity analysis was conducted for the full set of NACCS storms, at approximately 19,000 NACCS output save point locations. From the analysis of the full set of storms over the full Maine-to-Virginia modeling domain, it was found that 85% of the 19,000 NACCS points have a nonlinearity value within 0.2 m. The analysis was used to adjust the storm set used for the hazard curves, which was based on the linear superposition of 96 random tides.

7.3 NLRs due to linear superposition of sea level change (SLC)

The NLRs due to SLC were assessed utilizing the results of the third set of simulations. The 1.0 m SLC condition is approximately equal to (or higher than) the “High” value of relative SLC for all 2068 USACE High SLC values across the NACCS study area. The value of 1.0 m for SLC is also a conservative estimate of SLC for the USACE Intermediate SLC values at 2100. The results from the modeled SLC scenario and analysis techniques informed all other SLC estimates within the modeling domain from Maine to Virginia. For analyses in which other future time periods are required, the SLC can be computed by linear superposition along with linearity adjustments as required.

Refinements and updates to this process of developing SLC contributions to the numerical modeling storm parameters can be developed for adjustment/correction terms as the uncertainty of the SLC projections lessen in the future and/or during updates to the storm surge modeling work, both of which are subsequent to completion of the NACCS numerical modeling work.

7.4 Combined NLR

The NLR due to the linear superposition of storm surge and astronomical tide ($\mu_{e_{tide}}$) combined with NLRs due to the linear superposition of storm surge and SLC ($\mu_{e_{SLC}}$) was computed as the summation of the individual biases:

$$\mu_{\varepsilon_{combined}} = \mu_{\varepsilon_{tide}} + \mu_{\varepsilon e_{SLC}} \tag{7-1}$$

The combined uncertainty ($\sigma_{e_{combined}}$) was computed as follows:

$$\sigma_{\varepsilon_{combined}} = \sqrt{\sigma^2_{\varepsilon_{tide}} + \sigma^2_{\varepsilon_{SLC}}} \tag{7-2}$$

8 Joint Probability Analysis of Coastal Storm Hazards

This chapter focuses on the statistical analyses of storm responses obtained from the numerical modeling of all storms, tropical and extratropical. As discussed in Section 2.1.2, JPM methodology generally consists of the following steps:

- characterization of storm climatology
- computation of spatially varying SRR
- storm parameterization and development of probability distributions of storm parameters
- discretization of probability distributions of storm parameters
- development of synthetic storm set
- meteorological and hydrodynamic simulation of synthetic storms
- estimation of errors and other secondary terms
- integration of joint probability of storm responses, including extratropical events.

8.1 Characterization of TC climate

The characterization of storm climate was previously discussed in Chapter 3. For the development of the synthetic TC suite, 45 historical landfalling and bypassing TCs were selected from HURDAT2 within the 1938–2013 period (Table 3-4). For the JPA of TC responses, the 45-TC historical set was expanded to 112 TCs with $\Delta p \geq 23$ hPa, either making landfall or passing within 300 km of the study area during the same period (Appendix E).

8.2 Computation of spatially varying SRR

The computation of SRR was discussed in detail in Chapter 4. The SRR_{200km} for low-intensity TCs (28 hPa $\leq \Delta p <$ 48 hPa) in the entire Atlantic basin for the 1938–2013 period are presented in Figure 8-1. The SRR_{200km} corresponding to high-intensity TCs ($\Delta p \geq 48$ hPa) for the same period are shown in Figure 8-2. The GKF SRR (adjusted by +10%) for low- and high-intensity TCs at the 23 locations are listed in Table 8-1.

Figure 8-1. SRR_{200km} for low-intensity TCs during the 1938–2013 period.

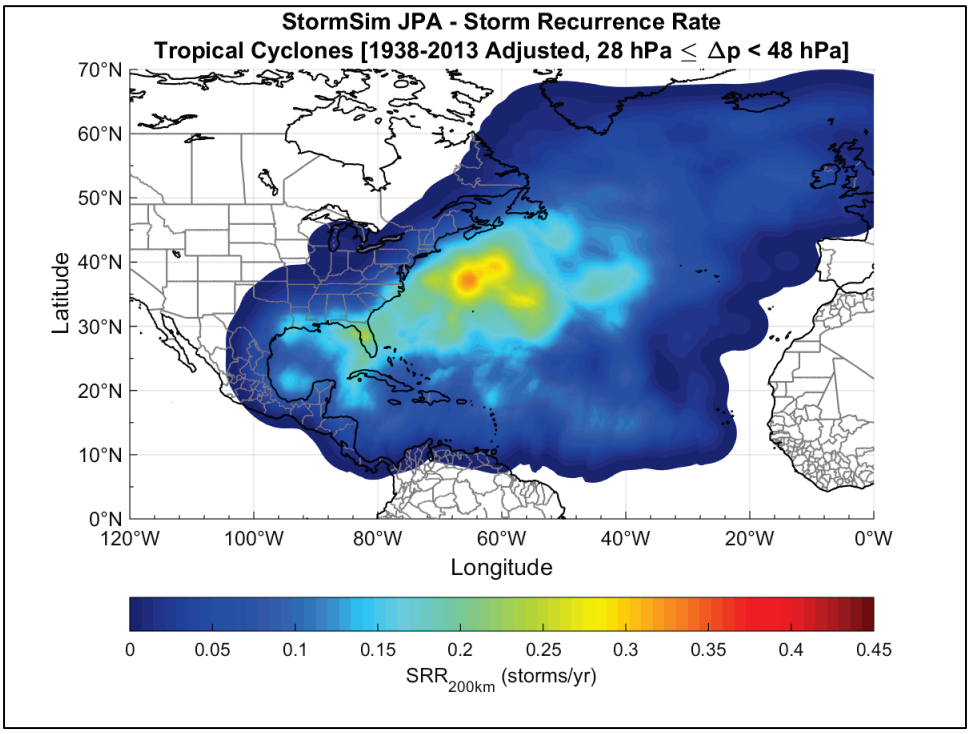

Figure 8-2. SRR_{200km} for high-intensity TCs during the 1938–2013 period.

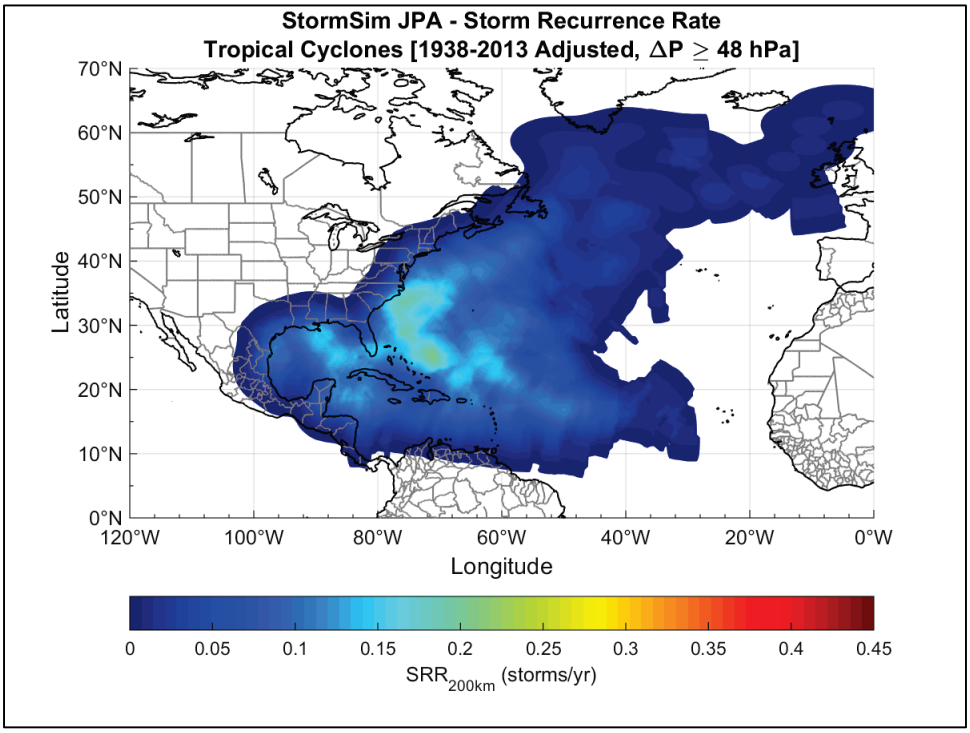

Table 8-1. GKF SRR adjusted by +10% for low- and high-intensity TCs.

Coastal Reference Location	Low Intensity TCs (28 hPa ≤ Δp < 48 hPa)		High Intensity TCs (Δp ≥ 48 hPa)	
	GKF SRR (storms/yr/km)	GKF SRR_{200km} (storms/yr)	GKF SRR (storms/yr/km)	GKF SRR_{200km} (storms/yr)
Eastport, ME	2.47E-04	0.10	5.85E-05	0.02
Bar Harbor, ME	2.46E-04	0.10	5.86E-05	0.02
Portland, ME	2.40E-04	0.10	3.88E-05	0.02
Boston, MA	2.64E-04	0.11	1.06E-04	0.04
Woods Hole, MA	3.50E-04	0.14	1.49E-04	0.06
Nantucket Island, MA	3.56E-04	0.14	1.50E-04	0.06
Newport, RI	3.18E-04	0.13	1.66E-04	0.07
Providence, RI	3.21E-04	0.13	1.66E-04	0.07
New London, CT	3.07E-04	0.12	1.67E-04	0.07
Montauk Point Light, NY	3.07E-04	0.12	1.67E-04	0.07
Kings Point, NY	2.08E-04	0.08	1.85E-04	0.07
The Battery, NY	2.03E-04	0.08	1.84E-04	0.07
Sandy Hook, NJ	2.03E-04	0.08	1.84E-04	0.07
Atlantic City, NJ	2.59E-04	0.10	2.14E-04	0.09
Cape May, NJ	2.72E-04	0.11	2.10E-04	0.08
Lewes, DE	2.89E-04	0.12	2.07E-04	0.08
Cambridge, MD	3.03E-04	0.12	2.08E-04	0.08
Baltimore, MD	2.89E-04	0.12	2.07E-04	0.08
Annapolis, MD	2.89E-04	0.12	2.07E-04	0.08
Solomons Island, MD	3.23E-04	0.13	2.23E-04	0.09
Washington, DC	3.03E-04	0.12	2.08E-04	0.08
Sewells Point, VA	3.77E-04	0.15	2.39E-04	0.10
Chesapeake Bay Bridge Tunnel, VA	3.77E-04	0.15	2.39E-04	0.10

8.3 Parameterization of TCs

The general methodology for the parameterization was presented in Chapter 5. There, a set of marginal distributions was developed corresponding to each subregion's MPCRL with the sole purpose of developing the synthetic TCs. Then the final JPA discussed in this chapter was done at a higher spatial resolution. Separate statistical analyses were performed at 200 CRLs throughout the NACCS region following an idealized coastline. The expanded historical TC set (Appendix E) was assessed at each of these CRLs, which are depicted in Figure 8-3.

Figure 8-3. NACCS CRL for JPA.

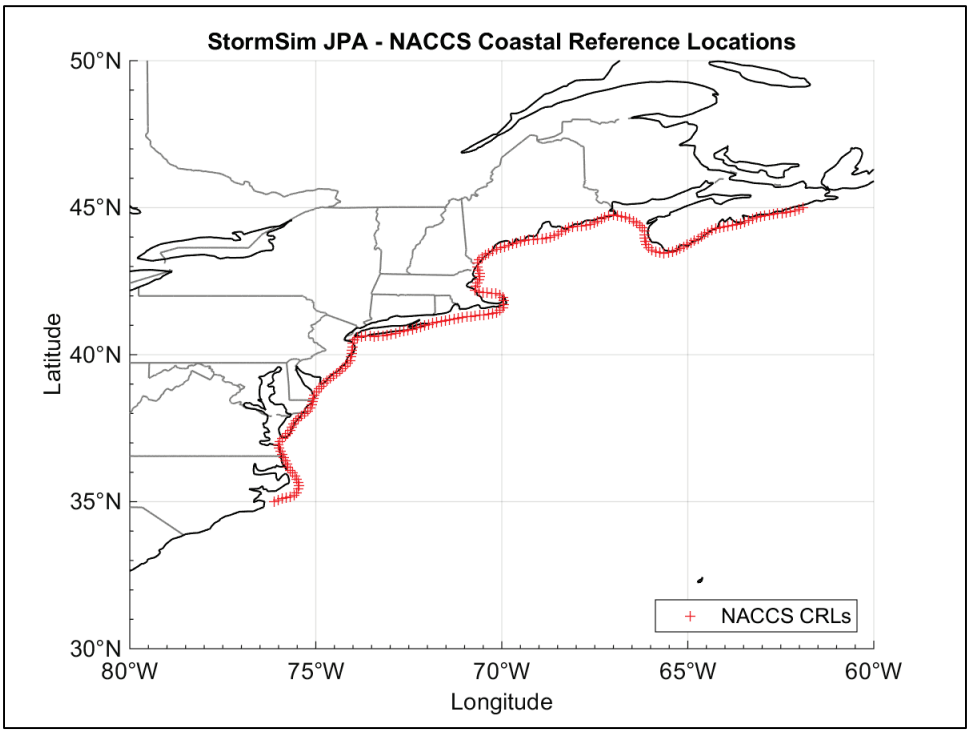

At each CRL, only those TCs with tracks passing within 1,000 km were retained for further analyses. The track point at which the storm parameters were extracted for each TC was determined based on the following intensity index function:

$$I_{\Delta p} = w(d_i)\Delta p_i \tag{8-1}$$

where: $I_{\Delta p}$ = TC intensity index; $w(d_i)$ = distance weights computed using the GKF (Equation 4-2); Δp_i = central pressure deficit at individual track points.

For each TC track, all storm parameters were identified at the track point that maximized the value of Equation 8-1. The TC parameter distributions were then computed following the methodology discussed in Section 5.1, where the historical values were adjusted based on the GKF weights, using the distances from the track points to the respective MPCRL of each subregion. In this case, however, the distances were computed from the track points to each of the 200 CRLs along the NACCS coastline. At a given CRL, the distance-weighted mean (μ_{dist}) of each parameter distribution was computed from Equation 5-1, and the individual storm parameter values were adjusted in order to comply with Equation 5-3.

8.3.1 Central pressure deficit (Δp)

For the JPA, a left-truncated Weibull distribution (LTWD) was fit to the Δp data. Then, a bootstrap resampling method was applied to determine the mean Δp distribution curve, similar to the procedure recommended in McGuire et al. (2005) and FEMA (2008). The LTWD has the following form:

$$F[\Delta p > x] = exp\left[-\left(\frac{x}{U}\right)^k\right] - exp\left[-\left(\frac{\Delta p_1}{U}\right)^k\right] \quad (8\text{-}2)$$

where: U = scale parameter; k = shape parameter; and Δp_1 = lower limit of Δp.

In this process, the initial LTWD best-fit was resampled 10,000 times, and each time a new LTWD was fit to the resampled values. This resulted in 10,000 LTWD fits from which a mean and CLs curves were computed. A final LTWD was fit to the mean curve.

Examples of these results are presented next for NACCS CRL 59. The location of CRL 59 is shown in Figure 8-4.

Figure 8-4. Location of NACCS CRL 59.

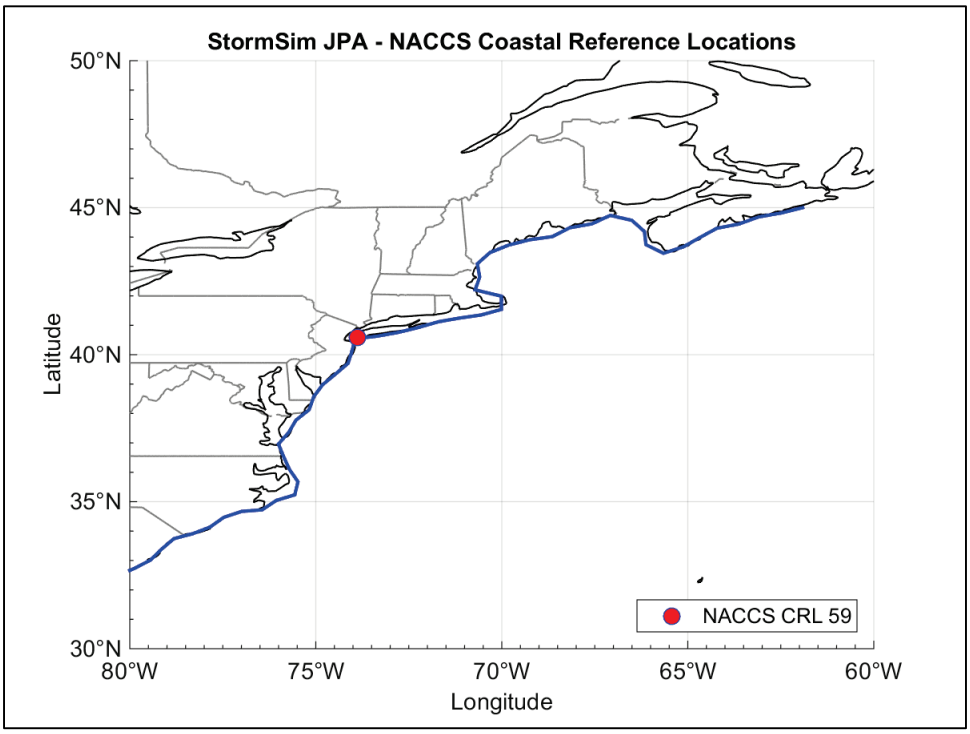

Figure 8-5 illustrates the initial LTWD best-fit, as well as mean curve, 16% and 84% CLs. In general, the LTWD fit to the mean curves tended to yield slightly lower Δp values than the initial best-fits.

Figure 8-5. Central pressure deficit bootstrap resampling results for CRL 59.

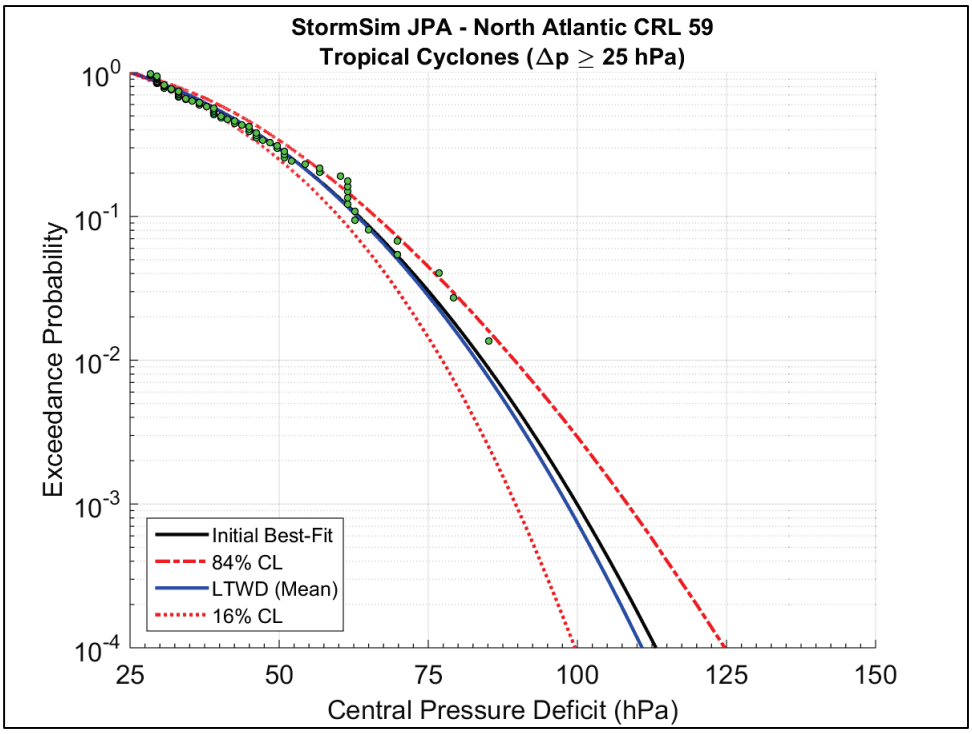

Since the storm probabilities are computed separately for low- and high-intensity TCs, the Δp distribution depicted in Figure 8-5 was truncated at 48 hPa. Then, the DTWD (previously given as Equation 5-5) was used to fit the Δp data corresponding to low-intensity TCs, while the LTWD was applied to fit the Δp data just from high-intensity TCs.

The scale and shape parameters corresponding to the LTWD fit in Figure 8-5 were held constant for the low- and high-intensity TC fits. Figure 8-6 shows the marginal distribution of Δp for-low intensity TCs corresponding to NACCS CRL 59. The lower truncation of this DTWD was adjusted to 25 hPa to allow the computation of probabilities for 28 hPa TCs. Figure 8-7 shows the marginal distribution of Δp for high-intensity TCs for CRL 59. Similar to the DTWD, the lower truncation of this LTWD was adjusted to 45 hPa. This 3 hPa overlap is necessary to compute the probabilities corresponding to TCs of 48 hPa.

Figure 8-6. Marginal distribution of central pressure deficit for low-intensity TCs at CRL 59.

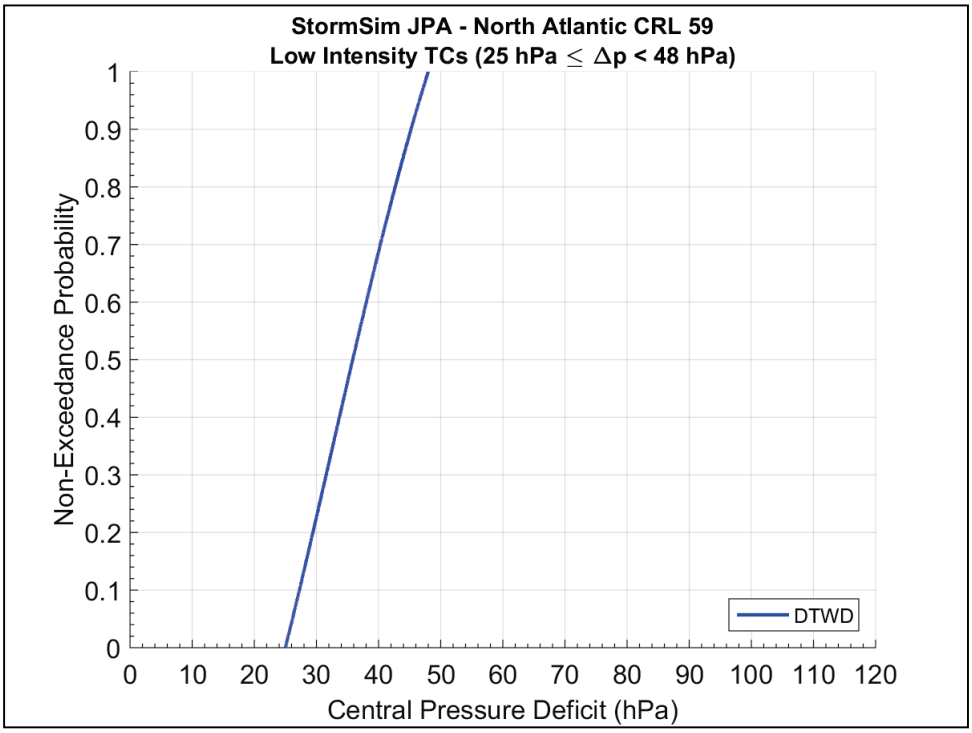

Figure 8-7. Marginal distribution of central pressure deficit for high-intensity TCs at CRL 59.

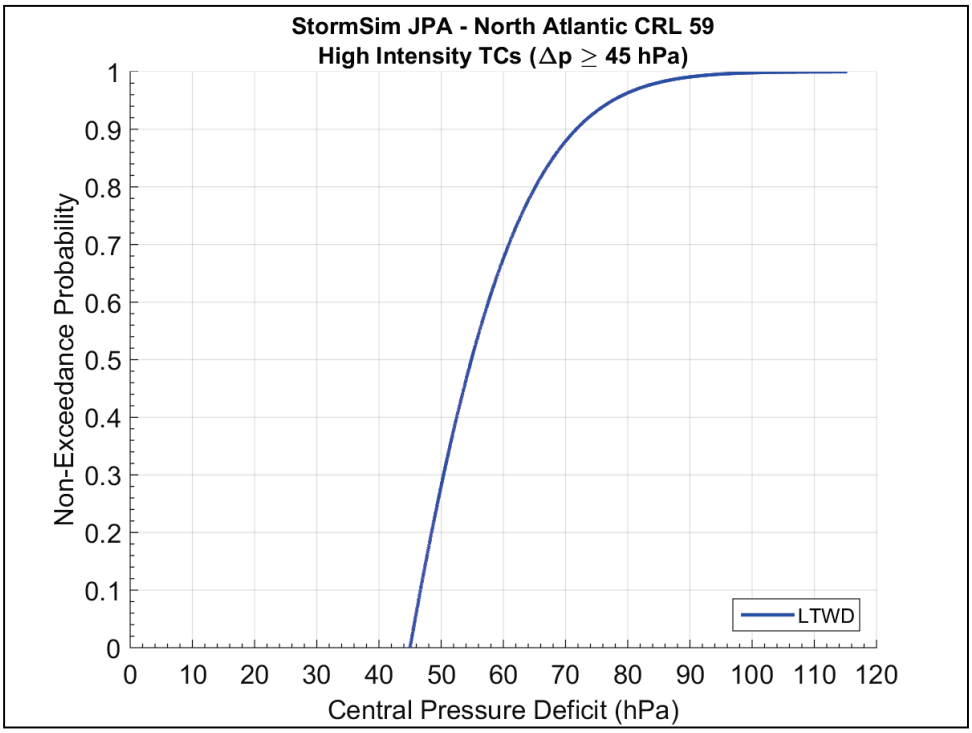

The scale parameter, shape parameter, and truncation limits of the Δp for CRL 59 are listed in Table 8-2.

Table 8-2. Central pressure deficit marginal distribution parameters for CRL 59.

TC Intensity	U	k	Δp_1	Δp_2
All (LTWD)	41.48	2.29	25	n/a
Low (DTWD)	41.48	2.29	25	48
High (LTWB)	41.48	2.29	45	n/a

8.3.2 Radius of maximum winds (R_{max})

As discussed in Section 5.1.2, the parameter R_{max} is represented by the lognormal distribution (Equation 5-6). For the JPA, however, the R_{max} values were partitioned based on TC intensity.

Figure 8-8 shows the marginal distribution of R_{max} for low-intensity TCs corresponding to NACCS CRL 59. The marginal distribution of R_{max} for high-intensity storms is depicted in Figure 8-9. The R_{max} lognormal distribution parameters corresponding to CRL 59 are listed in Table 8-3.

Figure 8-8. Marginal distribution of radius of maximum winds for low-intensity TCs at CRL 59.

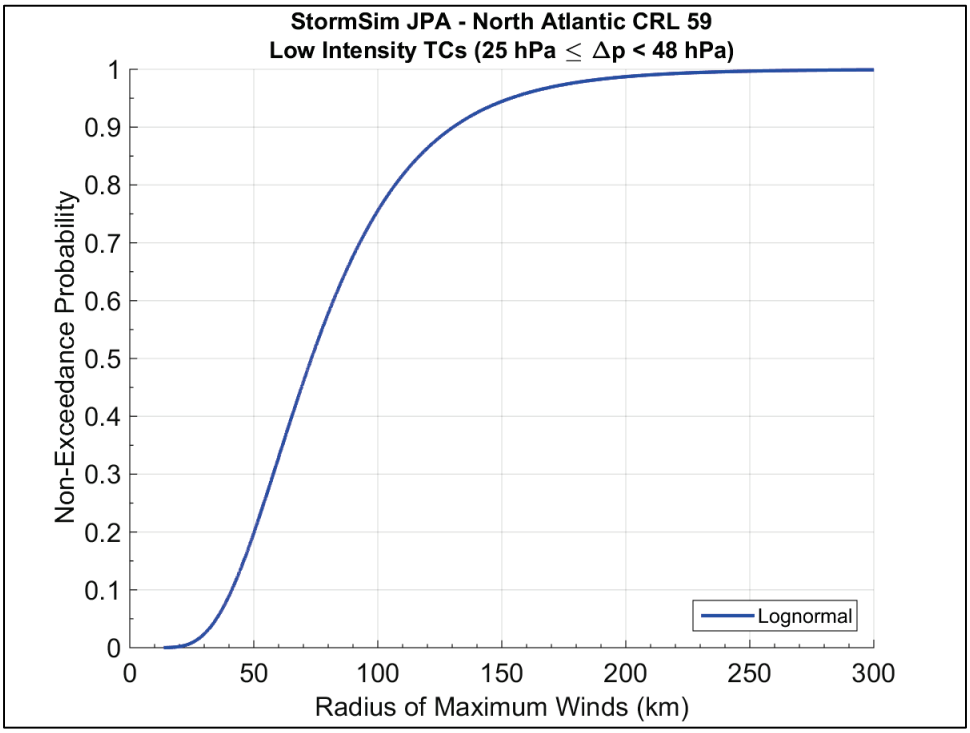

Figure 8-9. Marginal distribution of radius of maximum winds for high-intensity TCs at CRL 59.

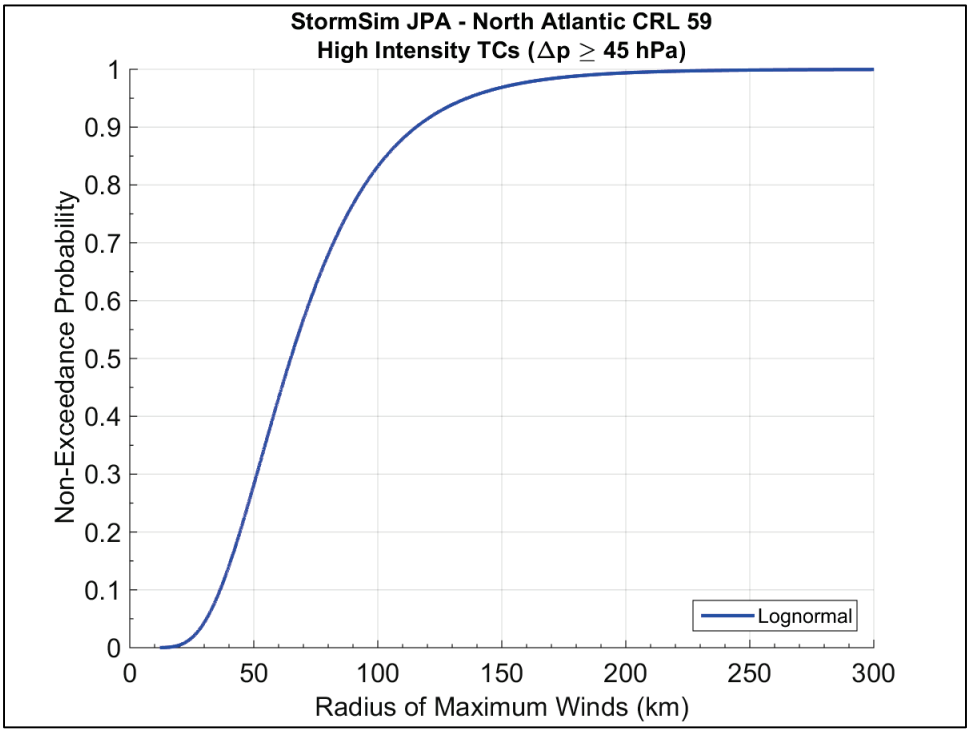

Table 8-3. Radius of maximum winds marginal distribution parameters for CRL 59.

TC Intensity	$\mu_{ln(x)}$	$\sigma_{ln(x)}$
Low	4.29	0.45
High	4.16	0.45

8.3.3 Translational speed (V_t)

The V_t marginal distribution is represented by the normal distribution, as discussed in Section 5.1.3. The V_t values were also partitioned based on the intensity of the TCs. Figure 8-10 shows the marginal distribution of V_t for low-intensity TCs corresponding to NACCS CRL 59.

The marginal distribution of V_t for high-intensity storms is depicted in Figure 8-11.

Figure 8-10. Marginal distribution of translational speed for low-intensity TCs at CRL 59.

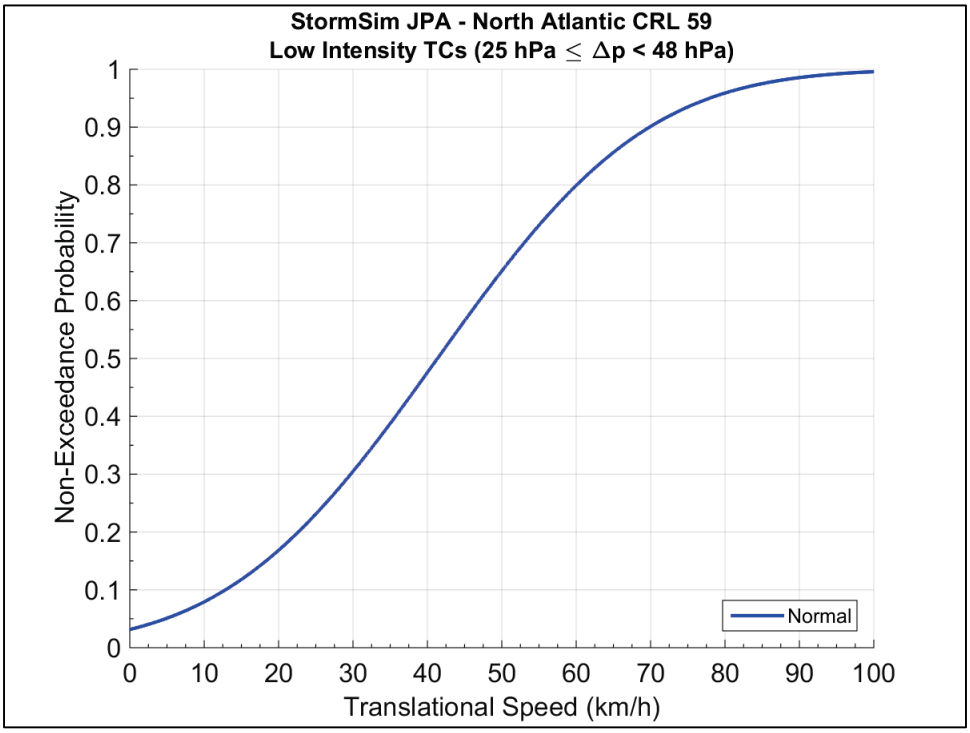

Figure 8-11. Marginal distribution of translational speed for high-intensity TCs at CRL 59.

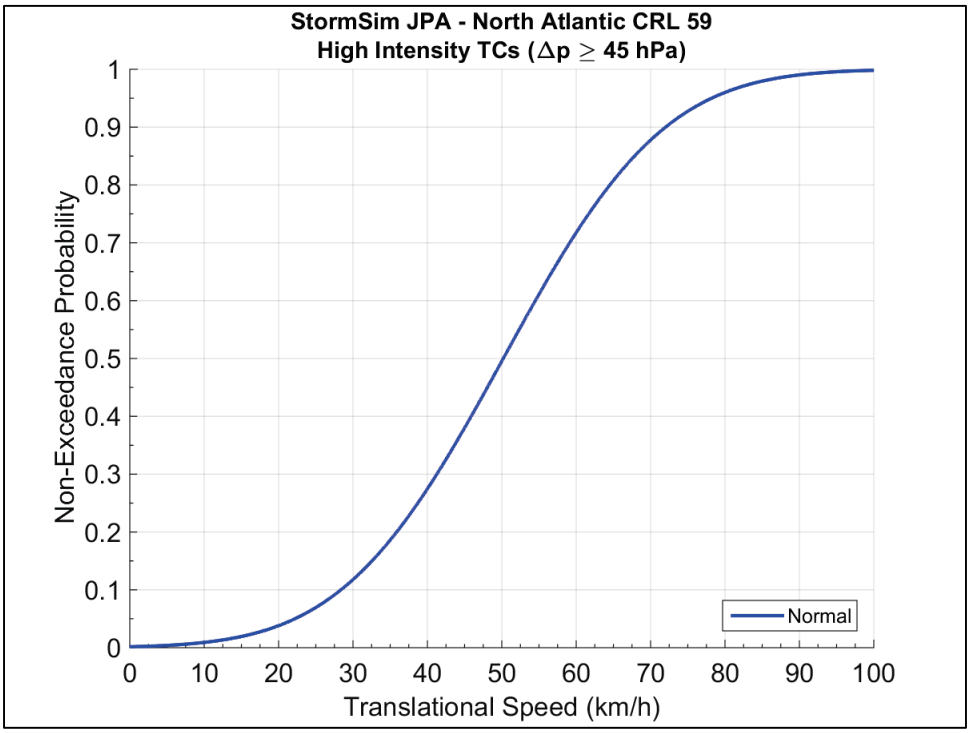

The V_t normal distribution parameters corresponding to CRL 59 are listed in Table 8-4.

Table 8-4. Translational speed marginal distribution parameters for CRL 59.

TC Intensity	μ	σ
Low	41.34	22.71
High	50.18	17.81

8.3.4 Heading direction (θ)

For the JPA, the θ marginal distribution was determined from the directional SRR (DSRR) computed based on the GKF model (Chouinard and Liu 1997). The DSRR is given by

$$\lambda_\theta = \frac{1}{T}\sum_i^n w(d_i)w(\theta_i) \tag{8-3}$$

$$w(\theta_i) = \frac{1}{\sqrt{2\pi}h_\theta} exp\left[-\frac{1}{2}\left(\frac{\theta_i}{h_\theta}\right)^2\right] \tag{8-4}$$

where λ_θ = the DSRR in storms/yr/km; T = record length in (yr); d_i = distance from location of interest to a storm data point (km); h_d = optimal kernel size (km); $w(\theta_i)$ = distance-adjusted weights from the heading direction Gaussian PDF (deg^{-1}); θ_i = heading direction (deg); h_θ = optimal directional kernel size (e.g., 30 deg); and $w(d_i)$ = distance weights computed using the GKF (Equation 4-2).

Figure 8-12 shows the marginal distribution of θ for low-intensity TCs corresponding to NACCS CRL 59. The marginal distribution of θ for high-intensity storms is depicted in Figure 8-13.

Figure 8-12. Marginal distribution of heading direction for low-intensity TCs at CRL 59.

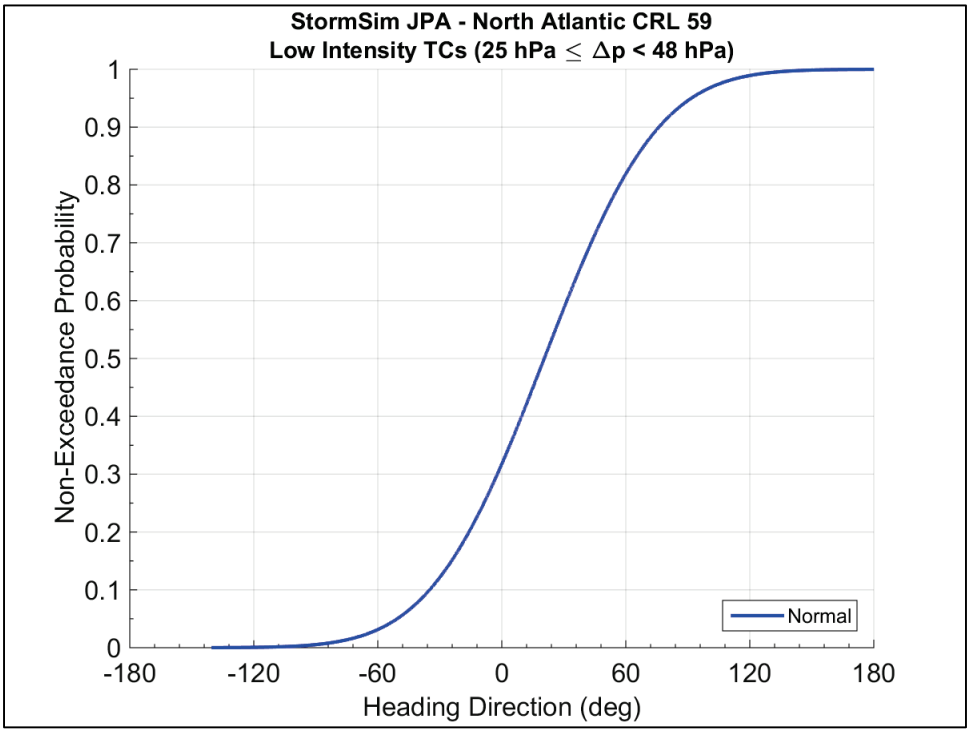

Figure 8-13. Marginal distribution of heading direction for CRL 59 high-intensity TCs.

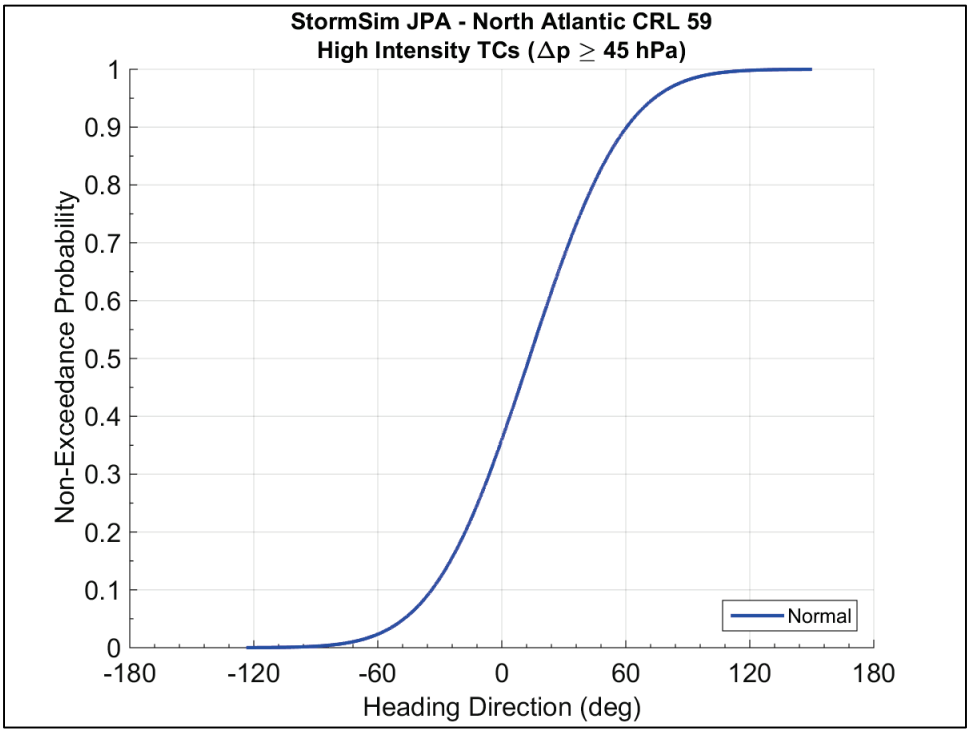

The θ normal distribution parameters corresponding to CRL 59 are listed in Table 8-5.

Table 8-5. Heading direction marginal distribution parameters for CRL 59.

TC Intensity	μ	σ
Low	20.54	43.28
High	13.24	36.79

8.4 Discrete distributions of TC parameters

The discrete probability distributions of TC parameters was determined as part of the JPA by computing the discrete weights of the synthetic TC suite. The optimal values of these weights were computed using a Bayesian Quadrature method. Examples of discrete distributions computed for the NACCS are presented in Table 8-6 through 8-9 for CRL 59.

Table 8-6. Discretized distributions for CRL 59 high-intensity TCs ($-60^0 \leq \theta \leq -20^0$).

High-Intensity TCs $-60^0 \leq \theta \leq -20^0$		Subregion 3	Subregion 2	Subregion 1
θ (deg)	-60	0.1899	0.1899	0.1899
	-40	0.2963	0.2963	0.2963
	-20	0.5138	0.5138	0.5138
Δp (hPa)	53	0.4327	0.6078	0.5765
	63	0.3058	0.1637	0.2118
	73	0.1327	0.1637	0.2117
	83	0.0644	0.0647	-
	93	0.0643	-	-
R_{max} (km)	30	0.1935	0.1900	0.1660
	60	0.4857	0.4962	0.4057
	90	0.1604	0.1475	0.3044
	120	0.1604	0.1474	0.1140
	150	-	0.0189	-
	180	-	-	0.0100
V_t (km/h)	15	0.2086	0.0784	-
	30	0.2086	0.1176	0.2672
	45	0.5828	0.4079	0.2673
	60	-	0.1981	0.2941
	75	-	0.1980	0.1713

Table 8-7. Discretized distributions for CRL 59 high-intensity TCs ($0^0 \leq \theta \leq 20^0$).

High-Intensity TCs $0^0 \leq \theta \leq 20^0$		Subregion 3	Subregion 2	Subregion 1
θ (deg)	0	0.3362	0.3362	0.3362
	20	0.3322	0.3322	0.3322
	40	0.3316	0.3316	0.3316
Δp (hPa)	48	0.1693	0.2114	0.2522
	53	0.1708	0.2054	0.2306
	58	0.1504	0.1698	0.1817
	63	0.1225	0.1302	0.139
	68	0.0963	0.0972	0.0985
	73	0.0760	0.0735	0.098
	78	0.0623	0.0563	-
	83	0.0540	0.0562	-
	88	0.0493	-	-
	93	0.0492	-	-
R_{max} (km)	30	0.1900	0.1900	0.1704
	60	0.4962	0.4962	0.4215
	90	0.1475	0.1475	0.2556
	120	0.1474	0.1474	0.0830
	150	0.0189	0.0189	0.0348
	180	-	-	0.0347
V_t (km/h)	15	0.0672	0.0876	0.0876
	30	0.2369	0.0876	0.0876
	45	0.2370	0.4197	0.4197
	60	0.4590	0.2415	0.2415
	75	-	0.1249	0.1249
	90	-	0.0388	0.0388

Table 8-8. Discretized distributions for CRL 59 low-intensity TCs ($-60^0 \leq \theta \leq -20^0$).

Low-Intensity TCs $-60^0 \leq \theta \leq -20^0$		Subregion 3	Subregion 2	Subregion 1
θ (deg)	-60	0.1899	0.1899	0.1899
	-40	0.2963	0.2963	0.2963
	-20	0.5138	0.5138	0.5138
Δp (hPa)	53	0.6629	0.6629	0.6629
	63	0.3371	0.3371	0.3371
R_{max} (km)	30	0.1880	0.1880	0.1880
	60	0.1880	0.1880	0.1880
	90	0.6240	0.6240	0.6240
V_t (km/h)	15	0.2774	0.3893	0.3893
	30	0.2775	0.2299	0.2299
	45	0.4451	0.2298	0.2298
	60	-	0.1510	0.1510

Table 8-9. Discretized distributions for CRL 59 low-intensity TCs ($0^0 \leq \theta \leq 20^0$).

Low-Intensity TCs $0^0 \leq \theta \leq 20^0$		Subregion 3	Subregion 2	Subregion 1
θ (deg)	0	0.3362	0.3362	0.3362
	20	0.3322	0.3322	0.3322
	40	0.3316	0.3316	0.3316
Δp (hPa)	33	0.3449	0.3449	0.3449
	38	0.3278	0.3278	0.3278
	43	0.3272	0.3272	0.3272
R_{max} (km)	30	0.1880	0.1357	0.1357
	60	0.1880	0.4329	0.4329
	90	0.6240	0.2158	0.2158
	120	-	0.2157	0.2157
V_t (km/h)	15	0.0672	0.0876	0.0784
	30	0.2369	0.0876	0.1176
	45	0.2370	0.4197	0.4079
	60	0.4590	0.2415	0.1981
	75	-	0.1249	0.198
	90	-	0.0388	-

8.5 Integration of joint probability of TC responses

In the JPA of coastal storm hazards, the AEP of the TC responses, such as water level, was computed by integrating the discrete form of the JPM integral, which was previously given in Equation 2-1:

$$\lambda_{r(\hat{x})>r} \approx \sum_i^n \lambda_i P[r(\hat{x}) > r|\hat{x}] \quad (2\text{-}1)$$

The peak responses produced by each synthetic TC at any given site are represented by the combined probability of the TC parameters. To estimate the water level AEP, for example, the first step is to compute the annual probability of each TC as the product of (1) the SRR, (2) the joint probability from the discrete distributions, and (3) the track spacing. These probabilities are then assigned to the respective response generated by each TC. The second step requires establishing a range of water elevation bins that encompass the entire range of water levels (e.g., 0 to 10 m at 0.01 m intervals). The third and final step involves the development of the complementary cumulative distribution function (CCDF) of the response by aggregating the probabilities of all water levels that exceed each of the established bins.

When the epistemic uncertainty associated with a given response is incorporated into the JPA, the JPM integral is modified as follows:

$$\lambda_{r(\hat{x})\pm\sigma_r>r} \approx \sum_i^n \lambda_i \, P[r(\hat{x})\pm\sigma_r > r|\hat{x}] \tag{8-5}$$

where σ_r = epistemic uncertainty of response (r).

In the NACCS, four nonexceedance CLs are provided. The nominal values of these CLs are 84%, 90%, 95%, and 98%. It is standard practice to represent epistemic uncertainty as a Gaussian distribution process with mean zero (Resio et al. 2007; Toro 2008; FEMA 2012). Therefore, this requires the correction of any statistically significant bias. The CLs are then computed as follows:

$$CL = \mu_r + z\sigma_r \tag{8-6}$$

where: CL = confidence limit; μ_r = mean value of a given TC response; z = Z-score or number standard deviations the CL is above μ_r; and σ_r = standard deviation of the response. The Z-score values associated with each CL are listed in Table 8-10.

Table 8-10. Normal distribution Z-scores associated with the NACCS CLs.

Nominal Confidence Limit (%)	Z-Score	Actual Confidence Limit (%)
84	1.0	84.134
90	1.282	90.008
95	1.645	95.002
98	2.0	97.725

8.6 Coastal storm hazards example

The TC frequencies computed for CRL 59 were used to compute the response statistics corresponding to NACCS save point (SP) 7672, shown in Figures 8-14 and 8-15. The water level hazard curve from JPA for SP 7672 is shown in Figure 8-16. The water level hazard curve due to XCs for SP 7672 is shown in Figure 8-17.

Figure 8-14. Location of NACCS SP 7672.

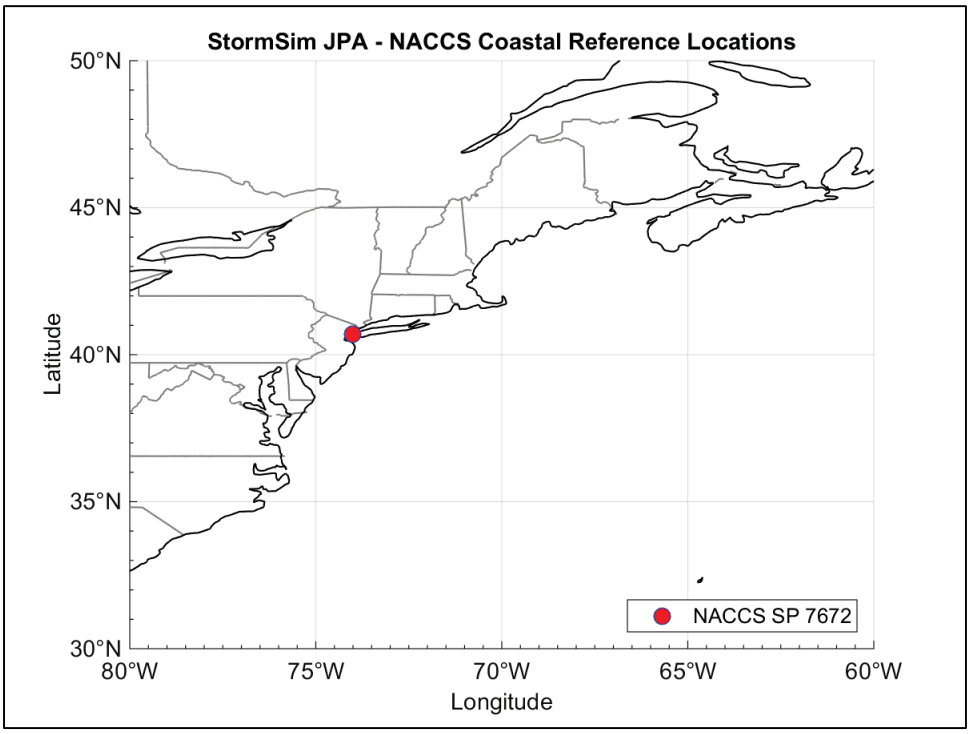

Figure 8-15. Aerial view of location of NACCS SP 7672 and NOAA water level gage at The Battery, NY.

Figure 8-16. Water level hazard curve due to TCs for NACCS SP 7672.

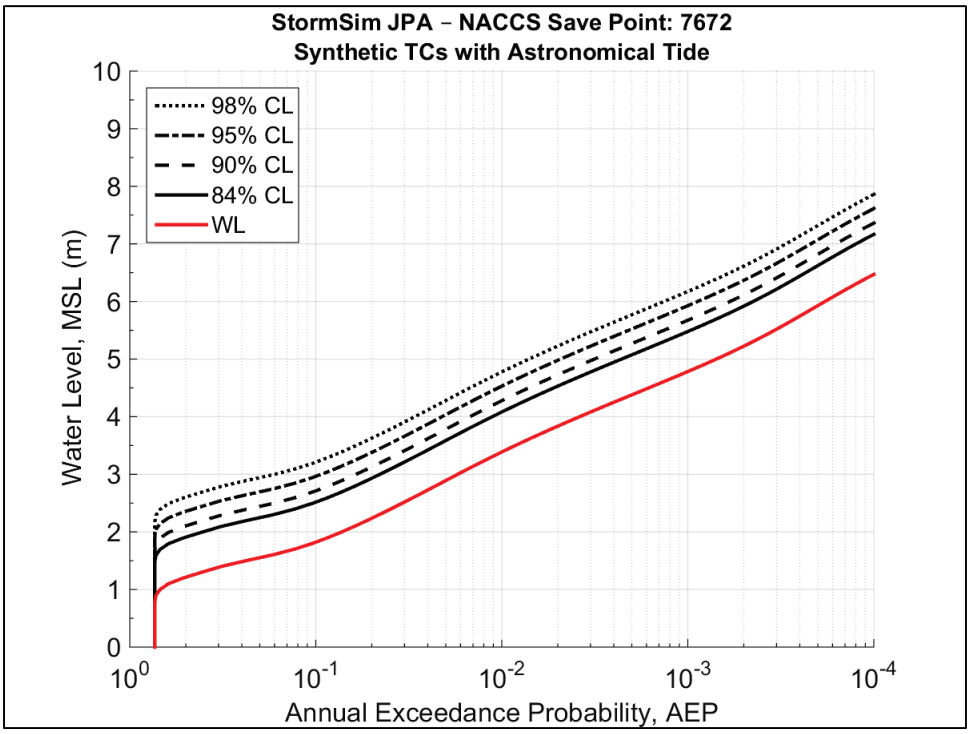

Figure 8-17. Water level hazard curve due to XCs for NACCS SP 7672.

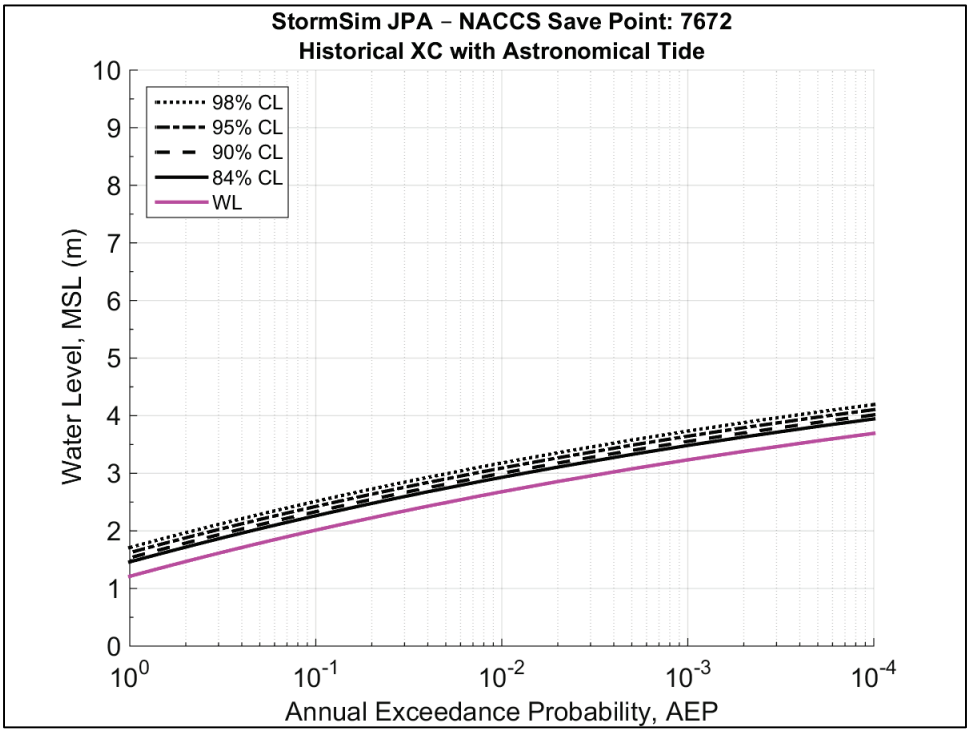

The final flood hazard curves combine the probabilities and responses from both TCs and XCs. The probabilities of these two storm populations are combined, assuming independence, as follows:

$$P(CC) = P(TC) + P(XC) \tag{8-7}$$

where: $P(CC)$ = combined probability of a given response due to both TCs and XCs; $P(TC)$ = probability of a given response due to TCs; $P(XC)$ = probability of a given response due to XCs. Figure 8-18 shows the TC and XC mean flood hazard curves as well and the combined curve for SP 7672. The water level hazard curve due to and TCs and XCs with CLs is shown in Figure 8-19.

Figure 8-18. Comparison of mean water level hazard curves for NACCS SP 7672.

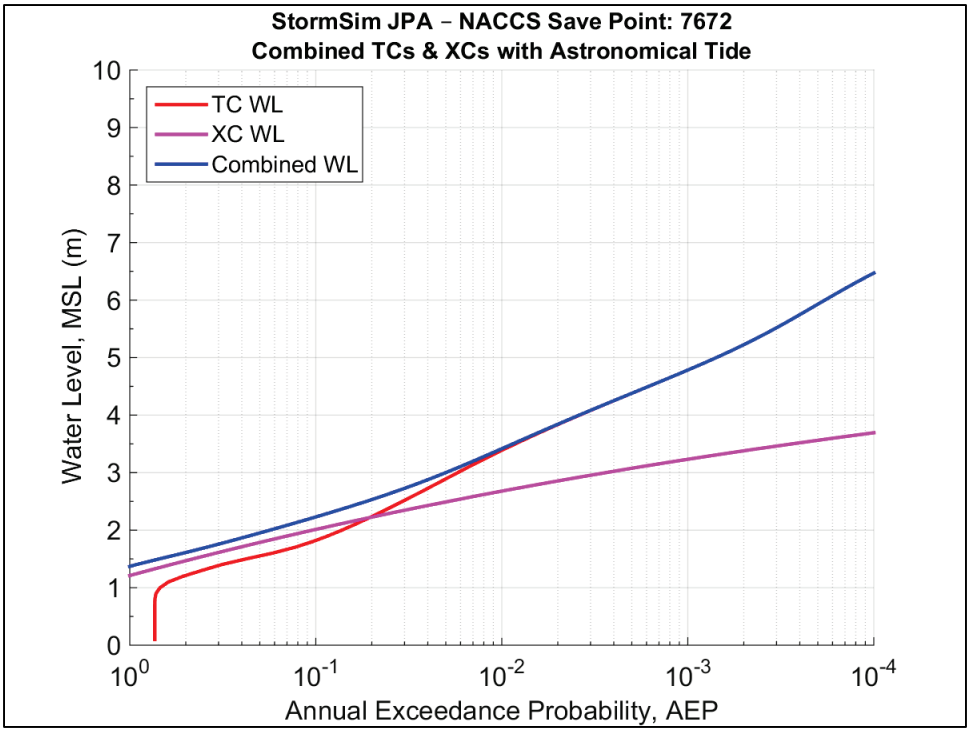

Figure 8-19. Water level hazard curve due to combined TCs and XCs for NACCS SP 7672.

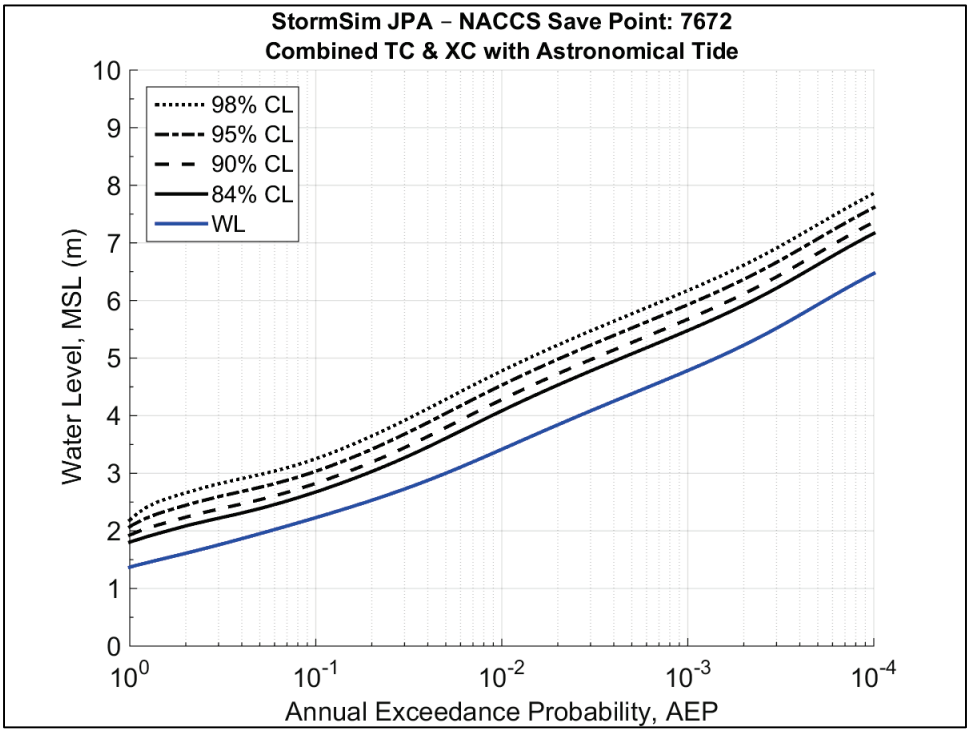

8.7 Comparison of NACCS joint probability analysis (JPA) results to other studies

In this section, NACCS JPA results are compared to results from previous studies.

8.7.1 Historical water levels

An extremal analysis of measured water levels was conducted by Nadal-Caraballo and Melby (2014). Figure 8-20 shows their results for The Battery gage along with the results for NACCS SP 7672. In general, the GPD based on measurements will be lower than that from the JPA because of the short record length and relatively sparse extreme storm occurrences.

Figure 8-20. Comparison between NACCS JPA and historical (GPD) water level hazard curves at NACCS SP 7672.

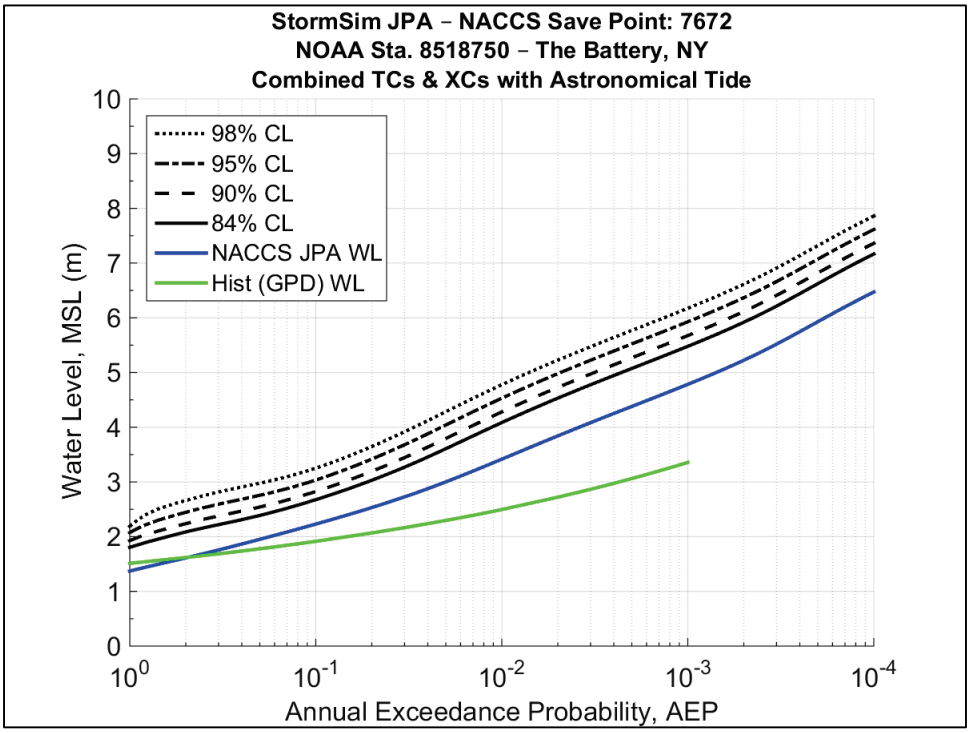

8.7.2 FEMA flood frequency curves

Figure 8-21 shows the comparison of NACCS JPA with varied confidence levels for NACCS SP 7672 vs FEMA Region II flood frequency results for the same location. The main difference is that epistemic uncertainties were incorporated into the aleatory uncertainty estimates for the FEMA Region II study using a Gaussian smoothing approach while epistemic uncertainties were treated explicitly for the NACCS. The reason for this difference is that the NACCS sought to quantify a range of confidence levels for varied engineering and planning applications. Generally, the FEMA results fall between the mean and 84% CL for the locations reviewed in this study.

Figure 8-21. Comparison between NACCS JPA and FEMA Region II water level hazard curves at NACCS SP 7672.

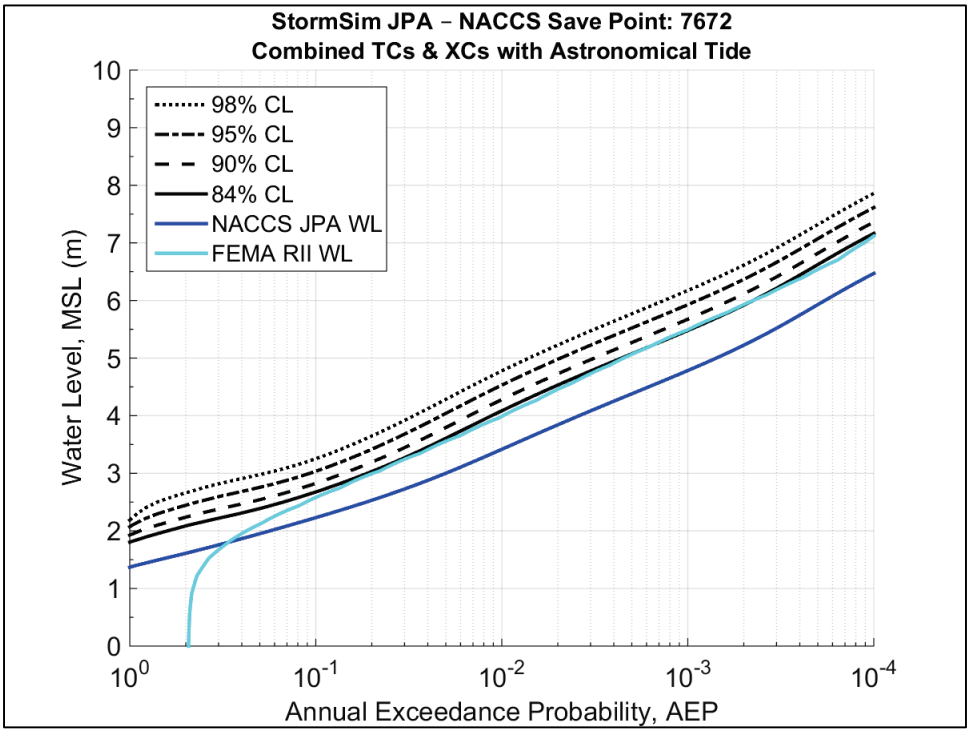

9 Coastal Hazards System (CHS)

The NACCS numerical modeling and statistical analysis effort generated a tremendous amount of data including storm forcing conditions, model results, and statistical analysis products for the coastal regions from Virginia to Maine. These data and data products will serve the coastal engineering and coastal management communities in the North Atlantic for many years. Managing and providing access to this vast quantity of information is made possible via the CHS, which is a national, coastal, storm-hazard data storage and mining system (Figure 9-1). It stores comprehensive, high-fidelity, storm-response computer modeling results including climatology, storm surge, total water level, wind, currents, and waves as well as measurements. Extremal statistics and epistemic uncertainties of the processes are also stored, and the data are easily accessed, mined, plotted, and downloaded through a user-friendly web interface.

Figure 9-1. Screen capture of the CHS with the NACCS region selected and highlighted on the map as tiles. The numbers on the tiles indicate the number of save points accessible within the area defined by the tile.

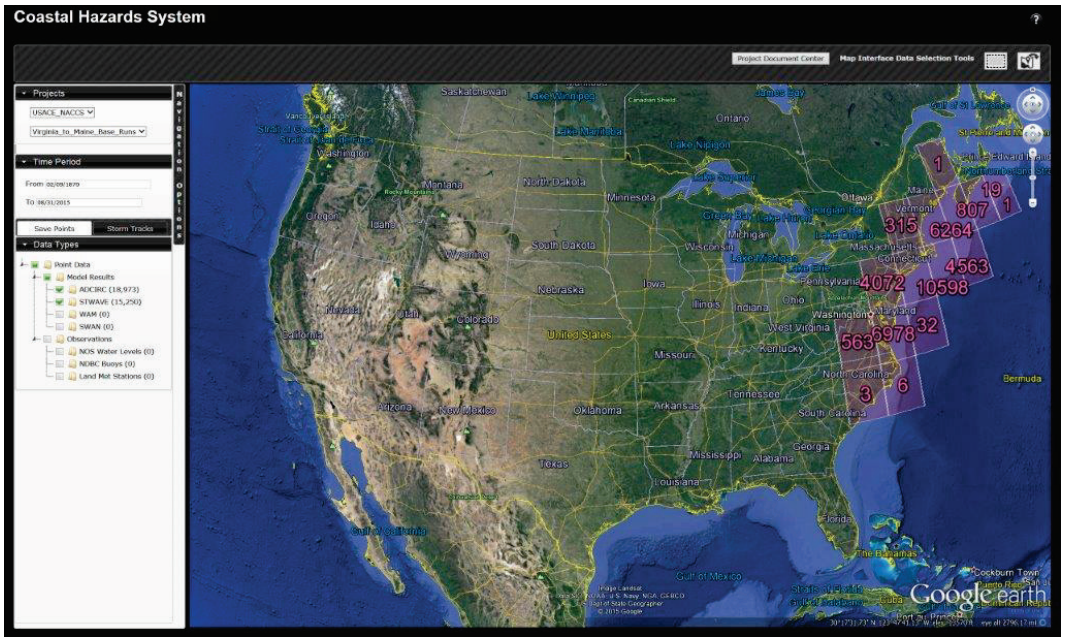

The CHS stores and distributes USACE and FEMA high-fidelity coastal storm data from formalized regional studies such as the FEMA National Flood Insurance Program and the USACE NACCS. Modeling results and associated measurements are converted into consistent and efficient

standards and formats and stored in a centralized system that is relatively easily maintained due to an innovative big-data design. The user-friendly web interface includes a multiaccess environment where the user can screen data through a map interface or through a text-based navigation window or some arbitrary combination of the two.

9.1 CHS data resources

CHS regional data are comprehensive, uniformly spanning the coastal region and practical probability space. The data are stored and accessed by project, and projects are usually regional. Each project contains subregions to better segregate the data. The types of data that are distributed include

- ADCIRC model output
- STWAVE and SWAN model output
- WAM model output
- TC tracks and parameters
- storm response statistics
- model grids
- wind and pressure field files
- historical measurements.

Both time-varying and maxima data are stored by save point location. Responses for all storms for a specific save point are stored in a unique file. The CHS native file formats are self-describing compressed HDF5. Matlab code snippets for reading and writing the data and are available in the online help. The capability for online conversion to comma-separated values (CSV) format exists within the system.

Aleatory and epistemic uncertainties, computed using the methods discussed in this report, are stored for each parameter for numerical model save points and observations. Model input files, such as grids, wind and pressure files, and other inputs, are stored in the Documents folder on the CHS system. Documentation for the system, data, and file formats is contained in technical reports in the Documents folder of the CHS.

9.2 Access

The CHS web application (https://chs.erdc.dren.mil) can be accessed through the CHS web site from the USACE Engineer Research and

Development Center Coastal and Hydraulics web site. In addition, a CHS wiki provides the latest up-to-date information on the system (https://wiki.erdc.dren.mil/Coastal_Hazards_System).

9.3 Applications

USACE and general Federal coastal projects, R&D studies, flood-risk mapping, and emergency response activities require storm data and extensive high-fidelity modeling in a statistical context in order to plan and design projects and assess risk. These data are usually generated for each study at great expense. A typical coastal engineering study requires expensive modeling and measurements that include time- and spatially varying waves, water level, wind, atmospheric pressure, and currents, among other data types. The CHS provides comprehensive coastal data and the associated uncertainties in easily ingestible standardized formats producing great potential for monetary savings as well as improved understanding of the complex processes. Integration of CHS file formats into the Surface Water Modeling System (SMS) and other USACE coastal software is underway.

10 Conclusions

The study summarized in this report is focused on the JPA of coastal storm hazards, including the statistical analysis of historical, regional, storm-induced water level responses, performed to support the NACCS. The overall NACCS climate, wave, and water level modeling study goals included simulating an efficient number of storms that blanketed a sufficient range of storm characteristics in order to accurately describe the statistical nature of coastal storm response over the entire region from Virginia to Maine. This information is required for modern probabilistic project design and for risk assessments. For this study, storm surge, tide, waves, wind, atmospheric pressure, currents, and SLC were the dominant responses computed. The significant advancements in this study included a dense spatial coverage of nearshore storm response for the region, high-fidelity computations, a complete description of the aleatory variability of response from frequent storm events to extremely rare events, a complete description of epistemic uncertainty, characterization of the statistical nature of the data in relatively simple data formats, and public distribution of data and statistics within the CHS, a web-based coastal storm data resource.

The NACCS region coastal storm hazard is primarily dependent on large ocean-based storms consisting of TCs, XCs, and transitional cyclones. It is common to group the storms into statistical families of tropical and extratropical with transitional storms that originated as tropical being categorized as tropical. In this study, tropical and extratropical storms were strategically selected to characterize the regional storm hazard. The storm suite was specifically designed to simulate coastal hydrodynamic response that efficiently spans practical parameter and probability spaces for each studied area.

Extratropical storms were selected by the methods of Nadal-Caraballo and Melby (2014) and Nadal-Caraballo et al. (2012) using an observation screening and sample-space optimization process. Storm surge and meteorological measurements were sampled to define significant extratropical events. The result was an efficient sample of 100 historical extratropical storms that were then modeled with high-fidelity climate and hydrodynamic numerical models.

The methods for sampling historical extratropical storms from historical measurements of response, such as storm surge, are not very useful for tropical storms because tropical storm response records on any specific section of coast are usually too sparse to derive accurate statistical models. Therefore, the tropical storm suite was developed with a modified version of the JPM with Bayesian optimized sampling techniques where synthetic tropical storms are defined from a probabilistic model of TC parameters. TC parameters for storms that impacted the region, such as storm size and intensity, were collected from databases such as HURDAT2 for the period 1938–2013, roughly corresponding to the period of modern aircraft reconnaissance missions. The primary parameters considered were landfall or CRL, heading direction, central pressure deficit, radius of maximum winds, and translational speed. Optimal sampling of the joint distributions of these parameters yielded 1,050 unique tropical storms that spanned the region spatially and encompassed the full range of practical hazard from frequent to very rare events. These tropical storms were also simulated with high-fidelity climate and hydrodynamic models.

A new JPM was developed to update the probabilities of each of the modeled storms in order to take advantage of more rigorous methods recently developed by the USACE. The simulation results were extracted at approximately 19,000 locations where probabilities of coastal storm hazards were sought. Storm surge, tide, waves, wind, atmospheric pressure, currents, and SLC were the dominant responses computed. The joint probabilities of these parameters were computed for separate tropical and extratropical storm statistical families and then combined. The statistical analysis of the 1,150 computed storms at 19,000 locations produced response statistics including AEP and ARI. In addition, epistemic uncertainty was quantified with specific confidence intervals.

References

Blake, E. S., C. W. Landsea, and E. J. Gibney. 2011. The deadliest, costliest, and most intense United States tropical cyclones from 1851 to 2010 (and other frequently requested hurricane facts). NOAA Technical Memorandum NWS NHC-6. Miami, FL: National Hurricane Center National Weather Service, National Oceanic and Atmospheric Administration.

Burkett, V. R., and M. A. Davidson, ed. 2012. Coastal impacts, adaptation and vulnerability: A technical input to the 2012 National Climate Assessment. Cooperative Report to the 2013 National Climate Assessment, 150. Washington, DC: Island Press.

Cardone, V.J., and A. T. Cox. 2009. Tropical cyclone wind field forcing for surge models: Critical issues and sensitivities. Natural Hazards 51: 29–47.

Cardone, V. J., and D. B. Ross. 1979. State-of-the-art wave prediction methods and data requirements. In Ocean Wave Climate, Vol. 8, ed. M. D. Earle and A. Malahoff. New York, NY: Plenum Publishing Corporation.

Cardone, V. J., W. J. Pierson, and E. G. Ward. 1976. Hindcasting the directional spectra of hurricane generated waves. Journal of Petroleum Technology 28:385–394.

Cardone, V. J., C. V. Greenwood, and J. A. Greenwood. 1992. Unified program for the specification of tropical cyclone boundary layer winds over surfaces of specified roughness. Contract Report CERC 92-1. Vicksburg, MS: U.S. Army Corps of Engineers Waterways Experiment Station.

Cardone, V. J., A. T. Cox, J. A. Greenwood, and E. F. Thompson. 1994. Upgrade of tropical cyclone surface wind field model. Miscellaneous Paper CERC-94-14. Vicksburg, MS: U.S. Army Corps of Engineers Waterways Experiment Station.

Cardone, V. J., and C. K. Grant. 1994. Southeast Asia meteorological and oceanographic hindcast study (SEAMOS). OSEA 94132. 10th Offshore Southeast Asia Conference, 6-9 December, Singapore.

Chouinard, L. M., and C. Liu. 1997. Model for recurrence rate of hurricanes in Gulf of Mexico. Journal of Waterway, Port, Coastal and Ocean Engineering 123(3):113–119.

Chow, S. H. 1971. A study of the wind field in the planetary boundary layer of a moving tropical cyclone. Master of Science thesis in meteorology, School of Engineering and Science, New York University.

Cialone M. A., T. C. Massey, M. E. Anderson, A. S. Grzegorzewski, R. E. Jensen, A. Cialone, D. J. Mark, K. C. Peavey, B. L. Gunkel, T. O. McAlpin, N. C. Nadal-Caraballo, J. A. Melby, and J. J. Ratcliff. 2015. North Atlantic Coast Comprehensive Study (NACCS) coastal storm model simulations: Waves and water levels. ERDC/CHL TR-15-14. Vicksburg, MS: U.S. Army Engineer Research and Development Center.

Church, J. A., and N. J. White. 2011. Sea-level rise from the late 19th to the early 21st century. Surveys in Geophysics 32(4–5):585–602.

Coastal Protection and Restoration Authority (CPRA). 2013. Greater New Orleans flood protection system notice of completion – Design assessment by non-federal sponsor. Bell City, LA: Lonnie G. Harper & Associates.

Coles, S. 2001. An introduction to the statistical modeling of extreme values. London, UK: Springer-Verlag, 45–49.

Federal Emergency Management Agency (FEMA). 1988. Coastal flooding hurricane storm surge model. Volume 1 Methodology. Washington, DC: Office of Risk Management, Federal Insurance Administration, FEMA.

_____. 2005. Guidelines for coastal flood hazard analysis and mapping for the Pacific Coast of the United States. Joint project by FEMA Region IX, FEMA Region X, and FEMA Headquarters. Oakland, CA: FEMA Region IX.

_____. 2008. Mississippi coastal analysis project. Final Report: HMTAP Task Order 18, prepared for the Federal Emergency Management Agency, Department of Homeland Security. Gaithersburg, MD: URS Group, Inc.

_____. 2012. Operating guidance No. 8-12 for use by FEMA staff and flood mapping partners: Joint probability – optimal sampling method for tropical storm surge. Washington, DC: Federal Emergency Management Agency, Department of Homeland Security.

_____. 2014. Redefinition of the coastal flood hazard zones in FEMA Region II: Analysis of the coastal storm surge flood frequencies. Final Report prepared for the Federal Emergency Management Agency, Department of Homeland Security. Fairfax, VA: Risk Assessment, Mapping, and Planning Partners.

Forristall, G. Z., R. C. Hamilton, and V. J. Cardone. 1977. Continental shelf currents in tropical storm Delia: Observations and theory. Journal of Physical Oceanography 7(4):532-546.

Forristall, G. Z., E. G. Ward, V. J. Cardone, and L. E. Borgman. 1978. The directional spectra and kinematics of surface waves in Tropical Storm Delia. Journal of Physical Oceanography 8(5): 888-909.

Forristall, G. Z. 1980. A two-layer model for hurricane driven currents on an irregular grid. Journal of Physical Oceanography 10(9):1417–1438.

Forristall, G. Z., and J. A. Greenwood. 1998. Directional spreading of measured and hindcasted wave spectra. In Proceedings 5th International Workshop on Wave Hindcasting and Forecasting. Melbourne, FL. January 26-30. Downsview, Ontario: Environment Canada Atmospheric Environment Service.

Ho, F. P. 1974. Storm tide frequency analysis for the coast of Georgia. NOAA Technical Memorandum NWS HYDRO-19. Silver Spring, MD: U.S. Department of Commerce.

Ho, F. P., and V. A. Myers. 1975. Joint probability method of tide frequency analysis applied to Apalachicola Bay and St. George Sound, Florida. NOAA Technical Report NWS 18. Silver Spring, MD: National Weather Service, National Oceanic and Atmospheric Administration.

Ho, F. P., J. C. Su, K. L. Hanevich, R. J. Smith, and F. P. Richards. 1987. Hurricane climatology for the Atlantic and Gulf Coasts of the United States. NOAA Technical Report NWS 38. Silver Spring, MD: National Weather Service, National Oceanic and Atmospheric Administration.

Holland, G. J. 1980. An analytic model of the wind and pressure profiles in hurricanes. Monthly Weather Review 108 (8):1212–1218.

Interagency Performance Evaluation Task Force (IPET). 2009. Performance evaluation of the New Orleans and Southeast Louisiana hurricane protection system. Final Report of the Interagency Performance Evaluation Task Force. Washington, DC: U.S. Army Corps of Engineers, Department of the Army.

Jarvinen, B. R., C. J. Neumann, and M. A. S. Davis. 1984. A tropical cyclone data tape for the North Atlantic basin, 1886–1983: Contents, limitations, and uses. NOAA Tech. Memo 22. Miami, FL: National Hurricane Center, National Weather Service.

Landsea, C. W., G. A. Vecchi, L. Bengtsson, and T. R. Knutson. 2010. Impact of duration thresholds on Atlantic tropical cyclone counts. Journal of Climate 23(10):2508–19.

Landsea, C. W., and J. L. Franklin. 2013. Atlantic hurricane database uncertainty and presentation of a new database format. Monthly Weather Review 141(10):3576–3592.

Mann, M. E., T. A. Sabbatelli, and U. Neu. 2007. Evidence for a modest undercount bias in early historical Atlantic tropical cyclone counts. Geophysical Research Letters 34(22):L22707.

McGuire, R. K., C. A. Cornell, and G. R. Toro. 2005. The case for using mean seismic hazard. Earthquake Spectra 21(3):879–886.

Myers, V. A. 1954. Characteristics of United States hurricanes pertinent to levee design for Lake Okeechobee, Florida. Hydrometeorological Report No. 32. Washington, DC: Weather Bureau, U.S. Department of Commerce.

Myers, V. A. 1970. Joint probability method of tide frequency analysis applied to Atlantic City and Long Beach Island, NJ. ESSA Technical Memorandum WBTM HYDRO 11. Washington, DC: Weather Bureau, U.S. Department of Commerce.

Myers, V. A. 1975. Storm tide frequencies on the South Carolina Coast. NOAA Technical Report NWS-16. Washington, DC: National Weather Service, National Oceanic and Atmospheric Administration.

Nadal-Caraballo, N. C., and J. A. Melby. 2014. North Atlantic Coast Comprehensive Study – Phase I: Statistical analysis of historical extreme water levels with sea level change. ERDC/CHL TR-14-7. Vicksburg, MS: U.S. Army Engineer Research and Development Center.

Nadal-Caraballo, N. C., J. A. Melby, and B. A. Ebersole. 2012. Statistical analysis and storm sampling approach for Lakes Michigan and St. Clair. ERDC/CHL TR-12-19. Vicksburg, MS: U.S. Army Engineer Research and Development Center.

National Oceanographic and Atmospheric Administration (NOAA). 2012. Global sea level rise scenarios for the U.S. National Climate Assessment. NOAA Technical Report OAR CPO-1. Silver Spring, MD: Climate Program Office.

Niedoroda, A.W., D. T. Resio, G. R. Toro, D. Divoky, H. S. Das, and C. W. Reed. 2010. Analysis of the coastal Mississippi storm surge hazard. Ocean Engineering 37(1):82–90.

Neumann, C. J., G. W. Cry, E. L. Caso, and B. R. Jarvinen. 1985. Tropical cyclones of the North Atlantic Ocean, 1871-1980. Asheville, NC: National Climatic Center.

Pirani, R., and L. Tolkoff. 2014. Lessons from Sandy: Federal policies to build climate-resilient coastal regions. Policy Focus Report. Cambridge, MA: Lincoln Institute of Land Policy. https://www.lincolninst.edu/pubs/2381_Lessons-from-Sandy

Powell, M. D., S. Murillo, P. Dodge, E. Uhlhorn, J. Gamache, V. Cardone, A. Cox, S. Otero, N. Carrasco, B. Annane, and R. St. Fleur. 2010. Reconstruction of Hurricane Katrina's wind fields for storm surge and wave hindcasting. Ocean Engineering 37:26–36.

Resio, D. T., S. J. Boc, L. Borgman, V. Cardone, A. T. Cox, W. R. Dally, R. G. Dean, D. Divoky, E. Hirsh, J. L. Irish, D. Levinson, A. Niedoroda, M. D. Powell, J. J. Ratcliff, V. Stutts, J. Suhada, G. R. Toro, and P. J. Vickery. 2007. White Paper on estimating hurricane inundation probabilities. Consulting Report prepared by USACE for FEMA. Vicksburg, MS: U.S. Army Engineer Research and Development Center.

Ross, D. B., and V. J. Cardone. 1978. A comparison of parametric and spectral hurricane wave prediction products. In Turbulent Fluxes through the Sea Surface, Wave Dynamics, and Prediction, ed. A. Favre and K. Hasselmann. New York, NY: Plenum Press.

Russell, L. R. 1968a. Stochastic models for hurricane prediction for the Texas Gulf Coast. Master's thesis, Stanford University.

Russell, L. R. 1968b. Probability distributions for Texas Gulf Coast hurricane effects of engineering interest. PhD dissertation, Stanford University.

Shapiro, L. J. 1983. The asymmetric boundary layer flow under a translating hurricane. Journal of the Atmospheric Sciences 40(8):1984–1998.

Smith, J. M., A. R. Sherlock, and D. T. Resio. 2001. STWAVE: Steady-state spectral wave model user's manual for STWAVE, version 3.0. ERDC/CHL SR-01-1. Vicksburg, MS: U.S. Army Engineer Research and Development Center.

Toro, G. R. 2008. Joint probability analysis of hurricane flood hazards for Mississippi – Final URS Group report in support of the FEMA-HMTAP flood study of the State of Mississippi. Boulder CO: Risk Engineering.

Thompson, E. F., and V. J. Cardone. 1996. Practical modeling of hurricane surface wind fields. ASCE Journal of Waterway, Port, Coastal and Ocean Engineering 122(4):195–205.

Toro, G. R., D. T. Resio, D. D., A. W. Niedoroda, and C. Reed. 2010. Efficient joint-probability methods for hurricane surge frequency analysis. Ocean Engineering 37(1):125–34.

U.S. Army Corps of Engineers (USACE). 2009a. Louisiana Coastal Protection and Restoration (LACPR). Final Technical Report. New Orleans, LA: New Orleans District, Mississippi Valley Division, USACE.

_____. 2009b. Mississippi Coastal Improvements Program (MSCIP), Hancock, Harrison, and Jackson Counties, Mississippi. Mobile, AL: Mobile District, South Atlantic Division, USACE.

_____. 2011. Flood insurance study: Coastal counties, Texas: Scoping and data review. Denton, TX: Federal Emergency Management Agency, Region 6.

_____. 2015. North Atlantic Coast Comprehensive Study: Resilient adaptation to increasing risk – Main report (Final). Brooklyn, NY: North Atlantic Division, USACE.

Vecchi, G. A., and T. R. Knutson. 2011. Estimating annual numbers of Atlantic hurricanes missing from the HURDAT database (1878–1965) using ship track density. Journal of Climate 24(6):1736–1746.

Vickery, P. J. 2005. Simple empirical models for estimating the increase in the central pressure of tropical cyclones after landfall along the coastline of the United States. Journal of Applied Meteorology 44(12):1807–1826.

Vickery, P. J., and B. O. Blanton. 2008. North Carolina coastal flood analysis system hurricane parameter development. Technical Report TR-08-06. Chapel Hill, NC: RENCI Renaissance Computing Institute.

Vickery, P. J., and D. Wadhera. 2008. Statistical models of Holland pressure profile parameter and radius to maximum winds of hurricanes from flight-level pressure and H*Wind data. Journal of Applied Meteorology and Climatology 47(10):2497–2517.

Vickery, P., D. Wadhera, A. Cox, V. Cardone, J. Hanson, and B. Blanton. 2013. Coastal storm surge analysis: Storm forcing – Report 3: Intermediate submission no. 1.3. ERDC/CHL TR-11-1. Vicksburg, MS: U.S. Army Engineer Research and Development Center.

Westerink, J. J., R. A. Luettich, Jr., A. M. Baptista, N. W. Scheffner, and P. Farrar. 1992. Tide and storm surge predictions using finite element model. Journal of Hydraulic Engineering 118(10):1373–1390.

Worley, S. J., S. D. Woodruff, R. W. Reynolds, S. J. Lubker, and N. Lott. 2005. ICOADS release 2.1 data and products. Journal of Climatology 25:823–842.

Appendix A: NACCS Historical XCs

The following table lists the 100 historical XCs that were identified for the NACCS study area. The "Total Number of Locations" column indicates the amount of NOAA gages where each storm was identified as a top-50 water level event. "Highest Rank" is the highest ranking achieved by each storm's water level response at any one NOAA gage. For each storm, the "NOAA Station ID" indicates the gage where the highest response was observed, as well as the "NACCS Subregion" where each NOAA station is located. Date indicates earliest peak surge (NTR) time among all stations where each storm was identified.

NACCS Historical Extratropical Cyclone ID	Year	Month	Day	Total Number of Locations	Highest Rank	NOAA Station ID	NACCS Subregion	NTR (m)
1	1938	1	25	2	11	8574680	3	1.03
2	1940	2	15	3	8	8443970	1	1.22
3*	2010	2	6	4	17	8638863	3	0.97
4	1943	10	27	2	6	8518750	2	1.67
5	1945	11	30	3	3	8443970	1	1.46
6	1947	3	3	2	11	8443970	1	1.17
7	1950	11	25	4	1	8531680	2	2.5
8	1952	3	11	2	8	8574680	3	1.13
9*	2000	12	17	2	17	8571892	3	0.86
10	1952	11	21	3	8	8594900	3	1.66
11	1953	11	7	4	10	8518750	2	1.4
12	1958	2	16	3	17	8443970	1	1.06
13	1960	2	19	4	15	8452660	1	0.93
14	1960	3	4	2	14	8443970	1	1.12
15	1961	2	4	4	10	8534720	2	1.12
16	1961	4	14	2	6	8443970	1	1.32
17	1962	3	7	6	1	8557380	3	1.77
18	1962	12	6	3	13	8534720	2	1.04
19	1964	1	13	4	9	8534720	2	1.12
20	1966	1	23	5	15	8536110	2	1.06
21	1966	1	30	3	16	8510560	2	1.04
22	1968	11	12	4	2	8557380	3	1.58
23	1970	12	17	4	16	8516945	2	1.66
24	1971	3	4	2	9	8452660	1	1.02
25	1971	11	25	5	16	8531680	2	1.39
26	1972	2	4	3	11	8452660	1	1

NACCS Historical Extratropical Cyclone ID	Year	Month	Day	Total Number of Locations	Highest Rank	NOAA Station ID	NACCS Subregion	NTR (m)
27	1972	2	19	6	5	8534720	2	1.32
28	1972	11	9	3	9	8516945	2	1.82
29	1972	12	16	3	12	8510560	2	1.12
30	1973	1	29	2	14	8452660	1	0.94
31	1974	12	2	5	6	8531680	2	1.66
32	1976	2	2	3	9	8447930	1	0.97
33	1977	1	10	4	13	8447930	1	0.9
34	1977	10	14	2	14	8536110	2	1.06
35	1978	1	20	3	17	8510560	2	1.01
36	1978	1	26	5	7	8574680	3	1.16
37	1978	2	7	3	3	8510560	2	1.28
38	1978	4	26	2	7	8638610	3	1.23
39	1978	12	25	3	12	8413320	1	0.71
40	1979	1	21	8	7	8413320	1	0.81
41	1980	10	25	7	12	8454000	1	1.15
42	1982	10	25	2	4	8638863	3	1.22
43	1983	2	11	5	9	8638863	3	1.12
44	1983	3	19	6	7	8577330	3	0.79
45	1983	11	25	4	5	8413320	1	0.84
46	1983	12	12	4	10	8577330	3	0.7
47	1983	12	23	2	9	8410140	1	0.87
48	1983	12	29	3	7	8454000	1	1.29
49	1984	2	29	3	16	8413320	1	0.68
50	1984	3	29	4	3	8449130	1	1.03
51	1985	2	13	6	17	8574680	3	0.98
52	1985	11	5	6	1	8577330	3	1.04
53	1987	1	2	4	11	8557380	3	1.17
54	1987	1	23	9	3	8418150	1	1.05
55	1988	4	13	3	13	8638863	3	1.03
56	1988	11	2	3	9	8413320	1	0.79
57	1990	11	11	3	11	8413320	1	0.72
58	1991	10	30	9	1	8449130	1	1.41
59	1992	1	4	3	9	8577330	3	0.71
60	1992	12	11	4	2	8516945	2	2.26
61	1993	3	5	4	10	8571892	3	0.88
62	1993	3	14	6	2	8510560	2	1.29
63	1993	11	28	5	4	8571892	3	0.98
64	1993	12	21	2	8	8413320	1	0.8
65	1994	1	4	5	7	8536110	2	1.11

NACCS Historical Extratropical Cyclone ID	Year	Month	Day	Total Number of Locations	Highest Rank	NOAA Station ID	NACCS Subregion	NTR (m)
66	1994	3	2	7	2	8531680	2	2.23
67	1994	12	24	4	4	8516945	2	2
68	1995	2	5	4	5	8418150	1	0.94
69	1995	11	15	4	10	8516945	2	1.73
70	1996	1	8	7	1	8536110	2	1.54
71*	2003	10	15	2	17	8413320	1	0.68
72	1996	10	20	3	14	8516945	2	1.69
73	1996	12	8	3	9	8418150	1	0.83
74	1997	1	10	5	15	8454000	1	1.08
75	1997	4	19	2	9	8449130	1	0.95
76	1998	1	28	4	3	8638863	3	1.36
77	1998	2	5	8	3	8557380	3	1.53
78	2000	1	25	4	10	8638863	3	1.1
79	2001	3	7	3	11	8449130	1	0.93
80	2003	12	11	4	15	8577330	3	0.7
81	2003	12	18	4	10	8418150	1	0.83
82	2006	10	7	2	15	8638863	3	0.99
83	2006	10	28	6	11	8454000	1	1.16
84	2006	11	17	4	13	8575512	3	0.9
85	2006	11	22	2	6	8638863	3	1.15
86	2007	4	16	7	8	8454000	1	1.24
87	2008	5	12	6	5	8577330	3	0.87
88	2008	12	22	2	2	8410140	1	0.97
89	2009	11	13	5	1	8638863	3	1.57
90	2009	12	9	3	16	8418150	1	0.78
91	2009	12	19	5	11	8638863	3	1.09
92	2009	12	26	5	16	8577330	3	0.69
93	2010	2	26	7	1	8443970	1	1.84
94	2010	3	13	3	10	8594900	3	1.52
95	2010	10	1	2	14	8577330	3	0.7
96	2010	10	15	2	11	8418150	1	0.82
97	2010	12	27	6	14	8418150	1	0.8
98	2011	4	17	4	6	8571892	3	0.95
99	2012	12	21	6	3	8571892	3	1.09
100	2012	12	27	4	12	8516945	2	1.72

*Substitute XCs. Original events were identified in POT analysis as having exceeded a surge (NTR) threshold, but based on wind analysis it was determined that these were actually nonstorm (rain) events and were therefore replaced by storm events from a list of substitutes.

Appendix B: NACCS Synthetic TC Master Tracks

Following are the 130 master tracks developed for the 1,050 NACCS synthetic TCs.

Master Track ID	NACCS Subregion	Heading Direction, θ (deg)	Reference Latitude (deg N)	Reference Longitude (deg W)
1	3	-60	34.05	74.18
2	3	-60	34.39	73.57
3	3	-60	34.89	73.30
4	3	-60	35.64	73.57
5	3	-60	36.22	73.48
6	3	-60	36.65	73.09
7	3	-60	37.08	72.71
8	3	-60	37.74	72.81
9	2	-60	38.06	72.19
10	2	-60	38.52	71.73
11	2	-60	39.07	71.50
12	2	-60	39.49	70.96
13	2	-60	39.71	69.97
14	2	-60	40.12	69.42
15	2	-60	40.19	68.12
16	1	-60	40.53	67.40
17	1	-60	41.49	68.00
18	1	-60	42.16	67.94
19	1	-60	42.66	67.48
20	1	-60	42.90	66.42
21	1	-60	43.21	65.53
22	1	-60	42.56	62.38
23	1	-60	43.02	61.82
24	1	-60	43.31	60.88
25	3	-40	33.64	74.75
26	3	-40	33.83	74.06
27	3	-40	34.67	74.08
28	3	-40	35.52	74.09
29	3	-40	36.03	73.75
30	3	-40	36.50	73.38
31	3	-40	37.52	73.59
32	2	-40	37.58	72.69
33	2	-40	38.12	72.30
34	2	-40	38.84	72.11
35	2	-40	38.97	71.29
36	2	-40	39.14	70.51

Master Track ID	NACCS Subregion	Heading Direction, θ (deg)	Reference Latitude (deg N)	Reference Longitude (deg W)
37	2	-40	39.60	70.05
38	2	-40	39.75	69.26
39	1	-40	39.89	68.44
40	1	-40	41.22	68.85
41	1	-40	41.79	68.43
42	1	-40	42.14	67.76
43	1	-40	42.30	66.88
44	1	-40	42.73	66.31
45	1	-40	42.89	65.42
46	1	-40	41.95	63.30
47	1	-40	42.33	62.67
48	1	-40	42.76	62.10
49	1	-40	42.98	61.28
50	3	-20	33.23	75.34
51	3	-20	33.64	74.82
52	3	-20	35.21	74.80
53	3	-20	35.80	74.36
54	3	-20	37.15	74.28
55	2	-20	37.26	73.55
56	2	-20	37.94	73.07
57	2	-20	38.50	72.55
58	2	-20	38.65	71.83
59	2	-20	38.84	71.14
60	2	-20	39.25	70.55
61	1	-20	39.51	69.88
62	1	-20	40.88	69.74
63	1	-20	41.57	69.23
64	1	-20	41.76	68.45
65	1	-20	42.34	67.86
66	1	-20	42.29	66.97
67	1	-20	42.51	66.22
68	1	-20	41.59	64.90
69	1	-20	41.58	64.03
70	1	-20	42.07	63.42
71	1	-20	42.33	62.67
72	3	0	32.45	76.88
73	3	0	33.11	76.10
74	3	0	35.62	75.44
75	3	0	36.79	74.78
76	2	0	37.80	74.05
77	2	0	38.43	73.31
78	2	0	38.59	72.57
79	2	0	39.06	71.84
80	2	0	39.29	71.10
81	1	0	41.33	70.30

Master Track ID	NACCS Subregion	Heading Direction, θ (deg)	Reference Latitude (deg N)	Reference Longitude (deg W)
82	1	0	41.63	69.48
83	1	0	41.90	68.66
84	1	0	42.31	67.85
85	1	0	42.52	67.04
86	1	0	42.11	66.22
87	1	0	41.23	65.41
88	1	0	41.82	64.60
89	1	0	42.22	63.78
90	1	20	45.00	70.55
91	1	20	45.00	69.60
92	1	20	45.00	68.66
93	1	20	45.00	67.71
94	1	20	45.00	66.76
95	1	20	45.00	65.82
96	1	20	45.00	64.87
97	1	20	45.00	63.93
98	2	20	41.50	74.08
99	2	20	41.50	73.25
100	2	20	41.50	72.43
101	2	20	41.50	71.60
102	2	20	41.50	70.78
103	2	20	41.50	69.95
104	2	20	41.50	69.13
105	2	20	41.50	68.30
106	2	20	41.50	67.47
107	3	20	39.00	75.37
108	3	20	39.00	74.65
109	3	20	39.00	73.94
110	3	20	39.00	73.22
111	3	20	39.00	72.51
112	3	20	39.00	71.79
113	1	40	45.00	68.33
114	1	40	45.00	67.17
115	1	40	45.00	66.01
116	1	40	45.00	64.85
117	1	40	45.00	63.69
118	1	40	45.00	62.53
119	2	40	41.50	72.55
120	2	40	41.50	71.54
121	2	40	41.50	70.53
122	2	40	41.50	69.51
123	2	40	41.50	68.50
124	2	40	41.50	67.49
125	3	40	39.00	74.90
126	3	40	39.00	74.03

Master Track ID	NACCS Subregion	Heading Direction, θ (deg)	Reference Latitude (deg N)	Reference Longitude (deg W)
127	3	40	39.00	73.15
128	3	40	39.00	72.27
129	3	40	39.00	71.40
130	3	40	39.00	70.52

Appendix C: NACCS Synthetic TC Parameters

Following is a list of the 1,050 synthetic TCs that were developed for the NACCS study area. Storm parameters assigned to each cyclone are heading direction (θ), central pressure deficit (Δp), radius of maximum winds (R_{max}), and translational speed (V_t).

NACCS Synthetic Tropical Cyclone ID	NACCS Subregion	Master Track ID	θ (deg)	ΔP (hPa)	R_{max} (km)	V_t (km/h)
1	3	1	-60	88	39	18
2	3	1	-60	78	108	29
3	3	1	-60	68	62	42
4	3	1	-60	58	47	32
5	3	1	-60	48	64	12
6	3	1	-60	38	72	19
7	3	1	-60	28	26	39
8	3	2	-60	88	114	25
9	3	2	-60	78	51	30
10	3	2	-60	68	26	31
11	3	2	-60	58	37	12
12	3	2	-60	48	77	44
13	3	2	-60	38	72	13
14	3	2	-60	28	39	39
15	3	3	-60	88	105	24
16	3	3	-60	78	50	30
17	3	3	-60	68	39	12
18	3	3	-60	58	26	29
19	3	3	-60	48	82	44
20	3	3	-60	38	68	15
21	3	3	-60	28	42	40
22	3	4	-60	88	50	40
23	3	4	-60	78	51	29
24	3	4	-60	68	107	26
25	3	4	-60	58	65	12
26	3	4	-60	48	28	34
27	3	4	-60	38	37	13
28	3	4	-60	28	75	38
29	3	5	-60	88	77	37
30	3	5	-60	78	35	26
31	3	5	-60	68	62	12
32	3	5	-60	58	109	25
33	3	5	-60	48	49	25
34	3	5	-60	38	58	40
35	3	5	-60	28	25	35

NACCS Synthetic Tropical Cyclone ID	NACCS Subregion	Master Track ID	θ (deg)	ΔP (hPa)	R_{max} (km)	V_t (km/h)
36	3	6	-60	88	72	31
37	3	6	-60	78	38	27
38	3	6	-60	68	53	35
39	3	6	-60	58	105	28
40	3	6	-60	48	64	14
41	3	6	-60	38	25	28
42	3	6	-60	28	61	46
43	3	7	-60	88	50	37
44	3	7	-60	78	78	12
45	3	7	-60	68	104	35
46	3	7	-60	58	41	12
47	3	7	-60	48	25	31
48	3	7	-60	38	48	20
49	3	7	-60	28	71	33
50	3	8	-60	88	47	18
51	3	8	-60	78	75	40
52	3	8	-60	68	104	21
53	3	8	-60	58	41	39
54	3	8	-60	48	67	36
55	3	8	-60	38	25	19
56	3	8	-60	28	58	13
57	3	25	-40	88	53	20
58	3	25	-40	78	105	21
59	3	25	-40	68	29	22
60	3	25	-40	58	73	41
61	3	25	-40	48	51	40
62	3	25	-40	38	38	36
63	3	25	-40	28	65	12
64	3	26	-40	88	54	30
65	3	26	-40	78	104	30
66	3	26	-40	68	37	12
67	3	26	-40	58	29	38
68	3	26	-40	48	80	13
69	3	26	-40	38	63	47
70	3	26	-40	28	50	23
71	3	27	-40	88	44	24
72	3	27	-40	78	66	45
73	3	27	-40	68	117	25
74	3	27	-40	58	52	17
75	3	27	-40	48	26	20
76	3	27	-40	38	39	41
77	3	27	-40	28	74	23
78	3	28	-40	88	69	43
79	3	28	-40	78	53	16

NACCS Synthetic Tropical Cyclone ID	NACCS Subregion	Master Track ID	θ (deg)	ΔP (hPa)	R_{max} (km)	V_t (km/h)
80	3	28	-40	68	37	42
81	3	28	-40	58	103	23
82	3	28	-40	48	29	19
83	3	28	-40	38	62	38
84	3	28	-40	28	60	25
85	3	29	-40	88	53	35
86	3	29	-40	78	79	22
87	3	29	-40	68	32	22
88	3	29	-40	58	105	28
89	3	29	-40	48	55	12
90	3	29	-40	38	31	47
91	3	29	-40	28	59	39
92	3	30	-40	88	53	21
93	3	30	-40	78	42	22
94	3	30	-40	68	115	40
95	3	30	-40	58	25	33
96	3	30	-40	48	83	24
97	3	30	-40	38	50	45
98	3	30	-40	28	46	13
99	3	31	-40	88	65	16
100	3	31	-40	78	54	44
101	3	31	-40	68	104	31
102	3	31	-40	58	44	17
103	3	31	-40	48	27	32
104	3	31	-40	38	46	25
105	3	31	-40	28	74	21
106	3	50	-20	98	66	38
107	3	50	-20	88	76	12
108	3	50	-20	78	42	21
109	3	50	-20	68	113	32
110	3	50	-20	58	25	23
111	3	50	-20	48	37	49
112	3	50	-20	38	62	30
113	3	51	-20	98	48	26
114	3	51	-20	88	117	29
115	3	51	-20	78	68	42
116	3	51	-20	68	47	24
117	3	51	-20	58	72	12
118	3	51	-20	48	33	41
119	3	51	-20	38	31	12
120	3	52	-20	98	63	28
121	3	52	-20	88	38	22
122	3	52	-20	78	115	26
123	3	52	-20	68	70	38

NACCS Synthetic Tropical Cyclone ID	NACCS Subregion	Master Track ID	θ (deg)	ΔP (hPa)	R_{max} (km)	V_t (km/h)
124	3	52	-20	58	25	25
125	3	52	-20	48	44	43
126	3	52	-20	38	63	12
127	3	53	-20	98	59	19
128	3	53	-20	88	116	33
129	3	53	-20	78	27	36
130	3	53	-20	68	37	20
131	3	53	-20	58	56	46
132	3	53	-20	48	75	21
133	3	53	-20	38	45	20
134	3	54	-20	98	49	33
135	3	54	-20	88	100	17
136	3	54	-20	78	87	44
137	3	54	-20	68	28	20
138	3	54	-20	58	50	12
139	3	54	-20	48	65	27
140	3	54	-20	38	38	46
141	3	72	0	88	42	31
142	3	72	0	83	53	12
143	3	72	0	78	77	35
144	3	72	0	73	133	26
145	3	72	0	68	40	16
146	3	72	0	63	26	13
147	3	72	0	58	29	38
148	3	72	0	53	55	21
149	3	72	0	48	51	48
150	3	72	0	43	71	15
151	3	72	0	38	59	39
152	3	72	0	33	98	35
153	3	72	0	28	33	20
154	3	73	0	88	53	27
155	3	73	0	83	39	12
156	3	73	0	78	145	20
157	3	73	0	73	49	46
158	3	73	0	68	79	29
159	3	73	0	63	27	28
160	3	73	0	58	42	12
161	3	73	0	53	87	12
162	3	73	0	48	76	42
163	3	73	0	43	39	33
164	3	73	0	38	25	13
165	3	73	0	33	50	12
166	3	73	0	28	83	24
167	3	74	0	88	93	28

NACCS Synthetic Tropical Cyclone ID	NACCS Subregion	Master Track ID	θ (deg)	ΔP (hPa)	R_{max} (km)	V_t (km/h)
168	3	74	0	83	59	31
169	3	74	0	78	41	31
170	3	74	0	73	64	12
171	3	74	0	68	40	16
172	3	74	0	63	25	25
173	3	74	0	58	69	47
174	3	74	0	53	114	25
175	3	74	0	48	78	21
176	3	74	0	43	45	36
177	3	74	0	38	67	26
178	3	74	0	33	25	53
179	3	74	0	28	53	16
180	3	75	0	88	51	24
181	3	75	0	83	29	38
182	3	75	0	78	140	32
183	3	75	0	73	64	25
184	3	75	0	68	59	51
185	3	75	0	63	73	12
186	3	75	0	58	38	14
187	3	75	0	53	42	40
188	3	75	0	48	25	25
189	3	75	0	43	52	22
190	3	75	0	38	92	32
191	3	75	0	33	71	21
192	3	75	0	28	39	36
193	3	107	20	88	63	29
194	3	107	20	83	33	26
195	3	107	20	78	140	29
196	3	107	20	73	71	49
197	3	107	20	68	60	12
198	3	107	20	63	56	12
199	3	107	20	58	73	28
200	3	107	20	53	31	46
201	3	107	20	48	35	48
202	3	107	20	43	88	21
203	3	107	20	38	25	17
204	3	107	20	33	41	22
205	3	107	20	28	59	35
206	3	108	20	88	59	33
207	3	108	20	83	104	35
208	3	108	20	78	46	24
209	3	108	20	73	53	12
210	3	108	20	68	31	29
211	3	108	20	63	47	37

NACCS Synthetic Tropical Cyclone ID	NACCS Subregion	Master Track ID	θ (deg)	ΔP (hPa)	R_{max} (km)	V_t (km/h)
212	3	108	20	58	142	13
213	3	108	20	53	69	17
214	3	108	20	48	43	59
215	3	108	20	43	27	12
216	3	108	20	38	73	34
217	3	108	20	33	25	27
218	3	108	20	28	55	33
219	3	109	20	88	40	27
220	3	109	20	83	75	18
221	3	109	20	78	106	50
222	3	109	20	73	63	36
223	3	109	20	68	135	21
224	3	109	20	63	25	38
225	3	109	20	58	48	12
226	3	109	20	53	54	27
227	3	109	20	48	38	45
228	3	109	20	43	34	33
229	3	109	20	38	79	34
230	3	109	20	33	31	12
231	3	109	20	28	40	29
232	3	110	20	88	54	15
233	3	110	20	83	140	18
234	3	110	20	78	66	25
235	3	110	20	73	56	44
236	3	110	20	68	79	19
237	3	110	20	63	29	18
238	3	110	20	58	33	44
239	3	110	20	53	33	19
240	3	110	20	48	51	33
241	3	110	20	43	100	35
242	3	110	20	38	25	34
243	3	110	20	33	74	12
244	3	110	20	28	46	29
245	3	111	20	88	44	18
246	3	111	20	83	104	19
247	3	111	20	78	25	42
248	3	111	20	73	95	36
249	3	111	20	68	55	19
250	3	111	20	63	71	23
251	3	111	20	58	86	52
252	3	111	20	53	49	45
253	3	111	20	48	67	12
254	3	111	20	43	25	12
255	3	111	20	38	41	29

NACCS Synthetic Tropical Cyclone ID	NACCS Subregion	Master Track ID	θ (deg)	ΔP (hPa)	R_{max} (km)	V_t (km/h)
256	3	111	20	33	32	29
257	3	111	20	28	71	27
258	3	112	20	88	67	23
259	3	112	20	83	85	16
260	3	112	20	78	44	16
261	3	112	20	73	62	49
262	3	112	20	68	44	38
263	3	112	20	63	137	33
264	3	112	20	58	28	31
265	3	112	20	53	27	26
266	3	112	20	48	47	28
267	3	112	20	43	79	27
268	3	112	20	38	60	12
269	3	112	20	33	38	49
270	3	112	20	28	45	19
271	3	125	40	98	76	28
272	3	125	40	93	51	23
273	3	125	40	88	68	46
274	3	125	40	83	89	20
275	3	125	40	78	139	30
276	3	125	40	73	26	20
277	3	125	40	68	55	12
278	3	125	40	63	41	28
279	3	125	40	58	35	35
280	3	125	40	53	25	34
281	3	125	40	48	61	35
282	3	125	40	43	79	21
283	3	125	40	38	47	27
284	3	126	40	98	92	33
285	3	126	40	93	45	35
286	3	126	40	88	34	27
287	3	126	40	83	125	23
288	3	126	40	78	62	26
289	3	126	40	73	61	30
290	3	126	40	68	74	15
291	3	126	40	63	25	31
292	3	126	40	58	25	31
293	3	126	40	53	83	44
294	3	126	40	48	42	59
295	3	126	40	43	35	12
296	3	126	40	38	63	47
297	3	127	40	98	68	20
298	3	127	40	93	132	22
299	3	127	40	88	55	37

NACCS Synthetic Tropical Cyclone ID	NACCS Subregion	Master Track ID	θ (deg)	ΔP (hPa)	R_{max} (km)	V_t (km/h)
300	3	127	40	83	50	12
301	3	127	40	78	40	50
302	3	127	40	73	30	27
303	3	127	40	68	98	31
304	3	127	40	63	60	17
305	3	127	40	58	90	21
306	3	127	40	53	34	13
307	3	127	40	48	43	12
308	3	127	40	43	38	21
309	3	127	40	38	26	40
310	3	128	40	98	92	40
311	3	128	40	93	44	27
312	3	128	40	88	60	42
313	3	128	40	83	75	18
314	3	128	40	78	67	39
315	3	128	40	73	126	30
316	3	128	40	68	62	12
317	3	128	40	63	30	39
318	3	128	40	58	26	42
319	3	128	40	53	58	51
320	3	128	40	48	25	15
321	3	128	40	43	39	17
322	3	128	40	38	73	26
323	3	129	40	98	61	27
324	3	129	40	93	71	46
325	3	129	40	88	121	22
326	3	129	40	83	46	22
327	3	129	40	78	25	34
328	3	129	40	73	70	15
329	3	129	40	68	50	54
330	3	129	40	63	42	12
331	3	129	40	58	48	38
332	3	129	40	53	27	16
333	3	129	40	48	88	34
334	3	129	40	43	64	33
335	3	129	40	38	57	12
336	3	130	40	98	104	12
337	3	130	40	93	87	31
338	3	130	40	88	46	12
339	3	130	40	83	40	25
340	3	130	40	78	61	36
341	3	130	40	73	79	12
342	3	130	40	68	28	35
343	3	130	40	63	103	31

NACCS Synthetic Tropical Cyclone ID	NACCS Subregion	Master Track ID	θ (deg)	ΔP (hPa)	R_{max} (km)	V_t (km/h)
344	3	130	40	58	56	19
345	3	130	40	53	42	33
346	3	130	40	48	45	57
347	3	130	40	43	53	32
348	3	130	40	38	26	14
349	2	9	-60	78	125	65
350	2	9	-60	68	52	26
351	2	9	-60	58	56	61
352	2	9	-60	48	57	25
353	2	9	-60	38	29	43
354	2	9	-60	28	93	37
355	2	10	-60	78	51	36
356	2	10	-60	68	127	55
357	2	10	-60	58	88	28
358	2	10	-60	48	67	64
359	2	10	-60	38	31	52
360	2	10	-60	28	47	25
361	2	11	-60	78	125	43
362	2	11	-60	68	61	26
363	2	11	-60	58	69	62
364	2	11	-60	48	39	53
365	2	11	-60	38	35	35
366	2	11	-60	28	82	39
367	2	12	-60	78	50	45
368	2	12	-60	68	139	48
369	2	12	-60	58	79	31
370	2	12	-60	48	75	67
371	2	12	-60	38	41	24
372	2	12	-60	28	34	64
373	2	13	-60	78	47	29
374	2	13	-60	68	77	56
375	2	13	-60	58	127	49
376	2	13	-60	48	56	61
377	2	13	-60	38	80	27
378	2	13	-60	28	30	52
379	2	14	-60	78	55	28
380	2	14	-60	68	126	42
381	2	14	-60	58	79	65
382	2	14	-60	48	48	58
383	2	14	-60	38	30	38
384	2	14	-60	28	76	32
385	2	15	-60	78	66	60
386	2	15	-60	68	44	30
387	2	15	-60	58	127	48

NACCS Synthetic Tropical Cyclone ID	NACCS Subregion	Master Track ID	θ (deg)	ΔP (hPa)	R_{max} (km)	V_t (km/h)
388	2	15	-60	48	81	23
389	2	15	-60	38	33	62
390	2	15	-60	28	65	50
391	2	32	-40	78	47	57
392	2	32	-40	68	130	42
393	2	32	-40	58	74	25
394	2	32	-40	48	26	45
395	2	32	-40	38	46	33
396	2	32	-40	28	76	59
397	2	33	-40	78	67	63
398	2	33	-40	68	126	45
399	2	33	-40	58	74	22
400	2	33	-40	48	44	38
401	2	33	-40	38	29	68
402	2	33	-40	28	78	50
403	2	34	-40	78	67	61
404	2	34	-40	68	42	32
405	2	34	-40	58	80	25
406	2	34	-40	48	127	50
407	2	34	-40	38	33	65
408	2	34	-40	28	63	50
409	2	35	-40	78	44	28
410	2	35	-40	68	64	60
411	2	35	-40	58	125	51
412	2	35	-40	48	67	55
413	2	35	-40	38	79	24
414	2	35	-40	28	33	58
415	2	36	-40	78	46	25
416	2	36	-40	68	62	62
417	2	36	-40	58	126	61
418	2	36	-40	48	94	30
419	2	36	-40	38	30	55
420	2	36	-40	28	59	41
421	2	37	-40	78	82	59
422	2	37	-40	68	61	24
423	2	37	-40	58	44	60
424	2	37	-40	48	128	36
425	2	37	-40	38	31	29
426	2	37	-40	28	70	48
427	2	38	-40	78	52	23
428	2	38	-40	68	126	40
429	2	38	-40	58	45	55
430	2	38	-40	48	81	69
431	2	38	-40	38	72	33

NACCS Synthetic Tropical Cyclone ID	NACCS Subregion	Master Track ID	θ (deg)	ΔP (hPa)	R_{max} (km)	V_t (km/h)
432	2	38	-40	28	26	34
433	2	55	-20	88	55	62
434	2	55	-20	78	82	27
435	2	55	-20	68	126	50
436	2	55	-20	58	28	52
437	2	55	-20	48	48	29
438	2	55	-20	38	76	57
439	2	56	-20	88	47	36
440	2	56	-20	78	130	42
441	2	56	-20	68	50	68
442	2	56	-20	58	73	23
443	2	56	-20	48	79	56
444	2	56	-20	38	36	44
445	2	57	-20	88	60	45
446	2	57	-20	78	129	43
447	2	57	-20	68	43	29
448	2	57	-20	58	75	63
449	2	57	-20	48	37	58
450	2	57	-20	38	72	28
451	2	58	-20	88	43	38
452	2	58	-20	78	82	29
453	2	58	-20	68	66	64
454	2	58	-20	58	128	52
455	2	58	-20	48	29	64
456	2	58	-20	38	51	32
457	2	59	-20	88	58	34
458	2	59	-20	78	50	35
459	2	59	-20	68	126	48
460	2	59	-20	58	68	66
461	2	59	-20	48	34	48
462	2	59	-20	38	80	29
463	2	60	-20	88	67	56
464	2	60	-20	78	126	41
465	2	60	-20	68	34	26
466	2	60	-20	58	66	22
467	2	60	-20	48	40	54
468	2	60	-20	38	78	57
469	2	76	0	78	74	38
470	2	76	0	73	89	79
471	2	76	0	68	112	14
472	2	76	0	63	35	36
473	2	76	0	58	62	50
474	2	76	0	53	25	54
475	2	76	0	48	58	47

NACCS Synthetic Tropical Cyclone ID	NACCS Subregion	Master Track ID	θ (deg)	ΔP (hPa)	R_{max} (km)	V_t (km/h)
476	2	76	0	43	42	66
477	2	76	0	38	126	47
478	2	76	0	33	52	19
479	2	76	0	28	71	60
480	2	77	0	78	58	75
481	2	77	0	73	61	32
482	2	77	0	68	143	30
483	2	77	0	63	36	33
484	2	77	0	58	97	59
485	2	77	0	53	60	29
486	2	77	0	48	49	58
487	2	77	0	43	98	39
488	2	77	0	38	25	56
489	2	77	0	33	61	54
490	2	77	0	28	60	18
491	2	78	0	78	117	38
492	2	78	0	73	73	62
493	2	78	0	68	42	43
494	2	78	0	63	76	21
495	2	78	0	58	56	68
496	2	78	0	53	25	30
497	2	78	0	48	45	29
498	2	78	0	43	80	50
499	2	78	0	38	132	45
500	2	78	0	33	39	66
501	2	78	0	28	61	40
502	2	79	0	78	82	47
503	2	79	0	73	46	42
504	2	79	0	68	96	68
505	2	79	0	63	74	18
506	2	79	0	58	130	32
507	2	79	0	53	33	14
508	2	79	0	48	94	45
509	2	79	0	43	28	55
510	2	79	0	38	64	38
511	2	79	0	33	58	66
512	2	79	0	28	46	39
513	2	80	0	78	71	26
514	2	80	0	73	76	56
515	2	80	0	68	140	50
516	2	80	0	63	44	44
517	2	80	0	58	52	88
518	2	80	0	53	25	56
519	2	80	0	48	51	50

NACCS Synthetic Tropical Cyclone ID	NACCS Subregion	Master Track ID	θ (deg)	ΔP (hPa)	R_{max} (km)	V_t (km/h)
520	2	80	0	43	83	69
521	2	80	0	38	37	14
522	2	80	0	33	99	35
523	2	80	0	28	62	38
524	2	98	20	78	73	38
525	2	98	20	73	86	82
526	2	98	20	68	83	32
527	2	98	20	63	50	55
528	2	98	20	58	37	34
529	2	98	20	53	137	39
530	2	98	20	48	59	22
531	2	98	20	43	28	49
532	2	98	20	38	92	51
533	2	98	20	33	59	58
534	2	98	20	28	45	35
535	2	99	20	78	41	33
536	2	99	20	73	69	61
537	2	99	20	68	108	22
538	2	99	20	63	145	50
539	2	99	20	58	26	50
540	2	99	20	53	70	17
541	2	99	20	48	58	39
542	2	99	20	43	41	77
543	2	99	20	38	50	47
544	2	99	20	33	41	39
545	2	99	20	28	100	49
546	2	100	20	78	70	34
547	2	100	20	73	36	60
548	2	100	20	68	144	52
549	2	100	20	63	73	22
550	2	100	20	58	70	56
551	2	100	20	53	44	39
552	2	100	20	48	60	60
553	2	100	20	43	25	41
554	2	100	20	38	103	42
555	2	100	20	33	50	74
556	2	100	20	28	61	23
557	2	101	20	78	77	32
558	2	101	20	73	62	65
559	2	101	20	68	33	42
560	2	101	20	63	138	49
561	2	101	20	58	62	27
562	2	101	20	53	93	58
563	2	101	20	48	101	23

NACCS Synthetic Tropical Cyclone ID	NACCS Subregion	Master Track ID	θ (deg)	ΔP (hPa)	R_{max} (km)	V_t (km/h)
564	2	101	20	43	42	14
565	2	101	20	38	48	46
566	2	101	20	33	61	48
567	2	101	20	28	33	84
568	2	102	20	78	60	44
569	2	102	20	73	96	33
570	2	102	20	68	57	73
571	2	102	20	63	145	43
572	2	102	20	58	32	55
573	2	102	20	53	31	24
574	2	102	20	48	90	51
575	2	102	20	43	35	39
576	2	102	20	38	85	14
577	2	102	20	33	57	46
578	2	102	20	28	57	46
579	2	103	20	78	44	34
580	2	103	20	73	78	33
581	2	103	20	68	139	65
582	2	103	20	63	65	61
583	2	103	20	58	111	29
584	2	103	20	53	30	49
585	2	103	20	48	58	29
586	2	103	20	43	50	53
587	2	103	20	38	42	60
588	2	103	20	33	41	14
589	2	103	20	28	95	51
590	2	104	20	78	68	57
591	2	104	20	73	141	37
592	2	104	20	68	58	26
593	2	104	20	63	32	55
594	2	104	20	58	79	44
595	2	104	20	53	33	43
596	2	104	20	48	39	14
597	2	104	20	43	83	17
598	2	104	20	38	54	50
599	2	104	20	33	55	60
600	2	104	20	28	100	54
601	2	105	20	78	68	48
602	2	105	20	73	128	60
603	2	105	20	68	67	22
604	2	105	20	63	66	56
605	2	105	20	58	62	78
606	2	105	20	53	56	24
607	2	105	20	48	32	53

NACCS Synthetic Tropical Cyclone ID	NACCS Subregion	Master Track ID	θ (deg)	ΔP (hPa)	R_{max} (km)	V_t (km/h)
608	2	105	20	43	38	28
609	2	105	20	38	62	63
610	2	105	20	33	100	37
611	2	105	20	28	52	47
612	2	106	20	78	118	25
613	2	106	20	73	61	51
614	2	106	20	68	36	28
615	2	106	20	63	58	36
616	2	106	20	58	74	29
617	2	106	20	53	50	59
618	2	106	20	48	93	57
619	2	106	20	43	126	34
620	2	106	20	38	27	62
621	2	106	20	33	57	27
622	2	106	20	28	51	62
623	2	119	40	88	66	31
624	2	119	40	83	94	43
625	2	119	40	78	76	60
626	2	119	40	73	46	45
627	2	119	40	68	45	88
628	2	119	40	63	129	56
629	2	119	40	58	98	29
630	2	119	40	53	29	50
631	2	119	40	48	46	14
632	2	119	40	43	66	53
633	2	119	40	38	52	34
634	2	120	40	88	69	39
635	2	120	40	83	137	57
636	2	120	40	78	47	14
637	2	120	40	73	64	79
638	2	120	40	68	60	45
639	2	120	40	63	33	29
640	2	120	40	58	34	56
641	2	120	40	53	102	41
642	2	120	40	48	54	41
643	2	120	40	43	72	17
644	2	120	40	38	64	67
645	2	121	40	88	105	33
646	2	121	40	83	67	59
647	2	121	40	78	46	36
648	2	121	40	73	50	53
649	2	121	40	68	33	76
650	2	121	40	63	126	38
651	2	121	40	58	68	21

NACCS Synthetic Tropical Cyclone ID	NACCS Subregion	Master Track ID	θ (deg)	ΔP (hPa)	R_{max} (km)	V_t (km/h)
652	2	121	40	53	28	31
653	2	121	40	48	85	49
654	2	121	40	43	88	69
655	2	121	40	38	54	54
656	2	122	40	88	146	44
657	2	122	40	83	54	27
658	2	122	40	78	63	71
659	2	122	40	73	67	36
660	2	122	40	68	87	14
661	2	122	40	63	25	28
662	2	122	40	58	63	44
663	2	122	40	53	43	29
664	2	122	40	48	115	44
665	2	122	40	43	32	59
666	2	122	40	38	68	45
667	2	123	40	88	75	58
668	2	123	40	83	48	35
669	2	123	40	78	136	40
670	2	123	40	73	37	73
671	2	123	40	68	92	33
672	2	123	40	63	27	34
673	2	123	40	58	54	47
674	2	123	40	53	76	28
675	2	123	40	48	105	58
676	2	123	40	43	53	52
677	2	123	40	38	40	14
678	2	124	40	88	158	62
679	2	124	40	83	46	51
680	2	124	40	78	62	49
681	2	124	40	73	51	16
682	2	124	40	68	90	17
683	2	124	40	63	70	45
684	2	124	40	58	62	80
685	2	124	40	53	29	71
686	2	124	40	48	27	34
687	2	124	40	43	105	56
688	2	124	40	38	51	46
689	1	16	-60	68	153	58
690	1	16	-60	58	51	36
691	1	16	-60	48	75	66
692	1	16	-60	38	95	35
693	1	16	-60	28	36	66
694	1	17	-60	68	53	48
695	1	17	-60	58	151	53

NACCS Synthetic Tropical Cyclone ID	NACCS Subregion	Master Track ID	θ (deg)	ΔP (hPa)	R_{max} (km)	V_t (km/h)
696	1	17	-60	48	89	33
697	1	17	-60	38	83	70
698	1	17	-60	28	28	51
699	1	18	-60	68	50	60
700	1	18	-60	58	154	46
701	1	18	-60	48	78	35
702	1	18	-60	38	92	68
703	1	18	-60	28	35	29
704	1	19	-60	68	69	66
705	1	19	-60	58	151	61
706	1	19	-60	48	98	37
707	1	19	-60	38	33	60
708	1	19	-60	28	53	34
709	1	20	-60	68	152	44
710	1	20	-60	58	52	60
711	1	20	-60	48	78	33
712	1	20	-60	38	92	67
713	1	20	-60	28	36	32
714	1	21	-60	68	79	61
715	1	21	-60	58	153	53
716	1	21	-60	48	48	37
717	1	21	-60	38	40	71
718	1	21	-60	28	91	28
719	1	22	-60	68	54	51
720	1	22	-60	58	154	49
721	1	22	-60	48	86	31
722	1	22	-60	38	88	68
723	1	22	-60	28	30	44
724	1	23	-60	68	50	61
725	1	23	-60	58	150	46
726	1	23	-60	48	79	36
727	1	23	-60	38	93	71
728	1	23	-60	28	38	28
729	1	24	-60	68	52	62
730	1	24	-60	58	150	42
731	1	24	-60	48	77	33
732	1	24	-60	38	96	67
733	1	24	-60	28	36	34
734	1	39	-40	68	51	49
735	1	39	-40	58	152	49
736	1	39	-40	48	86	31
737	1	39	-40	38	85	68
738	1	39	-40	28	26	50
739	1	40	-40	68	151	44

NACCS Synthetic Tropical Cyclone ID	NACCS Subregion	Master Track ID	θ (deg)	ΔP (hPa)	R_{max} (km)	V_t (km/h)
740	1	40	-40	58	77	35
741	1	40	-40	48	50	62
742	1	40	-40	38	37	30
743	1	40	-40	28	93	68
744	1	41	-40	68	54	64
745	1	41	-40	58	151	40
746	1	41	-40	48	70	29
747	1	41	-40	38	94	61
748	1	41	-40	28	35	40
749	1	42	-40	68	51	34
750	1	42	-40	58	151	59
751	1	42	-40	48	74	65
752	1	42	-40	38	96	34
753	1	42	-40	28	36	63
754	1	43	-40	68	51	37
755	1	43	-40	58	151	55
756	1	43	-40	48	78	64
757	1	43	-40	38	94	30
758	1	43	-40	28	37	67
759	1	44	-40	68	68	66
760	1	44	-40	58	152	65
761	1	44	-40	48	101	39
762	1	44	-40	38	54	32
763	1	44	-40	28	34	57
764	1	45	-40	68	51	65
765	1	45	-40	58	150	43
766	1	45	-40	48	76	36
767	1	45	-40	38	95	67
768	1	45	-40	28	37	34
769	1	46	-40	68	48	36
770	1	46	-40	58	151	55
771	1	46	-40	48	79	61
772	1	46	-40	38	42	71
773	1	46	-40	28	91	29
774	1	47	-40	68	52	65
775	1	47	-40	58	151	41
776	1	47	-40	48	71	30
777	1	47	-40	38	92	61
778	1	47	-40	28	36	41
779	1	48	-40	68	50	61
780	1	48	-40	58	153	45
781	1	48	-40	48	78	34
782	1	48	-40	38	91	67
783	1	48	-40	28	38	29

NACCS Synthetic Tropical Cyclone ID	NACCS Subregion	Master Track ID	θ (deg)	ΔP (hPa)	R_{max} (km)	V_t (km/h)
784	1	49	-40	68	48	60
785	1	49	-40	58	80	36
786	1	49	-40	48	151	47
787	1	49	-40	38	89	69
788	1	49	-40	28	40	29
789	1	61	-20	78	52	36
790	1	61	-20	68	76	66
791	1	61	-20	58	154	54
792	1	61	-20	48	93	33
793	1	61	-20	38	36	64
794	1	62	-20	78	49	37
795	1	62	-20	68	150	52
796	1	62	-20	58	79	65
797	1	62	-20	48	87	32
798	1	62	-20	38	40	66
799	1	63	-20	78	63	35
800	1	63	-20	68	103	57
801	1	63	-20	58	150	30
802	1	63	-20	48	58	72
803	1	63	-20	38	33	48
804	1	64	-20	78	52	64
805	1	64	-20	68	75	35
806	1	64	-20	58	151	41
807	1	64	-20	48	97	67
808	1	64	-20	38	37	35
809	1	65	-20	78	51	63
810	1	65	-20	68	150	45
811	1	65	-20	58	78	35
812	1	65	-20	48	92	69
813	1	65	-20	38	39	33
814	1	66	-20	78	51	36
815	1	66	-20	68	78	63
816	1	66	-20	58	152	55
817	1	66	-20	48	94	30
818	1	66	-20	38	37	67
819	1	67	-20	78	51	36
820	1	67	-20	68	79	66
821	1	67	-20	58	153	53
822	1	67	-20	48	37	66
823	1	67	-20	38	91	34
824	1	68	-20	78	59	69
825	1	68	-20	68	166	50
826	1	68	-20	58	34	49
827	1	68	-20	48	93	49

NACCS Synthetic Tropical Cyclone ID	NACCS Subregion	Master Track ID	θ (deg)	ΔP (hPa)	R_{max} (km)	V_t (km/h)
828	1	68	-20	38	58	29
829	1	69	-20	78	52	61
830	1	69	-20	68	151	43
831	1	69	-20	58	95	67
832	1	69	-20	48	36	32
833	1	69	-20	38	78	34
834	1	70	-20	78	49	60
835	1	70	-20	68	81	35
836	1	70	-20	58	150	48
837	1	70	-20	48	87	68
838	1	70	-20	38	42	32
839	1	71	-20	78	38	67
840	1	71	-20	68	156	55
841	1	71	-20	58	92	33
842	1	71	-20	48	77	65
843	1	71	-20	38	49	37
844	1	81	0	68	89	43
845	1	81	0	63	55	49
846	1	81	0	58	154	54
847	1	81	0	53	32	60
848	1	81	0	48	86	52
849	1	81	0	43	74	73
850	1	81	0	38	70	18
851	1	81	0	33	44	43
852	1	81	0	28	104	42
853	1	82	0	68	64	51
854	1	82	0	63	84	62
855	1	82	0	58	156	46
856	1	82	0	53	28	58
857	1	82	0	48	80	25
858	1	82	0	43	43	33
859	1	82	0	38	49	64
860	1	82	0	33	104	55
861	1	82	0	28	61	60
862	1	83	0	68	72	60
863	1	83	0	63	162	50
864	1	83	0	58	58	72
865	1	83	0	53	49	31
866	1	83	0	48	32	53
867	1	83	0	43	100	26
868	1	83	0	38	72	38
869	1	83	0	33	105	59
870	1	83	0	28	51	58
871	1	84	0	68	80	59

NACCS Synthetic Tropical Cyclone ID	NACCS Subregion	Master Track ID	θ (deg)	ΔP (hPa)	R_{max} (km)	V_t (km/h)
872	1	84	0	63	57	48
873	1	84	0	58	107	70
874	1	84	0	53	153	49
875	1	84	0	48	32	41
876	1	84	0	43	100	34
877	1	84	0	38	42	73
878	1	84	0	33	54	27
879	1	84	0	28	73	57
880	1	85	0	68	85	30
881	1	85	0	63	52	51
882	1	85	0	58	154	47
883	1	85	0	53	103	54
884	1	85	0	48	78	35
885	1	85	0	43	83	72
886	1	85	0	38	36	38
887	1	85	0	33	38	79
888	1	85	0	28	59	48
889	1	86	0	68	79	25
890	1	86	0	63	151	48
891	1	86	0	58	80	67
892	1	86	0	53	52	46
893	1	86	0	48	45	83
894	1	86	0	43	33	43
895	1	86	0	38	98	59
896	1	86	0	33	99	40
897	1	86	0	28	57	53
898	1	87	0	68	104	68
899	1	87	0	63	70	29
900	1	87	0	58	54	53
901	1	87	0	53	163	40
902	1	87	0	48	32	52
903	1	87	0	43	97	42
904	1	87	0	38	56	65
905	1	87	0	33	49	29
906	1	87	0	28	79	56
907	1	88	0	68	83	56
908	1	88	0	63	50	44
909	1	88	0	58	168	43
910	1	88	0	53	80	28
911	1	88	0	48	42	79
912	1	88	0	43	59	67
913	1	88	0	38	104	61
914	1	88	0	33	36	38
915	1	88	0	28	71	42

NACCS Synthetic Tropical Cyclone ID	NACCS Subregion	Master Track ID	θ (deg)	ΔP (hPa)	R_{max} (km)	V_t (km/h)
916	1	89	0	68	76	61
917	1	89	0	63	83	41
918	1	89	0	58	170	52
919	1	89	0	53	48	46
920	1	89	0	48	26	53
921	1	89	0	43	64	25
922	1	89	0	38	101	44
923	1	89	0	33	75	74
924	1	89	0	28	50	56
925	1	90	20	68	50	41
926	1	90	20	63	94	37
927	1	90	20	58	66	78
928	1	90	20	53	162	47
929	1	90	20	48	57	54
930	1	90	20	43	30	55
931	1	90	20	38	72	20
932	1	90	20	33	93	61
933	1	90	20	28	59	60
934	1	91	20	68	89	40
935	1	91	20	63	60	47
936	1	91	20	58	31	54
937	1	91	20	53	174	45
938	1	91	20	48	102	72
939	1	91	20	43	56	69
940	1	91	20	38	38	32
941	1	91	20	33	98	38
942	1	91	20	28	54	30
943	1	92	20	68	87	51
944	1	92	20	63	101	31
945	1	92	20	58	52	50
946	1	92	20	53	50	45
947	1	92	20	48	155	51
948	1	92	20	43	27	45
949	1	92	20	38	87	61
950	1	92	20	33	49	81
951	1	92	20	28	75	28
952	1	93	20	68	55	50
953	1	93	20	63	112	16
954	1	93	20	58	35	54
955	1	93	20	53	165	52
956	1	93	20	48	75	45
957	1	93	20	43	67	79
958	1	93	20	38	51	17
959	1	93	20	33	102	49

NACCS Synthetic Tropical Cyclone ID	NACCS Subregion	Master Track ID	θ (deg)	ΔP (hPa)	R_{max} (km)	V_t (km/h)
960	1	93	20	28	48	53
961	1	94	20	68	100	38
962	1	94	20	63	82	74
963	1	94	20	58	59	47
964	1	94	20	53	151	53
965	1	94	20	48	64	59
966	1	94	20	43	34	71
967	1	94	20	38	41	35
968	1	94	20	33	78	25
969	1	94	20	28	94	49
970	1	95	20	68	62	42
971	1	95	20	63	92	57
972	1	95	20	58	156	29
973	1	95	20	53	35	57
974	1	95	20	48	113	57
975	1	95	20	43	50	46
976	1	95	20	38	61	69
977	1	95	20	33	74	36
978	1	95	20	28	42	26
979	1	96	20	68	109	71
980	1	96	20	63	88	28
981	1	96	20	58	52	57
982	1	96	20	53	28	51
983	1	96	20	48	152	46
984	1	96	20	43	77	51
985	1	96	20	38	50	29
986	1	96	20	33	88	54
987	1	96	20	28	55	73
988	1	97	20	68	85	59
989	1	97	20	63	83	25
990	1	97	20	58	40	66
991	1	97	20	53	68	66
992	1	97	20	48	150	36
993	1	97	20	43	59	34
994	1	97	20	38	108	50
995	1	97	20	33	30	38
996	1	97	20	28	62	65
997	1	113	40	78	82	56
998	1	113	40	73	156	48
999	1	113	40	68	45	34
1000	1	113	40	63	82	23
1001	1	113	40	58	34	64
1002	1	113	40	53	69	83
1003	1	113	40	48	58	52

NACCS Synthetic Tropical Cyclone ID	NACCS Subregion	Master Track ID	θ (deg)	ΔP (hPa)	R_{max} (km)	V_t (km/h)
1004	1	113	40	43	113	52
1005	1	113	40	38	69	45
1006	1	114	40	78	117	64
1007	1	114	40	73	58	51
1008	1	114	40	68	73	19
1009	1	114	40	63	56	54
1010	1	114	40	58	152	39
1011	1	114	40	53	29	57
1012	1	114	40	48	40	29
1013	1	114	40	43	73	77
1014	1	114	40	38	87	43
1015	1	115	40	78	157	53
1016	1	115	40	73	55	23
1017	1	115	40	68	71	45
1018	1	115	40	63	51	73
1019	1	115	40	58	74	48
1020	1	115	40	53	96	75
1021	1	115	40	48	31	49
1022	1	115	40	43	113	36
1023	1	115	40	38	57	48
1024	1	116	40	78	65	47
1025	1	116	40	73	154	47
1026	1	116	40	68	39	67
1027	1	116	40	63	35	27
1028	1	116	40	58	100	26
1029	1	116	40	53	70	79
1030	1	116	40	48	104	58
1031	1	116	40	43	71	36
1032	1	116	40	38	53	45
1033	1	117	40	78	83	67
1034	1	117	40	73	88	27
1035	1	117	40	68	156	45
1036	1	117	40	63	45	52
1037	1	117	40	58	33	28
1038	1	117	40	53	73	44
1039	1	117	40	48	64	42
1040	1	117	40	43	53	81
1041	1	117	40	38	107	53
1042	1	118	40	78	174	43
1043	1	118	40	73	77	62
1044	1	118	40	68	58	66
1045	1	118	40	63	39	61
1046	1	118	40	58	74	32
1047	1	118	40	53	39	33

NACCS Synthetic Tropical Cyclone ID	NACCS Subregion	Master Track ID	θ (deg)	ΔP (hPa)	R_{max} (km)	V_t (km/h)
1048	1	118	40	48	69	32
1049	1	118	40	43	114	50
1050	1	118	40	38	59	57

Appendix D: NACCS Analysis of Nonlinear Residuals White Paper

White Paper
Focus Study on Nonlinear Residuals and Uncertainty Associated with the Use of Linear Superposition to Estimate Coastal Storm Extreme Water Levels

U.S. Army Engineer Research and Development Center, Coastal and Hydraulics Laboratory (ERDC-CHL)

Written by
Norberto C. Nadal-Caraballo, Jeffrey A. Melby, and Victor M. Gonzalez

(3/28/2015)

Incorporating contributions by
Mary A. Cialone, Fatima Diop, Brittany L. Gunkel, Thomas C. Massey, Tate O. McAlpin, and Kimberly C. Pevey

Executive Summary

The North Atlantic Coast Comprehensive Study (NACCS) wave and water level modeling and statistical analysis study addresses the coastal storm hazard for the east coast of the United States from Maine to Virginia. The primary goal is to determine, as accurately as possible, coastal storm effects, including coastal flooding, wave and wind characteristics for ocean-front locations throughout the region. The information developed here can be used in project design and evaluation, as well as in a wide range of other studies such as risk assessments and critical infrastructure evaluations.

Within the NACCS, coastal storm waves and water levels are being modeled for a suite of 1150 storms covering a range of storm sizes, intensities, and landfall locations. The project includes three storm suites that each encompasses a full range of storm frequencies from frequent to rare. The three storm suites include (1) a base case where storms are modeled on the current mean sea level, (2) a case with a single random tide per storm, and (3) a case with a single random tide per storm and a single sea level change (SLC) scenario. If Suite 1 is used for engineering studies, water level components (e.g., surge, tide, and SLC) will be obtained by linear superimposition. However, in reality, these water level components interact in a complex, nonlinear way. As a result, linear superposition generates an error, or nonlinear residual (NLR), that must be accounted for with further calculations.

The focused study described in this paper addresses the uncertainty in applying linear superposition of water level components. To address this problem prior to completing NACCS high-fidelity modeling, a focused study was conducted using recent modeling performed for the Federal Emergency Management Agency (FEMA) Region II Risk Mapping Assessment and Planning (Risk MAP) study for a smaller region of the East Coast. The premise of the focused study was to relatively quickly compute and assess the error produced by applying the linear superposition technique within the FEMA Region II Risk MAP study region, thus providing a *proof-of-concept* for application of the linear superposition technique to the larger domain NACCS modeling effort. The focused study concentrated on the New York and New Jersey coastal region, with reduced Advance Circulation (ADCIRC) (Westerink et al. 1992) model resolution outside that area. The focused study used the computational mesh and storm climatology suite applied in the FEMA

Region II Risk MAP study, which had fewer synthetic storms (159) sampled from the joint probability model (FEMA 2014) than the more detailed NACCS effort. Only one SLC realization (1.0 m) was analyzed for the focused study.

The focused study also assumes a stationary climate for TC activity in the region. The assumption of stationarity means that the future conditions can be described within the envelope of aleatory variability observed in the past (Milly et al. 2008). As a result, the only long-term climate change considered is the SLC scenario. For future time horizons, the impacts of climate change could potentially alter TC hazards beyond what is presented by this analysis (e.g., beyond changing sea levels). However, recent studies do project changes in Atlantic TC climate over the twenty-first century, including Knutson et al. (2013) and Emanuel (2013).

The analysis shows that the linear superposition of water level components adequately represents extreme water levels with a correction factor for the small bias over the majority of the coastal region. However, in some areas characterized by constrained geometric features like small interior bays and canals, the NLR can be non-negligible. Unfortunately, many of these areas are the most highly developed areas. For most of these areas, the NLR can be accounted for within the statistical analysis, but in some areas, or for certain types of studies, the NACCS full simulation (nonlinear) results must be used.

D1 Introduction

This white paper summarizes the methodology and results of a focused study on the nonlinear effects on extreme water levels due to the interaction of storm surge with astronomical tide and SLC. This study was done as part of the U.S. Army Corps of Engineers (USACE) NACCS. It is common practice in engineering studies to separately model storm surge, tide, and SLC and then linearly superimpose these time series or the peaks. However, as is described in this paper, these processes interact in a nonlinear way. Linear superposition introduces an error that is called the nonlinearity or the NLR. This error can vary spatially and temporally depending on a number of factors including the tide phase, relative phase between tide and surge, water depth, shoreline geometry, and bathymetry, among other things.

The study described in this paper included modeling a range of storm surge, tide, and SLC conditions on the FEMA Region II domain model, which reasonably meets the objective of discerning the NLRs. Although NACCS spans the entire coastal region from Virginia to Maine, for this focus study, efforts were concentrated on quantifying the NLR within a subregion consisting of the coastal areas of New York and New Jersey using FEMA Region II ADCIRC mesh. This subregion is representative of the larger region with respect to these processes. The focused study took advantage of the readily available storm climatology, as well as a smaller, more efficient mesh that eases the computational burden. This focused effort was required to inform the larger and more detailed NACCS modeling study in a timely manner and to avoid significant impacts to the overall schedule and budget.

D1.1 Background

Storm surge is a temporary increment of the water surface elevation caused primarily by wind stress and atmospheric pressure deficit associated with moving storm systems such as tropical and extratropical cyclones, TC and XC, respectively. Storm water levels can reach high elevations along the coastline and can cause extensive damage to coastal and inland areas. Shelf geometry, interaction with astronomical tide, and SLC play significant roles in altering the basic storm surge response to wind and pressure forcing. For the NACCS region, storm surges due to TCs are typically higher than those generated by XCs. In addition, tides make a much larger contribution to total storm water level in this area than in lower latitudes (e.g., Gulf of Mexico).

The nonlinear interactions between storm surge, astronomical tides, and SLC have been well documented in the technical literature. In one of the first studies to address the issue of surge-tide nonlinearity, Proudman (1957) developed a general solution to the linear terms of the continuity and momentum equations, representing the interaction of storm surge and astronomical tide within an idealized estuary. Approximations of nonlinear terms were also considered. For a finite length estuary it was found that the surge-tide interaction results in an increased storm surge elevation when the peak surge occurs during high tide compared to when the peak surge occurs during low tide. Those results were attributed to the shallow water terms of the evaluated equations. For an estuary of infinite length, where the frictional term dominates over the shallow water terms, the opposite nonlinear effects were observed.

Prandle and Wolf (1978) examined the interaction of storm surge and astronomical tide in the North Sea as surges propagate southwards through different coastal regions of Great Britain. Results from previous model studies showed that in the North Sea region, peak water levels tend to occur at high tide. However, among the studied areas, it was found that in the River Thames, the peak storm surge generally occurred during rising tide, regardless of the interaction between storm surge and tidal phase in the northern North Sea. As part of the study, a statistical analysis of recorded surges was performed to assess surge-tide interaction. Also, a method was developed to resolve the processes involved in the storm surge and tide interaction consisting of an analytical model of tidal propagation and a model of surge propagation. Results showed that the NLR was proportional to the product of the storm surge elevation and the amplitude of the astronomical tide. The authors also concluded that the quadratic friction term represented the principal mechanism that dominated the nonlinear interaction between surge and tide in the River Thames.

Wolf (1978) examined the nonlinear interaction between storm surge and astronomical tide in semi-infinite uniform channels. Using the methodology developed by Proudman (1957) as a starting point, an analytical solution for progressive tidal waves in a semi-infinite channel was developed and applied to model the southward progression of surge and tide down the east coast of Great Britain. This study complemented the previous study by Prandle and Wolf (1978) on the interaction of surge and tide in the River Thames. The author concluded that the largest nonlinear effect of surge and tide was a result of the quadratic friction term, followed by shallow water and convective terms. The quadratic friction term reduced the residual at high tides whereas the shallow water and convective terms produced larger residuals on rising tides than at other phases. In general, it was found that the nonlinear surge-tide interaction increased as depth decreased.

Bernier and Thompson (2007) studied the nonlinear interactions between surge and tide along the east coast of Canada and the northeastern United States using a combination of statistical analyses and numerical modeling to identify and quantify its causes. Statistical analysis of 23 tide gages resulted in the identification of the occurrence of surge-tide interactions in the Northumberland Strait and the Gulf of Maine/Bay of Fundy. A combined surge-tide hindcast was compared with the linear superposition of surge-only and tide-only hindcasts through modeling in order to assess

the nonlinear effects. Significant nonlinearity was found in the Grand Banks, Gulf of Main/Bay of Fundy, and the Strait of Belle-Isle, with the largest NLRs being observed in the Northumberland Strait. Similar to other studies, nonlinearity was found to be primarily caused by the bottom friction component.

Kim et al. (2008) studied the nonlinear effects on storm surge, wave setup, and total water level (TWL) due to tidal variations. They compared two sets of numerical simulation results: one with tide, wind, and radiation stress as input forcing and one with only tide. The difference between these two, referred to as the residual surge component, was evaluated at eight distinct tidal phases. They identified the peak values of the storm surge during the eight tidal phases. It was found that the maximum differences in the peak residuals occurred during high and low tides. Storm surge occurring during high tide resulted in augmentation of the surge elevation whereas storm surges occurring during low tide were reduced. The differences in surge when observed at midrising and midreceding tides were negligible. These differences became larger as the amplitude of the astronomical tide increased. Differences in peak values of wave setup magnitude followed the same pattern as the peak storm surge. Results from the study by Kim et al. (2008) also indicated that differences in TWL associated with low-amplitude tides, roughly 0.5 m to 1.0 m, were very small, varying from 0.03 m to 0.06 m. For higher tidal amplitudes ranging from 2.0 m to 3.0 m, the differences in TWL varied from 0.14 m to 0.24 m. It was concluded, based on all evaluated components, that tidal variation reduced TWL near high tide and increased TWL near low tide, due to the frictional effects being more prominent at low tide.

Loder et al. (2009) evaluated changes in peak storm surge elevation and wave elevation in shallow marsh areas due to TCs. Numerical simulations of storm surge were performed using ADCIRC (Westerink et al. 1992) and STWAVE (Smith et al. 2001). It was observed that storm surge elevations are reduced in areas of increased bottom friction due to slower surge propagation. However, potential storm surge elevation increases with TC intensity, thus diminishing the effectiveness of bottom friction on reducing surge elevation.

In other recent studies, Rego (2009) and Rego and Li (2010) investigated the nonlinear effects of astronomical tide and shelf geometry on storm surge. The impact of storm surge to the coasts of Louisiana and Texas was

examined by using a finite volume coastal ocean model to simulate the surges caused by Hurricanes Rita and Ike. An investigation into the role of shelf geometry and tides was conducted, which included an examination of the nonlinear interaction between tide and surge. Nonlinearity was computed by subtracting the sum of the tide-only and surge-only elevations from the total elevation. The study found that east of the landfall point, the NLR opposes the tide so that the surge is reduced when the tide is high and increases when the tide is low. For the modeled condition, the NLR was found to reach 70% of the tidal amplitude. For hurricane landfalls occurring at the midrising tide or midreceding tide, the NLR was found to oppose the tide before and after peak storm tides but had the same peak water level as linear superposition; in other words, in this case the linear superposition and the full simulation water level peaks were found to be similar in magnitude. The NLR was listed from greatest to smallest in the following order: landfall at low tide, landfall at high tide, and landfall at midrising or midreceding tides. The study concluded that ignoring the nonlinearity may lead to significant underestimation of surge in the particular case of landfall at low tide.

Lin et al. (2012) quantified the tide-surge nonlinearity for TCs affecting the Battery, New York area. Using SLOSH (Jelesnianski et al. 1992) simulations, 210 intense TCs were identified as having recurrence intervals of 10 years or greater. The SLOSH simulations were performed using a polar grid with a 1 km resolution. Each of the 210 storms was replicated eight times in order to vary the arriving time at 3-hour intervals. It was proposed that nonlinear relationships based on the premise that the water level response is amplified when the peak of the storm surge coincides with receding or low tide. Conversely, it was proposed that the water level response is dampened when the peak of the storm surge coincides with rising or high tide. However, the study focused in a region with relatively uniform water depths; therefore, possible nonlinear effects due to shallow water or water depth variation were unaccounted for. Lin et al. (2012) also found that the nonlinear effects due to SLC to be very small for the Battery area. SLC scenarios lower than 1.0 m resulted in negligible NLRs whereas SLC scenarios larger than 1.5 m resulted in small residuals fluctuating almost symmetrically around zero. It was observed that even for the higher SLC scenarios, the net effect of superposition was statistically small, and therefore, the nonlinearity was negligible. Linear superposition of storm surge and SLC was recommended as the desired approach.

D1.2 Previous approaches for integration of astronomical tide in joint probability studies

Recent studies concerning the joint probability analysis (JPA) of storm surge have addressed the nonlinear interaction between surge and astronomical tide employing very distinct methodologies. Resio et al. (2007) and IPET (2009) discussed nonlinearity while focusing on extreme TCs affecting southeast Louisiana, where tidal amplitudes are relatively small compared to storm surge response. They recognized that although there is a degree of nonlinearity, numerical experiments have shown the linear superposition usually results in reasonable estimates of total water level response. It was recommended the integration of tide as part of a JPA by assuming linear superposition and statistically accounting for the degree of error introduced by this approach. For the Gulf of Mexico, it is suggested performing numerical simulation of storm surge assuming zero tidal elevation and accounting for the tidal component in the form of an error, or uncertainty, term. This requires the assumption that the NLRs are independent and unbiased.

Additional flood hazard studies conducted for Mississippi (FEMA 2008) and Texas (FEMA 2011a) excluded astronomical tides from hydrodynamic simulations, and the contributions of tides were later accounted for as part of the JPA, similar to the above studies. However, FEMA (2011b) followed a different method to incorporate the astronomical tide in a JPA for the New York-New Jersey coastal area (FEMA Region II). A single tide with random phase and amplitude was included in each of the 159 synthetic TCs simulated with ADCIRC. A Monte Carlo simulation method, involving linear superposition of surge and tidal phases, was then employed for validation of the approach and to determine if the use of just one random tide per synthetic storm adequately represented the complete range of tidal variation in the total water level extremal statistics. It was noted that the purpose of the validation process was to assess the probabilistic stability of the approach and not to verify the validity of the linear superposition assumption.

FEMA (2012a) operating guidance recommends the use of the linear superposition approach or accounting for tidal variation as an added correction term in the event that tidal amplitudes are small relative to the storm surge elevation. Similar to the approach suggested by Resio (2007) and IPET (2009), the astronomical tide would be represented as a random uncertainty term characterized as a standard deviation around zero mean.

In a recent FEMA Region III storm surge study (FEMA 2012b), the astronomical tides were incorporated in the joint probability analysis by replicating each storm surge response 100 times and then linearly adding to each surge replicate a tide randomly sampled from the astronomical tide cumulative distribution function. Although an uncertainty term representing modeling skill was included in the joint probability integration, no correction or uncertainty term was used to account for the nonlinear interaction between storm surge and astronomical tide.

The above studies illustrate the regional differences in nonlinear interaction of surge and tide and recent storm water level hazard assessment methodologies that incorporate these processes. In the Gulf of Mexico, where tides are relatively small, the nonlinearity is less significant, and total water level peak coincides with the storm surge peak for extreme water levels. In this case, the common practice of incorporating tide as an uncertainty in total water level statistics is reasonable. In the North Atlantic coastal region, the tide plays a much larger role in the total storm water level response, and this impact increases with increasing latitude. For this region, the most extreme water levels coincide with high tide. Tide and extreme surges are of similar magnitude. Nonlinearity is dependent on the relative phasing between tide and surge and tends to be negligible on rising and falling tides but can be significant at low and high tides. In addition, nonlinearity is greater at low tide and in shallower depths with bottom friction, and to a lesser extent, convection playing a role. In the following, the focus is on quantification of the nonlinearity with specific attention on relative phase and the overall nonlinearity for extreme water levels. Current understanding is that no previous USACE or FEMA joint probability study has accounted for surge-SLC nonlinear interactions.

D2 General Methodology

Based on the summarized literature, it is expected that linear superposition is generally a reasonable approximation for extreme water levels. Also, based on previous studies, it was expected that a nonlinear uncertainty factor could be quantified to reasonably approximate the water level response using linear superposition for other situations. The general purpose of this focused study of nonlinear water level response was to determine under what conditions linear superposition of surge and tide is a valid approximation for the North Atlantic coastal region and where a correction or uncertainty term must be applied. The study also sought to characterize conditions under which the nonlinearity was too

large to apply linear superposition. This study determined the minimum number of tidal realizations needed so that the water level response approximates the probability distributions for total storm water levels. A nonlinear tidal correction factor will reduce the number of tidal permutation simulations required within the high-fidelity modeling component of a coastal study.

D2.1. Hydrodynamic numerical simulations

The ADCIRC model (Westerink et al. 1992) was used to simulate storm water levels as well as tides for this study. The ADCIRC mesh developed as part of the most recent FEMA Region II coastal flood hazard study (FEMA 2011b) consisted of 604,790 computational nodes. For purposes of this nonlinearity assessment, which focused on the New York and New Jersey coastal areas, the ADCIRC results analyzed were limited to all nodes above latitude 38.5^0 N and below latitude 41.5^0 N. Note that the subsequent NACCS mesh development began with the FEMA Region II and FEMA Region III meshes which are all referenced to mean sea level (MSL); therefore, NACCS modeled water levels are referenced to MSL. This information about datums is important because USACE projects must comply with existing policy and guidance (USACE 2009; USACE 2010). Any application that requires water levels referenced to NAVD88 can apply the mesh-wide key derived from VDATUM for converting water levels to NAVD88 that is provided with the Coastal Hazards System (CHS).

The initial step in the analysis was to simulate a tidal time period to use as the tide-only simulation condition and for randomly selecting a tidal start time for the surge-and-tide simulations. Based on tidal data analysis of 18 years of National Oceanic and Atmospheric Administration (NOAA) water level data, September 2010 was determined to be the most appropriate month to use for the tide-only simulation and for selecting the random tidal start times. The selection was based on the analysis of tidal data extracted from the NOAA website for five locations along the east coast: Atlantic City, NJ; Boston, MA; Portland, MD; Sewells Point, VA; and The Battery, NY. In the five-gage analysis, the average monthly tide ranges for the months August through November were extracted for the years 1995 through 2012. The August-through-November time period was chosen because these are the most active months for hurricanes for this region.

A range of the most commonly occurring monthly-averaged tide ranges was determined and used to identify specific months that possess average tide range conditions. It was determined that tides from September 2010 would be ideal because this period contained the highest standard deviation in the tide ranges. The higher standard deviation was desired as this provided the most variability in tide range which was beneficial to the random tide selection and analysis.

As part of the nonlinearity analysis, 157 synthetic tropical cyclones were simulated and used for the evaluation of nonlinear affects. This set of synthetic storms was originally developed as part of the most recent FEMA Region II coastal flood hazard study (FEMA 2014). The wind and pressure fields used to drive the ADCIRC model obtained from the FEMA study. ADCIRC was run for each storm to simulate surge-only response for the 157 synthetic TCs at MSL. Then, the 157 storms were simulated four times, each with a unique random tidal phase, resulting in an augmented set of 628 unique ADCIRC storm water level simulations.

This approach provides a coverage of responses that augments the range of tidal phases at landfall so that an increased range of nonlinearity can be discerned. Comparisons were made between the total storm water level computed for the full ADCIRC simulation of tides and storm surge and the water level calculated as the linear sum of the responses of the surge-only and tide-only simulations. The difference between these two is termed the nonlinearity or the nonlinear residual (NLR), herein.

D2.2 Computation of nonlinear residuals (NLRs)

The nonlinearity assessment sought the quantification of the nonlinear residuals, *NLR*, due to the interaction of storm surge and tide, and due to the interaction of storm surge and SLC, independently. In both cases, NLR is generally defined as the difference in storm water levels, S*WL*, computed with linearly superimposed components, SWL_{LS}, and computed with full numerical simulation of total storm water level, SWL_{FS}. The general equation used to compute NLR at every time-step of a time series, t_n, has the form

$$NLR(t_n) = SWL_{LS}(t_n) - SWL_{FS}(t_n) \quad \text{(D1)}$$

A positive $NLR(t_n)$ value occurs when linear superposition overestimates the water level response. Conversely, a negative $NLR(t_n)$ value indicates underestimation of the total water level.

For linear superposition, a base condition was first established by simulating only storm surge. Then, astronomical tide was linearly added to surge-only simulations. Four unique tides were coupled with each simulated storm to compute both $SWL_{FS}(t_n)$ and $SWL_{LS}(t_n)$. For the relative phase analysis, Equation 1 was computed for all 628 storms and at every time-step by summing the surge-only responses with the astronomical tides.

Another approach used in this study consisted of analyzing NLRs computed as the difference between the maximum (max) or peak water level estimated by linear superposition and the peak water level from the full simulation of storm water level time series:

$$NL = max[SWL_{LS}(t)] - max[SWL_{FS}(t)] \quad \text{(D2)}$$

The assessment of NLRs due to SLC was done with an additional set of numerical simulations. All 157 synthetic TCs were used to simulate storm surge-only but including a static adjustment of water level representing a future SLC scenario of 1.0 m. In this case, since tides are not involved, the NLRs due to SLC resulting from the difference between the peak water level estimated by linear superposition and the peak water level from the full simulation were computed using Equation D2.

D3 Nonlinearity Due to Astronomical Tide

A goal of the nonlinearity assessment was to evaluate the effect of the tidal phase on the interaction between storm surge and astronomical tide. Two distinct analyses described in this section focused on the estimation of NLRs, first, across the entire time series of storm water levels and second, based on the difference between peak water levels.

D3.1 Temporal variability of NLR

In order to investigate the surge-tidal phasing relationship, the results of the medium-fidelity model where analyzed at 105 save point locations corresponding to NOAA water level stations along the entire NACCS coastal region from Virginia to Maine (Figure D1). As previously discussed,

four realizations of 157 storms were run with random astronomical tide, for a total of 628 storms. In order to assess the effect of tidal phasing, the NLRs were computed at each time-step for each of the model runs for each station. An average NLR was calculated at each time-step considering all storms. The mean NLR time series was plotted with the astronomical tide for each station. In addition, CLs of 98% and 2% were calculated and plotted to convey the range of nonlinearity with the elimination of extreme outliers.

The main observed temporal behavior of the mean NLR consisted of an oscillation approximating 0.0 m. Although there were many locations where the amplitude was very small, making it difficult to visually establish a pattern, there were numerous locations were the oscillation was clearly appreciable. Figure 1 shows all 105 save points. Two points highlighted in this analysis are Cape May, NJ (green circle), and The Battery, NY (red circle).

Figure D1. Locations of 105 save points used for tidal phasing assessment.

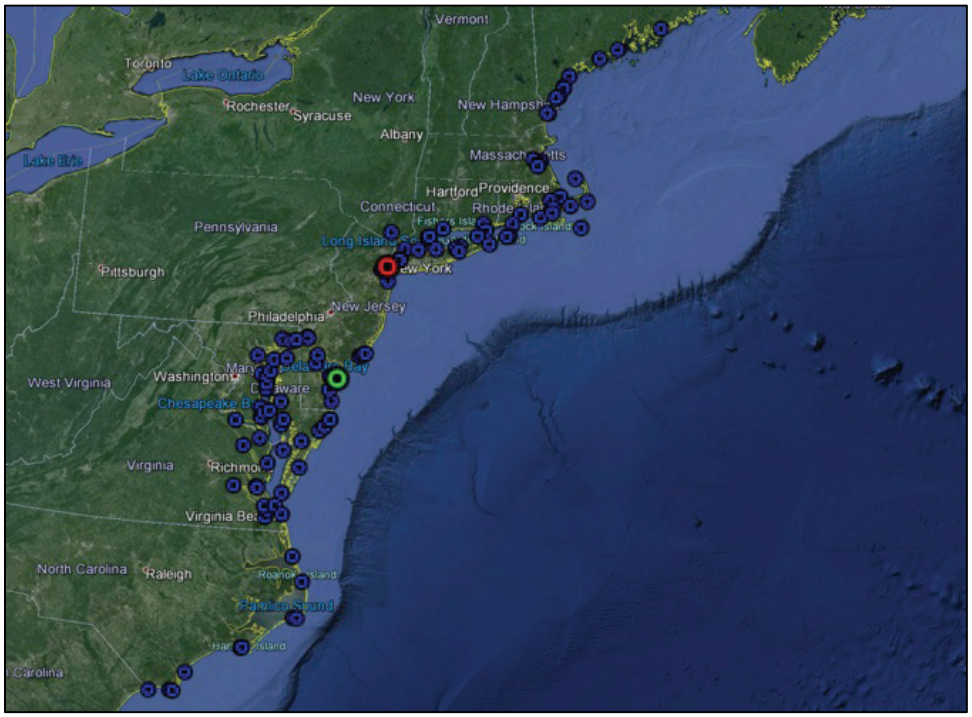

Figures D2 and D3 present the time series for Cape May, NJ, over a time interval of 25 days and a time interval of 5 days, respectively. It can be observed at this station that nonlinearity increased with the rising tide and decreased with the receding tide. For Cape May, the amplitude of the astronomical tide ranges from 0.5 m to 0.9 m. The range of NLRs

corresponding to the 98% and 2% confidence levels vary from 0.1 m to 0.5 m. However, the mean NLRs observed at Cape May are negligible in comparison to the tidal amplitude. In general, the maximum positive NLRs are observed at or near high tide while the maximum negative NLRs are usually observed near low tide. In accordance with the adopted definition of nonlinearity, the storm surge is reduced with rising tide and increased with receding tide for all 105 save point locations, agreeing with previous observations.

Figure D2. Time series of nonlinearity for Cape May, NJ.

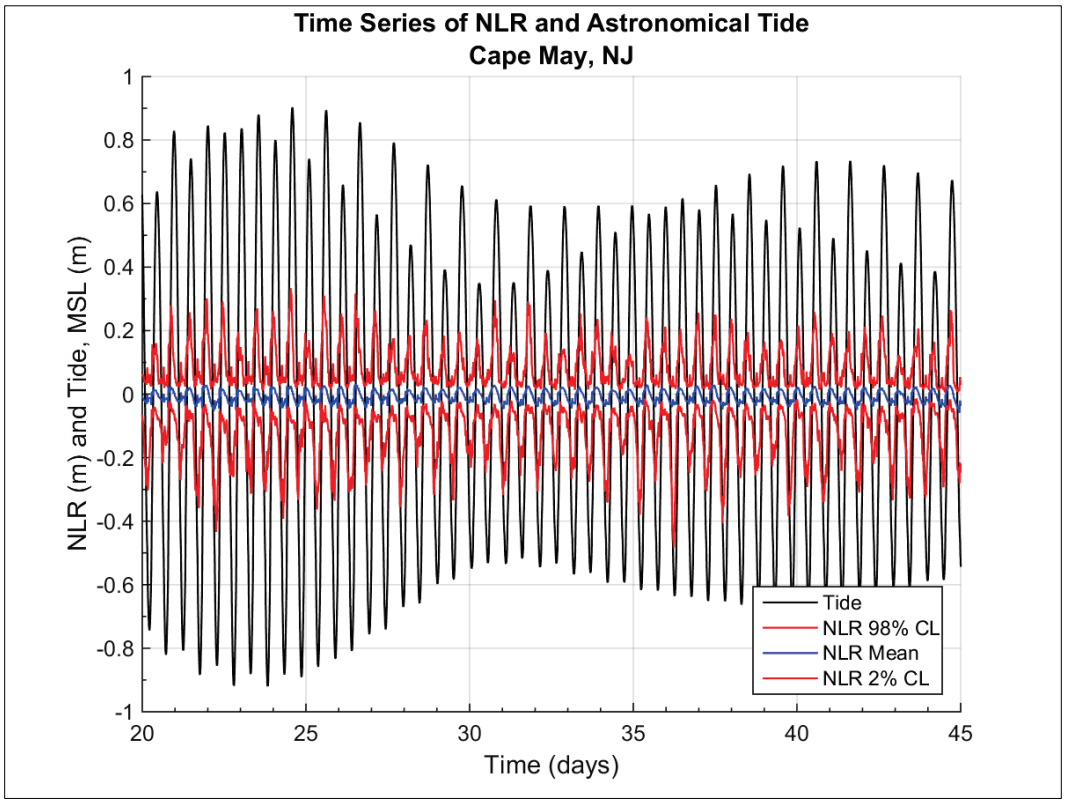

Figure D3. Five-day time series of nonlinearity for Cape May, NJ.

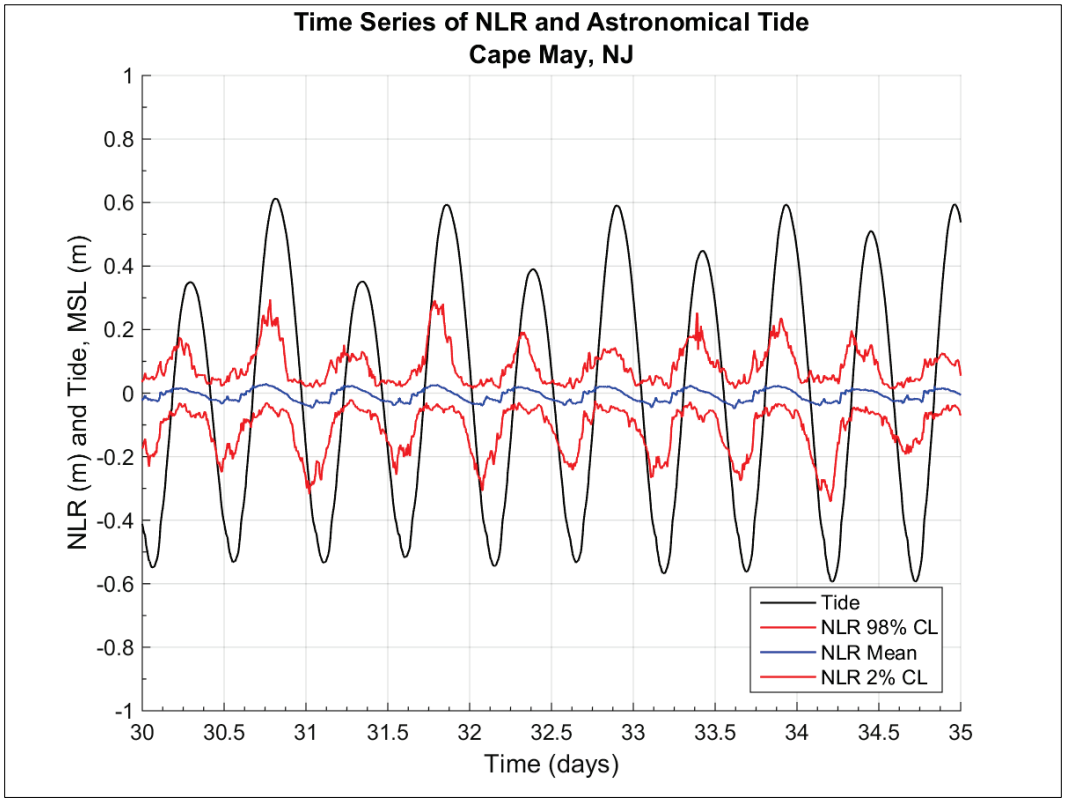

Figures D4 and D5, for The Battery, NY, show similar characteristics of the nonlinearity variability with tidal phase. In general, the NLRs were very small. For The Battery, the amplitude of the astronomical tide ranges from 0.5 m to 1.0 m. The NLRs corresponding to the 98% and 2% confidence levels vary from 0.2 m to 0.8 m. Similar to the mean NLRs observed at Cape May, the residuals for The Battery are negligible relative to the tidal amplitude.

Figure D4. Time series of nonlinearity for The Battery, NY.

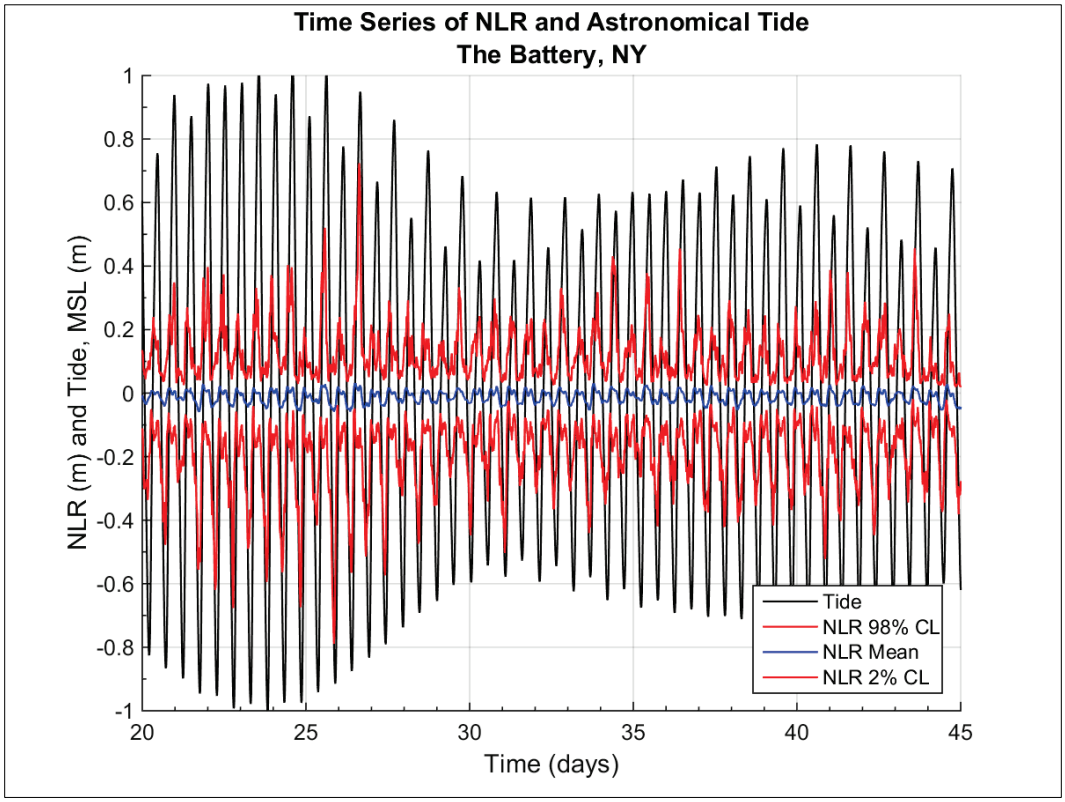

Figure D5. Five-day time series of nonlinearity for The Battery, NY.

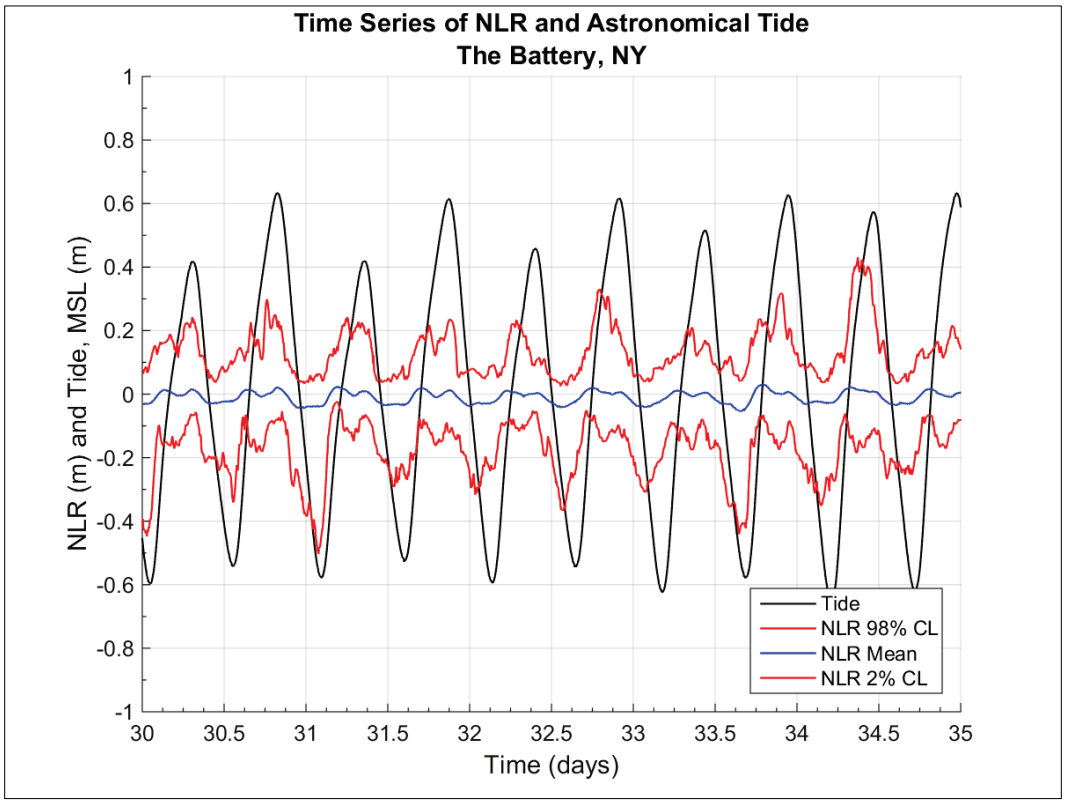

A second approach to evaluate the effect of tidal phase on the surge-tide interaction consisted of determining the tide phasing at the time of the peak surge and evaluating the effect on the peak water level NLR. For this approach, the *NLR* was computed for all 105 save point locations using Equation D2. The base case, which includes all tidal phases, is presented in Figure D6. Shown in this figure are the NLR mean, and the 98%, 84%, 16%, and 2% CLs as a function of water depth. The blue curves indicate overestimation by linear superposition of total water level response while the red curves indicate underestimation.

Figure D6. NLRs in peak water level as a function of water depth.

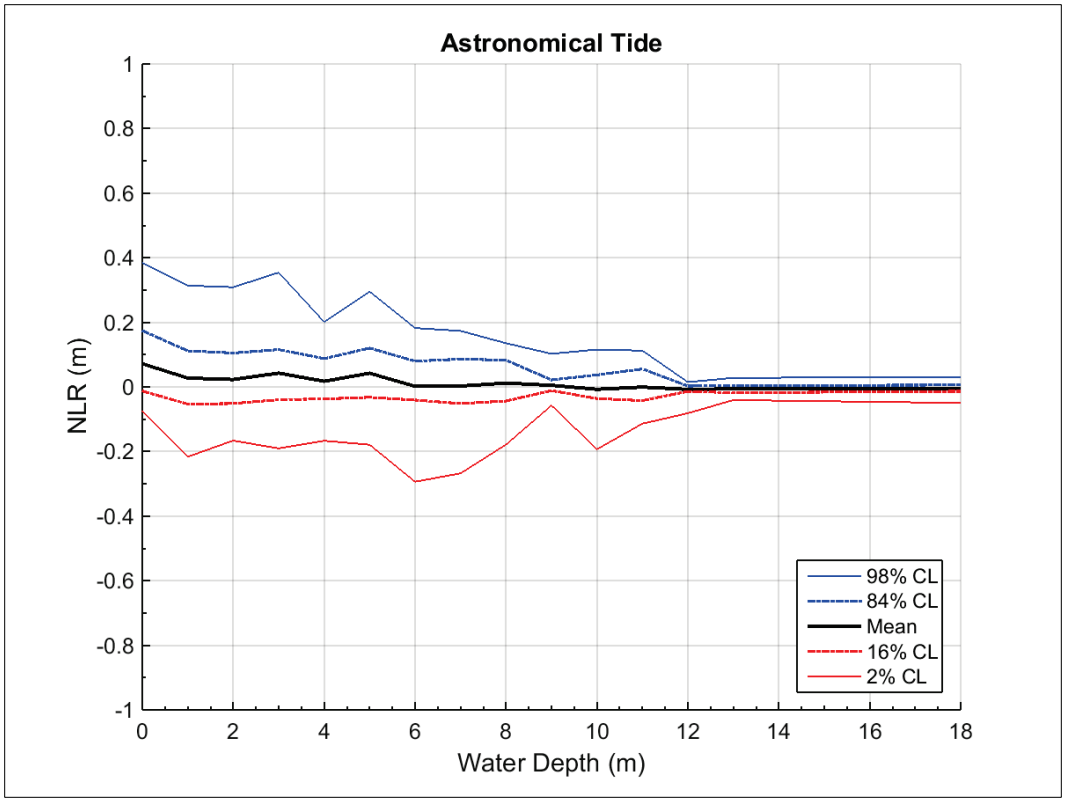

In addition, the relative phase between surge and tide was examined for all 628 simulated storms at each of the 105 stations and identified as rising, high, receding, or low tide. The NLRs were classified based on this distinction. Figure D7 presents four subplots showing NLRs due to the relative phase between peak storm surge and tide, as discussed above. Based on these results, no relationship was observed between the relative phase between surge and tide and the corresponding NLRs. The results shown in Figure D7 exhibit the same general relationship of reduced NLR with increasing water depth that was shown in Figure D6. No substantial

differences are observed in the mean NLRs when segregated into rising, high, receding, and low tide.

Figure D7. NLRs in peak water levels due to the relative phase between peak storm surge and astronomical tide.

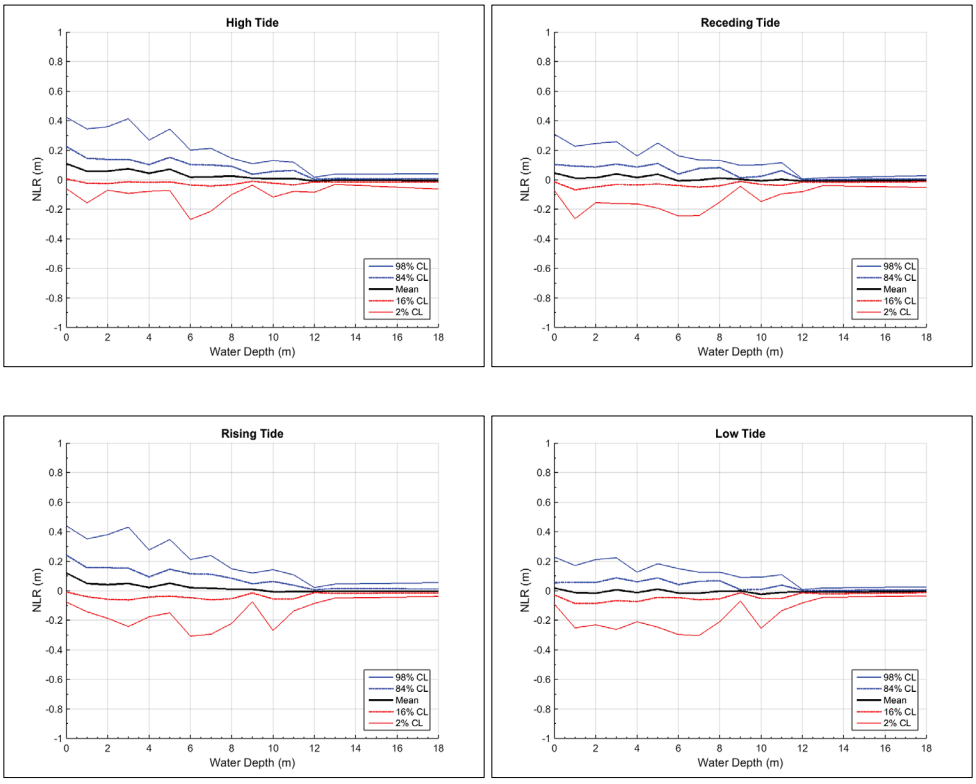

D3.2 Spatial variability of NLR

Having characterized the temporal behavior of the nonlinearity and investigated the effect of relative phase between peak surge and tide for 105 save points, it is of interest to analyze the spatial behavior of peak water level nonlinearity throughout the modeled region. This analysis, which was limited to the New York-New Jersey coastal region, allowed for the investigation of the effect of the varying coastal topographic and bathymetric features on NLRs. This part of the analysis focused on evaluating NLRs resulting from differences between the peak water level estimated by linear superposition and the peak water level from full simulation, irrespective of relative tidal phase.

For purposes of this analysis, the ADCIRC mesh was divided into two parts, in order to independently focus on New York and New Jersey. The New York subregion, bounded by latitudes 40.5^0 N and 41.5^0 N, had

80,876 nodes. The New Jersey region, bounded by latitudes 38.5^0 N and 40.5^0 N, consisted of 132,006 nodes. Figure D8 shows the NLRs as a function of depth for the New York subregion. This figure also shows the NLR mean and the 98%, 84%, 16%, and 2% CLs as a function of water depth. Positive mean NLRs represent overestimation by the linear superposition of peak water levels whereas negative mean values are indicative of underestimation. The uncertainty associated with the NLRs, defined as the standard deviation of NLR, is plotted in Figure D9. Overall, these curves exhibit the general trend of NLR increasing as the water depth decreases. There is a clear transition at a depth of approximately 35 m corresponding to typical water depths in Long Island Sound (Figure D10). Similar patterns are also observed in the vicinity of New York Bay (Figure D11).

Figure D8. NLRs in the New York region due to astronomical tide.

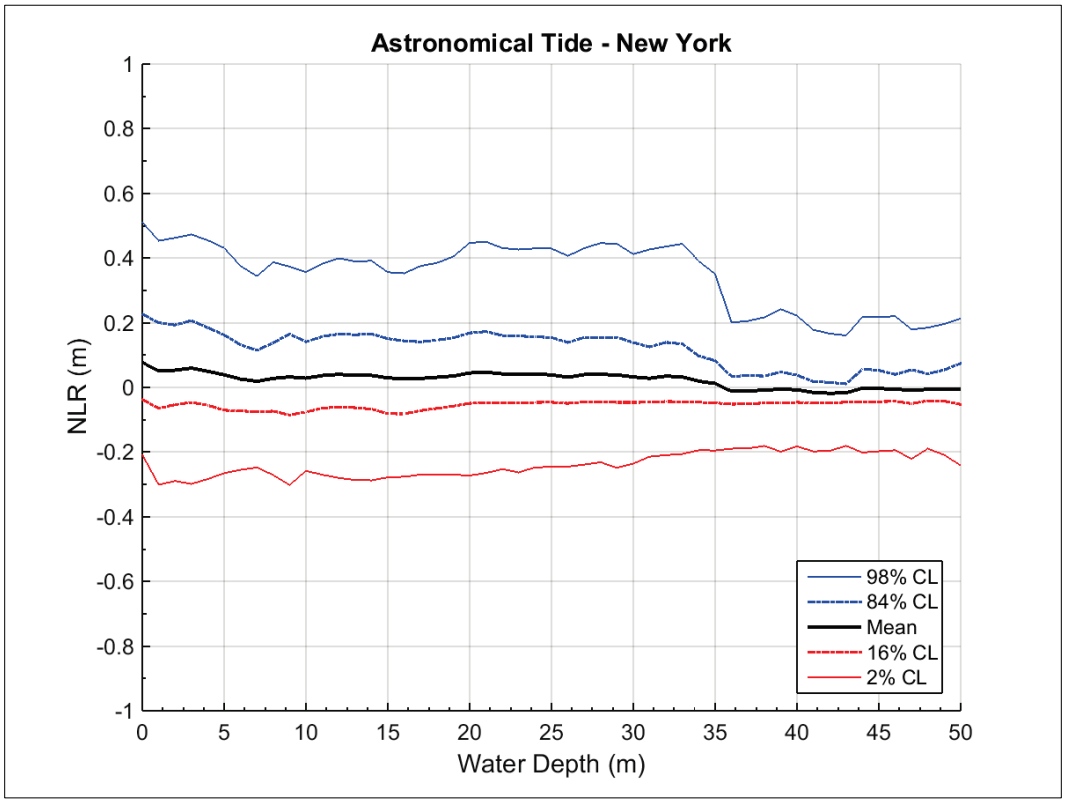

Figure D9. Uncertainty associated with NLRs in the New York subregion due to astronomical tide.

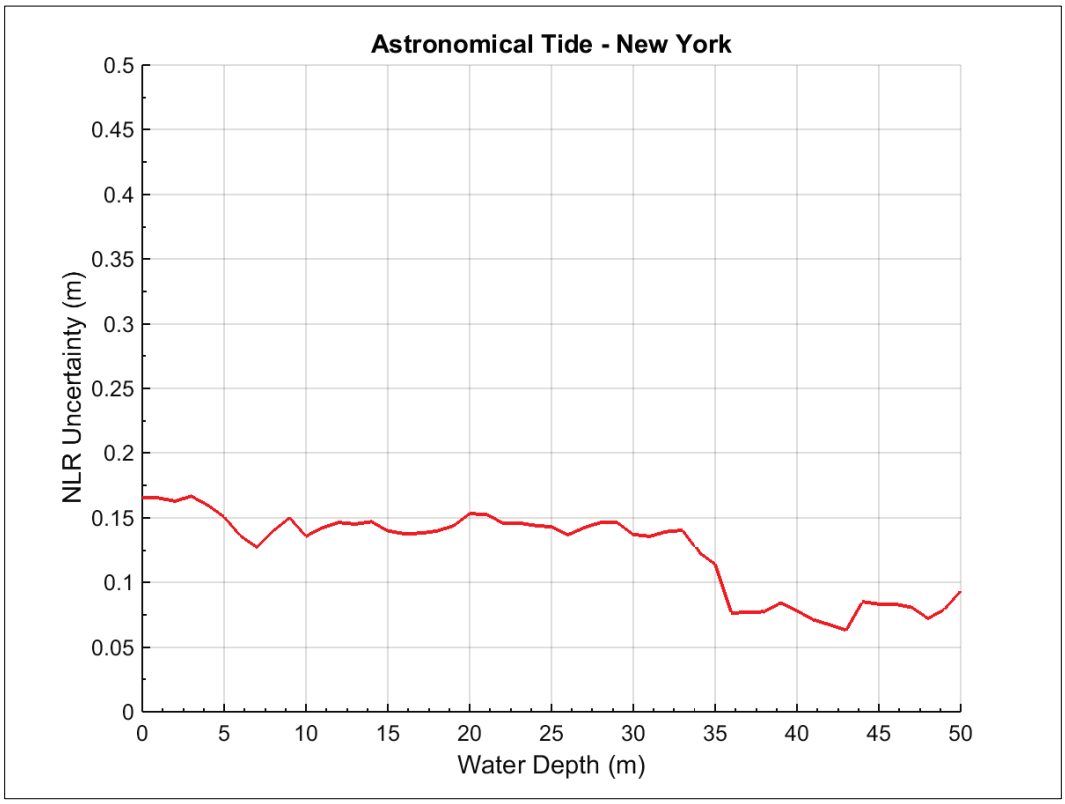

As discussed above, although in the New York area NLR increases as water depth decreases, as expected, the magnitude of positive residuals corresponding to semienclosed areas like Long Island Sound and New York Bay is slightly higher when compared to open coasts. Figures D10 and D11 show mean NLR or bias for each node due to surge-tide interaction. As shown in Figure D10, the peak water levels are consistently overestimated using linear superposition by an average of 0–0.1 m throughout most of Long Island Sound, as well as the Gardiners Bay and Great Peconic Bay areas. The range of overestimation increases to 0.1–0.2 m in the western part of the Sound and adjacent to the northern and southern shorelines where the geometry of the sound contracts. The Great South Bay area, located south of Long Island, also shows overestimation of peak water levels of 0–0.1 m. Throughout most of the coastlines from Montauk Point to Long Beach, the peak water levels are underestimated using linear superposition by an average of 0–0.1 m. Figure D11 focuses on the New York Bay area and shows positive mean NLR of 0–0.1 m. The magnitude of the positive residuals decreases then transitions to negative residuals on the open coast near the Sandy Hook area.

Figure D10. Mean NLRs due to tidal interaction in the Long Island, NY, area.

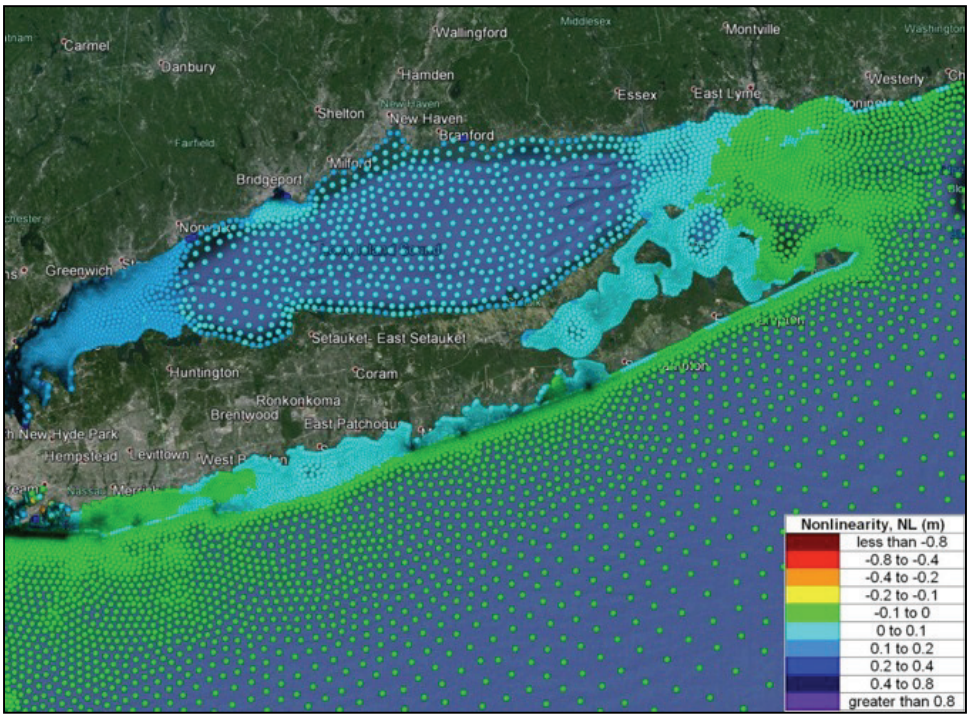

Figure D11. Mean NLRs around the New York Bay area.

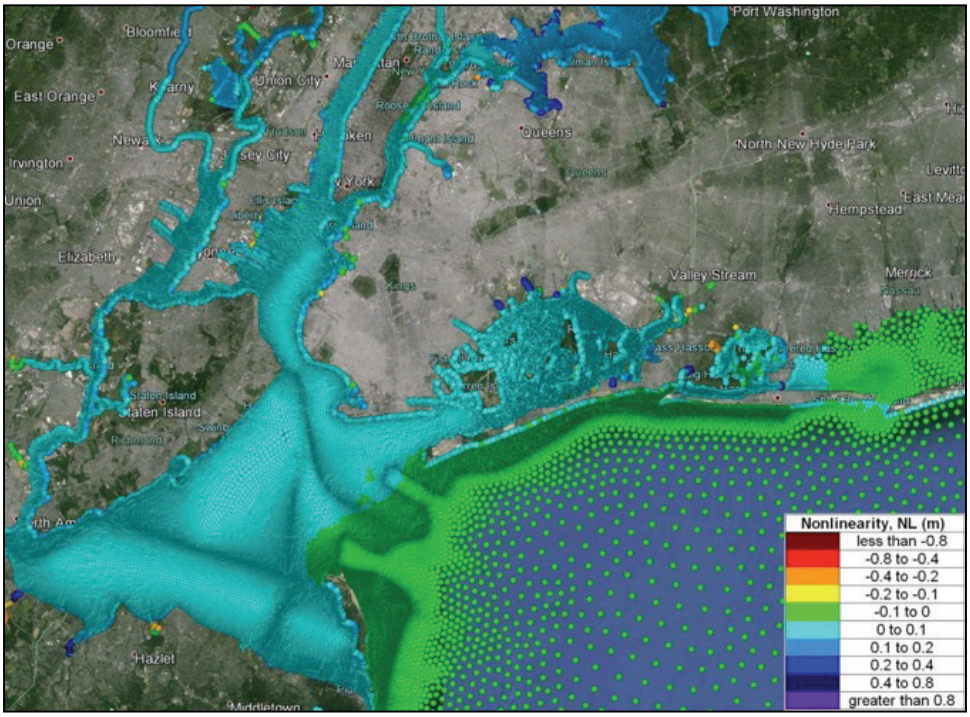

The mean NLR and confidence limits (CLs) as a function of water depths for the New Jersey subregion are shown in Figure D12. The majority of the nodes in this region are located along open coastlines where the inverse

relationship between NLRs and water depth is exhibited. The NLR curves in Figure D12 for New Jersey are smoother than the New York curves (Figure D8). Figure D12 clearly shows that NLR decreases with depth, and it is absent of the geometric confinement effects represented in Figure D8. A slight increase in both positive and negative residuals is observed in depths of 15 m or shallower. Figure D13 shows the uncertainty associated with the NLRs.

Figure D12. NLRs in the New Jersey subregion due to astronomical tide.

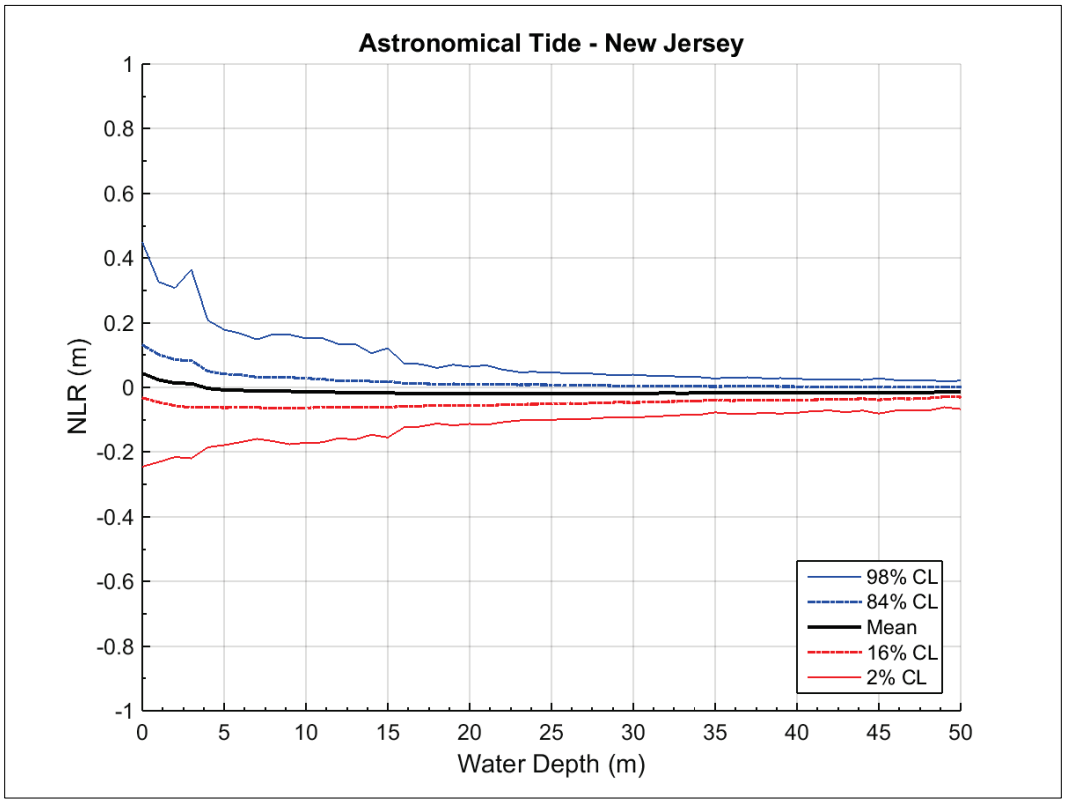

Figure D13. Uncertainty associated with NLRs in the New Jersey subregion due to astronomical tide.

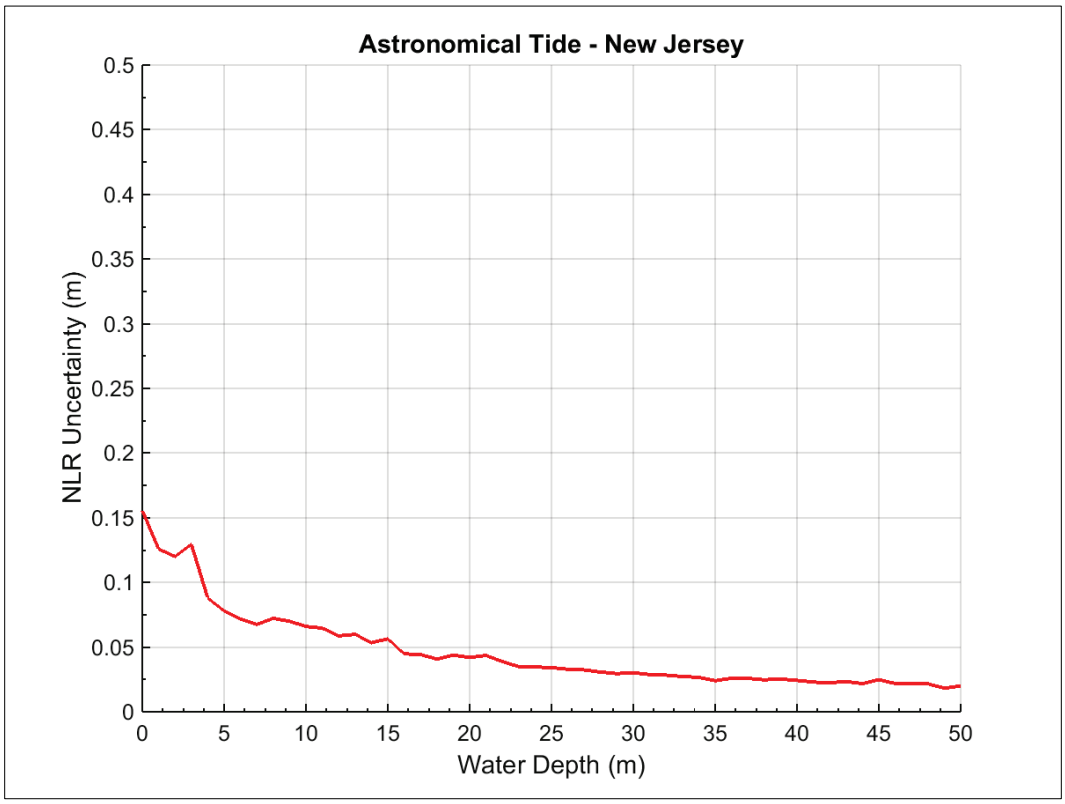

Figure D14 shows that throughout most of the New Jersey coastlines the peak water levels are underestimated by an average of 0–0.1 m. The sheltered areas immediately landward of the barrier islands in the Atlantic City area exhibit positive NLR of 0–0.1 m, indicating slight overestimation of the peak water levels by linear superposition. Overestimations in the range of 0.2–0.8 m, while observed throughout this area, are highly localized, being confined to relatively small scale geometric features such as canals and streams.

Figure D14. Mean NLRs around the New Jersey coastal region.

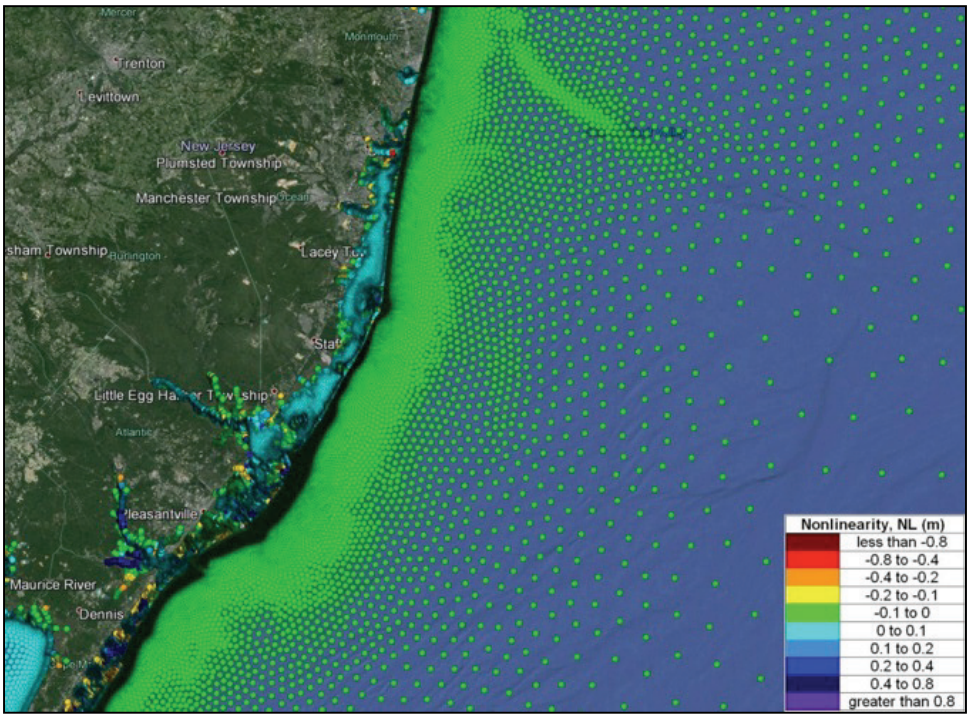

Figure D15 focuses on the Atlantic City area while Figure D16 presents a closer look at the area near Absecon Inlet, NJ. The majority of the nodes in this area located in open water exhibit mean NLR underestimating peak water levels by 0–0.1 m. Most shallow waters located inland show overestimation of peak water levels by 0–0.1 m. The exceptions are very specific locations such as canals and relatively small, sheltered areas. An example of these exceptions is the marina located behind the Absecon Inlet, which is shown in Figure 16 as a group of blue dots indicating overestimation of peak water levels of 0.2–0.4 m.

Figure D15. Mean NLRs in the Atlantic City, NJ, area.

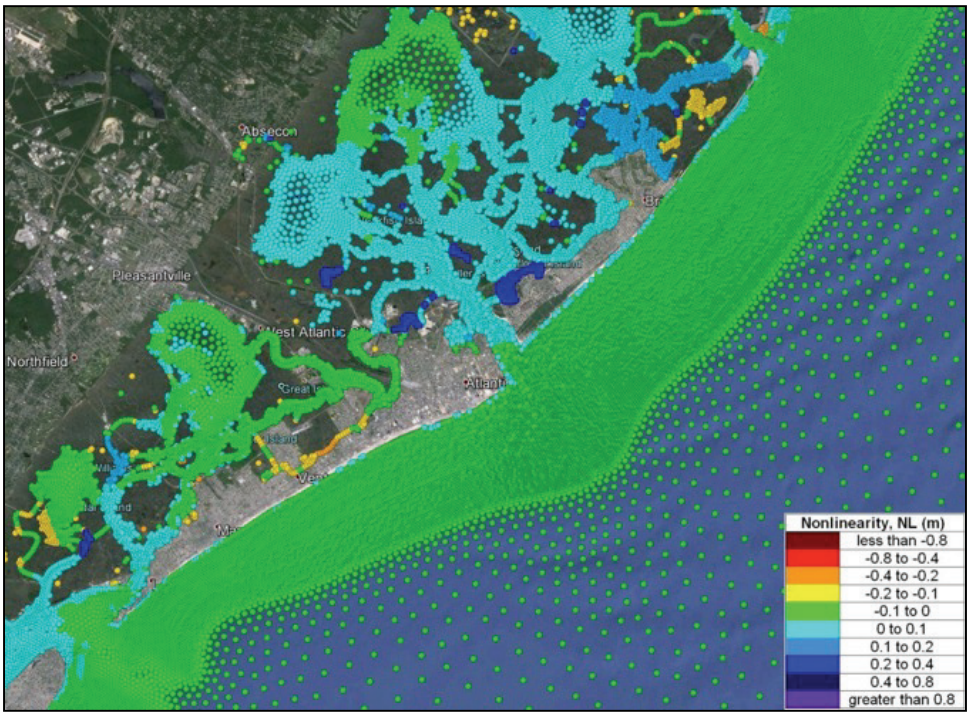

Figure D16. Mean NLRs near the Absecon Inlet area in NJ.

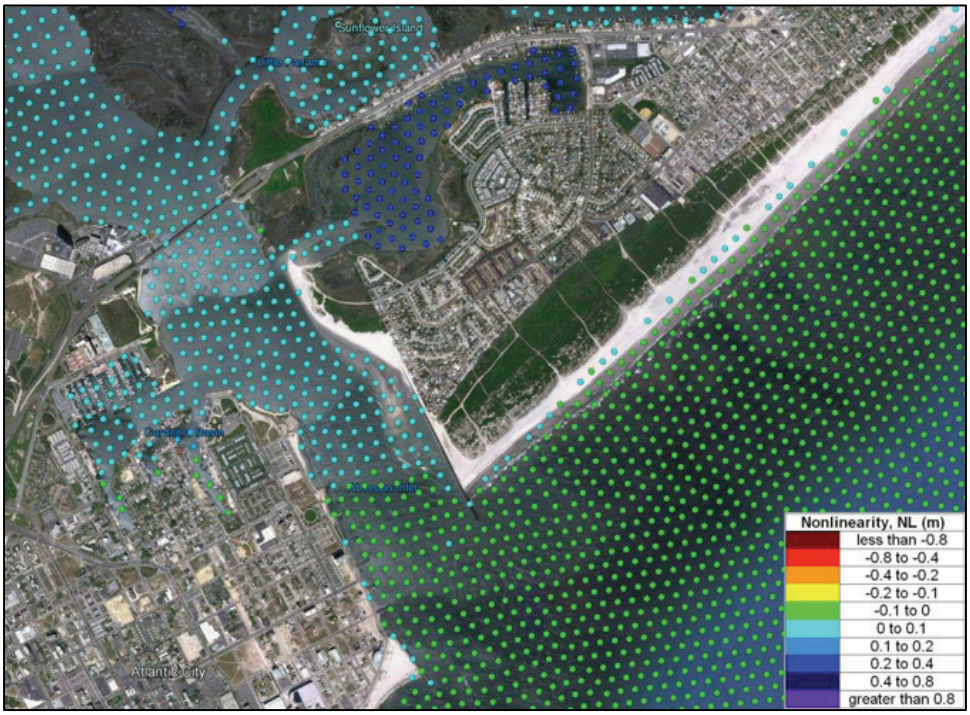

D4 Nonlinearity Due to Sea Level Change (SLC)

Another goal of the nonlinearity assessment was to evaluate the effect of SLC on the magnitude of the storm surge. For this purpose, all 157 synthetic TCs were simulated with a static water level adjustment representing a future SLC scenario of 1.0 m and no astronomical tides. In order to investigate the surge-SLC relationship, the results were analyzed for the New York-New Jersey coastal region, based on 80,876 nodes in the New York coastal area and 132,006 nodes in New Jersey. The approach followed in this section focuses on the estimation of NLRs based on the difference between the peak water level estimated by linear superposition and the peak water level from the full simulation (Equation D2).

It was found that the magnitude of the mean NLRs due to SLC in general increases in shallow areas, sheltered water bodies, in nearshore areas of complex geometry but is almost negligible along open coasts. Figure D17 shows the NLR mean and the 98%, 84%, 16%, and 2% CLs as a function of water depth, for the New York subregion. Positive mean NLRs represent overestimation by the linear superposition peak water levels, while negative mean values are indicative of underestimation. Figure D18 shows the uncertainty associated with the NLRs. Similar to the surge-tide cases, these curves exhibit the general trend of NLRs increasing as the water depth decreases. The observed trend is consistent for water depths of 10 m or greater. The dispersion of the confidence levels increases at shallower water depths.

Figure D17. NLRs in the New York subregion due to SLC.

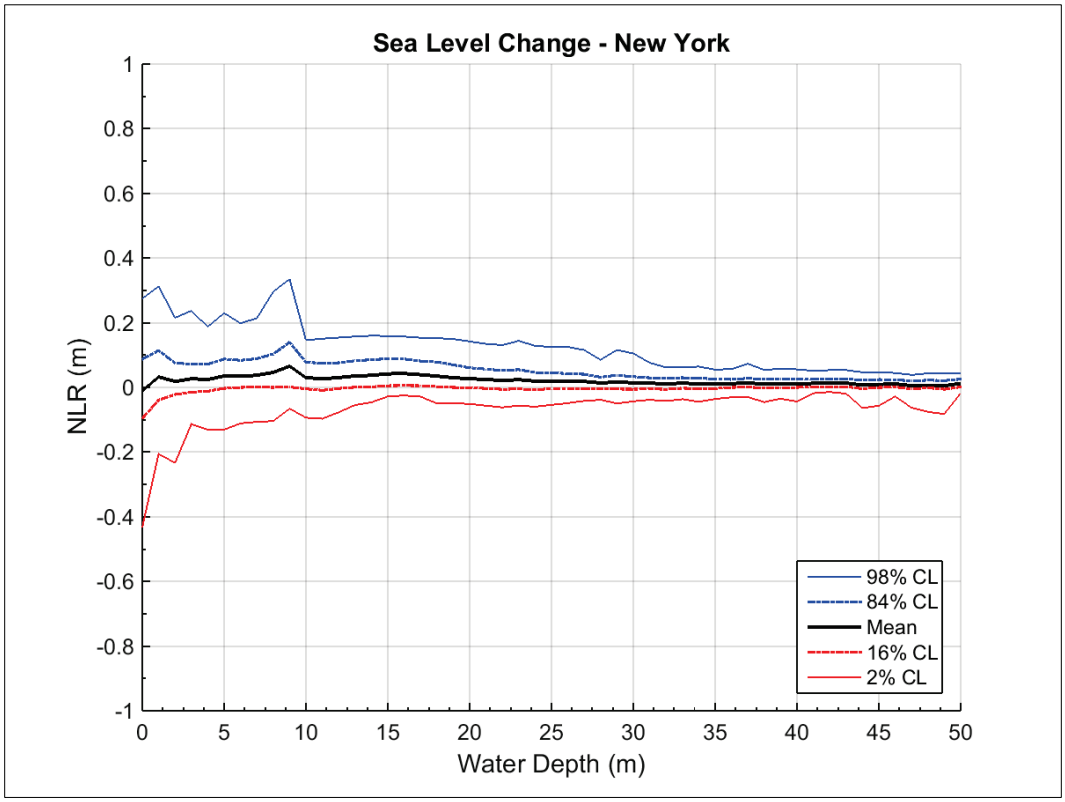

Figure D18. Uncertainty sssociated with NLRs in the New York subregion due to SLC.

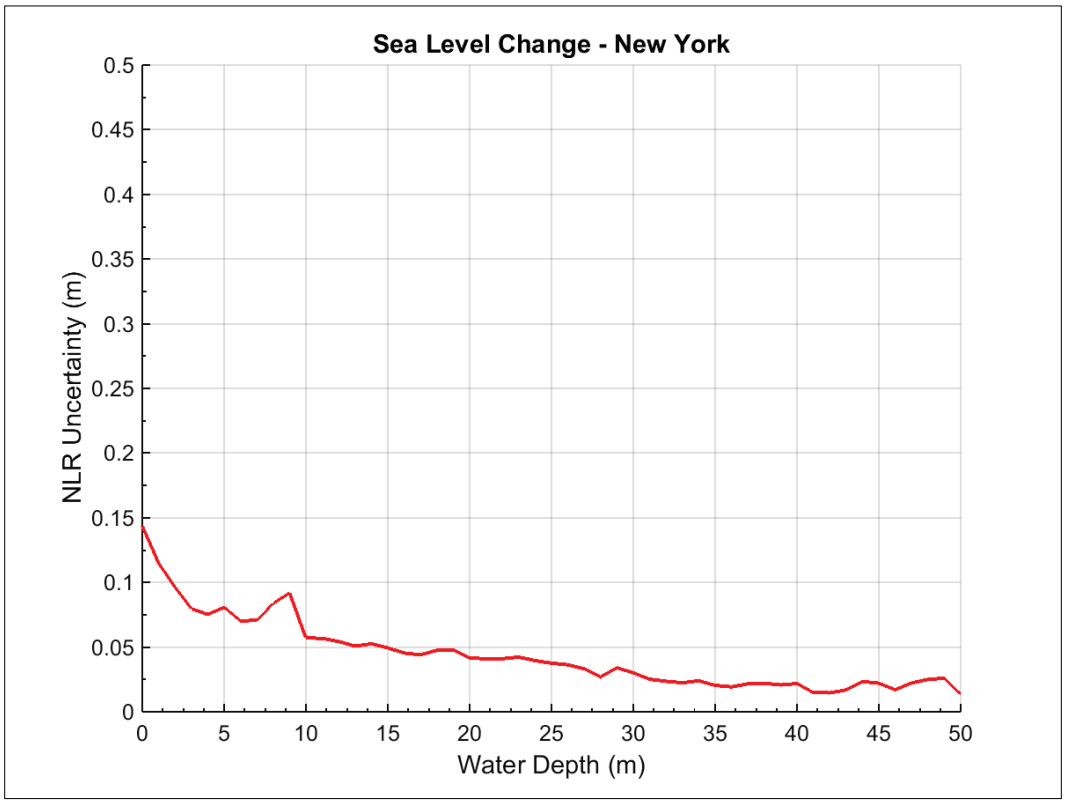

Figure D19 shows the Long Island Sound area, where the mean NLRs typically vary from -0.1 m to 0.1 m. Significant underestimation of the peak water levels in the range of 0.2–0.8 m can be observed for shallow, sheltered waters south of Long Island such as South Oyster Bay and Moriches Bay.

Figure D19. Mean NLRs due to SLC in Long Island, NY.

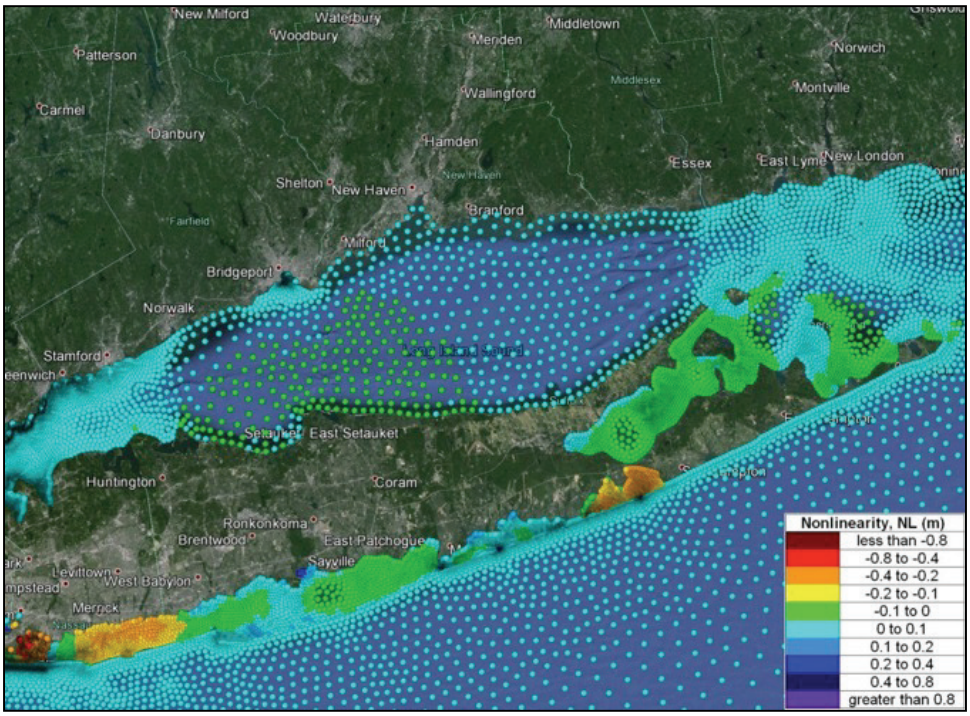

Figure D20 focuses on the Long Beach, NY, area and shows positive mean NLRs on the order of 0–0.1 m. Mean negative NLRs, ranging from 0.2 to 0.8m can be observed in the marsh areas north of Long Beach, NY.

Figure D20. Mean NLRs due to SLC near Long Beach, NY.

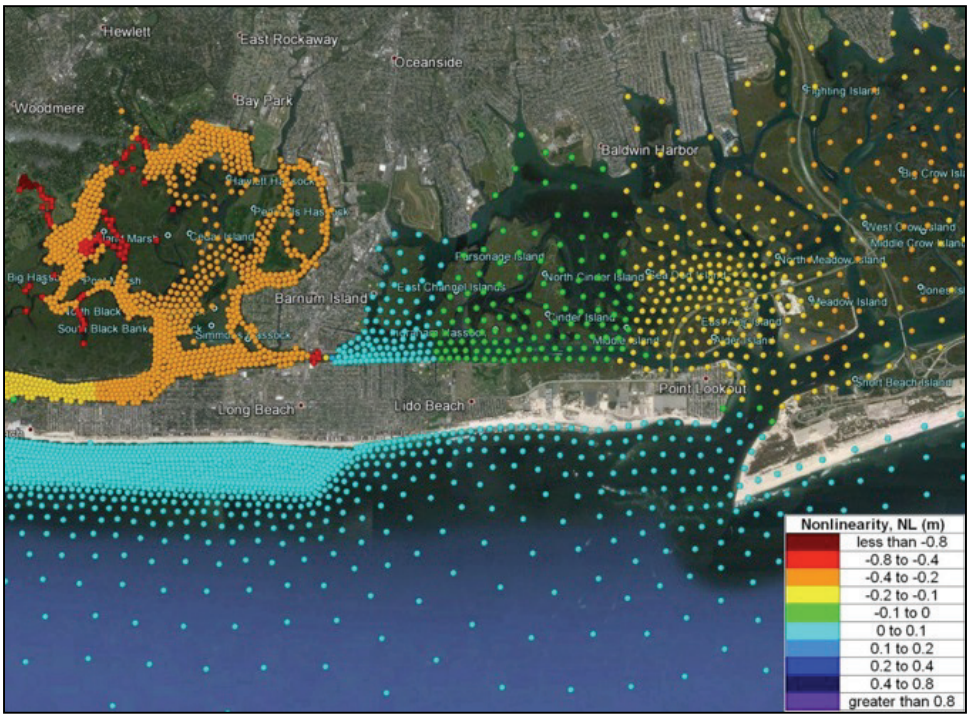

The mean NLRs for the New Jersey subregion due to surge-SLC interaction are shown in Figure D21. The figure also shows the NLR mean and CLs as a function of water depth. The majority of the nodes in this region are located in open water, emphasizing the inverse relationship between NLRs and water depth. A slight increase in both positive and negative NLRs is observed in depths of 10 m or less. Figure D22 shows the uncertainty associated with the NLRs.

Figure D21. NLRs in the New Jersey subregion due to SLC.

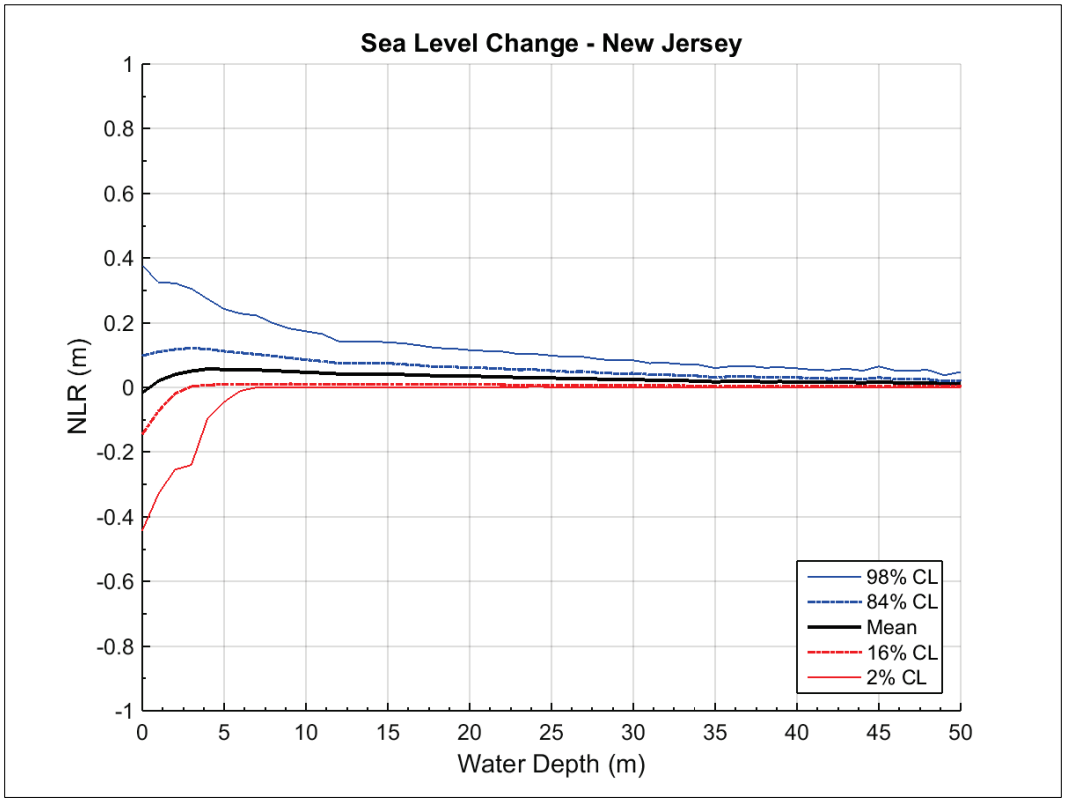

Figure D22. Uncertainty associated with NLRs in the New Jersey subregion due to SLC.

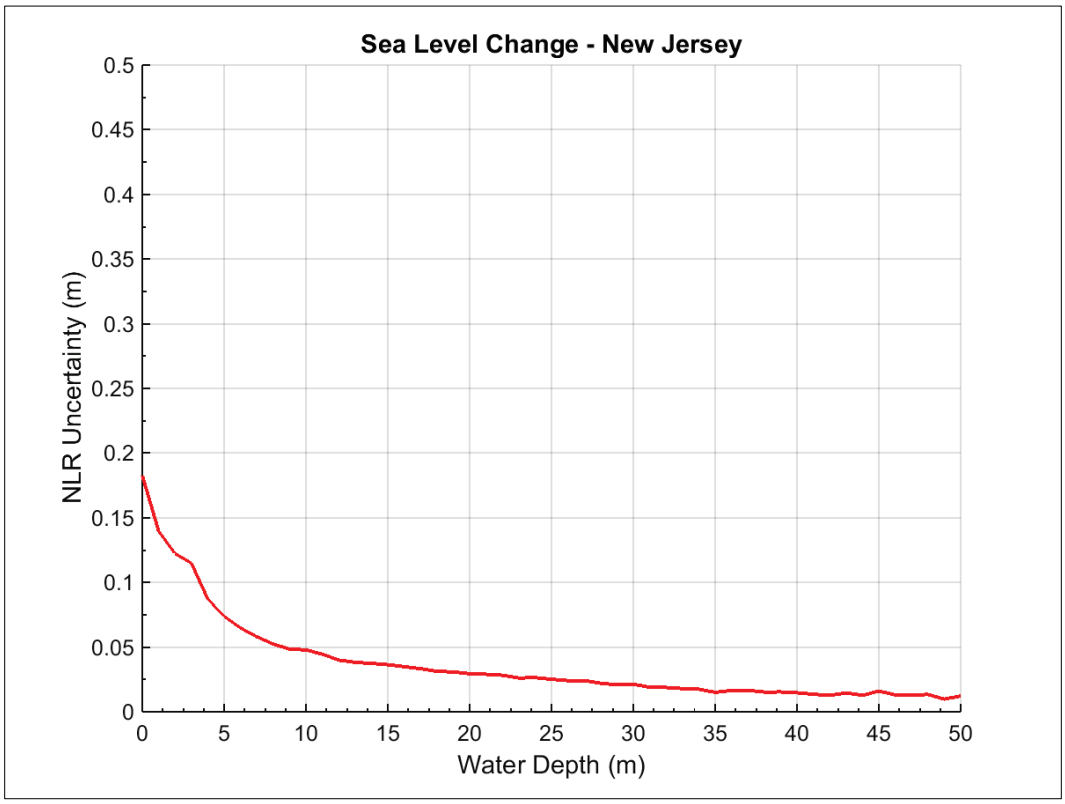

Figure D23 shows that throughout most of the New Jersey coastlines, the peak water levels are overestimated by an average of 0–0.1 m. The sheltered areas immediately landward of the barrier islands in the Atlantic City area exhibit negative NLRs on the order of 0–0.1 m, indicating slight underestimation of the peak water levels, with marsh areas showing underestimation in the range of 0.2–0.8 m.

Figure D23. Mean NLRs due to SLC in the New Jersey subregion.

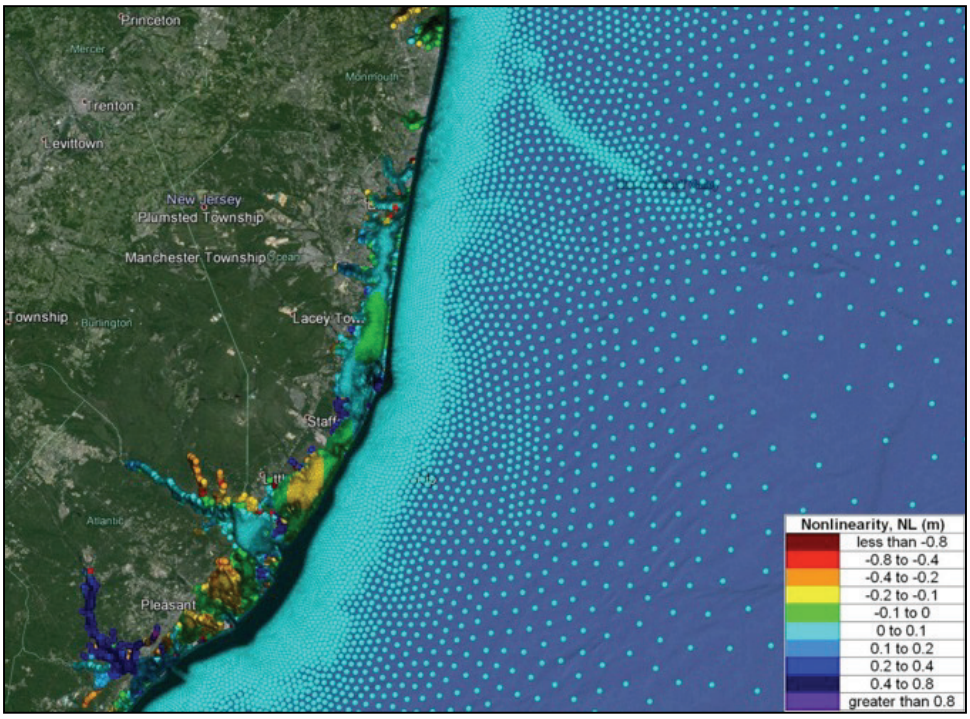

Figure D24 shows the Atlantic City area while Figure D25 presents a zoomed-in view of an area with canals near Ventnor City, NJ. The majority of the nodes in this area located in open water exhibit mean NLRs that indicate overestimation of peak water levels by 0–0.1 m. Most shallow marsh areas show underestimation of peak water levels by 0.2–0.8 m. Figure D25 shows an area of small canals used for small-boat navigation where the mean NLRs vary roughly from negative 0.8 m to positive 0.8 m, as an example of areas where these simulations might not be sufficiently resolved local hydrodynamics.

Figure D24. Mean NLRs due to SLC in the Atlantic City, NJ, area.

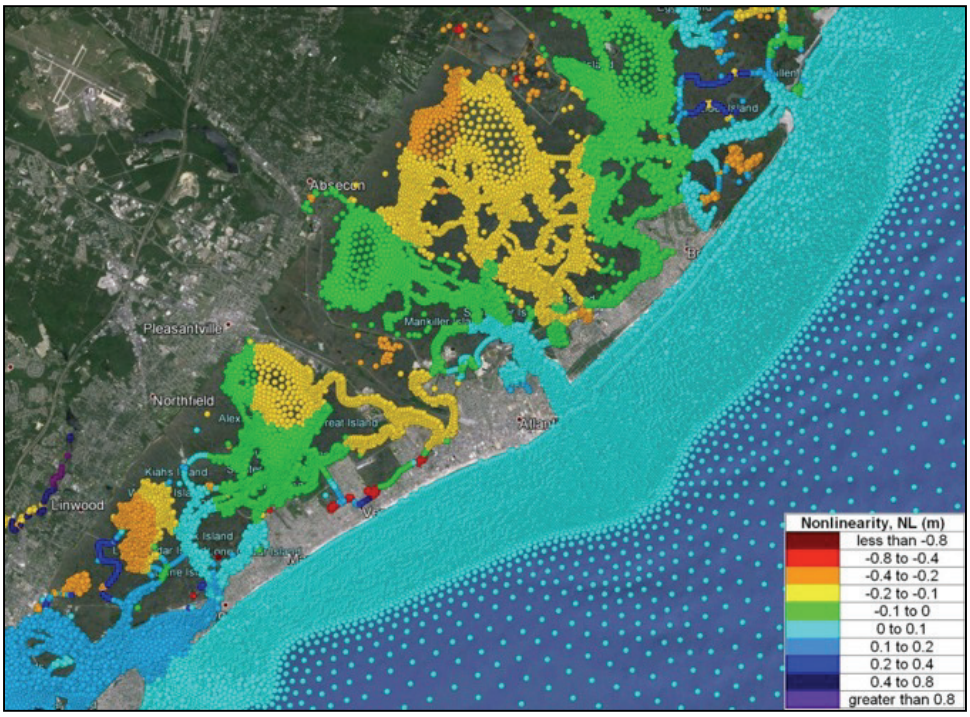

Figure D25. Mean NLRs due to SLC in the Atlantic City, NJ area.

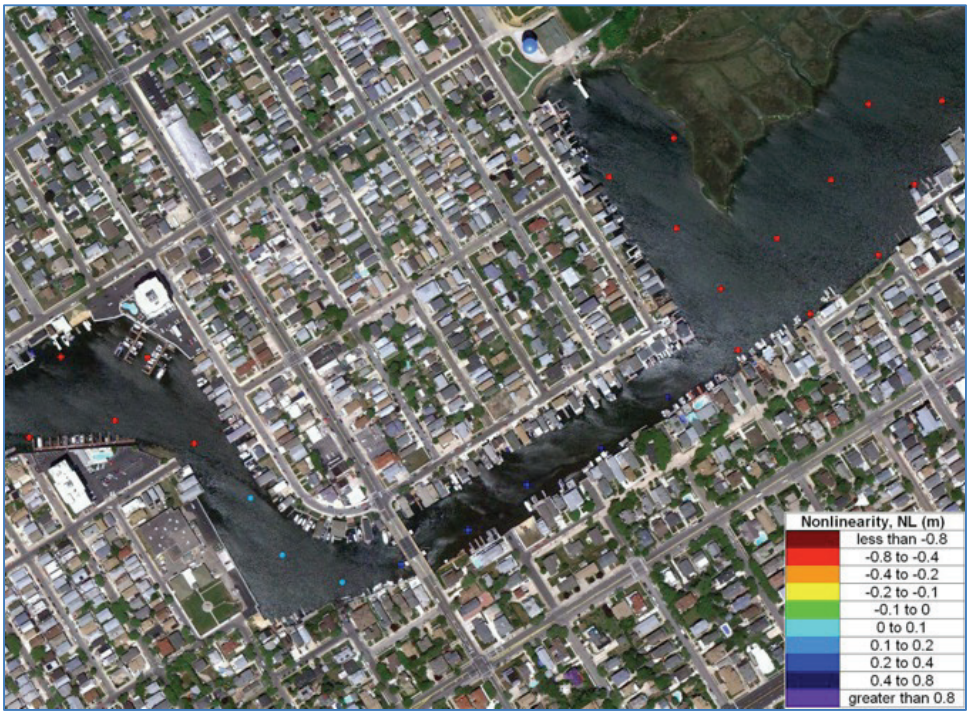

D5 Discussion and Conclusions

This study focused on the statistical analysis of NLRs. The primary goals were to determine the magnitude of the NLRs, identify where these NLRs are acceptable and where they may be too large to apply directly, and to evaluate the feasibility of using correction and uncertainty terms to account for nonlinearity as part of the joint probability of storm water levels. The bias from linear superposition of separate components of storm water levels can be large at very specific locations characterized by enclosed bays, canals, and streams. Unfortunately, many of these locations in the study area coincide with densely populated areas or areas with large investments in industry or critical infrastructure. The results shown indicate that, in general, the NLR bias is negligible over most of the vast majority of the region (Table D1). The analyses in sections D3 and D4 suggest that for most regions, the storm water level components can be modeled separately and linearly superimposed with little error. It was shown that over most of the New York-New Jersey coastal region, the bias was less than 0.2 m but could be more than 0.2 m in the bay near Long Beach, NY, and Amityville, NY.

Bias in general statistical terms refers to a systematic deviation from the expected value and is calculated as the mean of the NLR. The bias can be accounted for by developing correction terms and integrating uncertainty in the joint probability computation similar to procedures in recent FEMA coastal Risk MAP studies. It is feasible within the NACCS study to compute a bias correction term and associated uncertainty for every location where the JPA of storm water levels is to be performed. The incorporation of both tides and SLC to the water level response can be handled with this approach. The statistical quantification of the nonlinearity and inclusion of uncertainty in the JPA is highly desirable since it is a cost-effective approach that fully quantifies uncertainty from nonlinearity.

It was shown that nonlinearity can be significant at specific locations such as canals and streams. Most of these locations exhibit bias that is still reasonably handled with correction and uncertainty terms within the joint probability approach when quantifying extreme water levels. However, some storms produce large NLRs within enclosed localized areas. For the cases where the NLR is too large to account for within the JPA, three approaches are proposed (Figure D26).

If specific storms are to be used within, for example, a life-cycle modeling approach or for any studies that incorporate a significant life-safety consideration, then the local areas with high nonlinearity should be handled by using the full NACCS modeling of tide, surge, and SLC or by using a nearby point that has a low NLR. The NACCS database will contain sufficient information to discern nonlinearity.

Table D1. Nonlinear bias and uncertainty associated with tide and SLC at selected locations.

Location	NACCS Save Point			Nearest ADCIRC Mesh Node	Tide (m)				SLC (m)			
	No.	Longitude (deg)	Latitude (deg)		Bias (m)	Uncertainty (m)	2% Confidence Limit	98% Confidence Limit	Bias (m)	Uncertainty (m)	2% Confidence Limit	98% Confidence Limit
Atlantic City – ocean side	5852	-74.4042	39.36418	210588	-0.02	0.06	-0.16	0.12	0.06	0.07	0.00	0.27
Atlantic City – bay side	3652	-74.4302	39.3912	344930	0.02	0.15	-0.33	0.27	0.01	0.14	-0.23	0.43
Long Beach, NY – ocean side	4501	-73.6776	40.58291	98703	-0.02	0.06	-0.16	0.12	0.06	0.07	0.00	0.25
Long Beach, NY – bay side	4386	-73.67	40.60316	228819	0.01	0.16	-0.39	0.30	-0.29	0.24	-0.75	0.12
Amityville – ocean side	4528	-73.4247	40.60915	38017	-0.02	0.05	-0.13	0.08	0.06	0.05	0.00	0.20
Amityville – bay side	4486	-73.4201	40.64827	175524	-0.02	0.07	-0.18	0.12	-0.21	0.16	-0.54	0.16
Fire Island – ocean side	4662	-73.2374	40.62466	30224	-0.02	0.04	-0.12	0.06	0.05	0.04	0.00	0.17
Fire Island – bay side	4622	-73.2355	40.63922	113971	0.06	0.09	-0.10	0.30	0.12	0.16	-0.10	0.57
Rockaway/Jamaica Bay – ocean side	6488	-73.8513	40.57034	154164	-0.01	0.07	-0.17	0.12	0.07	0.07	0.00	0.26
Rockaway/Jamaica Bay – bay side	4289	-73.8588	40.59074	268982	0.02	0.15	-0.36	0.32	0.02	0.05	-0.03	0.12
Coney Island	4238	-73.9809	40.57071	251389	0.01	0.10	-0.23	0.20	0.04	0.04	0.00	0.13
Staten Island	4024	-74.0742	40.57669	343245	0.01	0.11	-0.23	0.23	0.04	0.04	-0.01	0.13
Perth Amboy	3939	-74.2623	40.49453	484560	0.02	0.14	-0.28	0.30	0.07	0.05	0.00	0.19
The Battery	4161	-74.0188	40.6987	473502	0.02	0.14	-0.29	0.30	0.06	0.05	0.00	0.18
Jersey City	4079	-74.0279	40.70741	482140	0.02	0.14	-0.31	0.30	0.06	0.05	0.00	0.17
Newark	4040	-74.1124	40.71291	509649	0.03	0.16	-0.32	0.36	0.10	0.12	-0.03	0.41
Newark	4085	-74.1447	40.73648	537214	0.05	0.18	-0.38	0.42	0.13	0.12	0.00	0.43

Figure D26. Proposed approaches for use of linear superposition for varying ranges of NLR and different cases of SLC.

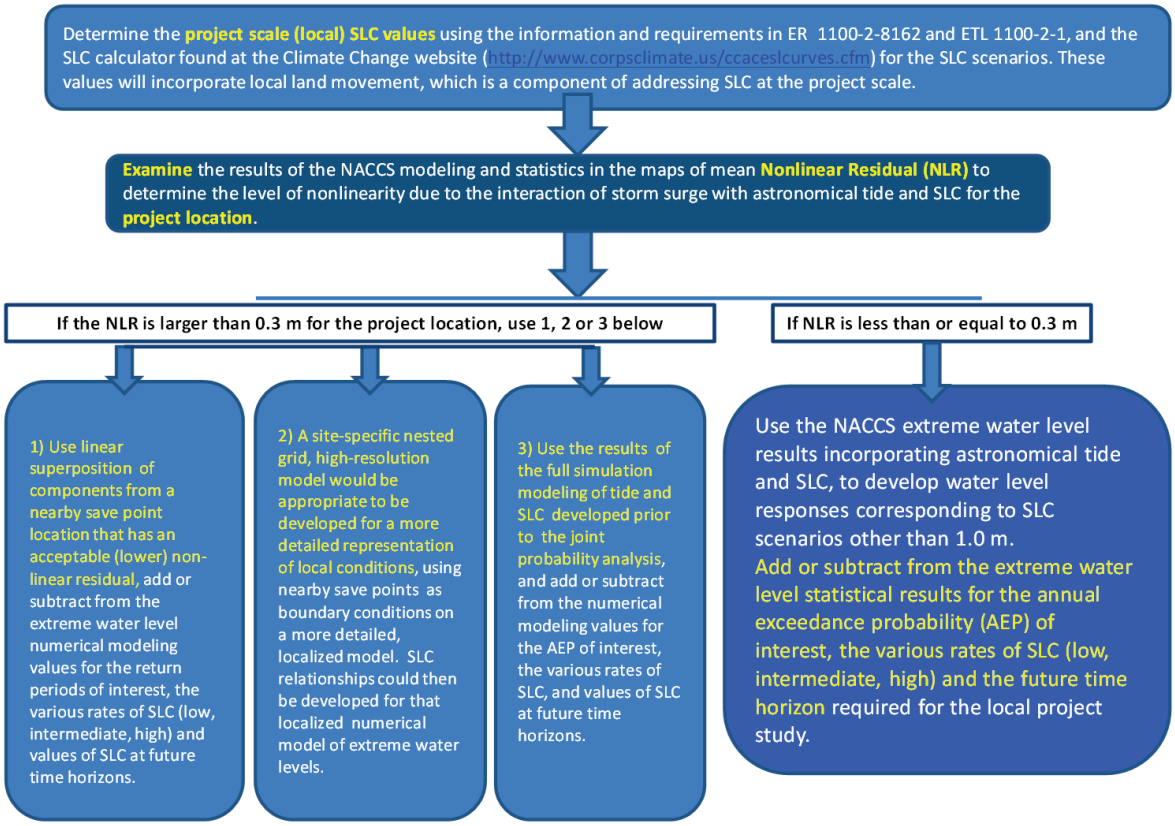

D6 References

Bernier, N. B., and K. R. Thompson. 2007. Tide-surge interaction off the east coast of Canada and northeastern United States. *Journal of Geophysical Research* 112:1–12

Emanuel, K. A. 2013. Downscaling CMIP5 climate models shows increased tropical cyclone activity over the 21st century. In *Proceedings of the National Academy of Sciences*, 110. doi/10.1073/pnas.1301293110.

FEMA. 2008. *Mississippi coastal analysis project: Coastal documentation and main engineering report*. Washington, DC: Federal Emergency Management Agency, Department of Homeland Security.

_____. 2011a. *Flood insurance study: Coastal counties, Texas*. Washington, DC: Federal Emergency Management Agency, Department of Homeland Security.

_____. 2011b. *Redefinition of coastal flood hazard zones in FEMA Region II: Analysis of the coastal storm surge flood frequencies*. Washington, DC: Federal Emergency Management Agency, Department of Homeland Security.

_____. 2012a. *Operating guidance No. 8-12 for use by FEMA staff and flood mapping partners: Joint probability – optimal sampling method for tropical storm surge*. Washington, DC: Federal Emergency Management Agency, Department of Homeland Security.

_____. 2012b. *FEMA Region III storm surge study*. Washington, DC: Federal Emergency Management Agency, Department of Homeland Security.

_____. 2014. *Region II storm surge project – Joint probability analysis of hurricane and extratropical flood hazards*. Washington, DC: Federal Emergency Management Agency, Department of Homeland Security.

Interagency Performance Evaluation Task Force (IPET). 2009. *Performance evaluation of the New Orleans and southeast Louisiana hurricane protection system*. Final Report of the Interagency Performance Evaluation Task Force. Washington, DC: Department of the Army, U.S. Army Corps of Engineers.

Jelesnianski, C. P., J. Chen, and W. A. Shaffer. 1992. *SLOSH: Sea, lake, and overland surges from hurricanes*. NOAA Technical Report NWS 48. Miami, FL: NOAA/National Weather Service, National Centers for Environmental Prediction, National Hurricane Center.

Kim, S. Y., T. Yasuda, and H. Mase. 2008. Numerical analysis of effects of tidal variations on storm surges and waves. *Applied Ocean Research* 30:311–322.

Knutson, T. R., J. J. Sirutis, G. A. Vecchi, S. T. Garner, M. Zhao, H.-S. Kim, M. A. Bender, R. E. Tuleya, I. M. Held, and G. Villarini. 2013. Dynamical downscaling projections of 21st century Atlantic hurricane activity: CMIP3 and CMIP5 model-based scenario. *Journal of Climate* 26(17). doi:10.1175/JCLI-D-12-00539.1.

Lin, N., K. Emanuel, M. Oppenheimer, and E. Vanmarcke. 2012. Physically based assessment of hurricane surge threat under climate change. *Nature Climate Change* 2:462-467. http://www.nature.com/nclimate/journal/v2/n6/abs/nclimate1389.html

Loder, N. M., M. A. Cialone, J. L. Irish, and T. V. Wamsley. 2009. *Idealized march simulations: Sensitivity of hurricane surge elevations and wave height to bottom friction*. ERDC/CHL CHETN-I-79. Vicksburg, MS: U.S. Army Engineer Research and Development Center.

Milly, P. C. D., J. Bentacourt, M. Falkenmark, R. M. Hirsh, Z. W. Kundezewicz, D. P. Lettenmaier, and R. J. Stouffer. 2008. Stationarity is dead: Whither water management? *Science* 319(5863): 573–574.

Prandle, D., and J. Wolf. 1978. The interaction of surge and tide in the North Sea and River Thames. *Geophysical Journal of the Royal Astronomical Society* 55:203–216

Proudman, J. 1957. Oscillations of tide and surge in an estuary of finite length. *Journal of Fluid Mechanics* 2:371– 382

Rego, J. L. 2009. Storm surge dynamics over wide continental shelves: Numerical experiments using the finite-volume coastal ocean model. PhD dissertation, Louisiana State University

Rego, J. L., and C. Li. 2010. Nonlinear terms in storm surge predictions: Effect of tide and shelf geometry with case study from Hurricane Rita. *Journal of Geophysical Research: Oceans* 115:1–19

Resio, D. T., S. J. Boc, L. Borgman, V. Cardone, A. T. Cox, W. R. Dally, R. G. Dean, D. Divoky, E. Hirsh, J. L. Irish, D. Levinson, A. Niedoroda, M. D. Powell, J. J. Ratcliff, V. Stutts, J. Suhada, G. R. Toro, and P. J. Vickery. 2007. *White paper on estimating hurricane inundation probabilities*. Consulting Report prepared by USACE for FEMA.

Smith, J. M., A. R. Sherlock, and D. T. Resio. 2001. *STWAVE: Steady-state spectral wave model user's manual for STWAVE, version 3.0*. ERDC/CHL SR-01-1. Vicksburg, MS: U.S. Army Engineer Research and Development Center.

U.S. Army Corps of Engineers (USACE). 2009. *Policies for referencing project elevation grades to nationwide vertical datums*. ER 1110-2-8160. Washington, DC: U.S. Army Corps of Engineers, Department of the Army.

_____. 2010. *Standards and procedures for referencing project elevation grades to nationwide vertical datums*. EM 1110-2-6056. Washington, DC: U.S. Army Corps of Engineers, Department of the Army.

Westerink, J., R. Luettich, A. Baptists, N. Scheffner, and P. Farrar. 1992. Tide and storm surge predictions using finite element model. *Journal of Hydraulic Engineering* 118(10):1373–1390.

Wolf, J. 1978. *Interaction of tide and surge in a semi-infinite uniform channel, with application to surge propagation down the east coast of Britain*. Merseyside, UK: Institute of Oceanographic Sciences, Bidston Observatory.

Appendix E: NACCS Expanded List of Historical TCs

Following is the expanded list of TCs ($\Delta p \geq 23$ hPa) identified from the HURDAT2 database as either making landfall or passing within 300 km of the study area during the 1938–2013 period.

NACCS Tropical Cyclone ID (Expanded Set)	Name	Year	National Hurricane Center ID	Maximum Wind Speed (km/h)	Minimum Central Pressure (hPa)
1	UNNAMED	1938	6	204	940
2	UNNAMED	1939	2	120	985
3	UNNAMED	1940	4	167	961
4	UNNAMED	1941	3	120	990
5	UNNAMED	1944	3	130	985
6	UNNAMED	1944	7	194	940
7	UNNAMED	1944	13	213	937
8	UNNAMED	1945	9	213	949
9	UNNAMED	1946	4	157	975
10	UNNAMED	1946	6	148	977
11	UNNAMED	1947	6	93	987
12	UNNAMED	1948	10	120	990
13	UNNAMED	1949	1	148	963
14	ABLE	1950	1	194	953
15	DOG	1950	4	204	953
16	BARBARA	1953	2	167	987
17	CAROL	1953	4	241	929
18	FLORENCE	1953	8	204	968
19	CAROL	1954	3	139	976
20	HAZEL	1954	9	204	937
21	CONNIE	1955	2	232	936
22	DIANE	1955	3	194	969
23	IONE	1955	9	185	938
24	FLOSSY	1956	7	120	980
25	DAISY	1958	4	194	935
26	HELENE	1958	8	204	934
27	UNNAMED	1959	3	120	974
28	GRACIE	1959	8	222	950
29	DONNA	1960	5	222	932

NACCS Tropical Cyclone ID (Expanded Set)	Name	Year	National Hurricane Center ID	Maximum Wind Speed (km/h)	Minimum Central Pressure (hPa)
30	ESTHER	1961	5	213	927
31	FRANCES	1961	7	204	948
32	GERDA	1961	8	102	987
33	ALMA	1962	1	120	986
34	DAISY	1962	4	157	965
35	GINNY	1963	8	176	958
36	CLEO	1964	5	250	950
37	DORA	1964	6	213	942
38	GLADYS	1964	9	232	945
39	ISBELL	1964	11	204	964
40	ALMA	1966	1	204	970
41	DORIA	1967	14	130	973
42	ABBY	1968	1	93	965
43	GLADYS	1968	14	130	965
44	CAMILLE	1969	9	278	900
45	GERDA	1969	16	204	979
46	BETH	1971	6	139	977
47	DORIA	1971	9	102	989
48	GINGER	1971	14	167	959
49	AGNES	1972	2	111	977
50	ALICE	1973	4	130	986
51	AMY	1975	2	111	981
52	BLANCHE	1975	4	139	980
53	BELLE	1976	7	194	957
54	BOB	1979	4	120	986
55	DAVID	1979	9	278	924
56	UNNAMED	1979	18	111	980
57	CHARLEY	1980	7	130	989
58	UNNAMED	1981	22	111	978
59	UNNAMED	1982	2	111	984
60	DIANA	1984	10	213	949
61	JOSEPHINE	1984	16	130	965
62	DANNY	1985	4	148	987
63	GLORIA	1985	9	232	920
64	KATE	1985	13	194	954
65	CHARLEY	1986	5	83	980
66	ARLENE	1987	2	120	987
67	HUGO	1989	11	259	918

NACCS Tropical Cyclone ID (Expanded Set)	Name	Year	National Hurricane Center ID	Maximum Wind Speed (km/h)	Minimum Central Pressure (hPa)
68	BERTHA	1990	3	130	973
69	LILI	1990	14	120	987
70	MARCO	1990	15	102	989
71	BOB	1991	3	185	950
72	UNNAMED	1991	12	111	972
73	EMILY	1993	5	185	960
74	GORDON	1994	12	139	980
75	ALLISON	1995	1	93	982
76	BARRY	1995	2	74	989
77	FELIX	1995	7	222	929
78	BERTHA	1996	2	185	960
79	EDOUARD	1996	5	232	933
80	FRAN	1996	6	194	946
81	HORTENSE	1996	8	222	935
82	JOSEPHINE	1996	10	83	970
83	DANNY	1997	5	130	984
84	BONNIE	1998	2	185	954
85	EARL	1998	5	102	964
86	DENNIS	1999	5	167	962
87	FLOYD	1999	8	250	921
88	IRENE	1999	13	176	958
89	GORDON	2000	11	130	981
90	HELENE	2000	12	111	986
91	UNNAMED	2000	19	102	976
92	KAREN	2001	13	130	982
93	GUSTAV	2002	8	148	960
94	KYLE	2002	12	139	980
95	ISABEL	2003	13	269	915
96	JUAN	2003	15	167	969
97	ALEX	2004	1	194	957
98	CHARLEY	2004	3	241	941
99	GASTON	2004	7	120	985
100	IVAN	2004	9	269	910
101	JEANNE	2004	11	194	950
102	OPHELIA	2005	16	120	976
103	ALBERTO	2006	1	102	969
104	ERNESTO	2006	6	111	985
105	BARRY	2007	2	74	990

NACCS Tropical Cyclone ID (Expanded Set)	Name	Year	National Hurricane Center ID	Maximum Wind Speed (km/h)	Minimum Central Pressure (hPa)
106	NOEL	2007	16	120	965
107	HANNA	2008	8	139	977
108	KYLE	2008	11	130	984
109	BILL	2009	3	204	943
110	EARL	2010	7	232	927
111	IRENE	2011	9	167	942
112	SANDY	2012	18	148	940

REPORT DOCUMENTATION PAGE

Form Approved
OMB No. 0704-0188

1. REPORT DATE	2. REPORT TYPE	3. DATES COVERED *(From - To)*
November 2015	Final	

4. TITLE AND SUBTITLE

Coastal Storm Hazards from Virginia to Maine

5a. CONTRACT NUMBER

5b. GRANT NUMBER

5c. PROGRAM ELEMENT NUMBER

6. AUTHOR(S)

Norberto C. Nadal-Caraballo, Jeffrey A. Melby, Victor M. Gonzalez, Andrew T. Cox

5d. PROJECT NUMBER
401426

5e. TASK NUMBER

5f. WORK UNIT NUMBER

7. PERFORMING ORGANIZATION NAME(S) AND ADDRESS(ES)
Coastal and Hydraulics Laboratory
U.S. Army Engineer and Development Center
3909 Halls Ferry Road
Vicksburg, MS 39180

8. PERFORMING ORGANIZATION REPORT NUMBER
ERDC/CHL TR-15-5

9. SPONSORING/MONITORING AGENCY NAME(S) AND ADDRESS(ES)
U.S. Army Corps of Engineers
Baltimore District
City Crescent Building, 10 South Howard Street
Baltimore, MD 21201

10. SPONSOR/MONITOR'S ACRONYM(S)

11. SPONSOR/MONITOR'S REPORT NUMBER(S)

12. DISTRIBUTION/AVAILABILITY STATEMENT
Approved for public release; distribution is unlimited.

13. SUPPLEMENTARY NOTES

14. ABSTRACT
The U.S. North Atlantic coast is subject to coastal flooding as a result of tropical cyclones (e.g., hurricanes) and severe extratropical cyclones (e.g., Nor'easters). The North Atlantic Coast Comprehensive Study (NACCS) seeks to quantify existing and future forcing for use in assessing potential engineering projects that would reduce flooding risk and increase resiliency. The study encompasses the coastal region from Virginia to Maine. This report describes the characterization of storm climate and statistical analysis of coastal storm hazards for the NACCS. The overall NACCS wave and water level modeling goals included simulating an efficient number of storms that blanketed a sufficient range of storm characteristics in order to accurately describe the statistical nature of coastal storm response over the entire region. This information is required for modern probabilistic project design and for risk assessments. For this study, storm surge, tide, waves, wind, atmospheric pressure, and currents were the dominant storm responses computed. The effect of sea level change on these storm responses was assessed. The significant advancements in this study included a dense spatial coverage of nearshore storm response for the region, high-fidelity computations, a comprehensive description of the aleatory variability of response from frequent storm events to extremely rare events, a description of epistemic uncertainty, characterization of the statistical nature of the data in easily ingestible, relatively simple data formats, and public distribution of data and statistics within the Coastal Hazards System, a web-based coastal storm data resource.

15. SUBJECT TERMS

Coastal storm hazards, extratropical cyclones, extreme value analysis, extreme water level, hurricanes, joint probability analysis, joint probability method, NACCS, North Atlantic Coast Comprehensive Study, optimal sampling, storm surge, synthetic storms, tropical cyclones, wave climate

16. SECURITY CLASSIFICATION OF:			17. LIMITATION OF ABSTRACT	18. NUMBER OF PAGES	19a. NAME OF RESPONSIBLE PERSON
a. REPORT	b. ABSTRACT	c. THIS PAGE			Norberto C. Nadal-Caraballo, PhD
Unclassified	Unclassified	Unclassified	SAR	222	19b. TELEPHONE NUMBER *(Include area code)* (601) 634-2008